Polycyclic aromatic hydrocarbon biodegradation for soil bioremediation : potential of microfluidics to understand benzo[a]pyrene uptake by the filamentous fungus Talaromyces helicus

Claire Baranger

Par **Claire BARANGER**

Polycyclic aromatic hydrocarbon biodegradation for soil bioremediation : potential of microfluidics to understand benzo[a]pyrene uptake by the filamentous fungus Talaromyces helicus

Thèse présentée
pour l'obtention du grade
de Docteur de l'UTC

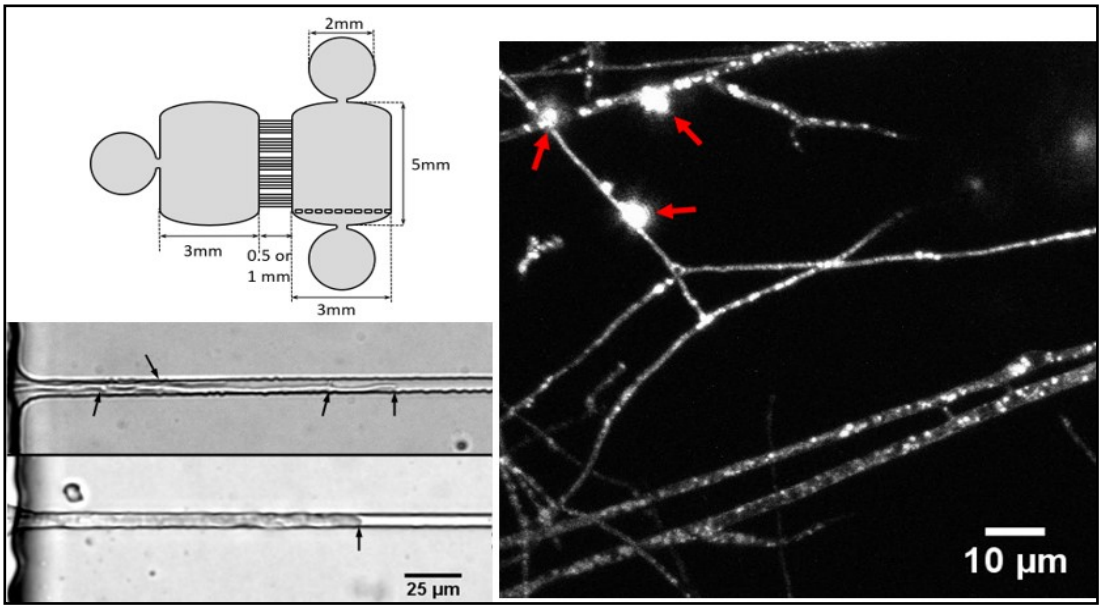

Soutenue le 22 juillet 2020
Spécialité : Bioprocédés et Bioingénierie : Transformations intégrées de la matière renouvelable (EA-4297)
D2559

Transformations Intégrées de la Matière Renouvelable - EA 4297 UTC-ESCOM

Biomécanique et Bioingénierie BMBI - UMR CNRS 7338

Spécialité : Bioprocédés et Bioingénierie

Polycyclic aromatic hydrocarbon biodegradation for soil bioremediation : Potential of microfluidics to understand benzo[*a*]pyrene uptake by the filamentous fungus *Talaromyces helicus*

Thèse présentée pour l'obtention du grade de docteur

de l'Université de Technologie de Compiègne

Ecole doctorale ED 71 UTC « Sciences pour l'ingénieur »

par

Claire Baranger

Soutenue le 22 juillet 2020, devant le jury composé de :

Craig FAULDS, Professeur, INRAE - Université d'Aix-Marseille	rapporteur
Philippe NGHE, Maître de Conférences, ESPCI Paris	rapporteur
Stéphanie DESCROIX, Directrice de Recherches, Institut Curie Paris	examinatrice
Christophe WATERLOT, Maître de Conférences (HDR), ISA Lille	examinateur
Olivier SCHOEFS, Professeur, UTC	examinateur
Isabelle PEZRON, Professeur, UTC	examinatrice
Antoine FAYEULLE, Maître de Conférences, UTC	directeur de thèse
Anne LE GOFF, Maître de Conférences, UTC	directrice de thèse

Remerciements

Je voudrais tout d'abord adresser mes remerciements à mon directeur et ma directrice de thèse, Antoine Fayeulle et Anne Le Goff, ainsi que ma co-encadrante Isabelle Pezron, pour leur grande disponibilité, leurs conseils précieux et leur patience, ainsi que les discussions scientifiques – et moins scientifiques – toujours enrichissantes qui m'ont permis d'avancer dans mes travaux.

Ma reconnaissance va aussi à toute l'équipe technique du département GPI et en particulier Bruno Dauzat pour son aide précieuse avec les analyses HPLC, ainsi qu'à Caroline Lefebvre au SAPC pour son expertise technique et son assistance au microscope confocal.

Je remercie également les personnes extérieures à l'UTC qui m'ont généreusement permis de profiter de leur savoir et de leurs ressources :

Alain Huré à Oxbiolab pour m'avoir permis de travailler avec des sols de sites contaminés, et m'avoir apporté une perspective essentielle sur les applications concrètes de la bioremédiation sur site, au-delà des essais en laboratoire.

Magali Deleu du laboratoire Biophysique Moléculaire aux Interfaces à l'Université de Liège, pour avoir accepté d'effectuer une simulation numérique du passage membranaire du BaP.

Sandrine Caristan chez Chromacim, qui a accepté d'analyser des échantillons en HPTLC, pour son contact chaleureux et pour son expertise sur la technique CAMAG qui m'a grandement aidée à interpréter les résultats.

J'adresse des remerciements tous particuliers aux étudiant·es et stagiaires qui ont participé, à l'échelle de quelques semaines ou de plusieurs mois, à ce projet et à l'obtention de certains résultats présentés dans ce manuscrit : Xue Sun, Roxane Valentin, Marie Valmori, Théo Guillerm, Estelle Canellas, Louis Mayer, Laurine de Lisiecki et surtout Laura Creusot, pour son sérieux et sa sympathie, et dont les travaux réalisés au cours de son stage ingénieur constituent la base expérimentale du chapitre I.

Merci à tous·tes mes collègues des deux laboratoires, TIMR et BMBI, et en particulier des équipes IFSB et MAB, avec qui j'ai partagé les pauses déjeuner et de (trop) nombreux cafés, et bien sûr les doctorant·es et de l'UTC avec qui j'ai traversé les hauts et les bas pendant ces quatre années. J'ai une pensée pour Doriane, Lorine, Mattia, Chunmei, Alex, Mégane, Gaël, Nabila, Nicolas, Baptiste, Diane, Thibaut, Audrey, Emma, Shruthi, et tous·tes les autres…

Merci à ma famille et notamment mes parents qui m'ont toujours supportée (dans tous les sens du terme) et qui m'ont permis d'arriver jusqu'ici. A mes amies toujours là même quand des milliers de kilomètres nous séparent. Et à Kiwi pour sa douceur et ses ronrons qui m'accompagnait déjà pendant les révisions du bac.

Merci enfin à mes camarades féministes, qui ont véritablement changé ma vie ces dernières années, et m'apportent chaque jour de la force et de l'espoir.

Résumé

Un grand nombre de polluants d'intérêt, dont les hydrocarbures et certains xénobiotiques, se caractérisent par une forte hydrophobie et une solubilité dans l'eau faible voire quasi-nulle. Certains de ces polluants, comme les hydrocarbures aromatiques polycycliques (HAP), ou des pesticides, sont préoccupants pour la santé animale et humaine, et l'environnement, en raison de leur persistance et de leur toxicité chronique. Etant donné la tendance de ces composés à s'adsorber plus ou moins fortement sur les surfaces hydrophobes ou la matière organique, leur taux de rétention élevé dans les sols peut à la fois être positif en minimisant l'exposition humaine et animale, et être une limitation à la remédiation efficace des sites contaminés. La fraction directement assimilable d'une molécule pour les organismes vivants est définie comme la fraction biodisponible : c'est donc cette fraction qui est dégradée ou accumulée préférentiellement par les organismes du sol au cours des processus d'atténuation naturelle d'une pollution. Les fractions les moins biodisponibles peuvent au contraire persister pendant des dizaines d'années.

Depuis la deuxième moitié du XXème siècle, la biodégradation des polluants organiques, et en particulier des hydrocarbures, par des champignons a été l'objet de nombreuses études. Les champignons sont partie intégrante des sols, à la fois en termes de structure et de fonctions, influençant leurs propriétés physiques et chimiques, en interaction dynamique avec les autres organismes vivants. Ainsi, les champignons développent un réseau mycélien très dense dans les sols, un gramme de sol pouvant contenir jusqu'à 10^4 m d'hyphes fongiques (Ritz et Young 2004). Ils affectent ainsi de façon notable l'agrégation et l'hydrophobie des sols (Rillig 2004, 2005). D'autre part, on estime que 90% des espèces végétales terrestres forment des associations mycorhiziennes avec des champignons (Bonfante et Genre, 2010). Evaluer les capacités de biodégradation fongique en elles-mêmes n'est donc pas suffisant pour comprendre leur rôle dans l'atténuation naturelle des contaminations du sol, et leur potentiel pour la bioremédiation: il est également nécessaire de prendre en compte leur écologie en temps qu'organismes natifs du sol et comment elle affecte la dynamique des polluants in situ.

La biodégradation concerne l'altération chimique des polluants par les organismes vivants, tandis que la biosorption est un phénomène physico-chimique passif de liaison des polluants au structures cellulaires. Ces deux phénomènes affectant les contaminants organiques de manière directe sont souvent examinés lorsque l'on étudie le potentiel d'une souche pour la bioremédiation. Cependant, les champignons sont également impliqués dans des modulations des propriétés du sol en lui-même, en particulier sa texture, son agrégation, la porosité, et son hydrophobie, affectant de manière

indirecte la rétention des polluants. Ainsi, les champignons contribuent à la structuration de la matrice du sol, à la fois en favorisant la formation d'agrégats, et en altérant les minéraux et la matière organique (Ritz and Young, 2004 ; Gadd et al., 2012).

La plupart des champignons du sol sont des organismes saprotrophes, qui contribuent au cycle du carbone des sols en décomposant et en minéralisant les matières organiques. Ils disposent d'outils enzymatiques adaptés à une large gamme de molécules d'origine biologique, et certaines souches ont démontré des capacités de biodégradation des hydrocarbures, de composés organiques synthétiques et même de matériaux polymériques. Les champignons, en coopération avec d'autres micro-organismes et plantes, participent ainsi à l'atténuation naturelle des polluants organiques hydrophobes notamment par leur altération chimique. Le métabolisme des hydrocarbures chez les champignons est en grande partie lié à celui des lipides. En effet, des activités lipolytiques intracellulaires et extracellulaires contribuent à leur conversion en acides gras suivie de leur biodégradation ou de leur incorporation dans la biomasse (Peter et al., 2012; Al-Hawash et al., 2019). En ce qui concerne les molécules contenant des cycles aromatiques, et en particulier les HAP et les certains colorants de synthèse, les enzymes fongiques de dégradation de la lignine ont été les plus étudiées pour leur potentiel de biodégradation. La voie ligninolytique implique notamment des oxido-réductases extracellulaires: des laccases, lignine-peroxydases, manganèse-peroxydases et tyrosinases qui catalysent la production d'agents oxydants et radicaux libres entraînant l'oxydation non-spécifique du substrat en quinones. L'autre voie majeure de métabolisation des aromatiques est la voie intracellulaire des cytochromes P450, qui apparaît comme la voie dominante chez les champignons non-ligninolytiques. Cette voie produit des dérivés plus réactifs et solubles que les polluants d'origine, dont des phénols, phtalates, dihydrodiols et autres dérivés carboxylés ou hydroxylés (Boll et al., 2015).

Les champignons produisent des molécules tensio-actives variées, qui remplissent des fonctions essentielles pour leur morphogenèse et leur mode de vie, notamment l'adhésion à des surfaces, l'interaction avec des substrats hydrophobes, et la formation d'hyphes aériens. Ces tensioactifs modulent à la fois les propriétés de surface des hyphes, et celles de leur environnement immédiat. Les hydrophobines et les glomalines sont des protéines fongiques extracellulaires capables de moduler les propriétés de surface du sol, affectant potentiellement l'adsorption des polluants et leur transport via des écoulements d'eau. Alors que les fonctions des glomalines et protéines apparentées au sein des sols sont relativement bien établies, les hydrophobines ont en revanche été principalement étudiées pour leur rôle physiologique et leurs applications industrielles, et les observations empiriques de leurs effets sur les sols sont encore peu documentées. Par ailleurs, les champignons produisent une large gamme de tensioactifs extracellulaires de nature non protéique, présentant des propriétés de dispersion ou de solubilisation de composés organiques hydrophobes. Cependant, leur implication

dans le cadre de mécanismes biologiques spécifiques pour le transport de ces composés n'est pas établie.

La mobilisation extracellulaire et l'adsorption en surface de molécules hydrophobes pourrait être une étape préalable favorisant leur incorporation dans la cellule. L'accumulation intracellulaire d'hydrocarbures par des champignons et connue au moins depuis les années 80, quand un premier mécanisme actif de transport des hydrocarbures a été proposé chez *Cladosporium resinae* (Lindley and Heydeman, 1986). Plus récemment, l'incorporation de HAP dans des organites de stockage dues lipides a été observée chez plusieurs espèces, dont l'ascomycète du sol *Fusarium solani* (Verdin et al., 2005; Fayeulle et al., 2014), le champignon mycorrhizien *Glomus intraradices* (Verdin et al., 2006), et un autre organisme eucaryote filamenteux, *Pythium ultimum* (Furuno et al., 2012). *P. ultimum* a été utilisé comme modèle d'organisme filamenteux pour mettre en évidence un double phénomène de dispersion susceptible d'augmenter la biodisponibilité des HAP dans les sols: d'une part via la translocation intracellulaire des corps lipidiques contenant des HAP accumulés, et d'autre part comme support à la migration de bactéries utilisatrices des HAP (Banitz et al., 2013). Des transports via les hyphes de champignons mycorhiziens pourraient également jouer un rôle dans l'accumulation de polluants des sols par les plantes. Les mécanismes permettant à ces molécules fortement hydrophobes hydrophobes de parvenir aux surfaces cellulaires, de traverser les parois fongiques et de pénétrer les cellules restent en revanche largement à élucider, bien que pour le passage des membranes et l'accès aux sites de stockage intracellulaire, des mécanismes de transport actif impliquant le cytosquelette soient suspectés (Fayeulle et al., 2014).

Le micro-organisme utilisé pour cette étude est une souche du champignon filamenteux *Talaromyces helicus* préalablement isolée à partir de sol d'un site industriel contaminé, et sélectionnées pour sa capacité de dégradation du benzo[*a*]pyrène (BaP). *T. helicus* est un champignon saprotrophe du sol, de répartition cosmopolite. Cette espèce est citée pour ses capacités de dégradation de plusieurs polluants organiques (Romero et al., 2010; Fayeulle et al., 2019) et d'accumulation de métaux (Romero et al., 2006) et a déjà été isolée à partir d'échantillons de sol contaminés (Fayeulle et al., 2019). D'autres espèces du genre *Talaromyces* ont également été identifiées dans des sols et sédiments contaminés à plusieurs occasions (Chaillan et al., 2004; Reyes-César et al., 2014), montrant leur adaptation à des conditions de stress et leur tolérance pour des contaminants toxiques tels que des polluants organiques et métaux lourds. Au cours de ce travail de thèse, le potentiel de cette espèce pour la biodégradation de polluants organiques a été examiné, et plus spécifiquement la dégradation du BaP utilisé comme modèle de polluant persistant fortement hydrophobe.

Afin d'évaluer l'efficacité de biodégradation de *T. helicus* vis-à-vis du BaP et d'autres polluants organiques, le premier chapitre décrit des tests de biodégradation menés selon deux approches complémentaires: dans un premier temps en cultures liquides en conditions contrôlées et avec le BaP comme unique contaminant modèle, et dans un deuxième temps en microcosmes de sol en utilisant des échantillons de sol issus de véritables sites pollués, présentant des contaminations multiples entre autres aux hydrocarbures, polychlorobiphényles (PCB), et HAP. Quatre stratégies visant à améliorer l'efficacité de bioremédiation ont été testées, en complément de la bio-augmentation avec *T. helicus*: la biostimulation par la supplémentation ou l'appauvrissement en azote, l'oxydation chimique par du peroxyde d'hydrogène, la bio-augmentation avec des bactéries métabolisant les hydrocarbures (suspension commerciale HC) ou produisant des surfactants (*Corynebacterium glutamicum*), et enfin l'addition de surfactants pour augmenter la biodisponibilité des polluants.

Concernant les expériences en milieu contrôlé, les taux de biodégradation du BaP ont été quantifiés après neuf jours de culture en milieu minéral supplémenté avec du BaP et du glucose comme cosubstrat carboné. Le BaP résiduel dans les cultures a ensuite été extrait par solvant en continu (méthode de Soxhlet), quantifié par HPLC et comparé à des témoins permettant d'évaluer les pertes abiotiques, par adsorption et du fait de l'extraction.

Les résultats obtenus confirment la capacité de biodégradation de *T. helicus* pour le BaP, avec un pourcentage de dégradation moyen de 38% par rapport au contrôle dans les conditions standard testées, ce qui est cohérent avec les taux de biodégradation rapportés dans la littérature dans des conditions similaires (Fayeulle et al. 2019). Le taux de dégradation est dépendant de l'approvisionnement en azote, et la dégradation apparaît fortement stimulée en milieu enrichi en azote (C/N = 8) avec un pourcentage de dégradation de 90%. L'ajout de surfactants (sophorolipides et Tween 20) pour solubiliser le BaP en revanche n'a pas eu d'effet significatif sur les pourcentages de biodégradation en milieu liquide, indiquant que la biodisponibilité n'est pas un facteur limitant pour la biodégradation dans ces conditions. D'autre part, les tests avec ajout de H_2O_2 à faible concentration montrent une inhibition de la biodégradation. Plusieurs produits de dégradation plus polaires que le BaP ont été détectés par HPLC dans les cultures, mais non identifiés plus précisément. Ces composés pourraient correspondre à des métabolites tels que des phénols, dihydrodiols, dérivés hydroxylés, carboxylés ou conjugués de sucres produits lors de la dégradation fongique.

Trois sols issus de sites localisés en Île-de-France et dans la région Pays-de-la-Loire ont été utilisés pour les tests de remédiation en microcosmes. Les sols n'ont pas été stérilisés afin de conserver la flore endogène, et ont été préalablement séchés et homogénéisés, puis humidifiés avec de l'eau distillée.

Les microcosmes ont été préparés dans des bouteilles en verre fermées et incubés dans pendant 30 jours avec une aération hebdomadaire.

T. helicus ainsi que le consortium bactérien HC étaient plus performants dans le sol présentant le contenu les plus important en matière organiques : les bactéries ont significativement réduit la contamination globale aux hydrocarbures, tandis que le champignon semble affecter spécifiquement les teneurs en HAP. En revanche, aucun des micro-organismes testés n'a stimulé l'élimination des polluants dans les échantillons de sols chaulés présentant un pH basique. Un résultat intéressant a été obtenu avec l'ajout d'un surfactant (un sophorolipide agrosourcé) qui a légèrement augmenté l'élimination des PCB et hydrocarbures totaux en présence de *T. helicus*. Enfin, la bio-augmentation avec *C. glutamicum* semble avoir spécifiquement stimulé la remédiation des PCB. L'efficacité de remédiation pour un micro-organisme donné dépend fortement des propriétés du sol considéré. Ainsi, les résultats obtenus en cultures liquides se sont révélés peu prédictifs de l'efficacité de la souche fongique dans des sols contaminés.

Le deuxième chapitre expérimental se concentre sur la production de biosurfactants extracellulaire par *T. helicus* et leur caractérisation partielle. Des surnageants de culture de *T. helicus* ont été produits en milieu minéral après 4 à 13 jours d'incubation, récoltés par filtration, et leur tension superficielle a été mesurée par un tensiomètre à lame de Wilhelmy. Un abaissement significatif de la tension de surface a été observé au cours de la croissance, de 69 mN/m avant inoculation jusqu'à 49 mN/m après 10 jours d'incubation. Cette diminution indique la libération de composés tensioactifs extracellulaires dans le milieu, coïncidant avec la phase de croissance du mycélium et la détection de faibles concentration de protéines dans le milieu, qui pourraient être entre autres des hydrophobines.

Des filtrats obtenus après 13 jours ont ensuite été analysés afin d'identifier leur composition, d'abord en réalisant une séparation sur résine d'exclusion de taille, puis en analysant les fractions récoltées par chromatographie sur couche mince (CCM) à haute performance. La combinaison de ces deux techniques vise à obtenir des informations à la fois sur le poids moléculaire et la nature chimique des tensioactifs présents dans les fractions actives. La CCM a été choisie car elle permet la détection d'une large gamme de composés de familles chimiques diverses grâce à l'utilisation de phases mobiles et de révélateurs appropriés. Cette adaptabilité de la technique est particulièrement intéressante dans le cas présenté ici, où les molécules d'intérêt sont inconnues et seulement définies au départ par leur capacité à abaisser la tension de surface du milieu. Les mesures de tension de surface dans les fractions issues de la chromatographie d'exclusion de taille révèlent au moins trois composés ou groupes de composés de masses moléculaires distinctes avec des propriétés tensio-actives. Cependant, leur

nature biochimique respective reste à caractériser plus précisément. Les premiers résultats de CCM indiquent que ces fractions contiennent des glucides, mais aucun lipide n'a été détecté.

L'effet des surnageants de culture sur la solubilisation apparente du BaP a ensuite été examiné en réalisant des tests de désorption. Une pastille de cellulose sur laquelle a été déposé 50 µg de BaP est incubée pendant 24h dans le filtrat de culture sous agitation, puis le BaP contenu sur la pastille de même que celui présent dans la phase aqueuse sont extraits séparément et quantifiés. Ces tests ne montrent pas une solubilisation significative du BaP en phase aqueuse par les tensioactifs fongiques en comparaison du milieu non inoculé, ce qui recoupe de précédents résultats obtenus avec la même espèce (Fayeulle 2013).

Le chapitre III décrit le développement d'un dispositif permettant la culture de champignons filamenteux sur puce microfluidique et le suivi de la mobilisation d'un polluant hydrophobe insoluble dans l'eau, le BaP. Ce dispositif est conçu pour servir de modèle d'un environnement compartimenté où d'une part la localisation de la source de polluant peut être contrôlée, et d'autre part le polluant peut être spatialement séparé de l'inoculum au début de l'expérience. Le contrôle de la géométrie, du confinement et de écoulements font des puces microfluidiques des outils intéressants pour le développement de modèles de « sol sur puce » non seulement pour l'étude des propriétés physico-chimiques des sols, mais également leur flore microbienne (Stanley et al., 2016). Ainsi les organismes peuvent être retenus ou transférés de manière contrôlée dans des compartiments définis, et observés en temps réel, ce qui est utile notamment pour l'étude des interactions entre micro-organismes. Ainsi des cultures fongiques dans un environnement compartimenté permettent de mettre en évidence l'hétérogénéité spatiale du mycélium, et sa capacité à déclencher des réponses localisées à des stimuli extérieurs. Cette compartimentation et le contrôle spatial du micro-environnement sont des caractéristiques particulièrement intéressantes dans le contexte des présents travaux de thèse, qui se concentrent sur le comportement d'un champignon en présence de polluants dans un environnement complexe et hétérogènes : le sol.

Dans un premier temps des tests de croissance ont été réalisés dans des puces de géométrie simple composées de deux chambres rectangulaires (4 mm x 800 µm) reliées par un canal unique (section 14 x 15 µm). Un motif « Ch50 » comportant deux chambres de 5 x 3 mm reliées par 50 micro-canaux de plus petites dimensions (6x12 µm) a également été dessiné. Ces puces sont fabriquées par une technique de lithographie douce, dans un polymère souple, transparent et bio-compatible, le polydimethylsiloxane (PDMS). Le PDMS non réticulé est coulé sur un wafer portant le motif de canaux en relief positif, et solidifié en activant la réticulation dans une étuve à 70°C. Le motif en relief négatif

est ensuite refermé en scellant le bloc d'élastomère sur une lame de verre après activation des surfaces par un plasma d'oxygène.

La vitesse de croissance de *T. helicus* dans les deux types de motifs a été mesurée et comparée avec la vitesse d'extension radiale de colonies sur milieu solide: le confinement dans les puces semble affecter la vitesse de croissance du mycélium, qui est ralentie. La vitesse d'extension apicale des hyphes dans les micro-canaux du motif Ch50 était de 47 µm/h, alors que la vitesse d'extension radiale des colonies sur milieu MYEA (qui ne peut être supérieure à la vitesse d'extension apicale) est de 112 µm/h.
Plusieurs modèles de puces microfluidiques avec des méthodes de fabrication différentes ont été testés pour déterminer si ils conviennent à des observations en microscopie de fluorescence. Bien que le PDMS est un matériau transparent, il possède des propriétés d'autofluorescence susceptibles de gêner l'observation de marquages fluorescents du mycélium. Ce désavantage peut être pallié par le photoblanchiment préalable des puces par exposition aux UV. Cependant, une autre source de bruit de fond fluorescent est le BaP lui-même, qui diffuse dans le polymère lorsqu'il est déposé dans les chambres. D'autres techniques de fabrications ont donc été testées pour minimiser ou contourner ce problème. Des puces construites à l'aide d'adhésif double face entre deux lamelles de verre étaient celles qui présentaient les meilleures propriétés optiques, mais ne permettaient pas de fabriquer des réseaux de canaux avec une résolution suffisante. Une autre option était d'utiliser un "sticker" de PDMS très fin sur lequel est moulé le motif, scellé entre deux lames de verre, cependant la fabrication de ce type de puces était particulièrement fastidieuse et demanderait à être optimisée. Finalement, les puces de PDMS sur verre classiques ont été choisies pour le suivi de l'incorporation du BaP. En effet l'utilisation d'un microscope confocal à balayage laser permet d'éliminer en grande partie le fond fluorescent en sélectionnant une profondeur de champ très faible et en n'excitant que les fluorophores à la profondeur désirée.

Le dernier chapitre concerne l'incorporation du BaP dans des cellules vivantes de *T. helicus* et son suivi au cours du temps par microscopie de fluorescence. Ces observations reposent sur la fluorescence naturelle du BaP pour détecter sa localisation au sein des cellules et leur micro-environnement.

Une première série d'expériences a été réalisée avec du mycélium incubé avec du BaP en milieu liquide, et observé à différents temps après la mise en contact. Ces conditions de cultures permettent un contact direct entre les hyphes du champignon et les cristaux de BaP en suspension dans le milieu, avec une agitation permanente. Un marquage fluorescent des hyphes est visible après seulement 30 minutes de mise en contact, et augmente en intensité au cours du temps au moins jusqu'à 24h. La fluorescence du BaP est localisée dans des vésicules intracellulaires bien distinctes, en particulier au niveau des apex et à la périphérie des segments dans les hyphes septés. Des expériences de

co-marquage avec un marqueur fluorescent de lipides, le BODIPY 500/510 C_4, C_9 montrent une colocalisation de ces vésicules avec les corps lipidiques révélés par le BODIPY. Ces résultats confirment l'incorporation du BaP dans des organites de stockage des lipides déjà observé chez d'autres espèces fongiques ou micro-organismes proches (Verdin et al., 2005, Furuno et al., 2012, Fayeulle et al., 2014).

Des observations en time-lapse d'un pellet de mycélium en contact avec des paillettes de BaP ont été réalisées sur 24 h avec une prise d'image toutes les 10 minutes. Ces observations ne mettent pas en évidence de manière claire des sites d'incorporation préférentielle, mais plutôt un marquage simultané des hyphes, bien qu'hétérogène. Des vésicules marquées sont visibles à partir de 2 h de contact et présentent une fluorescence de plus en plus intense jusqu'à 7 h. Ces observations suggèrent un transport rapide du BaP le long des hyphes, pourtant les vésicules observées semblent statiques à l'échelle de temps et la fréquence d'acquisition choisies. Le transport du BaP pourrait emprunter un trafic vésiculaire intracellulaire via la diffusion dans les lipides membranaires, plutôt qu'une translocation des corps lipidiques plus volumineux. Cette hypothèse est appuyée par des résultats d'une simulation informatique de la traversée de la membrane plasmique par le BaP, réalisée avec le logiciel IMPALA. Cette simulation montre une stabilité maximale du BaP au niveau du feuillet central de la bicouche lipidique, où se trouvent les queues hydrophobes des phospholipides. La molécule est en revanche très instable dans la phase aqueuse et au niveau des têtes polaires, ce qui rend peu probable un transport par la phase aqueuse en l'absence d'agent de solubilisation.

Enfin, les puces microfluidiques portant le motif Ch50, développées dans le chapitre précédent, ont été utilisées pour mettre en place un environnement de culture compartimenté permettant le suivi de l'incorporation du BaP sur plus d'une semaine, à partir d'un état initial où il n'y a pas de contact entre l'inoculum et la source de polluant. Les systèmes ont été inoculés avec des explants de mycélium prélevés sur des cultures sur milieu solide, et du BaP a été injecté avec dans la chambre opposée à l'inoculum. Les observations en microscopie confocale révèlent un marquage diffus des hyphes, plus intense que le témoin sans BaP, après seulement 3 jours de culture et alors que le mycélium n'a pas encore atteint les cristaux de BaP déposés dans la chambre opposée. Ces résultats suggèrent une phase précoce d'incorporation sans que le contact avec la source ne soit nécessaire, qui devra être confirmée par des tests supplémentaires. De plus, le BaP est susceptible de se dissoudre et de diffuser à travers des phases organiques non aqueuses, et se comporte apparemment de manière similaire dans le réseau polymérique du PDMS. Cependant, la sécrétion de biosurfactants fongiques permettant un transport facilité par des micelles en phase aqueuse n'est pas à exclure. Si la production d'agents de mobilisation du BaP est confirmée, deux modes d'actions complémentaires sont possibles : d'une part un effet détergent favorisant la fragmentation des cristaux de BaP et leur détachement des surfaces solides, et d'autre part un effet stabilisant des petites particules de BaP en suspension dans

la phase aqueuse. Le rôle potentiel des tensioactifs fongiques dans la stabilisation de composés organiques hydrophobes en phase aqueuse, et leur entrée dans les cellules, reste à déterminer.

En ce sens, des recherches plus poussées sont nécessaires pour élucider l'implication de tels agents de mobilisation, et en particulier le rôle éventuel des tensioactifs mis en évidence dans le chapitre II. Les données actuelles dans la littérature suggèrent que le BaP se comporte de manière similaire aux lipides neutres dans les cellules fongiques, et sa mobilisation extracellulaire de même que les mécanismes d'incorporation sont vraisemblablement similaires pour d'autres substrats lipophiles. De plus, et bien que certaines souches soient capables d'utiliser le BaP comme seule source de carbone, la dégradation du BaP par les champignons non ligninolytiques est généralement considérée comme un co-métabolisme, remplissant une fonction de détoxification non spécifique. Plusieurs voies métaboliques intracellulaires et extracellulaires participent vraisemblablement à la biodégradation des HAP, et leur caractérisation chez *T. helicus* pourrait être réalisée plus précisément par l'identification des activités enzymatiques exprimées ainsi qu'une caractérisation des métabolites produits.

Un modèle de sol simplifié a été mis au point sous forme d'une puce microfluidique, visant ici à élucider des mécanismes biologiques fondamentaux. La perspective à plus long terme pour ce type de dispositif serait de développer un modèle versatile dans une perspective « soil-on-chip ». Le design présenté ici nécessite d'être optimisé et complexifié pour intégrer de nouveaux paramètres expérimentaux. Dans l'optique de mettre en place un outil permettant de mimer les paramètres d'un sol, la prédictibilité et la reproductibilité des résultats obtenus devra être validée en les comparant à ceux obtenus sur site. Différentes stratégies de biostimulation pourraient ainsi être testées de manière personnalisée pour la mise au point de protocoles de bioremédiation.

Table of contents

List of abbreviations

AcN	acetonitrile
AMF	arbuscular mycorrhizal fungi
ATP	adenosine triphosphate
BaP	benzo[*a*]pyrene
BHI	brain-heart infusion broth
BODIPY	5-butyl-4,4-difluoro-4-bora-3a,4a-diaza-*s*-indacene-3-nonanoic acid
BSA	bovine serum albumin
BTEX	benzene, toluene, ethylbenzene, xylene
C. g.	*Corynebacterium glutamicum*
CMC	critical micelle concentration
CMR	carcinogenic, mutagenic, reprotoxic
C/N	carbon/nitrogen ratio
DAPI	4’,6-diamidino-2-phenylindole
DDT	dichlorodiphenyltrichloroethane
DNS	dinitrosalicylic acid
DW	dry weight
DMSO	dimethysulfoxide
FID	flame ionization detection
FITC	fluorescein isothiocyanate
GC	gas chromatography
GRSP	glomalin-related soil protein
HC	bacterial suspension for hydrocarbon degradation
HIC	hydrophobic interaction chromatography
HMW	high molecular weight
HOC	hydrophobic organic compound
HPLC	high performance liquid chromatography
HPTLC	high-performance thin layer chromatography
LSCM	laser scanning confocal microscope
MATH	microbial adhesion to hydrocarbons
MEL	mannosylerythritol lipid
MM	mineral medium
MOPS	3-(*N*-morpholino)propanesulfonic acid
MPYC	malt, peptone, yeast extract and casamino-acid medium

MS	mass spectrometry
MYEA	malt yeast extract agar
NAD	nicotinamide adenine dinucleotide
NAPL	non-aqueous phase liquid
PDMS	polydimethylsiloxane
PAH	polycyclic aromatic hydrocarbon
PCB	polychlorobiphenyl
POP	persistent organic pollutant
PTFE	polytetrafluoroethylene
Rf	retention factor
ROS	reactive oxygen species
SDS-PAGE	sodium dodecyl sulfate – polyacrylamide gel electrophoresis
SEC	size-exclusion chromatography
SL	sophorolipid
T. h.	*Talaromyces helicus*
TLC	thin-layer chromatography
TNT	trinitrotoluene
TSA	tryptone-soy agar
Tw20	Tween 20 (polysorbate 20)

List of figures

List of tables

Introduction générale

La désindustrialisation progressive de l'Europe dans la deuxième moitié du XXème siècle, au profit de l'essor du secteur tertiaire, a laissé de nombreuses friches industrielles à l'abandon. Actuellement en Europe persistent des pollutions anciennes liées aux deux révolutions industrielles, en particulier des métaux lourds et hydrocarbures. La délocalisation des industries lourdes, manufacturières et du traitement des déchets des pays occidentaux vers les territoires du Sud global, s'accompagne d'une délocalisation des pollutions sans pour autant faire disparaître leur origine. Même lorsque certains composés préoccupants cessent localement d'être utilisés suite à des mesures légales (le DDT aux Etats Unis ou le chlordécone aux Antilles en sont des exemples), les contaminations peuvent persister pendant des décennies et affecter plusieurs générations. Parallèlement, la production de nouveaux produits de spécialité à haute valeur ajoutée a entraîné l'apparition d'une grande variété de polluants organiques émergents dont notamment des produits phytosanitaires, cosmétiques et pharmaceutiques. L'exposition de la population aux diverses sources de pollutions est ainsi très inégalement répartie, non seulement à l'échelle internationale mais également à l'échelle d'un même territoire où elle recoupe souvent des inégalités socio-économiques.

Un site pollué se définit comme un espace délimité présentant une contamination par des composés toxiques posant un risque sanitaire ou environnemental. Cette toxicité peut affecter l'être humain (risque pour la santé) ou l'écosystème (notamment une dégradation des fonctions biologiques du sol et des milieux aquatiques). L'Agence Européenne de l'Environnement estimait en 2011 le nombre de sites potentiellement pollués à 2,5 millions en Europe (pour 33 pays dont les 28 Etats de l'Union Européenne, la Suisse, le Liechtenstein, la Norvège, l'Islande et la Turquie) (EEA, 2019). Les principales sources de pollution des sols sont les activités industrielles ainsi que le traitement de déchets. En France, 7256 sites pollués ou potentiellement pollués sont recensés en janvier 2020 par la base de données en ligne BASOL. 12% de ces sites présentent une pollution aux hydrocarbures, et 5,5 % une contamination par des hydrocarbures aromatiques polycycliques. Cette base de données se concentre sur des pollutions localisées provenant d'activités industrielles passées, mais pas les sites industriels et décharges en activité. Les pollutions diffuses telles que celles dues à l'agriculture ou aux retombées dues au trafic automobile sont quant à elles impossibles à quantifier en termes de nombre de sites affectés, mais peuvent être évaluées par des mesures de contamination des eaux, des sols et de l'air.

La gestion des sites pollués et les mesures éventuelles de remédiation sont un enjeu économique et de santé publique. La nécessité de dépolluer se pose en particulier lorsque la réhabilitation d'un site

est envisagée, dans le but d'en faire un nouvel usage commercial ou résidentiel par exemple. Le but d'un processus de réhabilitation est donc rarement de restaurer l'état initial du sol tel qu'il existait avant la pollution, mais de le rendre sûr et fonctionnel pour une utilisation donnée. La réutilisation de sols dépollués comme remblai ou support de cultures non alimentaires est une forme de recyclage, évitant d'excaver des sols sains et fertiles. En effet, les sols sont une ressource non renouvelable, menacée par l'érosion, l'étalement urbain et une artificialisation croissante.

Différentes techniques de remédiation peuvent être mises en œuvre selon le type de pollution, les critères de qualité à atteindre, les contraintes techniques et économiques. Les techniques de désorption thermique ou d'oxydation chimique nécessitent le plus souvent une excavation coûteuse du sol, et altèrent sa structure et les propriétés physico-chimiques. L'élimination des polluants par ventilation ou lavage en revanche peut être mise en place in situ et est moins destructrice. Enfin, la bioremédiation consiste à utiliser des organismes vivants - le plus souvent des plantes, bactéries ou champignons pour diminuer le risque environnemental associé à une pollution, et est réputée avoir un moindre impact environnemental en conservant l'intégrité du sol traité. L'introduction de micro-organismes ou plantes exogènes doit pourtant être considérée avec précaution puisqu'elle peut impliquer des risques pour l'équilibre de la flore microbienne autochtone, ou pour la santé humaine et animale s'il s'agit de potentiels pathogènes. L'efficacité d'un procédé de bioremédiation suppose que les organismes vivants utilisés puissent avoir accès aux polluants et les mobiliser. Les polluants organiques persistants (POP) se caractérisent par leur faible biodégradabilité, leur capacité à être transportés sur de longues distance par voie aérienne ou aquatique et par un risque important de bio-accumulation dans la chaîne alimentaire. Ils sont préoccupants du fait de leurs effets sur la santé, en particulier la toxicité chronique (perturbations endocriniennes, cancérogénicité, mutagénicité, reprotoxicité). Sur des sites présentant des contaminations anciennes, les métaux et composés organiques hydrophobes tendent à s'adsorber fortement sur la matière organique ou à la surface des particules, dans des porosités très fines difficilement accessibles. La faible biodisponibilité des polluants signifie une moindre exposition des organismes vivant sur le site, et un moindre risque de lixiviation (d'autant plus si ce sont des composés peu solubles dans l'eau), mais est également un frein à leur remédiation.

La morphologie filamenteuse des champignons leur permet d'explorer d'importants volumes de sol, et la grande diversité de leurs outils enzymatiques permet de métaboliser un large panel de composés organiques, y compris certains des plus récalcitrants à la dégradation. De plus, certaines souches isolées de sols pollués ont ainsi une résistance à des pollutions multiples et des capacités de biodégradation particulièrement intéressantes. C'est le cas du champignon filamenteux *Talaromyces helicus* qui est le modèle d'étude de cette thèse. Il s'agit d'une espèce d'ascomycète du sol dont le

potentiel pour la bioremédiation a été identifié relativement récemment, dans un contexte où les capacités de biodégradation des champignons non ligninolytiques vis-à-vis de polluants organiques aromatiques suscitent un intérêt croissant.

Les mécanismes de mobilisation des polluants organiques hydrophobes dans un milieu poreux et insaturé en eau tel quel le sol sont mal connus. Ainsi, le rôle d'agents de mobilisation extracellulaires pour l'émulsification d'hydrocarbures est étudié en milieu liquide, mais rarement dans les sols. L'influence des champignons sur la biodisponibilité des polluants passe aussi par des transformations chimiques : ainsi la production de métabolites plus polaires et donc plus mobiles en phase aqueuse à partir de contaminants hydrophobes augmente leur biodisponibilité. Si la minéralisation n'est pas complète, il est important de déterminer si ces métabolites sont plus facilement biodégradables pour d'autres micro-organismes ou au contraire toxiques. Plusieurs voies de métabolisation des hydrocarbures aromatiques sont identifiées chez les champignons, dont certaines impliquent des enzymes extracellulaires (laccases, manganèse peroxydases et lignine peroxydases) et d'autres intracellulaires (cytochrome P450). Certains champignons sont ainsi capables d'incorporer des polluants et de les métaboliser à l'intérieur des cellules, cependant le lien entre incorporation et dégradation n'est pas systématique: ainsi une incorporation efficace ne signifie pas forcément une dégradation efficace. D'autre part, l'existence de plusieurs voies de dégradation implique que l'incorporation n'est pas toujours nécessaire à la biodégradation.

Ce projet de thèse vise à examiner différents aspects de la bioremédiation fongique des HAP selon trois grands axes : mobilisation, incorporation, biodégradation. Cette étude se concentre sur les interactions entre le polluant, le champignon, et l'environnement à travers l'exemple de la mobilisation du benzo[*a*]pyrène, un composé CMR bien étudié comme modèle de polluant hydrophobe, par *Talaromyces helicus*, un champignon du sol récemment identifié comme présentant un intérêt pour la dépollution de contaminations multiples.

Par une meilleure compréhension des mécanismes d'accès à des polluants peu biodisponibles, et le lien entre incorporation et dégradation, l'enjeu est de développer des protocoles de bioremédiation plus efficaces. La prédictibilité des résultats en fonction des caractéristiques du site à traiter est en effet un verrou en matière de bioremédiation, ainsi il est important de disposer d'outils expérimentaux adaptés pour identifier des stratégies de biostimulation pertinentes au cas par cas. Plusieurs modèles expérimentaux sont ainsi utilisés. Dans un premier temps, des tests en cultures liquides ont été réalisés afin de quantifier la biodégradation dans des conditions contrôlées. Les microcosmes de sol sont aussi une approche classique pour l'étude de la bioremédiation de pollutions, qui permettent d'évaluer les capacités de la souche dans un milieu plus proche d'un site réel, et de tester des paramètres de

biostimulation. Enfin, un environnement modèle compartimenté a été mis en place sous la forme d'une puce microfluidique, dans le but de développer un milieu poreux modèle transparent et adaptable pour étudier à une micro-échelle la mobilisation et l'incorporation de polluants par un organisme non motile.

General introduction

Over the second half of the 20th century, gradual deindustrialization in Europe, in favor of the rising service industry, left behind a number of abandoned brownfields. Currently, historical pollutions resulting from both industrial revolutions persist in Europe, especially heavy metal and hydrocarbon pollutions. The relocation of heavy industries, manufacturing, and waste treatment from western countries to the global South is accompanied by a relocation of pollution sources, without eliminating them. Even when some concerning compounds locally stop being used after regulatory measures are taken (DDT in the US or chlordecone in the Caribbean being examples), contaminations can persist for decades and affect several generations. Meanwhile, the production of new high-value specialty products caused the rise of a wide variety of emerging organic pollutants, including phytosanitary products, cosmetics and pharmaceuticals among others. The exposition of populations to various sources of pollution is thus unevenly distributed, not only at the international scale but also at the scale of one territory where it often intersects with social and economical inequalities.

A polluted site is defined as a delineated area contaminated with toxic compounds which pose an environmental or health hazard. This toxicity can affect humans (health hazards) or the ecosystem (in particular, through a deterioration of biological functions in soils or aquatic habitats). In 2011, the European Environment Agency evaluated the number of potentially contaminated sites to be about 2,5 millions in Europe (for 33 countries including the 28 EU states, Switzerland, Liechtenstein, Norway, Iceland and Turkey) (EEA 2019). The main sources of soil pollution are industrial activities and waste treatment. In France, 7256 polluted of potentially polluted sites are listed on the online database BASOL as of January 2020. 12% of these sites are contaminated with hydrocarbons, and 5,5 % with polycyclic aromatic hydrocarbons. This database focuses on localized pollutions originating from past industrial activities, but not currently active industrial sites and landfills. Diffuse pollutions such as those generated by agriculture or car traffic are impossible to quantify in terms of number of affected sites, but they can be assessed by contamination level measurements in soils, water, and air.

Contaminated site management and the potential remediation measures are thus an economical and public health issue. The need for depollution especially arises when site rehabilitation is considered, in the aim of making a new commercial or residential use of it for example. Rehabilitation processes therefore rarely aim at restoring the initial state of the soil as it existed before contamination, but rather at rendering it safe and functional for a given use. Re-using a soil after treatment as fill material or substrate for non-edible crops is a form of recycling, avoiding the

excavation of healthy and fertile soil. Indeed, soil is a non-renewable resource, threatened by erosion, urban sprawl and increasing artificialization.

Several remediation techniques can be implemented depending on the type of contamination, quality requirements to be met, and technical and economical constraints. Thermal desorption or chemical oxidation techniques most often require a costly excavation of the soil to be treated, and alter its structural and physico-chemical properties. Pollutant removal through venting, washing in contrast can be used *in situ* and are typically less destructive. Finally, bioremediation consists in the use of living organisms – most often plants, bacteria or fungi – to reduce environmental risks associated with a pollution. It is generally regarded as having a lower environmental impact and preserving the soil integrity. Introducing exogenous microorganisms and plants however should be considered carefully, as it can potentially destabilize the equilibrium of the autochthonous flora, or threaten human and animal health if pathogens are used.

Bioremediation efficiency requires for the organisms used to have access to the pollutants and mobilize them. Persistent organic pollutants (POP) are characterized by their low biodegradability, their susceptibility to be transported over long distances by air or water, and by an important risk of bioaccumulation in food chains. POP are particularly concerning due to their health effects, especially their chronic toxicity (endocrine disruption, carcinogenicity, mutagenicity, reprotoxicity). On sites with aged contaminations, metallic elements and hydrophobic organic compounds tend to be strongly sorbed to organic matter or solid particles, and in hardly accessible fine porosities. The low bioavailability of such pollutants implies a lesser exposition of nearby living organisms, and a lesser risk of leaching (especially in the case of compounds which have a low water solubility), but it is also a limitation to their remediation.

The filamentous morphology of fungi enables them to explore large volumes of soil, and the diversity of their enzymatic tools allow the metabolization of a wide variety of organic compounds including some that are recalcitrant to biodegradation. Moreover, some strains isolated from polluted soils are resistant to multiple contaminations and particularly interesting biodegradation potential. This is the case of the filamentous fungus *Talaromyces helicus*, which is the working model of the present study. *T. helicus* is a soil ascomycete of which the potential for bioremediation was identified fairly recently, in a context where the abilities of non-lignolytic fungi for aromatic organic pollutant biodegradation are subjected to a growing interest.

The mobilization mechanisms of hydrophobic organic pollutants in a porous and water-unsaturated medium such as the soil are poorly known. Thus, the role of extracellular biosurfactants for the emulsification of hydrocarbons was studied in liquid media, but rarely in soil. The influence of

fungi on pollutant bioavailability is also related to their chemical alteration : indeed, the bioavailability of hydrophobic contaminants can be increased through their conversion into metabolites that are more polar and therefore more mobile in water. If mineralization is not completed, it is important to determine whether these metabolites are more easily biodegradable for other microorganisms, or on the contrary more toxic. Several metabolic routes for the degradation of aromatic hydrocarbons have been identified in fungi, including some involving extracellular enzymes (laccases, manganese-peroxidases, lignin peroxidases) and others intracellular enzymes (P450 cytochrome). Some fungi are able to internalize contaminants and metabolize them inside of their cells, however the relationship between uptake and biodegradation is not mandatory : thus, efficient uptake does not necessarily imply an efficient degradation. Besides, the coexistence of several biodegradation pathways means that uptake is not always necessary for biodegradation.

The present project aims at examining several aspects of fungal bioremediation of polycyclic aromatic hydrocarbons, following three main axes : mobilization, uptake ad biodegradation. This study focuses on the interactions between the pollutant, fungus and the environment through the example of benzo[*a*]pyrene (BaP) mobilization by *Talaromyces helicus*. BaP is a carcinogenic, mutagenic and reprotoxic compound well-studied as a model hydrophobic pollutant, while *T. helicus* in a soil fungus recently identified as holding potential for the remediation of multiple contaminations.

A better understanding of mechanisms involved in the access to low-bioavailability pollutants, and of the relationships between uptake and degradation, would be a useful insight for developing more efficient bioremediation protocols. Result predictability depending on each site's characteristics is a limitation in the field of bioremediation, and having adapted experimental tools is important to identify relevant biostimulation strategies on a case-by-case basis. Therefore, several experimental set-ups were used. As a first step, tests in liquid cultures were carried out to quantify BaP degradation in controlled conditions. Soil microcosms are also a classical approach for the study of pollution remediation, which allow the evaluation of the strain's performance in conditions closer to a real site, and the testing of biostimulation parameters. Finally, a compartmentalized model environment was set up in the form of a microfluidic chip, the goal being to develop a transparent, adaptable model of porous medium to study pollutant mobilization and uptake by a non-motile organism at the microscale.

Literature Review: Fungal influence on hydrophobic organic pollutant dynamics within the soil matrices

An edited version of this literature review was published as: Baranger C., I. Pezron, A. Le Goff, A. Fayeulle (2020). Fungal influence on hydrophobic organic pollutants dynamics within the soil matrices. In: V. Kumar [ed.]. Rhizomicrobiome Dynamics in Bioremediation, CRC Press (in press) - reprinted here with the editor's authorization

1. Introduction: hydrophobic pollutants in soils

Organic pollutants found in soils include linear, branched and cyclic alkanes, aromatic hydrocarbons including the BTEX family (benzene, toluene, ethylbenzene, xylene) and polycyclic aromatic hydrocarbons, halogenated hydrocarbons, and other synthetic molecules including pesticides, dyes, drugs, etc. Many display low solubility in water and higher affinity for organic phases: their hydrophobicity depends on the length of carbon chains, molecular weight and type of functional groups. Long term exposure to environmental contaminants, even when present in low amounts, is preoccupying due to carcinogenic, mutagenic, reprotoxic (CMR), or endocrine disrupting effects. Some of these hydrophobic organic compounds (HOC) are considered as persistent organic pollutants (POP), which are a class of environmental contaminants defined by their hazardous nature and their low degradability, causing a high bioaccumulation potential and possible transport over long distances (Ritter et al., 1995). Many persistent contaminants contain one or more aromatic rings, which impart their high chemical stability.

Anthropogenic sources of pollution with organic compounds are diverse. Hydrocarbons occur naturally in crude oil, natural gas and coal tar, which are mainly composed of alkanes of various chain lengths, and contain aromatic molecules such as biphenyls, BTEX and PAH in varying proportions. As a result they are found in sites contaminated by oil spills or any petroleum derivatives. PAHs are also unintentionally synthesized and released during the combustion of organic matter or fossil fuels at high temperatures, in industrial furnaces, car engines, or domestic waste incinerators. In this case they are found as particles disseminated through the air and water, rather than associated to other hydrocarbons in a non-aqueous phase liquid (NAPL). Agriculture is an important source of contamination with xenobiotics as well, especially halogenated compounds: pesticides are intentionally spread on crop fields on a large scale and can persist in agricultural soils for decades, leaching into surface and groundwater, while drugs for animal farming are found as contaminants in wastewater. Synthetic dyes and pigments from the textile industry, and chlorinated aromatics released as by-products of pulp and paper bleaching are other examples of significant organic pollutants.

Soil contaminants are subjected to a combination of chemical, physical and biological processes affecting their natural attenuation, persistence or transfer between different compartments. Volatile and relatively water-soluble compounds tend to have lower retention times in the soil since they either volatilize or leach into ground waters, potentially leading to an expansion of the contaminated area (Ortega-Calvo et al., 2013). Chemical or biological degradation of organic contaminants lowers the contamination levels by altering their chemical structure. This can lead to the release of metabolites with varying degrees of toxicity and bioavailability, or even to complete mineralization. As natural attenuation occurs, non-volatile hydrophobic pollutants with a high chemical stability tend to persist in soils in higher ratios than other compounds more easily removed through chemical or biological processes. As a result, the remaining fraction in aged contaminated soils is the least bioavailable (Ortega-Calvo et al., 2013).

The bioavailable fraction of a compound in the soil can be defined as the fraction immediately available for assimilation by living organisms (Semple et al., 2004). In environmental science this concept is used to refer to nutrient uptake by plants, and was extended to interactions between environmental contaminants and organisms. The term is used in toxicology to describe the fraction of a drug able to reach systemic circulation in animals. A given compound can be divided between several soil compartments: in solution, adsorbed or complexed with minerals or organic matter, as part of the minerals themselves. Bioavailability depends on both soil properties and the ability of a given organism to mobilize the molecule of interest. Bioaccessibility is a concept closely related to bioavailability; Semple et al. (2004) propose in the same work a definition of the bioaccessible fraction broader than the bioavailable fraction, as it includes what is potentially bioavailable but may only become so on a longer time scale (from days to years) or after physical or chemical alteration occurs. HOC typically associate with solid mineral particles, especially clays that display hydrophobic surfaces, or dead organic matter. Association with soil components is driven by adsorption - immobilization by reversible binding onto a surface – and absorption - immobilization by diffusion into a solid phase.

The aim of remediation is to lower the risk associated to a polluted site as much as possible, and restore a sufficient functionality for its intended use (agriculture, housing, natural area, commercial buildings, etc). This can be achieved by removal of the contaminant, transformation into harmless compounds, and/or stabilization into a non-bioavailable form. Chemical (oxidation, reduction, solvent or tension-active assisted extraction) and physical (venting, sparging, combustion, thermal or electric desorption) treatments are the most widely used to this date. Bioremediation is usually considered a more environmentally friendly approach to pollutant removal, although the longer time needed for soil rehabilitation is a drawback. When they can be implemented *in situ* without excavation, bioremediation techniques preserve the functional and structural integrity of the soil. In contrast,

physicochemical treatments can be too expensive or poorly adapted to some cases (Chen et al., 2015). In addition to the technical and financial advantages of bioremediation, these techniques receive a relatively good acceptance from the public. Khalid et al. (2017) reported a high acceptance of phytoremediation techniques for the removal of heavy metals, including microbe-assisted phytoextraction. However, opinions in regard to the open-field use of genetically modified micro-organisms appear to be mixed, as showed by a survey conducted in New Zealand about bacterial remediation of the organochloride DDT (Hunt et al., 2003). The release of genetically engineered organisms in the wild raises safety concerns, and is subject to prior authorization in some parts of the world, including the European Union (Directive 2001/18/EC of the European Parliament). As result, most research nowadays focuses on the use of naturally occurring strains, often isolated from contaminated areas.

Research on the potential of fungi for environmental remediation dates back to the 1950's with a study about wastewater cleanup by aquatic fungi (Harvey, 1952). Less than two decades later, as concern started to emerge about environmental consequences of the intensification of agricultural practices, the first studies on atrazine degradation by soil ascomycetous fungi were conducted (Kaufman and Blake, 1970). Ligninolytic fungi or "white rots" have been extensively studied for the biodegradation of aromatic pollutants, as they express extracellular enzymatic machinery able to non-specifically degrade a wide range a compounds with a similar structure to lignin. Non-ligninolytic soil fungi have drawn interest more recently, especially native strains isolated from contaminated soil and sediment. Fungi are abundant in the soil, making up for 50 to 1000 µg/g dry weight of soil, and developing networks in the order of 10 km hyphae per gram (Osono et al., 2003; Ritz and Young, 2004). They play a key role in terrestrial ecosystems, both as a structural component of the soil and through their interactions with other organisms (Ritz and Young, 2004). Filamentous fungi are non-motile organisms which colonize their environment through hyphal growth, thereby forming a mycelial network in 3 dimensions. The filamentous form allows them to grow in confined environments and colonize porous solid matrices, either in the soil or in plant tissues. This morphology is adapted to their heterotrophic mode of nutrition, enabling the fungus to efficiently scout large volumes of soil for heterogeneously distributed nutrients, and develop a high exchange surface.

Fungi affect soil structure and chemistry by breaking down organic matter, modulating surface properties and promoting particle aggregation. As a consequence, the fungal flora could greatly affect pollutant retention and alteration in soils, both directly (through biosorption and biotransformation) and indirectly (by modifying the soil matrix properties). Bioavailability of the pollutants is both a limitation to bioremediation efficiency, and a potential source of environmental risk, as mobile pollutants are more susceptible to diffusing to nearby areas and/or leaching into ground waters

(Ortega-Calvo 2013). In this regard, understanding the mechanisms underlying pollutant dynamics in the soil is key to a better assessment of environmental risk and improvement of remediation strategies. This chapter will discuss how fungi - either native strains or added for bioaugmentation purposes - affect pollutant stability and mobility in soils.

2. Fungal influence on soil hydrophobicity and pollutant retention

Fungi produce several types of surface active molecules, which play essential functions in their lifestyle and morphogenesis. These compounds modulate both their own cell surface properties and surface properties of their immediate environment, enabling the fungus to cross air/water interfaces, adhere to solid surfaces, and interact with organic substrates such as lignin and oils.

2.1. Extracellular fungal proteins modulating soil hydrophobicity

Filamentous fungi are known to produce extracellular surface-active proteins called hydrophobins that regulate fungal interactions with surfaces and air-water interfaces. Hydrophobins are a family of small cystein-rich proteins (< 15 kDa) displaying both a hydrophilic and a hydrophobic domain, explaining their surfactant properties. By self-assembling into amphiphilic layers at hydrophilic/hydrophobic interfaces, they lower interfacial tension and allow fungal hyphae to break through air/water interfaces as well as attach to hydrophobic substrates (Wösten et al., 1999). Hydrophobins are divided in two classes with differing structures and displaying various biological functions (Table 0.1). Class I hydrophobins, defined after the CS3 hydrophobin from *Schizophyllum commune,* form insoluble and extremely stable rodlets. Class II hydrophobins like HFBI and HFBII from *Trichoderma reesei* self-assemble at interfaces into monolayers (Szilvay et al., 2007; Linder, 2009). Hydrophobins are the most potent surfactant proteins known to this day (Wösten, 2001; Berger and Sallada, 2019): class II hydrophobins from *T. reesei* are able to lower the surface tension in water phases to up to 25 $mN.m^{-1}$, and are active at concentrations in the order of 0,1 $\mu mol.L^{-1}$ (Cox et al., 2007). They have also been shown to stabilize oil-in-water emulsions and foams (Lumsdon et al., 2005; Tchuenbou-Magaia et al., 2009; Lohrasbi-Nejad et al., 2016).

These modulations of surface properties in the microenvironment of fungi are closely linked to the fungal lifestyle: they are adapted to their heterogeneous habitat, solid porous substrates partially filled with aqueous phases. Hydrophobins help to retain moisture in cell walls and impart water-repellant properties to the mycelium by forming a coat at the surface of hyphae, allowing it to grow into the air and form aerial reproductive structures (Talbot, 1997). Indeed, the formation of aerial mycelium is impaired in hydrophobin-deficient strains of the basidiomycete *S. commune* (Wösten et al., 1999). Hydrophobins are also involved in the formation of mycorrhizae by mediating hyphal attachment to

the plant host cells (Mankel et al., 2002), and form a protective layer on fungal spores, playing a role in spore dispersal and attachment (Zhang et al., 2011).

Table 0.1 : Diversity of hydrophobins in filamentous fungi and their identified properties

Function/property	protein	species	reference
Surface hydrophobicity of conidia	Hyd1, Hyd2 (class I)	*Beauveria bassiana*	Zhang et al., 2011
	HCf-1, HCf-2, HCf-3, HCf-4 (class I) HCf-5 and HCf-6 (class II)	*Cladosporium fulvum*	Lacroix and Spanu, 2009
	Ccg2	*Neurospora crassa*	Bell-Pedersen et al., 1992
	Hyd1, Hyd2, Hyd3 (class I) Hyd4, Hyd5 (Class II)	*Fusarium verticilloides*	Fuchs et al., 2004
	RodA, DewA-E (class 1)	*Aspergillus nidulans*	Grünbacher et al., 2014
Cell wall of vegetative aerial hyphae and fruiting body		*Mucor mucedo* *Phanerochaete chrysosporium* *Penicillium chrysogenum* *Coprinus cinereus* *Schizophyllum commune*	de Vries et al., 1993
	POH1 (fruiting body) POH2, POH3 (vegetative)	*Pleurotus ostreatus*	Ásgeirsdóttir et al., 1998; de Vries et al., 1993
	Class I: ABH1 (fruiting body), ABH3 (vegetative)	*Agaricus bisporus*	Lugones et al., 1996, 1998
Interaction with plant host - pathogenesis	cerato-ulmin (class II)	*Ceratocystis ulmi*	Zhang et al., 2018
	MPG1 (class I)	*Magnaporthe grisea*	Talbot et al., 1996
Interaction with plant host - mycorrhizae	Hyd1 (class I)	*Tricholoma terreum*	Mankel et al., 2002
Stabilization of oil-in-water emulsions and foams	HFBI, HFBII (class II)	*Trichoderma reesei*	Cox et al., 2007 Lohrasbi-Nejad et al., 2016
	Class I and II	*Acremonium sclerotigenum* *Penicillium roseopurpureum* *And other marine fungi*	Cicatiello et al., 2016
Solubilization of hydrophobic compounds	SC3 (class I)	*Schizophyllum commune*	Haas Jimoh Akanbi et al., 2010
	unknown	*Aspergillus brasiliensis*	Sánchez-Vázquez et al., 2018

By coating the surface of soil particles, thereby reversing their hydrophobic or hydrophilic properties, hydrophobins could significantly impact the water flow through pores and the overall wettability of soil matrices (Rillig, 2005; Rillig et al., 2007). Hydrophobins self-assemble into membranes at oil/water interfaces as well (Zhang et al., 2018). They are likely to behave in a similar way at liquid/liquid

interfaces between soil water and NAPLs containing hydrocarbons, possibly enabling hyphae to penetrate NAPLs and promoting the access to hydrophobic contaminants.

Glomalin is a glycoprotein found abundantly in soils, produced by arbuscular mycorrhizal fungi of the Glomerales family. It was first identified as a soil protein fraction referred to as glomalin-related soil protein (GRSP), which likely includes a mix of extracellular fungal proteins (Rillig, 2004; Gadkar and Rillig, 2006). Glomalin itself is thought to be a protein component of the cell wall in arbuscular mycorrhizal fungi that persists in the soil after hyphal death and degradation (Driver et al., 2005). GRSP is known to promote the aggregation of soil particles, affecting soil hydrophobicity and texture. In relation to its role as a structural soil component displaying binding properties, GRSP has been linked to the retention of heavy metals in soils (González-Chávez et al., 2004). Chen et al. (2018) showed that added GRSP in a soil enhances the accumulation of PAHs in ryegrass plants. The authors attributed the increased sorption to plant roots in part to a higher PAH sorbed fraction at the root surface, suggesting that glomalin may act as a "glue" between the pollutant and the root cell wall. Another study demonstrated that the addition of GRSP in a phenanthrene-spiked soil could increase the extractible fraction of phenanthrene in n-butanol (Gao et al., 2017). These results indicate the ability of dissolved GRSP to mobilize PAH and facilitate its transfer to other organisms. In a similar way, cell-wall bound glomalin could mediate the sorption of HOC to the surface of living hyphae.

2.2. Fungal surfactants and emulsifiers enhance pollutant partition into aqueous phases

Hydrophobins and similar fungal proteins can affect the bioavailability of hydrophobic contaminants in the soil by promoting their dispersion in the aqueous phase. Indeed, a partial solubilization of hydrophobic drugs and increase of their bioavailability has been achieved using the SC3 hydrophobin from the basidiomycete *Schizophyllum commune* (Haas Jimoh Akanbi et al., 2010), and possible hydrophobin-like proteins able to solubilized PAH have been found in *Aspergillus brasiliensis* (Sánchez-Vázquez et al., 2018). Due to these versatile surface-active properties, hydrophobins have been proposed as a tool for oil recovery (Blesic et al., 2018)

In addition to hydrophobins, fungi produce a wide range of biosurfactants and emulsifiers with diverse chemical natures (Table 0.1). Although both categories overlap to some extent, surfactants are molecules able to lower interfacial tension between water and air or organic phases, while emulsifiers are defined by the ability to stabilize oil-in-water emulsions. Most of these molecules or molecular complexes can be classified in three broad categories: glycoproteins/glycopeptides, lipoproteins/lipopeptides, and glycolipids. Biosurfactants from fungi, and especially yeast and yeast-like strains, have been known for decades, yet until recently little information was available about biosurfactants from filamentous fungi (Bhardwaj, 2013). However, as the demand for bio-sourced and

biodegradable compounds in general increased over the last 10 years, microbial surfactants became a growing field of research.

Based on the overview presented in table 0.2, glycolipids appear to be the most widespread among fungal surfactants and emulsifiers. The high molecular weight glycoprotein liposan from *Candida lipolytica* (Cirigliano and Carman, 1985), sophorolipids from *Starmerella (Candida) bombicola* (Cooper and Paddock, 1984), and ustilagic acid, a cellobiose lipid from the zygomycete *Ustilago maydis* (Frautz et al., 1986), were the first main biosurfactants characterized in fungi. Mannosylerythritol lipids (MEL) produced by several smut fungi (Arutchelvi et al., 2008) and polyol lipids found in *Aureobasidium pullulans* and oleaginous yeasts of the *Rhodotorula* genus (Garay et al., 2018) are two other more recently identified classes of fungal surfactants. Several functions have been proposed for these extracellular surfactants: in a similar way to hydrophobins, they are likely involved in regulating the interaction of hyphae with surfaces. Polyol lipids and sophorolipids in particular may favor fungal growth on plant tissues by assisting the breakdown of cuticular wax. In addition, other functions have been identified: the mobilization of hydrophobic substrates, and defense against competing microorganisms through antibacterial or antifungal properties (Puchkov et al., 2002; Arutchelvi et al., 2008; Garay et al., 2018). Some appear to be produced constitutively, while others are induced by cultivation in presence of oil, and may be derivatives of lipid catabolism.

The potential industrial applications of biosurfactants was the main driver for research rather than the understanding of fungal physiology and ecology, hence the limited knowledge of their biological function in nature. Interestingly, many surfactant-producing fungal strains were identified as such while investigating their potential for the remediation of hydrocarbons and other hydrophobic soil contaminants (Batista et al., 2010; de Luna et al., 2015; Azin et al., 2018; Zadeh et al., 2018; do Amaral Marques et al., 2019; Pele et al., 2019), including PAH (Deziel et al., 1996; Nikiforova et al., 2009; Deng et al., 2010; Veignie et al., 2012). Rafin et al. showed an increase in Benzo[*a*]pyrene (BaP) concentration over time in fungal culture filtrates, suggesting the production of extracellular mobilizing agents able to partially stabilize BaP in the water phase (Rafin et al., 2013; Fayeulle et al., 2019). There is also evidence of emulsification of aliphatic and aromatic hydrocarbons by *Penicillium citrinum* (Camargo-de-Morais et al., 2003). Complexation agents are also produced by some strains known for biodegradation of hydrocarbons such as *Fusarium solani* (Veignie et al., 2012).

Remediation enhancement in presence of surfactant is likely driven by two main mechanisms involving (i) solubilization and transport of organic compound into micelles, and ii) displacement of entrapped NAPLs due to interfacial tension reduction (Paria, 2008). Indeed, when in presence of surfactant, the fraction of HOC found in micellar form is directly available for degrading bacteria , in a similar way to

Table 0.2 : Fungal strains identified as sources of extracellular biosurfactants or bioemulsifiers, and chemical nature thereof (when characterized).

		Species	Biosurfactants/bioemulsifier	references
Zygomycetes	Mucorales	*Cunninghamella echinulata*	glycolipoprotein	Andrade Silva et al., 2014
		Mucor circinelloides	lipopeptid glycolipid	do Amaral Marques et al., 2019 Zadeh et al., 2018
		Mucor indicus	glycolipid	Oje et al., 2016
		Rhizopus arrhizus	glycoprotein	Pele et al., 2019
		Cunninghamella echinulata	glycolipoprotein	Andrade Silva et al., 2014
Ascomycetes	Saccharomycetales " budding yeasts"	*Candida glabrata*	unknown	de Luna et al., 2009
		Candida tropicalis	unknown	Batista et al., 2010
		Dipodascus (Candida) ingens	(fatty acids)	Amézcua-Vega et al., 2007
		Kluyveromyces lactis (Candida sphaerica)	unknown	de Luna et al., 2015
		Kluyveromyces marxianus	mannoprotein	Lukondeh et al., 2003
		Lachancea thermotolerans	sophorolipid	Mousavi et al., 2015
		Nakazawaea (Candida) ishiwadae	monoglycerides	Thanomsub et al., 2004
		Saccharomyces cerevisiae	parietal mannoprotein	Cameron et al., 1988
		Starmerella (Candida) bombicola	sophorolipid	Cooper and Paddock, 1984
		Wickerhamomyces anomalus	glycolipid	Texeira Souza et al., 2017
		Wickerhamiella domercqiae	sophorolipid	Ma et al., 2014
		Yarrowia (Candida) lipolytica	high molecular weight glycoprotein "Liposan"	Cirigliano and Carman, 1985
	Filamentous ascomycetes	*Fusarium fujikuroi*	(trehalolipid)	Loureiro dos Reis et al., 2018
		Fusarium neocosmosporiellum	unknown	Azin et al., 2018
		Fusarium proliferatum	fatty amide	Bhardwaj et al., 2015
		Fusarium solani	carbohydrate	Veignie et al., 2012
		Fusarium sp.	unknown	Sena et al., 2018
		Phialemonium sp.	unknown	Guimarães Martins et al., 2006

		Penicillium chrysogenum	lipopeptide	Gautam et al., 2014
		Penicillium citrinum	lipopolysaccharide	Camargo-de-Morais et al., 2003
		Penicillium sp.	Lipids, carbohydrates, protein	Luna-Velasco et al., 2007
		Penicillium sp.	unknown	Sena et al., 2018
		Aspergillus flavus	phenyl glycoside	Ishaq et al., 2015
		Aspergillus fumigatus	unknown	Guimarães Martins et al., 2006
		Aspergillus ustus	glycolipoprotein	Kiran et al., 2009
		Aspergillus niger	unknown	Costa Sperb et al., 2018
		Aureobasidium pullulans	polyol lipids "liamocins"	Price et al., 2013
		Aureobasidium thailandense	fatty acid ester	Meneses et al., 2017
		Exophiala dermatitidis	monoglyceride	Chiewpattanakul et al., 2010
		Trichoderma sp.	unknown	Sena et al., 2018
Basidiomycetes	" white rots"	*Ceriporia lacerata*	mannosylerythritol lipids	Niu et al., 2017
		Pleurotus djamor	glycolipoprotein	Velioglu and Urek, 2016
		Pleurotus ostreatus	unknown	Nikiforova et al., 2009
		Trametes versicolor	lipopeptid	Lourenço et al., 2018
	Ustilaginales	*Pseudozyma spp.*	mannosylerythritol lipids cellobiose lipids	Kitamoto et al., 1993, Morita et al., 2007 Morita et al., 2013
		Sporisorium sp.	mannosylerythritol lipids	Alimadadi et al., 2018
		Ustilago maydis	cellobiose lipid « ustilagic acid »	Frautz et al., 1986
		Ustilago spp.	mannosylerythritol lipids	Spoeckner et al., 1999; Morita et al., 2008, 2009
	Oleaginous yeasts	*Cutaneotrichosporon curvatum (Cryptococcus curvatus)*	sophorolipid	Ma et al., 2014
		Rhodotorula babjevae	sophorolipid	Sen et al., 2017
		Rhodotorula spp.	polyol lipids	Garay et al., 2018
		Vanrija (Cryptococcus) humicola	cellobiose lipid "mycocin"	Puchkov et al., 2002

the dissolved fraction of HOC (Brown, 2007). Biosurfactant-enhanced desorption of phenanthrene from suspended clays and humic acid was observed by Garcia-Junco (Garcia-Junco et al., 2003). Similar mechanisms may be involved for fungal surfactants, increasing the bioavailability of HOC in soils to both the fungus itself and other microorganisms.

2.3. Alteration of the soil matrix and effect on the retention of hydrophobic pollutants

Soil structure is determined by the aggregation of its components, including minerals (clays and other silicates, calcium carbonate, metallic oxides) and organic matter. The relative content in particles of various size ranges defines soil texture, regardless of their chemical nature. Fungi greatly contribute to shaping the soil matrix by simultaneously promoting aggregate formation, and altering minerals and organic matter (Gadd et al., 2012; Ritz and Young, 2004). In combination with organic matter content, porosity is one of the main parameters affecting the retention of contaminants. Indeed, small pores and high total pore volume mean a high surface available for adsorption, and inaccessibility to degrading organisms and solutions (Ren et al., 2018; Yu et al., 2018). HOC are known to have a greater affinity for fine particles, and tend to sorb onto clay minerals which exhibit hydrophobic surfaces in a layered structure (Jaynes and Boyd, 1991; Yu et al., 2018). As a result, pollutant retention is usually higher in soils with a finer texture (Amellal et al., 2001).

Filamentous fungi develop extensive hyphal networks in the soil and can penetrate solid materials while exploring the substrate. Growing hyphal tips are subjected to swelling/shrinking cycles due to changes in intracellular osmotic pressure, exerting a mechanical force on the surfaces encountered, and cause biomechanical weathering of minerals through penetration into cracks and micropores (Fomina et al., 2006). Fungal weathering is also biochemical: fungi acidify their immediate surroundings by excreting organic acids (acetic, citric, oxalic, formic acid…) present in hyphal exsudates, as well as dissolved respiratory CO_2, thus promoting mineral dissolution. Zhang et al., (2016) suggest that organic acids produced through the metabolization of alkanes could in turn enhance the porosity of the solid matrix by dissolving carbonated minerals, thus increasing the accessibility of oil deposits. Metal chelators including siderophores and phenols are also involved in the chemical alteration of soil minerals, destabilizing their chemical structure by solubilizing the metallic elements (Gadd et al., 2012). Such chemical and physical alteration of minerals can enhance the release of inaccessible contaminant droplets or particles trapped in the soil solid matrix. Erosion phenomena lead to the fragmentation of the solid substrate into smaller particles or colloids susceptible to be carried through soil pores by water flows. Colloid-facilitated transport may contribute to the dispersion of sorbed contaminants in soils (de Jonge et al., 2004): indeed, some studies show that transport in a particle-bound form account

for a significant proportion of the leaching of hydrophobic pesticides through macropores (Villholth et al., 2000; Kjær et al., 2011)

One of the major functions of saprotrophic fungi affecting soil structure and chemical cycles is the biodegradation of dead organic matter. Fungi secrete a wide range of extracellular lytic enzymes including cellulases, xylanases, lipases, proteases, and lignin-degrading enzymes in the case of white rots. Through the enzymatic hydrolysis and dissolution of complex macromolecules, fungi disrupt organic matter aggregates, rendering bound HOC more accessible due to two complementary effects: the removal of physical hindrances preventing micro-organisms from accessing the source of pollutant, and the release of mobile organic matter fragments promoting the dispersal of sorbed HOC. Soluble humic acids act as carriers increasing the mobility and bioacessibility of HOC despite very low aqueous concentrations, and making them directly available for uptake even without desorption and solubilization in the water phase (Smith et al., 2009). Hydrophobic contaminants tend to sorb onto suspended humic acid-clay complexes (Garcia-Junco et al., 2003). Moreover, the biodegradation of organic matter by fungi also increases the dissolved organic carbon content, which has been linked to facilitated diffusion of HOC from NAPLs to the water phase (Smith et al., 2011).

3. Mobilization of hydrophobic pollutants by fungi

Access to the pollutant depends on the ability of micro-organisms to explore the substrate. The mechanisms involved differ among organisms: bacteria can rely on motility, while fungi explore the substrate through mycelial growth. Although various utilizing microorganisms exhibit chemotaxy for moderately soluble organic compounds, such mechanisms are not known for the most hydrophobic HOC such as Benzo[*a*]pyrene. The ability to detect minute concentrations of the pollutant and to grow towards the source could be crucial for its degradation (Ortega-Calvo et al., 2013).

3.1. Surface properties of the mycelium and biosorption of organic pollutants

Biosorption refers to the removal of a compound from the solution by a microorganism, through the combination of adsorption onto the cell surface and absorption into the cell. Many studies quantify total biosorption and do not differentiate the respective contribution of both mechanisms. However Adsorption by mycelia could account for a significant part of hydrophobic compound retention in the soil, given the extremely high surface/volume ratio developed by mycelial networks.

Water-insoluble, microfibrillar glucans and chitin are the main components of the fungal cell wall. Parietal α-1,3-glucans appear to play a decisive role in hyphal adhesion to the substrate (He et al., 2018). Ma et al. investigated the adsorption of PAHs to isolated fungal cell wall components, and although the highest affinity was for lipid components, a significant effect of the carbohydrate fractions

(chitin, chitosan, glucan and mannan) was found (Ma et al., 2016). Considering their relative abundance, parietal carbohydrates could account for a substantial proportion of PAH adsorption by the whole cell wall. Specific mechanisms may control cell surface properties in presence of HOC, enabling direct contact: first evidence of a modified cell wall structure associated with enhanced hydrocarbon adsorption was reported in *Candida tropicalis* when grown in presence of hexadecane (Käppeli et al., 1984). Similarly, the addition of naphtalene in culture media induces changes in surface hydrophobicity and emulsifying properties in several yeast strains (Deng et al., 2010). In filamentous fungi, hydrophobins modulate the surface hydrophobicity of the cell wall and affect cell adhesion to hydrophobic surfaces (see section 2.1) as well as hydrocarbons (Zhang et al., 2011).

Adsorption of hydrophobic molecules onto fungal hyphae could be a first step promoting subsequent absorption; however the mechanisms by which hydrocarbons cross the cell wall and enter fungal cells are still unclear. A mechanism of alkane incorporation involving adsorption onto the mycelium followed by active absorption was first proposed in *Cladosporium resinae* (Lindley and Heydeman, 1986). Adsorption of PAHs and crude oil onto the mycelium of a hydrocarbon-degrading *Aspergillus* strain was reported by Al-Hawash et al., as well as intracellular accumulation: absorption rates of up to 89% were found for pyrene in submerged culture (Al-Hawash et al., 2019). Incubation with the water-insoluble HAP benzo[*a*]pyrene induces morphological differences at the surface of hyphae in another *Aspergillus* strain, which displayed a roughness attributed to BaP deposits (Wu et al., 2009). Fayeulle (2013) demonstrated that preventing direct contact between the mycelium of *F. solani* and solid BaP flakes strongly decreased biosorption, while the same was not true for phenanthrene. These results suggests that removal of highly hydrophobic molecules such as BaP from the medium is dependent on their prior adsorption onto the mycelium, while moderately soluble compounds such as phenanthrene could be directly recovered from the aqueous phase.

3.2. Uptake and intrahyphal transport of hydrophobic molecules

Intracellular uptake of hydrocarbons by fungi has been studied since the 1980's, a first active hydrocarbon transport mechanism was demonstrated for dodecane in the "kerosene fungus" *C. resinae* (Lindley and Heydeman, 1986). Al-Hawash et al. (2019) showed that selective adsorption and absorption of crude oil and low molecular weight PAHs occurred in the mycelium of an *Aspergillus sp.* strain. Uptake and intracellular storage of PAH in lipid bodies has been observed in several other fungal species, including BaP in the ascomycete *Fusarium solani* (Verdin et al., 2005; Fayeulle et al., 2014) and anthracene in the arbuscular mycorrhizal fungus *Glomus intraradices* associated with chicory roots (Verdin et al., 2006). The cytochrome P450 oxidation and the β-oxidation of fatty acids are intracellular

pathways involved in the biodegradation of alkanes and aromatic hydrocarbons, which means the uptake of organic contaminants is a crucial step preceding their oxidation through these pathways.

Intrahyphal translocation of phenanthrene through storage and transport in lipid vesicles was demonstrated in the oomycete *Phythium ultimum* (Furuno et al., 2012a). The same species was found to increase the accessibility of fluorene to the PAH-degrading bacteria *Burkholderia sartisoli* after transport by the mycelium (Schamfuß et al., 2013). Although *P. ultimum* is a water mold, it shares a similar filamentous morphology and saprotrophic lifestyle with true fungi. This suggests that similar mechanisms of PAH redistribution could be at work in the mycelium of soil fungi.

Indeed, filamentous fungi are able to redistribute nutrients in the mycelium and propagate chemical signals through intrahyphal cytoplasmic flow. Simultaneous localized response to pathogen attack and glucose translocation was shown in *Coprinopsis cinerea* (Schmieder et al., 2019). This mechanism allows for accommodation of the heterogeneous environment, since a mycelium can cover large volumes and be locally exposed to different conditions in different areas. This is especially important in nutrient-deprived or contaminated lands. The incorporation of PAH into lipid bodies in *F. solani* is dependent on actin, which is consistent with the hypothesis intracellular hydrocarbon transport through cytoskeleton-dependent vesicular traffic (Fayeulle et al., 2014). Intracellular vesicle traffic is especially active at the growing tips of hyphae which are rich in secretory vesicles bringing “building materials” such as membrane lipids and cell wall precursors. Hydrophobic pollutants incorporated into vesicles could thus be released outside of hyphae and hereby become accessible for degradation by other microorganisms.

3.3. Enhancement of the bioaccessibility for other organisms

Water films along aerial hyphae of the oomycete *Phytium ultimum* enable the migration of motile bacteria following chemotactic gradients (Furuno et al., 2010). Here the mycelial network functions as a “highway” promoting the dispersal of PAH-degrading bacteria living at the surface of hyphae. Through the incorporation of fat-soluble pollutants into cell membranes and diffusion thereof, hyphae are likely to act as “conductor wires” transmitting HOC gradients and thus guiding utilizing bacteria towards the source (Furuno et al., 2010, 2012b). This mechanism highlights one of the ways fungi interact with other micro-organisms as structural components of the soil, and not solely through trophic exchanges. In combination with intrahyphal translocation of pollutants, it could contribute to enhance the access of unicellular micro-organisms to heterogeneously distributed hydrophobic pollutants in the soil (Banitz et al., 2013).

Many fungal species are able to form mutualistic interactions with plants though mycorrhizae. Indeed, 90% of plant species are currently thought to display such symbiotic associations (Bonfante and Genre, 2010). Filamentous fungi form mycorrhizes by developing hyphae in plant root tissue and exchanging nutrients with the cells. They provide the plant partner with inorganic phosphorus and nitrogen, while taking up sugars from the plant. In this regard, the mycelium of mycorrhizal fungi functions as an extension of the root network enabling a greater exchange surface for nutrient uptake.

Mycorrhizae may help with bioaccumulation of pollutants in plants, though incorporation, hyphal transport and transfer to plant cells among various exchanged molecules. Wu et al. (2008) found a better removal of phenanthrene from spiked soil with alfalfa plants colonized by the arbuscular mycorrhizal fungus *Glomus etunicatum* compared to plants without mycorrhizae. Enhanced accumulation and degradation of PAH in spiked soils was also shown for the legume *Sesbania cannabina* in triple symbiosis with *Glomus mosseae* and rhizobia (Ren et al., 2017). A similar result was obtained for the accumulation of uranium by another *Sesbania* species, in triple symbiosis as well with *G. etunicatum* and rhizobia (Ren et al., 2019). In arbuscular mycorrhizal fungi, parietal glomalin or freely dissolved GRSP may be involved in the biosorption of contaminants by mycorrhizal fungi, and its transfer to plant roots (see section 2.1). POP degrading abilities have also been found in various ectomycorrhizal basidiomycetes, covering a range of aromatic and/or halogenated hydrocarbons, pesticides and pharmaceuticals (Meharg and Cairney, 2000). Ectomycorrhizae in poplar tree for instance have been shown to enhance the removal of diesel oil from the soil (Gunderson et al., 2007). Even when they are not known themselves for biodegradation properties, other mycorrhizal fungi could thus contribute to remediation by mediating the transfer of pollutants to plant roots and/or rhizosphere bacteria.

4. Chemical alteration and fate of the degradation products

Soil-dwelling fungi are saprotrophic organisms which contribute to carbon cycling in soils by breaking down decaying organic matter. Their enzymatic machinery is adapted to the biodegradation of a wide range of organic molecules, and some strains have demonstrated biodegradation abilities towards hydrocarbons, synthetic organic compounds and even polymers. Fungi, in cooperation with other microorganisms and plants, thus participate in the natural attenuation of HOC through chemical alteration.

4.1. Biotransformation of pollutants by fungi

Hydrocarbon metabolism in fungi is in large part connected to lipid catabolism. Both intracellular lipolytic activity and extracellular enzymatic complexes contribute to the biodegradation of

hydrocarbons (Peter et al., 2012; Al-Hawash et al., 2019). Alkanes are first oxidized into fatty acids by mono-oxygenases and NAD-dehydrogenases before entering the intramitochondrial β-oxidation pathway (Singh, 2006a) leading either to total mineralization or incorporation into the biomass. Biotransformation of alkanes by fungal enzymes leads to the release of gases and water-soluble organic acids such as oxalate and propionate (Zhang et al., 2016). The use of abundant lipids (or alkanes) as a carbon source could also enhance the biodegradation of more recalcitrant compounds through the release of reactive oxygen species (ROS), as shown for the co-metabolization of vegetable oil and PAH in *F. solani* (Delsarte et al., 2018). This suggests that the fungal degradation of aromatics may be more efficient when they are associated with NAPLs that contain more easily assimilated linear hydrocarbons. Extracellular lipolytic enzymes also play a significant role in the breakdown of linear and cyclic hydrocarbons as well as aromatics: in particular heme peroxidases presenting a functional similarity to intracellular P450 oxidases have been found to calatyse the breakdown of a wide range of hydrocarbons and organic compounds (Harms et al., 2011; Peter et al., 2012).

Fungal lignolytic enzymes have been extensively studied for their potential in the biodegradation of organic contaminants containing aromatic rings, and especially PAHs and dyes, due to their structural similarity with lignin. Many white rot fungi have been identified as depolluting fungi, including *Phanerochaete chrysosporium*, *Pleurotus ostreatus*, *Trametes versicolor* (Lladó et al., 2013), *Anthracophyllum discolor* (Acevedo et al., 2011). The lignolytic pathway involves extracellular oxidoreductases: laccases, lignin peroxidases, manganese peroxidases, and tyrosinases which catalyse the production of oxidizing agents and free radicals leading to the non-specific oxidation of substrates into quinones. The reaction of aromatics with free radicals can also lead to their covalent binding with soil organic matter, as demonstrated during the degradation of trinitrotoluene through fungal laccases purified from *Trametes modesta* (Nyanhongo et al., 2006). The formation of such bound adducts can result in a lower acute toxicity of the degradation products, but also render them less available for further degradation.

Intracellular degradation through the cytochrome P450 mono-oxygenase pathway appears to be the dominant metabolic pathway for aromatics degradation in non-lignolytic fungi, and yields substituted derivatives that are more reactive and more soluble than the original pollutants: phenol, phthalate, hydroxyl-, carboxy- and dihydrodiol derivates that may in a second step be conjugated with sugar moieties (Boll et al., 2015). The fungal metabolization of biphenyls can yield water-soluble conjugates, such as glucuronide and sulfate conjugates as found in *Cunninghamella elegans* (Singh, 2006b). PCBs are typically oxidized into hydroxy- and dihydroxybiphenyls, more polar than the original compound (Singh, 2006b). Boll et al. showed that PAH metabolites produced by *C. elegans* had radically different behaviors compared to the parent PAHs, and tended to partition into the water phase at much higher

rates (Boll et al., 2015). On one hand, the release of such polar metabolites can increase environmental risk as they are more prone to leaching and can spread to surface and groundwater. On the other hand, higher mobility and bioavailability could enhance their further biodegradation by other organisms.

4.2. Biotransformation by microbial consortia

In the soil, fungi and bacteria co-exist in close vicinity, as the mycelial network constitutes a favorable microhabitat for soil bacteria. Furuno et al. (2012b) showed that several bacterial strains known for their degradation abilities towards HOC (*Pseudomonas, Xanthomonas, Rhodococcus, Arthrobacter*) could be selectively isolated from the surface of hyphae, highlighting the close link between physical and metabolic interactions regarding the biodegradation of pollutants. Indeed, fungi excrete proteins, polysaccharides and organic acids that can be used as carbon and nitrogen sources by bacteria (de Boer et al., 2005). Dashti et al. showed that bacterial and fungal organisms cooperate in the degradation of alkanes, and that fungi are able to take up and metabolize products released after primary oxidation by alkane-degrading bacteria, such as fatty acids, alkanols and alkanals (Dashti et al., 2008). Co-cultures of fungi and bacteria were also shown to work in synergy for the degradation of aromatic pesticides, by further metabolizing one another's degradation products, thus avoiding the accumulation of toxic intermediates responsible for an inhibition of degradation in pure cultures (Zhao et al., 2016)

Fungi are usually regarded as more efficient than bacteria for the transformation of HOC that are particularly recalcitrant due to their poor mass transfer rates (high molecular weight hydrocarbons including PAH) and/or low nutritional interest (highly oxidized compounds such as nitrated and chlorinated hydrocarbons) (Harms et al., 2011). This higher efficiency is attributed to enzymatic diversity and co-metabolic degradation mechanisms absent from bacteria. However many bacterial species have been identified as good degraders of lower molecular weight aromatic compounds, mostly members of the genera *Burkholderia, Pseudomonas, Acinetobacter, Rhodococcus, Streptomyces*. Bacterial metabolism of polycyclic aromatics differs from the fungal metabolism by the initiation of ring attack, through a dioxygenase activity as opposed to mono-oxygenase in fungi (Cerniglia, 1992). However, more recently dioxygenase activities involved in the biodegradation of lignin and BTEX have also been described in fungi (Gunsch et al., 2005). A new degradation pathway of phenolic compounds that was only known in bacteria thus far has been identified in *Aspergillus sp*. (Yang et al., 2018). Redundancy of metabolic functions in bacteria and fungi may thus be more frequent that was previously thought.

Bacteria and fungi can cooperate for the biodegradation of lignin: biphenyl derivatives from lignin can be further metabolized by *Pseudomonas, Streptomyces* (Vicuña et al., 1993), and *Sphingomonas* strains

(Peng et al., 2002) after a first depolymerization step by white rots. Due to the structural similarity between lignin monomers and aromatic pollutants, similar metabolic cooperation mechanisms are likely to occur during biodegradation processes of these compounds. Indeed, metabolic synergies between fungal and bacterial microorganisms can enhance the biodegradation of HOC compared to the yields obtained with individual strains, especially in the case of recalcitrant PAH (Han et al., 2008; Machín-Ramírez et al., 2010), azo-dyes (Lade et al., 2012; Zhou et al., 2014) or pesticides (Hai et al., 2012; Zhao et al., 2016).

Co-metabolization of HOC by several taxa could be of critical importance to avoid the accumulation of toxic intermediates. In soil microcosms, the white-rot fungi *Phanerochaete chrysosporium* and *Trametes versicolor* were able to mineralize 3 and 4 cycles PAH completely, while quinones produced by *Pleurotus ssp* accumulated as a dead-end metabolite (Andersson and Henrysson, 1996). This accumulation was attributed to an inhibiting effect of the fungus towards the autochthonous microflora, which appears to play an essential role in the further degradation of fungal metabolites. Antagonistic effects can also hinder the degradation efficiency, due to the production of anti-microbial compounds and/or competition for resources (Thion et al., 2012).

5. Experimental strategies to investigate pollutant mobilization

Bioremediation can be studied at several scales from batch biodegradation tests in the lab to field experiments. Biodegradation is usually assessed by quantifying the remaining pollutants and/or metabolites after treatment. Studying the availability and mobilization of contaminants is a complex problematic as it involves multiscale interactions between living organisms, dead organic matter, inorganic particles, gas phase and aqueous phase, and contaminants themselves. Investigating individual mechanisms often requires using simplified models for a specific subsystem, with varying degrees of complexity.

5.1. Characterizing contaminant bioavailability in soils

The bioavailable fraction of a contaminant is by definition the immediately available fraction to micro-organisms, and assumed to be the most soluble and easily extractible in mild conditions. Chemical techniques to measure the bioavailable fraction in contaminated soils include partial extraction with polar organic solvents such as ethanol or butanol, subcritical water extraction, or supercritical CO2 extraction. Co-solvent extractions using water in combination with a miscible solvent may be used as well. However solvent-based approaches are subject to discussion regarding their relevance to estimate the fraction actually available for microorganisms. Indeed, their recovery yields can be relatively close to those of exhaustive extractions techniques used to quantify total contamination,

suggesting they may be too harsh and lead to an overestimation of the bioavailable fraction (Cachada et al., 2014).

It is important to note that bioavailability is dependent on a number of dynamic processes, either physical, chemical and biological. That is why some approaches focus on assessing pollutant retention times and desorption kinetics rather than quantifying the available fraction at a single point in time. Other techniques aim at mimicking the effect of pollutant consumption by living organisms through biosorption and degradation, and allow to quantify desorption rates. Desorption behavior can be evaluated directly by measuring the dissolved fraction in water phase over time (Heister et al., 2013) or through resin-aided solid phase extraction (Kan et al., 2000). Solid-phase extraction is an aqueous extraction-based approach where instead of measuring pollutant concentration at equilibrium in the water phase, a hydrophobic resin such as Tenax is used as a trap to deplete the water phase from HOC. This promotes the desorption of compounds reversibly bound to the soil matrix (Breedveld and Karlsen, 2000). The freely dissolved HOC fraction in water or soil slurries can be measured *in situ* using passive samplers for environmental monitoring, however this type of device is poorly suited for use in unsaturated soil (Cui et al., 2013).

All these methods may give very different results depending on whether they are used on contaminated environmental samples or artificially spiked soil: indeed, the age of a contamination greatly influences sorption to the matrix. The aim can be different as well. In the case of soil samples from a polluted site, the availability of HOC can be evaluated as part of risk assessment and preliminary evaluation before treatment. When using spiked samples, the aim is to evaluate the sorption properties of a given soil, by measuring the differential partitioning of a pollutant between the sample and solvent or water.

5.2. Fungal-mediated desorption and solubilization assays

As developed in part III, fungi are able to mobilize hydrophobic compounds through several direct and indirect effects, by facilitating their transport in aqueous phase, and affecting their retention in soil. Experimental approaches to characterize fungal mechanisms of emulsification or facilitated transport can focus on the properties of specific molecules (particularly extracellular biosurfactants), or the whole organism.

Surface tension measurements are a simple way to assess the presence of surface active molecules in microbial extracts, and are commonly used in first approach to identify surfactant producing fungal strains (Kitamoto et al., 1993; Méndez-Castillo et al., 2017; Alimadadi et al., 2018; Al-Hawash et al., 2019). However, surface tension at the air-water interface does not yield direct information about the

behavior of biosurfactants in presence of hydrophobic compounds. Alternatively, interfacial tension measurements in contact with an immiscible organic phase can be performed (Kitamoto et al., 1993). Oil displacement assays are a cheap and quick method to compare the surfactant activity of fungal extracts without the need of costly equipment: in a Petri dish, a known volume of surfactant solution is dropped onto an oil film and the area cleared of oil is measured. This test has been used to rapidly detect surfactant activities in cell-free culture supernatants of several fungal species (Gautam et al., 2014; Meneses et al., 2017; Al-Hawash et al., 2019; Pele et al., 2019).

The ability of biosurfactants to solubilize hydrophobic compounds can be estimated by partitioning assays with a principle similar to octanol-water partitioning assay. The octanol-water partitioning coefficient (K_{ow}) is a classic measurement tool used to estimate the relative affinity of a given compound for aqueous or organic phases. It is determined by dissolving the tested compound in a mix of octanol and water, and expressed as the ratio of concentrations at equilibrium in both phases. The same method can be adapted so that culture supernatants or a solution of biosurfactants are used as the hydrophilic phase, and the enhanced partitioning of hydrocarbons into the aqueous phase containing microbial extracts is compared to the partitioning into pure water. In the same way, octanol may be substituted with any other NAPL of interest (Garcia-Junco et al., 2003).

Estimating the emulsifying activity of fungal extracts is a relevant approach to investigate their behavior towards NAPLs. (Sánchez-Vázquez et al., 2018) determined the emulsifying activity of a bioemulsifier towards dodecane, diesel oil and PAH dissolved in organic solvents by measuring the optical density of the oil-in-water emulsion or average oil droplet size. A similar protocol was used to estimate the emulsification index towards waste oil (Batista et al., 2010). Emulsification abilities of hydrophobins towards a decane and toluene mix in synthetic sea water were shown by measuring the relative height of the emulsified layer after mixing and resting (Blesic et al., 2018).

The auto-fluorescence properties of some aromatics, and more specifically PAHs, allow for their detection in spectro-fluorometry or fluorescence microscopy. Some desorption assays thus rely on fluorescence measurements in aqueous samples after incubation in direct contact with a solid deposit of PAH (Rafin et al., 2013; Fayeulle et al., 2019). A similar protocol followed by liquid-liquid extraction of PAH from the aqueous phase was used to demonstrate the ability of the bacterial emulsifier alasan to solubilize several PAH (Barkay et al., 1999).

Spatial compartmentalization of the pollutant source and microorganism can be used to demonstrate pollutant translocation. Solid culture of filamentous fungi on agar blocks separated by gap, only bridged by hyphal filaments showed fungal-mediated transport of PAH from the spiked block to the block inoculated with fungus, without PAH (Furuno et al., 2012a; Schamfuß et al., 2013).

Compartmentalization can be achieved with a dialysis membrane to prevent direct contact between the fungus and the solid pollutant deposit, allowing access to the solubilized fraction in aqueous phase only (Fayeulle, 2013). The use of a microfluidic device for fungal cultivation has also been proposed to spatially control the contact with a pollutant source (Baranger et al., 2018)

There is a need for new tools to simulate complex environments such as the soil. In this context, the use of micro-fluidic devices to study the interactions between micro-organisms is a recent field of research (Stanley et al., 2016). The importance of fungal-bacterial interactions for the degradation of organic pollutants is pointed out by the authors. These devices enable the modeling of heterogeneous, compartmentalized microbial habitats, with or without water flow, and allow for a direct coupling between microbial culture and multiscale observations from the single cell level to a several millimeter colony.

5.3. Surface properties of fungi and biosorption

Adsorption onto the cell surface and absorption into fungal cells both contribute to the removal of HOC from the soil in a non-destructive way, and can be a preliminary step leading to biodegradation. The sum of both mechanisms is quantified as total biosorption, however some studies attempt to quantify their respective contribution, differentiating between the reversible adsorption of HOC and their incorporation into the biomass. Several techniques have been used to selectively recover the adsorbed fraction and quantify it, the main issue being to find extraction conditions sufficient to recover HOC bound to the extracellular matrix without permeating the cell membrane. Assessing passive biosorption of pesticides and PAH with autoclaved mycelium is one of the approaches used (Hai et al., 2012; Thion et al., 2012). Al-Hawash et al. (2019) used sonic bath extraction to quantify the fraction adsorbed to mycelium pellets. The surface-adsorbed fraction can also be selectively extracted by cold washing the fresh or autoclaved mycelium with organic solvents (Al-Hawash et al., 2019). Chau et al. (2010) demonstrated a correlation between surface hydrophobicity of mycelial mats of several fungal taxa, including *Fusarium*, *Cladosporium*, *Mortierella* and *Penicillium* ssp, and their capacity to absorb ethanol solutions of increasing concentrations: this result suggests a relation between surface hydrophobicity and affinity for organic solvents. The affinity of whole fungal cell walls and insoluble cell wall components for PAH can be tested measuring their partitioning rates in a water-cosolvent mixture (Ma et al., 2016).

Microbial adhesion to hydrocarbons (MATH) assays estimate the surface hydrophobicity of a given microorganism's cell wall, by measuring its affinity for hydrocarbon-water interfaces. The microbial cell suspension is brought into contact with a hydrophobic phase, and the equilibrium concentration of cells that remain suspended in the aqueous phase is quantified by optical density measurements.

The decrease of suspended cell concentration, due to increased cell adhesion at the hydrocarbon-water interface, therefore reflects the cell surface hydrophobicity (Hazen, 1990; Rosenberg, 2006). This test was primarily designed for bacteria, and then extended to yeasts and fungal spores, but is limited to unicellular organisms. Although MATH has been used to assess the hydrophobicity of young hyphal germ tubes of *Candida albicans* (Rodrigues et al., 1999), it is impossible to implement for filamentous fungi at more advanced growth stages, since they form mycelial pellets in submerged culture rather than homogeneous cell suspensions. Hydrophobic interaction chromatography (HIC) has been adapted to assess the affinity of unicellular micro-organisms for a hydrophobic matrix: the microbial suspension is filtrated through the column and a retention index is measured. Similarly to MATH assays, HIC can be used for spores and yeast cells (Hazen, 1990; Holder et al., 2007)

Surface hydrophobicity of the mycelium can be assessed by measuring the contact angle with water droplets of whole colonies. Several fungal culture methods have been developed to allow for imaging of contact angles in controlled conditions, including growing mycelial mats on cellulose acetate filters (Smits et al., 2003), glass microscope slides that can be mounted directly on a sample stage (Chau et al., 2009), or producing fungal biofilms in submerged culture wells (Siqueira and Lima, 2012). The main advantage of contact angle measurements is that they are done on the filamentous form of fungi rather than a homogeneous suspension of germinating spores or broken mycelium fragments, more accurately representing the properties of whole mycelia. The apparent surface hydrophobicity of a mycelial mat does not solely depend on cell wall composition and the coating of hyphae with hydrophobins, but also on geometric parameters: hyphal diameter and tightness of the mycelial network affect the surface roughness of the mycelium and thus contact angles with water. Studies comparing the fungal surface hydrophobicity in different growth conditions highlight differentiated cell wall properties and/or morphology depending on water saturation and circadian growth cycles (Chau et al., 2009; Siqueira and Lima, 2012). However contact angle measurements do not account for local changes in cell surface properties at the microscale, and whole colony hydrophobicity does not necessarily reflect cell surface properties of individual hyphae. Soil-dwelling mycelia develop in mostly water-unsaturated environments and may thus present frequent variations in the local cell surface properties due to the heterogeneous nature of their microenvironment. Microsphere attachment assays can be implemented with whole hyphae or even small mycelial pellets, and may more accurately reflect local surface hydrophobicity. This method could be a useful tool to identify preferential sites of adsorption and uptake of hydrophobic molecules, and help better understand incorporation mechanisms.

6. Working model of the thesis

6.1. A candidate for soil mycoremediation: *Talaromyces helicus*

Talaromyces helicus (anamorph: *Penicillium helicum*) is a filamentous ascomycete belonging in the Trichocomaceae family of the Eurotiales order (Stolk and Samson, 1972; Yilmaz et al., 2014). The genus *Talaromyces* comprises species associated to the *Penicillium*, *Paecilomyces* and *Geosmithia* anamorph genera, which are polyphyletic. *T. helicus* grows as a white to cream-colored mycelium on MYEA agar, displaying septate hyphae of 2-3 µm in diameter, and produces biverticillate conidiophores holding chains of asexual spores of about 3 µm in diameter. Some strains display a yellow color due to the production of pigments of the azaphilone family, helicusins (Yoshida et al., 1995).

T. helicus is a saprotrophic soil-dwelling fungus, reported in agricultural topsoil (Romero et al., 2009), and in the rhizosphere of some edible crops (Scervino et al., 2010; Wu et al., 2016), as well as in urban polluted soils (Fayeulle et al., 2019) and agricultural and municipal waste (Olagoke, 2014). Isolates of the species were found in environmental samples from various parts of the world, including Ohio, USA (Huang and Schmitt, 1975), Indonesia (Oudot et al., 1993), Mexico (Romero et al., 2009), Argentina (Scervino et al., 2010), Nigeria (Olagoke, 2014), China (Wu et al., 2016), and France (Fayeulle et al., 2019). This indicates a cosmopolitan distribution of the species in areas with temperate to tropical climates.

Talaromyces marneffei, a close relative of *T. helicus*, is an opportunistic pathogen mostly known to cause lethal infections in immunocompromised HIV patients (Limper et al. 2017). In contrast, *T. helicus* appears to be safe for humans, having been reported only in two cases of opportunistic infection in dogs (Tomlison et al. 2011, Whipple et al. 2019). It is therefore considered a group I organism, which means it is not known to present any risk of causing disease in humans, and it requires no specific containment measures (INRS, 2018). In the field of industrial biotechnology, *T. helicus* has been identified as a producer of thermophilic amylases (Olagoke, 2014), and other species of the *Talaromyces* genus are used as sources of lignocellulolytic enzymes, including xylanases from *Talaromyces emersonii* (Tuohy and Coughlan, 1992), several glycosyl hydrolases from *Talaromyces cellulolyticus* (Inoue et al., 2014), and β-glucosidases from *Talaromyces thermophilus* (Nakkharat and Haltrich, 2006). *T. helicus* has also been studied as a biocontrol agent against phytopathogenic fungi (Manoch and Dethoup, 2011) and for its ability to enhance the solubilization of phosphate salts in soils (Scervino et al., 2010), which suggests possible future applications in agriculture. However, it is also an occasional plant pathogen and can cause root infection in edible tubers (Wu et al., 2016).

T. helicus was previously cited for its detoxification abilities towards several environmental contaminants, such as biphenyl , heavy metals , and the herbicide isoproturon (Romero et al., 2005, 2006, 2009). It can also simultaneously degrade several types of PAH including BaP (Fayeulle et al., 2019). Several strains of *T. helicus*, including the one used in this study, were previously isolated from polluted soil samples. Other species from the genus *Talaromyces* have been identified in contaminated soils and sediment on several occurrences , showing their adaptation to high-stress conditions and their tolerance towards toxic organic contaminants and heavy metals. For these reasons, *T. helicus* appears as a promising candidate for environmental remediation.

6.2. A model of persistent organic pollutants: benzo[*a*]pyrene

Benzo[a]pyrene, a well-studied PAH both in in the field of environmental science and toxicology, was chosen as a model for hydrophobic persistent pollutants in the following works. BaP is a persistent environmental pollutant, found mostly as part of PAH mixtures in natural deposits of petroleum, coal tar, and as products of high-temperature combustion of organic matter. It is thus found in creosote-contaminated soils and waste, industrial sites, and as particulate pollution from cookeries, traffic, waste incineration….

The effects of BaP on animal and human health are the best studied among PAH: it is classified as carcinogenic, mutagenic and reprotoxic (Bonnard et al., 2007) and shows immunotoxic properties (IARC, 2012). BaP absorption by mammals can occur through the oral, cutaneous or respiratory route. In humans, exposition mostly occurs through food and, to a lesser extent, through the particle pollution of air and drinking water. Estimates of the average dietary intake of BaP in humans range from 6 ng to 3.4 µg per day and per person, with great variations depending on the population considered and method of estimation (Domingo and Nadal, 2015). There is little epidemiological data in humans about specific PAH, as they almost always occur as a mixture and in association with other potentially carcinogenic pollutants. However a higher incidence of skin, lung and bladder cancer was noted in workers exposed to PAH (IARC, 2010). The mutagenicity of high molecular weight PAH was shown in bacteria (Mersch-Sundermann et al., 1992; Nylund et al., 1992). According to a number of studies reviewed by the International Association for Cancer Research (IARC, 2010), BaP administration is tumorigenic in mice (through oral, transdermal and subcutaneous routes) and hamsters (respiratory, oral and subcutaneous). In animals including humans, BaP is oxidized into dihydrodiol epoxides by P450 cytochromes in the liver, following a metabolic pathway similar to the one found in fungi (see section 4.1). These reactive metabolites can then form adducts covalently bound to biological macromolecules, including DNA, causing genotoxic effects (Brignon and Soleille, 2006; IARC, 2012).

BaP is a high molecular weight PAH BaP consisting in 5 conjugated unsubstituted benzene rings, with a molecular mass of 252.3 g/mol, and is nearly insoluble in water (aqueous solubility: $3.8 \cdot 10^{-3}$ mg/L at 25°C) (IARC, 2012). Like many aromatic compounds including PAH, BaP displays fluorescence properties when excited with UV light, with a maximum excitation at 297 nm and maximum emission in blue at 405 nm (Rivera-Figueroa et al., 2004). This property is used for detection and quantification, as well as direct observation in fluorescence microscopy (Plant et al., 1985). Due to its very high hydrophobicity, BaP is present in water only as traces, and as particle pollution in air (Brignon and Soleille, 2006). In soils, the availability of PAH is greatly dependent on its adsorption to organic matter and solid particles such as clay minerals (Amellal et al., 2001; Yu et al., 2018).

Due to its hazardous nature and high persistence in the environment, BaP is the most regulated PAH in environmental policies (Jennings, 2012). In France, the maximum exposure value recommended for occupational exposure is 150 ng/m^3 BaP in the air. The European directive n° 98/83/EC on the quality of water intended for human consumption (1998) sets a limit of 10 ng/L of BaP in drinkable water, and 0.10 µg/L for the sum of benzo[*b*]fluoranthene, benzo[*k*]fluoranthene, benzo[*ghi*]perylene and indeno[*1,2,3-cd*]pyrene. BaP is classified as a priority substance according to the European directive n° 2455/2001/CE (2001), and part of the list of 16 PAH defines as priority pollutants by the USEPA. BaP is also used as an indicator for PAH pollution in the environment: its abundance is often assumed to be representative of the presence of PAH contamination.

7. Summary and purpose of the thesis

Fungi are major actors of soil ecology and structure, and affect the retention and transfer of organic pollutants in contaminated soils. They impact pollutant dynamics on three levels: shaping of the soil structure and physico-chemical properties, mobilization of contaminants by facilitated transport and intracellular accumulation, and chemical alteration.

In particular, filamentous fungi promote soil aggregation, and modulation its physico-chemical properties through the release of amphiphilic proteins (hydrophobins and glomalin), likely to affect pollutant adsorption and transport through water flows. Fungi also produce a wide range of non-protein extracellular surfactants able to emulsify or solubilize HOC, however it is not known whether these are part of specific transport and incorporation mechanisms. Some fungal species are able to assimilate organic contaminants, including PAH, into their cells and translocate them through intrahyphal transport. They may thus function as dispersion routes for contaminants in the soil, promoting their transfer towards other degrading organisms. How aromatic hydrocarbons cross the cell wall and membrane before accumulating into intracellular organelles is still unclear.

The fungal degradation of organic pollutants has also been subjected to extensive research, with early works focusing mostly on non-specific extracellular oxidation by ligninolytic enzymes, but broadening more recently to include non-ligninolytic fungi. Other metabolization pathways have thus been identified in fungi, including intracellular detoxification through the cytochrome P450 pathway. In addition, metabolic synergies between fungal and bacterial microorganisms can enhance the biodegradation of HOC, especially in the case of recalcitrant compounds. The interactions between fungi and other soil organisms, including plants and other micro-organisms, should be taken into account as a whole to get a global picture of pollutant dynamics in the soil. Indeed, inter-organismal cooperation can yield very different outcomes compared to the single organisms in terms of pollutant mobilization, transport, and degradation. Although some communities work in synergy, competition may hinder efficient remediation.

The high influence of soil physicochemical properties on bioremediation efficiency on field is frequently reported as a limitation to the development of this type of techniques. To this date, the mechanisms driving hydrophobic pollutant mobilization, and uptake and transport by fungi are poorly understood and need to be further investigated. In order to adapt bioremediation protocols to each site's characteristics, there is a need for new faster laboratory-scale screening tools allowing a fine control of physicochemical parameters. Experimental approaches to investigate bioremediation involve biodegradation assays in homogeneous liquid microbial cultures or in soil microcosms/mesocosms (with historically contaminated or artificially spiked soil). "Soil-on-chip" microfluidic models have been recently proposed as a novel approach to investigate interactions between soil organisms at the microscale in a heterogeneous environment, and certainly hold potential to study pollutant mobilization and incorporation.

In this context, the works presented in this dissertation deal with the mobilization, incorporation and biodegradation of benzo[*a*]pyrene, chosen as a model of hydrophobic persistent pollutant, and the filamentous fungus *Talaromyces helicus.* The potential of the strain for bioremediation will be evaluated through biodegradation tests in liquid cultures and soil microcosms, as well as the analysis of potential fungal mobilizing agents. In complement to these traditional experimental approaches used to assess biodegradation efficiency, the purpose of this thesis is to examine pollutant mobilization and incorporation using a novel microfluidics-based approach. Hence, a microfluidic device will be designed and used as a model compartmentalized environment to monitor pollutant incorporation at the cell scale.

Chapter I: Biodegradation of hydrophobic organic contaminants by *Talaromyces helicus* under different experimental setups

1. Introduction

Ligninolytic fungi, including the wood-decaying basidiomycetes « white rots », have been the most extensively studied for bioremediation of aromatic organic contaminants, due to their capacity to degrade lignin. Although high degradation rates can be achieved in laboratory conditions, white rots are adapted to a wooden habitat and usually perform poorly in soils, mostly due to competition with the autochthonous flora. For these reasons, the potential of non-ligninolytic fungi for the degradation of recalcitrant organic compounds has drawn significant attention (Marco-Urrea et al., 2015). In non-ligninolytic fungi, including *Penicillium spp*, the degradation of high molecular weight PAH occurs as a co-metabolism and is thought to be a non-specific detoxification mechanism towards xenobiotics. Few fungi are known to actually use these compounds as sole carbon source for growth, and mineralization of PAH into CO_2 is rarely completed (Cerniglia and Sutherland, 2010). However, partial oxidation into metabolites of lesser toxicity, or more available to other degrading organisms, may be useful to initiate the natural attenuation of such compounds in soils. Indeed, cooperation between organisms can be a way to overcome metabolic limitations of specific strains: some fungi are be particularly efficient at oxidizing high molecular weight PAH but unable to mineralize them (Harms et al., 2011), while bacteria are usually more efficient to degrade lower molecular weight organic molecules, and some can use degradation metabolites from other organisms (Dashti et al., 2008; Zhao et al., 2016).

In this chapter, we investigated the potential of *Talaromyces helicus* for the biodegradation of organic contaminants, and more specifically benzo[*a*]pyrene (BaP) used as a model of recalcitrant and highly hydrophobic pollutant. *T. helicus* is a soil ascomycete previously cited for its detoxification abilities towards biphenyl (Romero et al., 2005), heavy metals (Romero et al., 2006), the herbicide isoproturon (Romero et al., 2009) and PAH including BaP (Romero et al., 2010; Fayeulle et al., 2019). Several strains of *T. helicus*, including the one used in this study, were previously isolated from polluted soil samples (Fayeulle et al., 2019). Other species from the genus *Talaromyces* have been identified in contaminated soils and sediment on several occurrences (Chaillan et al., 2004; Reyes-César et al., 2014), showing their adaptation to high-stress conditions and their tolerance towards toxic organic contaminants and heavy metals. It was also isolated from sewage sludge and reported to enhance particle flocculation by forming small pellets rather than large mycelial mats (Murugesan et al., 2014). *T. helicus* produces abundant conidiospores when grown on malt yeast extract agar (MYEA), which is convenient for propagation in liquid cultures.

In order to evaluate the biodegradation efficiency of *T. helicus* towards BaP and other organic contaminants, biodegradation experiments were carried out with two complementary approaches: in batch liquid cultures with controlled conditions and BaP as sole model contaminant, and in soil microcosms with actual polluted soil samples presenting multiple organic contaminations, including PAH in low amounts. Three soils from contaminated sites located in the Île-de-France and Pays-de-la-Loire regions in France were used for this purpose. Biodegradation in soil microcosms is a classical technique used to assess remediation efficiency at the laboratory scale, both for research purposes and for the diagnostic of real contaminated sites. This technique can be applied to native or sterilized soil, slurries, sludges, or even contaminated water. When soil is used, water is usually added and adjusted depending on soil texture to reach an optimal hydric potential for microbial activity. However this requires a precise knowledge of soil composition. Such a set-up allows comparing a large number of bio-augmentation and/or bio-stimulation conditions on small amounts of soil. Liquid cultures typically require shorter incubation times compared to microcosms, and allow a fine control over biodegradation conditions. These simplified set-ups are better suited to evaluate the influence of specific parameters individually and optimize them.

Here four strategies to improve bioremediation efficiency were tested, in complement to bio-augmentation with *T. helicus*: biostimulation by nitrogen supplementation or depletion, chemical oxidation with H_2O_2 to assist microbial metabolism, bio-augmentation with hydrocarbon-utilizing bacteria (*Corynebacterium glutamicum* and a commercial bacterial suspension “HC” for hydrocarbon degradation), and addition of surfactants to enhance the bioavailability of pollutants. Some conditions were tested in liquid cultures, soil microcosms, or both, and biodegradation rates were quantified.

Moreover, the nature of metabolites released during biodegradation processes will be discussed based on the results obtained in degradation experiments and previous literature. Indeed, degradation products including phenol, phthalate, hydroxyl-, carboxy- and dihydrodiol derivates or sugar conjugates are likely to be more reactive and more water-soluble than the BaP molecule (Boll et al., 2015). Some degradation products including coumarins, ketones or quinones are toxic, and can increase environmental risk as they are more susceptible to leaching due to their solubility in water. In this regard, gaining insight into the fate of degradation products is important to assess the efficiency of a method, and optimize it to achieve actual detoxification, if not complete mineralization.

2. Materials and methods

2.1. Reagents and chemicals

Benzo[*a*]pyrene (≥96%) in powder form was purchased from Sigma-Aldrich (St Quentin-Fallavier, France). Tween 20, a non-ionic polysorbate detergent synthesized from sorbitol, was purchased from Sigma-Aldrich. The commercial surfactant Sophoclean is a sophorolipid detergent derived from wheat and rapeseed oil, obtained from Wheatoleo (Pomacle, France)

HPLC grade dichloromethane, acetone and acetonitrile were purchased from Fisher Scientific (Illkirch-Graffenstaden, France) or VWR chemicals (Fontenay-Sous-Bois, France). Culture media were prepared with microbiology grade ingredients from VWR Chemicals, Fisher Scientific or Sigma-Aldrich. Demineralized water was used throughout all experiments.

2.2. Microorganisms and culture media

A strain of the filamentous fungus *Talaromyces helicus* previously isolated from an industrial contaminated soil, and selected for its PAH biodegradation properties, was used for this study. It was maintained on malt yeast extract agar medium (MYEA), at 22°C with a 12 h – 12 h light - dark cycle, and transplanted onto fresh medium every 10 days. A rich broth containing malt extract, yeast extract, peptone and casamino-acids (MYPC) was used for mycelium production in liquid cultures (recipes for all media are described in Table I.1).

A bacterial suspension “HC” for the biodegradation of hydrocarbons was kindly provided by Oxbiolab (Venette, France). This commercial preparation is intended for the remediation of soil polluted with linear hydrocarbons, and its precise composition is confidential. Bacteria are supplied as a suspension in a buffered medium at pH = 7, and stored at 4°C in the dark until use.

Mineral medium (MM1) at pH = 5.5 with 20 g/L glucose was used for all biodegradation tests unless specified otherwise, and MPYC was used as a rich medium for mycelium production in liquid pre-cultures. A stock solution of D-glucose (500 g/L) was prepared separately and added after autoclave when necessary. All solutions were sterilized by autoclaving (for media) or by filtration on a 0.2 µM syringe filter (for H_2O_2 and surfactants) before inoculation with microbial strains. For tests requiring varying carbon/nitrogen ratios, modified mineral media with higher or lower nitrogen content were prepared based on the recipe described in Table I.1, with varying concentrations of ammonium nitrate (NO_3NH_4) used as the sole nitrogen source (Table I.2).

Corynebacterium glutamicum (ATCC13032) was maintained in liquid culture in commercial brain-heart infusion broth (BHI) (Thermoscientific) or on TSA at 30°C. Modified GCXII medium (Hoffmann and Altenbuchner, 2014), a defined medium specifically designed for corynebacteria, was used for liquid pre-cultures.

Table I.1 : Media used for microbial cultures

Mineral medium pH = 5.5 (MM1)	qs 1L	
KCl	250	mg
$NaH_2PO_4.2H_2O$	1.54	g
Na_2HPO_4	8	mg
$MgSO_4.7H_2O$	244	mg
NO_3NH_4	1.0	g
Micro-nutrient solution	10	mL
Glucose 500g·L^{-1}	40	mL

Micro-nutrient solution for MM1 (100x)	qs 1L	
$ZnSO_4.7H_2O$	100	mg
$MnCl_2.4H_2O$	10	mg
$FeSO_4.5H_2O$	100	mg
$CuSO_4.7H_2O$	50	mg
$CaCl_2.2H_2O$	10	mg
MoO_3	20	mg

Malt-peptone-yeast rich medium (MPYC)	qs 1L	
Malt extract	10	g
Soy peptone	10	g
Yeast extract	4	g
Casamino-acid	2	g

Malt Yeast Extract Agar (MYEA)	qs 1L	
Malt extract	20	g
Yeast extract	2	g
Agar (Microbiological grade)	15	g

Tryptone Soy Agar (TSA)	qs 1L	
Tryptone	15	g
Soy peptone	5	g
NaCl	5	g
Agar (Microbiological grade)	15	g

Table I.1 : (continued) Media used for microbial cultures

Modified GCXII medium pH = 7	qs 1L	
MOPS	21	g
$(NH_4)_2SO_4$	5	g
Urea $CO(NH_2)_2$	5	g
KH_2PO_4	1	g
K_2HPO_4	1	g
$MgSO_4.7H_2O$	250	mg
$CaCl_2.2H_2O$	10	mg
Biotin 2g/L	1	mL
Micro-nutrient solution (1000x)	1	mL

Micro-nutrient solution for GCXII (1000x)	qs 1L	
$FeSO_4.7H_2O$	10	g
$MnSO_4.H_2O$	10	g
$FeSO_4.7H_2O$	1	g
$CuSO_4$	200	mg
$NiCl_2.6H_2O$	20	mg

Table I.2 : NO_3NH_4 concentrations in modified MM1 media

C/N ratio	$[NO_3NH_4]$ (mol·L^{-1})	qs 1L (g)
8	$3.58 \cdot 10^{-3}$	2.86
23 (standard MM1)	$1.25 \cdot 10^{-3}$	1.0
26	$1.10 \cdot 10^{-3}$	0.88
30	$9.50 \cdot 10^{-4}$	0.76
32	$8.88 \cdot 10^{-4}$	0.71

2.3. Biodegradation assays in batch cultures

The protocol for biodegradation assays was adapted from (Fayeulle, 2013). The experimental workflow is described schematically in Fig. I.1.

Mycelium in active growth phase is produced in MPYC medium in two steps. First, a spore suspension is prepared from solid cultures of *T. helicus* older than two weeks, by harvesting the spores from the surface in 10 mL of glucose-free MM1. Spores are then counted on a hemocytometer, and shaking flasks containing 50 mL of MPYC medium are inoculated with the spore suspension, the inoculation volume being adjusted so that the final concentration in pre-cultures is 10^4 spores/mL. The flasks are incubated 3 days at 22°C with a 12 h – 12 h light-dark cycle and orbital shaking. After 3 days, 5 mL of the first pre-culture was transferred to a new flask containing 50 mL of fresh MPYC medium. The second step pre-culture flasks were incubated for 2 to 5 days in the same conditions, until mycelium

was produced in a sufficient amount to inoculate all the shaking flasks needed for biodegradation assays. The mycelium was then harvested by vacuum-filtration on glass fiber filters with a Büchner funnel, rinsed with sterile MM1, chopped with a scalpel to separate the bigger pellets, and weighted.

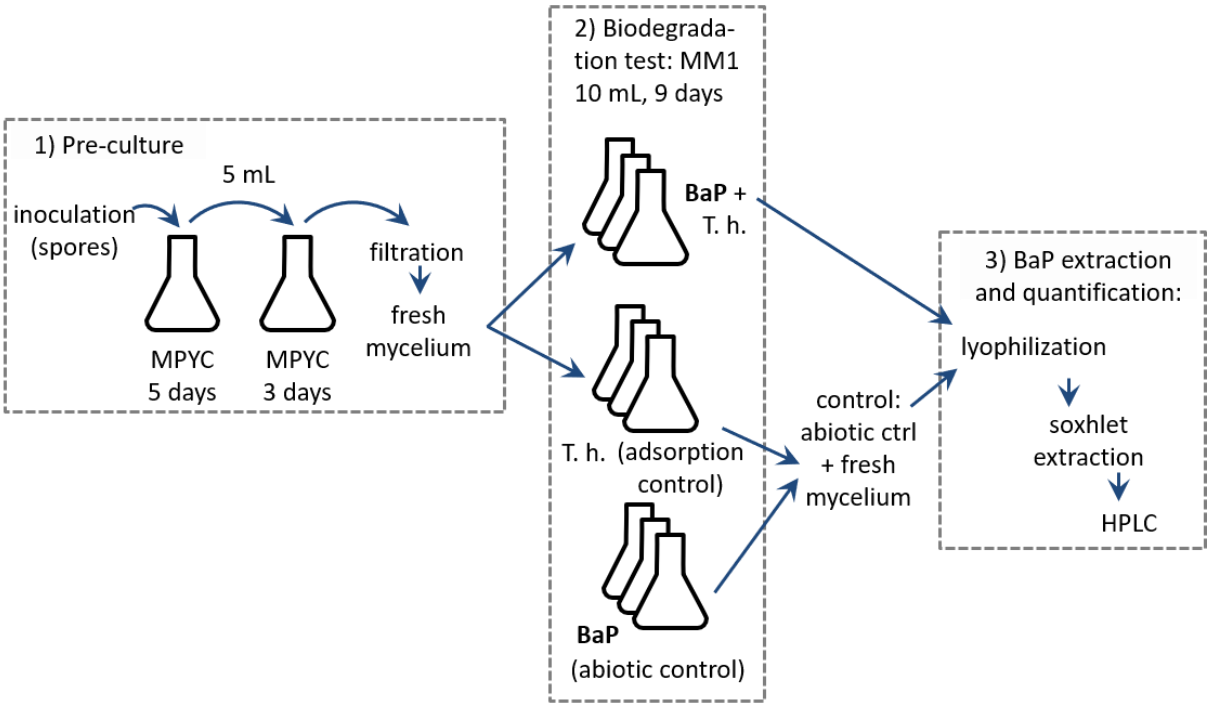

Fig. I.1 : experimental workflow of biodegradation assays in batch liquid cultures

Experimental conditions for BaP biodegradation tests, each tested in triplicate, were as follows:

- *T. helicus* (T.h.): 200 µg BaP is deposited in clean 50 mL shaking flasks by introducing 250 µL of a 0.8 mg/L stock solution in acetone and evaporating the acetone completely under a fume hood. 9.6 mL of MM1 is added to each flask. After autoclave, glucose stock solution is added to reach a concentration of 20 g/L in a final volume of 10 mL, and 75 mg of fresh mycelium is introduced in each flask. All flasks are incubated for 9 days at 22°C with a 12 h – 12 h light - dark cycle and orbital shaking. After incubation, all samples are frozen then lyophilized.

- Control (Ctrl): For the abiotic degradation control, BaP-containing flasks were prepared as described previously, but no glucose was added, and the flasks were not inoculated with mycelium. For the biosorption control, BaP-free flasks containing 10 mL of MM1 with 20 g/L glucose were prepared and inoculated with 75 mg fresh mycelium. All flasks were incubated for 9 days in the same conditions described previously. After incubation, the mycelium from each biosorption control was harvested by vacuum-filtration and transferred to one of the abiotic controls. The flasks were incubated for 10 min at room temperature with orbital shaking to allow sorption onto the mycelium, and then frozen.

- Carbon/nitrogen ratio (C/N): Test cultures were prepared as described for *T. helicus* alone, but using modified MM1 with C/N ratios of 8, 23, 26, 30 or 32 (see Table I.2)

- H_2O_2 : Test cultures were prepared as described for *T. helicus* alone, with an appropriate volume of 5% (w/v) H_2O_2 added before inoculation to reach final concentrations of $5{\cdot}10^{-2}$, $5{\cdot}10^{-3}$ and $5{\cdot}10^{-4}$ mol/L.

- Biostimulation with surfactants (SL and Tw20): Flasks containing 10 mL MM1 with 20 g/L glucose were prepared as described for *T. helicus* alone. Before inoculation with fresh mycelium, Sophoclean was added at $1{\cdot}10^{-2}$ g/L, $1{\cdot}10^{-1}$ g/L or 1 g/L, or Tween 20 at 0.01, 0.1 or 1 g/L

Code letters for all biodegradation experiments and the corresponding conditions tested are summarized in Table I.3.

Table I.3: Summary of all experimental conditions tested in liquid cultures

Exp.	Ctrl	T.h.	C/N	Tw20 (M)	SL (g/L)	H_2O_2 (mol/L)
A	x	x	23, 26, 30, 32			
B	x	x	8, 23, 30	10^{-6}, 10^{-5}, 10^{-4}		
C	x		23		0.01, 0.1, 1	$5{\cdot}10^{-2}$, $5{\cdot}10^{-3}$, $5{\cdot}10^{-4}$
D	x	x	23			

2.4. BaP extraction and quantification by HPLC analysis

Extraction - Residual BaP in the cultures was recovered with a soxhlet extractor. The lyophilized biomass was scraped off the inside of the shaking flasks with a spatula and transferred to a paper thimble. 100 mg of anhydrous magnesium sulfate was added to each thimble to absorb any residual moisture. The shaking flasks were then rinsed three times with 10 mL CH_2Cl_2 and the rinsing solvent was collected in round-bottom flasks used for the extraction. After adjusting the CH_2Cl_2 volume to 50 mL, the round-bottom flasks and sample thimbles were placed in the soxhlet extractor and heated to reflux at 60°C for 16 h.

The extracts were then concentrated in 1.5 mL glass vials under an air flow until the volume was under 700 µL, then each sample was filtered with a PTFE syringe filter to eliminate any residual impurities, and completed with an equal volume of acetonitrile (CH_3CN). A standard concentration scale was prepared by dissolving 10, 50, 100 and 250 µg BaP in 1:1 CH_2Cl_2:AcN, as well as a blank with the same solvent mixture.

HPLC quantification - Samples were analyzed by HPLC using a C18 reverse-phase column (Syncronis aQ, Thermoscientific, bed dimensions 250 x 4.6 mm, particle size 5 µm). BaP was eluted with an acetonitrile:water gradient from 75:25 to 100:0 over 25 min, at a solvent flowrate of 1 mL/min. BaP was detected at 380 nm as a single peak at 20 min of elution, and its concentration was calculated by measuring the peak area and comparing it to the standard scale. The residual mass of BaP m_{spl} in each sample was then calculated in µg by multiplying the concentration with the known sample volume. The residual quantity in the control sample m_{ctrl} represented 0% of biodegradation, the loss of BaP being only due to abiotic degradation, sorption onto the mycelium and loss during the extraction procedure. The biodegraded mass of BaP was expressed as the difference between the control and each sample, and biodegradation rates D were calculated as the ratio between mass loss in samples and residual mass in the control.

Degradation rate = 1-(residual mass in sample)/(residual mass in control)

$$D(\%) = 1 - \frac{m_{spl}}{m_{ctrl}}$$

The dispersion of values in each triplicate is represented by the standard deviation. In order to evaluate the significance of differences between each condition, an unpaired bilateral Student's t-test was performed for each couple of conditions. Conditions were considered significantly different for $p < 0.05$.

2.5. Soil samples

Samples of contaminated soil from three polluted sites were supplied by the partner company Oxbiolab (Venette, France). Relevant information regarding each sample's characteristics and analysis results for the site of origin are summarized in Table I.4. Preliminary analyses of soils from Noisy-le-Sec were conducted by Eurofins (Saverne, France) through acetone/hexane extraction followed by GC/FID (total hydrocarbon content) or GC/MS/MS (PAH and PCB). The total hydrocarbon content in soil from Ecommoy was analyzed at Flandres Analyses (Cappelle-la-Grande, France) by solvent extraction followed by GC/FID.

Soil samples were manually rid of bigger debris such as stones, wood, scrap metal and glass shards. Samples were then spread onto plastic trays and left to dry at room temperature under a fume hood for a week. They were mixed manually every day and bigger clumps are broken by hand, to ensure that the distribution of both contaminants and microflora is as uniform as possible. Dry soil was then sifted through a 2 mm sieve. Aggregates bigger than 2 mm were ground for 30 s with an IKA M20 mill (Ika Werke, Staufen, Germany) until a fine powder was obtained. The powder was weighted and mixed

with the sifted fraction in the same proportions for each soil. Residual water content was measured by weighting a sample of soil (≈ 1 – 2 g) before and after overnight drying in a 105°C oven. Samples were then stored in closed vessels at 4°C in the dark until use for biodegradation assays.

Table I.4 : Soil sample characteristics and indicative contamination levels.

	1	2	3
location	Noisy-le-Sec	Ecommoy	Noisy-le-Sec
Origin of the contamination	industrial	Construction vehicle fire	industrial
description	Light-colored, clay-limestone like texture	Dark, humus-like with many plant debris	Light-colored, sandy texture
Total hydrocarbon content (C10-C40)	442 mg/kg	9550 mg/kg	94.3 mg/kg
PAH content (16)	3.4 mg/kg	n/a	2.6 mg/kg
BaP content	0.27 mg/kg	n/a	0.21 mg/kg
pH	(9.2 – 9.4)*	(6.8)*	10.5
* pH in soils n° 1 and 2 was only measured after incubation in microcosms; no data was available about the site of origin			

2.6. Biodegradation assay in soil samples

Pozzolana granules were purchased from a gardening supplies store and used as an inert substrate to carry the micro-organisms and inoculate soil microcosms. Granules measuring between 1 and 1.5 cm were sorted and autoclaved in distillated water. Shake flasks containing 50 mL MM1 were prepared and 30 pozzolana granules were added per flask. Media were then inoculated with a spore suspension of *T. helicus* prepared as described in section 2.3 to reach a final concentration of 10^4 spores/mL, and incubated for 8 days at 22°C. When bacteria were used, the bacterial suspension was added in the same shaking flasks containing the fungus after 6 days of preculture to reach a final density of 10^4 bacterial cells/mL, and media were supplemented with 1 mL of glucose stock solution (500 g/L). For assays with *C. glutamicum*, modified BHXII medium was used for the co-culture instead of MM1.

Biodegradation tests were performed in 500 mL glass bottles. 120 g of dry unsterilized soil is introduced in each bottle, and distillated water is added so that the soil is visibly moist but not saturated. The final water percentage (w/w) was 10% for soil n°1, 25% in soil n°2, and 13% in soil n°3. Pozzolana granules carrying the micro-organisms are then mixed in and the wet soil is packed with a

flat spatula to a density of 1.3 g/cm^3. In microcosms containing sophorolipids, the soil was wetted with a sterile solution of sophorolipid at 1 g/L in place of distilled water.

The soil microcosms were incubated for 30 days or 4 months in the dark at room temperature. The atmosphere was renewed once a week by placing the open bottles for 30 s under a compressed air flow. After incubation, soil samples were transferred to plastic dishes and dried for a week under a fume hood, then shipped for analysis at Eurofins (Saverne, France) to quantify residual contaminants. Briefly, soil samples were analyzed through acetone/hexane extraction followed by GC/FID (total hydrocarbon content) or GC/MS/MS (PAH and PCB). The lower quantification threshold was 15 mg/kg (dry soil weight) for hydrocarbons, 0.05 mg/kg for individual PAH, and 0.01 mg/kg for individual PCB.

Table I.5 : Summary of tests performed on each soil sample (each condition in triplicate), water percentage and incubation times: 1 or 4 months

n°	Sample name	Water percentage (mL/g DW)	*T. helicus*	Bacterial suspension « HC »	*C. glutamicum*	Sophoclean
1	Noisy E4	0.11	1m/4m	4m	1m	1m
2	Ecommoy	0.35	1m	1m		
3	Limed soil	0.19	1m	1m		
			Incubation time (months)			

2.7. Data analysis

Data obtained was treated using the Microsoft Excel 2010 software. The mean residual content in pollutants of each family was calculated for each triplicate, and expressed in mg/kg of dry weight. When the content in a particular chemical compound was below its quantification threshold, the value was considered to be zero. The dispersion of values in each triplicate is represented by the standard deviation. In order to evaluate the significance of differences between each condition, an unpaired bilateral Student's t-test was performed for each couple of conditions.

3. Biodegradation of BaP in liquid cultures

3.1. Biodegradation with *T. helicus* in mineral medium

Testing the biodegradation of a given compound in liquid mineral medium is a rapid and simple way to assess the biodegradation abilities of a microorganism or microbial consortia, with complete control over the nutritional environment and specifically carbon and nitrogen sources. Several degradation

tests were carried out to evaluate the degradation rate over 9 days of incubation. Here, experiments were run with 200 g of BaP initially introduced in each flask for 10 mL of mineral medium unless specified otherwise. BaP loss measured at the end of the experiment accounts for a combination of biodegradation, abiotic degradation, sorption to the mycelium, and loss during the extraction itself. Biodegradation rates may vary depending on the initial quantity introduced: indeed, BaP abundance may affect the metabolic state of the fungus and favor hydrocarbon-degrading metabolic pathways. Sorption onto the mycelium is likely solely dependent on the quantity of biomass, and there would be a maximal amount of BaP that can be sorbed per mg of mycelium. As a result, BaP loss may not be proportional to the initial amount introduced.

The quantity of BaP recovered in controls was relatively consistent between experiments, amounting to 170 ± 43 µg for experiments where 200 µg of BaP was initially introduced in each flask (Fig. I.2). The amount recovered in experiments A, B and C was not significantly different. The recovery yield in controls was 85% (± 22%) on average, which represent 15% loss due to abiotic degradation, adsorption to the mycelium and loss during the extraction procedure combined.

Experiment A showed a decrease of the BaP quantity compared to the control, with 63.5 ± 10 g of BaP recovered. In contrast, no significant degradation occurred in exp. B, where the residual quantity in flasks inoculated with *T. helicus* was 111.7 ± 22 µg. The average degradation rate for both experiments was 38%, which is consistent with previous results obtained with the same strain (Fayeulle et al., 2019). However the variation between experiments is significant, this variation could be in part explained slight differences in incubation times for the pre-cultures, resulting in mycelium at different growth stages.

Experiment D was run with 500 µg BaP initially introduced in each flask, while 371 ± 22 µg BaP was recovered from the control, and 63.5 ± 10 µg from samples incubated with *T. helicus* (Fig. I.2). The recovery yield for the control was 74%, which is within the range found for experiments carried out with 200 µg. It must be noted that losses may not be proportional to the initial amount; a fixed amount may be adsorbed to the mycelium and/or lost during extraction. The degradation rate was 75% for this experiment, which is higher than the average degradation rate found when 200 µg BaP was initially introduced (exp. A, B, C). The ratio between BaP quantity and total volume was conserved across experiments, however since BaP is not soluble in the medium, biodegradation rates by the fungus may be influenced by the volume of the culture. In experiment C, biodegradation conditions with *T. helicus* alone in standard MM1 were not tested, hence the lack of data shown on the graph.

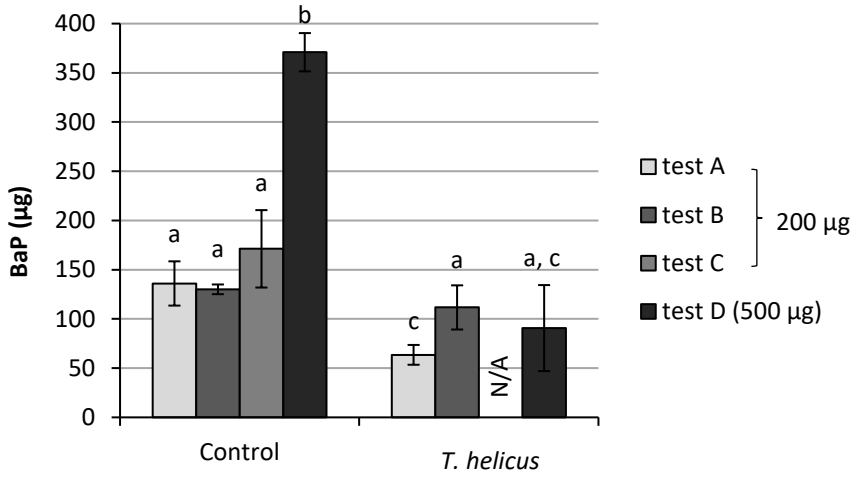

Fig. I.2 : Residual BaP mass after 9 days of incubation in control flasks vs flasks inoculated with *T. helicus* in 10 mL of mineral medium supplemented with 200 µg BaP (or 25 mL MM with 500µg BaP in the case of test D). Groups of values that are not significantly different are indicated with the same letter.

3.2. Influence of the nitrogen supply

Nitrogen supply in the soil is one of the major parameters determining the metabolic state of living organisms and their trophic interactions. Nitrogen enrichment was found to enhance hydrocarbon removal from soils through natural attenuation (Silva-Castro et al., 2013) or bioaugmentation with both ligninolytic and non-ligninolytic fungal strains (Lladó et al., 2012; Azin et al., 2018). In *P. chrysosporium,* the degradation of PAH yields different metabolites depending on the nitrogen supply in the medium, indicating different metabolic pathways influenced by nitrogen supply in white rots: quinones were preferentially produced under low-nitrogen conditions, as opposed to dihydrodiols in high-nitrogen conditions (Cerniglia and Sutherland, 2010). This suggests that high nitrogen in the medium may promote the intracellular pathway in white rots. However, so far there is no evidence of a similar mechanism in non-ligninolytic fungi, where degradation mainly occurs through the P-450 monooxygenase pathway. On the contrary, Fayeulle et al. (2019) found lower PAH biodegradation rates in N-enriched conditions with *Talaromyces helicus*, when tests were conducted in soil microcosms. The authors hypothesized that nitrogen may stimulate the development of the native microflora competing with *T. helicus* and thereby hinder the PAH removal efficiency of the fungus. Incidentally, there is evidence of some fungi developing particularly well in nitrogen-starved conditions, by efficiently scavenging nitrogen from substrates with high C/N ratios, and relocating it within the mycelium (Watkinson et al., 2006).

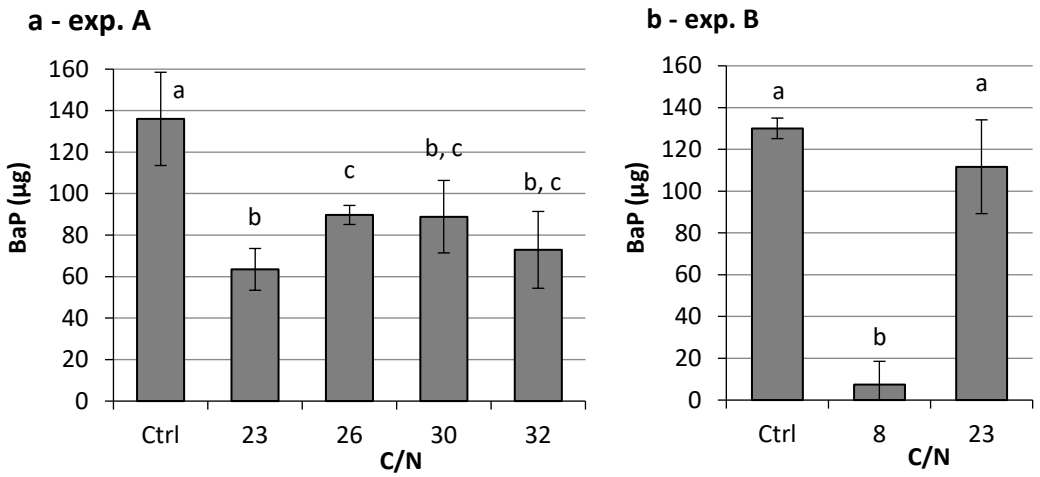

Fig. I.3 : Residual BaP mass after 9 days of incubation in cultures inoculated with *T. helicus* in 10 mL of modified mineral medium with varying supplies of nitrogen. Groups of values that are not significantly different are indicated with the same letter - a: exp. A (C/N = 23, 26, 30 or 32) – b: exp. B (C/N = 8 or 23)

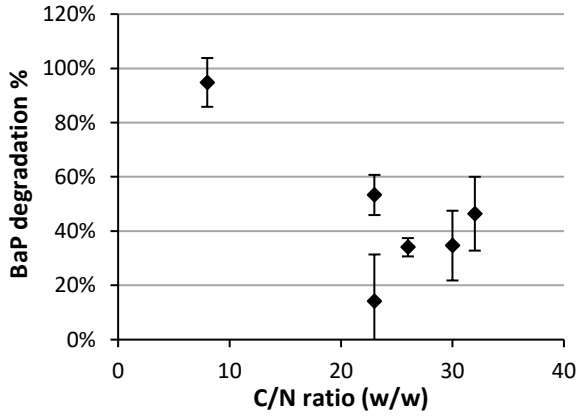

Fig. I.4: BaP degradation by *T. helicus* in exp. A and B expressed as a percentage of the quantity recovered in control flasks, depending on the C/N ratio of the medium

The influence of carbon/nitrogen ratio on the biodegradation efficiency was tested in liquid cultures. Several modified mineral media were prepared based on the MM1 recipe, with a fixed glucose concentration as sole carbon source, and varying ammonium nitrate concentrations as the sole nitrogen source. MM1 has a C/N ratio of 23. One N-enriched medium with a C/N ratio of 8 and three N-depleted media with C/N ratios of 26, 30 and 32 were used. Two separate experiments were carried out: the first one (exp. B) comparing the standard MM1 with the enriched medium (C/N = 8) and the deprived medium (C/N = 30), the second one (exp. A) comparing the standard MM1 with three N-depleted media (C/N = 26, 30 and 32).

The results of exp. B presented in Fig. I.3.b show that fungal biodegradation in N-enriched medium (C/N = 8) was extremely efficient, reaching about 90% compared to the control. In contrast,

degradation rates in the N-depleted media (C/N = 26, 30 or 32) were lower or equivalent to the standard medium, as shown by exp. A. (Fig. I.3.a). The average biodegradation rates for carbon/nitrogen ratios of 23, 26, 30 and 32 were respectively 53%, 34%, 35% and 46%. Above C/N = 23, no particular tendency could be observed in function of C/N variations, as degradation percentages were not significantly different from each other (Fig. I.4). These results indicate a stimulating effect on BaP biodegradation by *T. helicus* when the medium is supplemented with a nitrogen source. It is apparently contradictory with the results found by Fayeulle et al. (2019) with the same species, however the authors considered the total PAH content and not only BaP, and the study was conducted in soil microcosms in presence of the native microflora. Incidentally, nitrogen supply may affect specific biodegradation pathways rather than the overall biodegradation efficiency, in a similar way to white rots.

3.3. Combined biodegradation and chemical oxidation with H_2O_2

In non-ligninolytic fungi, an alternative PAH degradation pathway was proposed involving non-enzymatic oxidation by reactive oxygen species (Rafin et al., 2006). Fenton-like degradation can occur when hydrogen peroxide (H_2O_2) from the fungal metabolism reacts with ionic iron and forms free radicals able to oxidize aromatic rings. This oxidation process was associated with high rates of mineralization, yielding more rapid ring fission than the more commonly described cytochrome P450 pathway. Chemical oxidation with H_2O_2 can also be used as a pre-treatment before bioremediation, which has been shown to enhance the biodegradation of diesel by the autochthonous microbial flora in contaminated soil (Silva-Castro et al., 2013).

In exp. C, H_2O_2 was added to test whether it could enhance the biodegradation of BaP by combining native enzymatic activities of *T. helicus* with chemical oxidation. Biodegradation tests were run with *T. helicus* in medium supplemented with H_2O_2 in increasing concentrations ($5{\cdot}10^{-2}$, $5{\cdot}10^{-3}$ and $5{\cdot}10^{-4}$ mol/L). After 9 days of incubation, a significant degradation of BaP was recorded in the cultures containing H_2O_2 at $5{\cdot}10^{-2}$ mol/L (Fig. I.5). Lower concentrations of hydrogen peroxide ($5{\cdot}10^{-3}$ and $5{\cdot}10^{-4}$ mol/L) inhibited the biodegradation by *T. helicus*, as residual BaP amounts found in the samples were higher than without H_2O_2 (Fig. I.5). This could be explained by toxicity towards the fungus. Indeed, *T. helicus* cultivated with $5{\cdot}10^{-2}$ mol/L H_2O_2 showed reduced biomass at the end of incubation compared to the cultures without H_2O_2. Lyophilized cultures contained a high amount of residual glucose that was not consumed during fungal growth, forming a viscous caramel-like substance that was not found in cultures without hydrogen peroxide. Considering that the fungus did not develop properly in cultures with $5{\cdot}10^{-2}$ mol/L H_2O_2, the degradation observed is likely mainly due to chemical oxidation of BaP rather than biodegradation. In cultures with $5{\cdot}10^{-3}$ and $5{\cdot}10^{-4}$ mol/L H_2O_2, it appears that the H_2O_2

concentration was sufficient to inhibit fungal growth and biodegradation of BaP, but too low to enable the chemical oxidation of BaP. Another explanation for the low degradation rates is the inactivation of fungal peroxidases due to the presence of excess hydrogen peroxide (Valderrama et al., 2002). This suggests that peroxidase activities are responsible for BaP oxidation by *T. helicus*. Indeed, peroxidase activities have been described in non-ligninolytic fungi including manganese-peroxidases (Fayeulle, 2013) extracellular lignin-peroxidases or laccases (Cao et al., 2020), or to the intracellular peroxidation of neutral lipids (Delsarte et al., 2018).

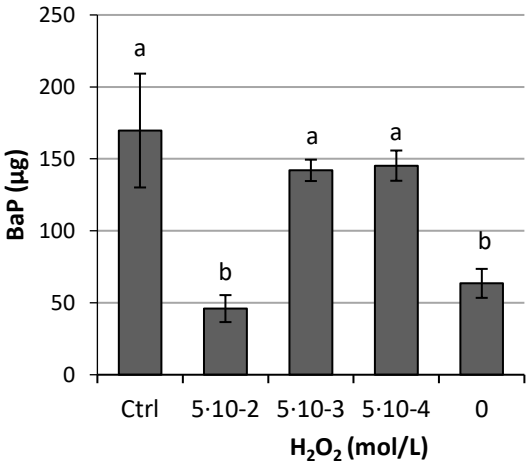

Fig. I.5 : Residual BaP mass after 9 days of incubation with *T. helicus* in 10 mL of mineral medium supplemented with increasing concentrations of H_2O_2 ($5 \cdot 10^{-4}$, $5 \cdot 10^{-3}$ and $5 \cdot 10^{-2}$ mol/L) or without H_2O_2 (value from exp. A). Groups of values that are not significantly different are indicated with the same letter.

3.4. Biodegradation in presence of surfactants

The addition of surfactants to contaminated soil is a common strategy to enhance the removal of hydrophobic contaminants, either as a washing method before extraction, or to assist bioremediation protocols. The supplementation of surfactants in soils can, on one hand, increase the bioavailability of bound HOC and render them more effectively degraded by micro-organisms, and on the other hand, inhibit microbial activity either because of inherent toxicity or by increasing the exposure to mobilized toxic contaminants (Ortega-Calvo et al., 2013). Tween 20 is a non-ionic polysorbate detergent commonly used in life sciences, as well as in pharmaceutical preparations due to its very low toxicity. Being a widely available, non-toxic and relatively cheap synthetic surfactant, Tween 20 has been investigated as a biostimulation agent for the remediation of aged contaminated soils (Leonardi et al., 2007). Low concentrations of synthetic surfactants including Tween 20 and SDS can enhance the biodegradation of PAH by bacteria, but the effect depends on the combination between strain,

surfactant and pollutant considered (Rodrigues et al., 2013). It is therefore useful to conduct studies at a laboratory scale beforehand to identify relevant strategies.

Bio-surfactants, and especially bacterial surfactants, have drawn a growing interest for their potential applications in soil remediation, rhamnolipids from *Pseudomonas aeruginosa* were for example used to assist the fungal remediation of aged oil-contaminated soil (Lladó et al., 2012). Bacterial surfactants can also be used to wash soils spiked with aromatic and heterocyclic organic pollutants (Ivshina et al., 2016). Bio-surfactants raised interest for two reasons: (i) – they can be produced from microbial fermentations without the need of petroleum-based synthesis, and (ii) – They are usually biodegradable in the environment, which is an interesting feature for sustainable remediation applications. Indeed, biodegradability of the molecules used is a concern, since surface-active compounds can durably disturb the biodiversity and soil wetting properties if they persist after the treatment, or leach into surface and groundwater. However, the applications of biosurfactants for large-scale uses such as contaminated soil treatment are still hindered by high production costs. Bio-based synthetic surfactants with good biodegradability are a cheaper alternative.

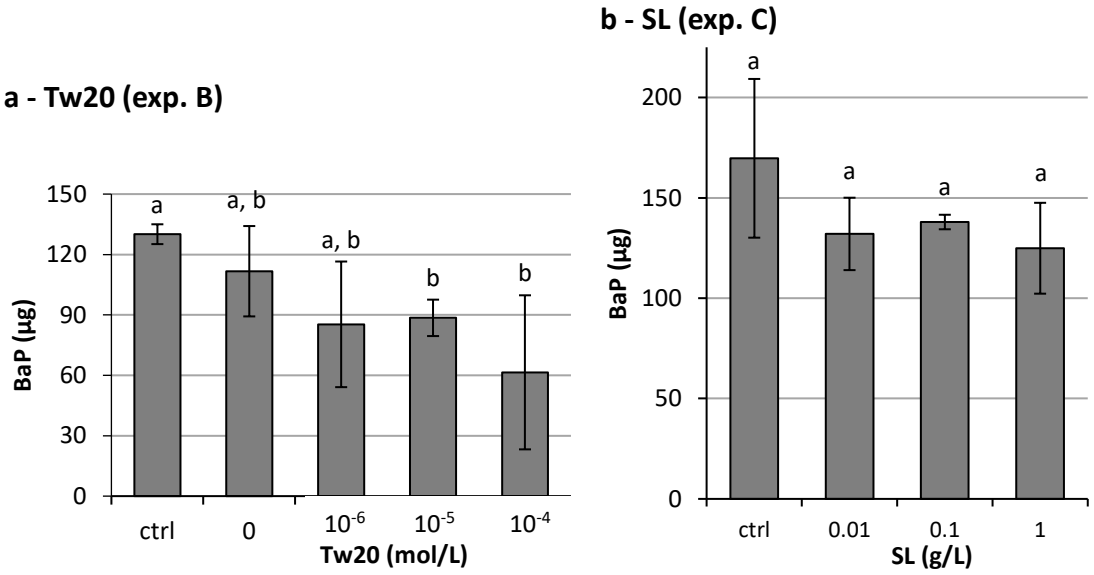

Fig. I.6 : Residual BaP mass after 9 days of incubation in control flasks vs flasks inoculated with *T. helicus* in 10 mL of mineral medium supplemented with surfactants : Tween 20 (Tw20) from 10^{-6} to 10^{-4} mol/L or Sophoclean (SL) from 10^{-2} to 1 g/L. Groups of values that are not significantly different are indicated with the same letter.

Here the effect of two surfactants on BaP biodegradation by *T. helicus* was tested: Tween 20 (exp. B) and the sophorolipid detergent Sophoclean (exp. C). The commercial surfactant Sophoclean itself is not a bio-surfactant, since it is chemically synthesized from plant-based raw materials. However sophorolipids are a class of glycolipid biosurfactants found in a wide number of fungal strains,

particularly yeasts. Surfactants were added in concentrations near their respective critical micelle concentration (CMC) and below. Values given for the CMC of Tween 20 in the literature are $5.1 \cdot 10^{-5}$ mol/L (Patist et al., 2000) or $8 \cdot 10^{-5}$ mol/L (Lu, 2016). According to the value given by the manufacturer, the CMC of Sophoclean is 30 to 50 mg/L (Agrobiobase, 2013).

In cultures where Tween 20 was added, residual BaP quantities were not significantly different from each other, however significant degradation of BaP was observed for concentrations near the CMC compared to the control. Degradation rates amounted to 32% at $1 \cdot 10^{-5}$ mol/L and 53% at $1 \cdot 10^{-4}$ mol/L. These degradation rates were higher but not significantly different from those recorded in surfactant-free cultures, showing that Tween 20 has little to no impact on the biodegradation efficiency for *T. helicus*, possibly slightly enhancing it. The surfactant may not be present in sufficient concentration to efficiently mobilize BaP, concentrations above the CMC could be tested to confirm whether this is the case. On the other hand, BaP bioavailability may not be a limiting factor in these conditions. Besides, high concentrations of Tw20 may lead to their preferential degradation by the fungus, as was observed by Kim and Weber (2003): for Tw20 concentrations above the CMC, which enhances the micellar solubilization of phenanthrene, some hydrocarbon-utilizing strains would preferentially degrade the surfactant rather than recalcitrant PAH, thus nullifying the effect of Tw20 on PAH bioavailability.

The addition of sophorolipid did not appear to enhance biodegradation, and may even have an inhibitory effect. The dispersion of values in each triplicate was high, and the residual amount after biodegradation for each concentration was neither significantly different from the control, nor between concentrations (Fig. I.6). When SL was added, the biodegradation rates for each concentration were 22%, 29% and 26% for SL concentrations of 0.01, 0.1 and 1 g/L respectively. This is significantly lower than the average biodegradation rate obtained with *T. helicus* in plain mineral medium in exp. A, but equivalent to the degradation obtained in exp. B (section 3.1).

The apparent inhibition of fungal degradation by added sophorolipids may have several explanations: (i) It could be due to a toxicity of the sophorolipid towards the fungus, impairing its normal growth by interfering with membranes and cell wall components. Indeed, some natural sophorolopids from yeasts can have antifungal properties (Sen et al., 2017). (ii) Another explanation is the preferential consumption of the surfactant itself as a carbon source by the fungus, since it is more readily biodegradable than BaP. A similar effect was reported during fungal biodegradation of PAH with added Tween 80 (Kotterman et al., 1998). Due to their chemical structure, the biodegradation of sophorolipid surfactants is likely to involve lipid metabolism and fatty acid oxidation pathways. Sophorolipids may

thus act as competitors of BaP for non-selective oxidation. (iii) Finally, the addition of surfactants may increase the toxicity of PAH to the fungus by increasing their bioavailability.

The accessibility of BaP is not a limiting factor for its biodegradation in liquid batch cultures, since the fungus is grown in a homogenous environment continuously shaken to maximize exchanges, and comes in direct contact with the BaP source. However BaP supplied as solid crystals is not necessarily in a bioavailable form, since it dissolves in the medium only in minute amounts. The addition of surfactants may enhance the partitioning of BaP in the aqueous phase through facilitated diffusion, however this will not have any effect on the efficiency of degradation if the pollutant reaches the cell surface faster than it can be incorporated and/or degraded. In this case either the degradation pathways are limiting, or the absorption mechanism. Moreover, *T. helicus* appears to be able to incorporate BaP through direct contact with solid particles suspended in the medium, as described in chapter IV. Surfactants may mediate the contact between the hydrophilic cell wall and the very hydrophobic crystals, and/or facilitate its crossing through the cell membrane by permeating the lipid bilayer.

3.5. Analysis of produced benzo[*a*]pyrene metabolites

Degradation products of PAH, and more specifically hydroxylated derivates including phenol, carboxy- and dihydrodiol compounds or sugar conjugates, are typically more reactive and more soluble in water than the original pollutants (Boll et al., 2015). Some of them such as quinones are toxic, and their greater mobility in water phase causes a higher risk of exposition compared to the parent PAH, hence the need to investigate the nature and potential toxicity of metabolites released during bioremediation processes. In this section, the detection of unidentified metabolites during BaP biodegradation by *T. helicus* is discussed.

Upon HPLC analysis, BaP was detected as a single peak at 20.2 min in standard scale vials, and the same peak was visible in degradation test samples (Fig. I.7).

On chromatograms obtained after degradation in N-enriched medium, four additional peaks were detected, which were not visible in standard mineral medium (Fig. I.7.b): a higher peak (n°3) at 17.8 min with roughly the same area as the BaP peak (37.5 mAU·min, compared to 36.7 mAU·min for BaP at 20.2 min), and smaller ones at 11.3 min (n°1), 11.9 min (n°2) and 19 min (n°4) with areas of 2.6, 1.4 and 2.2 mAU·min respectively. In samples presenting the highest degradation rates, the BaP peak was still visible considerably smaller than shown in Fig. I.7 (1.8 and 0.8 mAU·min), while peak n°3 became the main one with areas of 64.9 and 108.6 mAU·min respectively. These additional peaks could

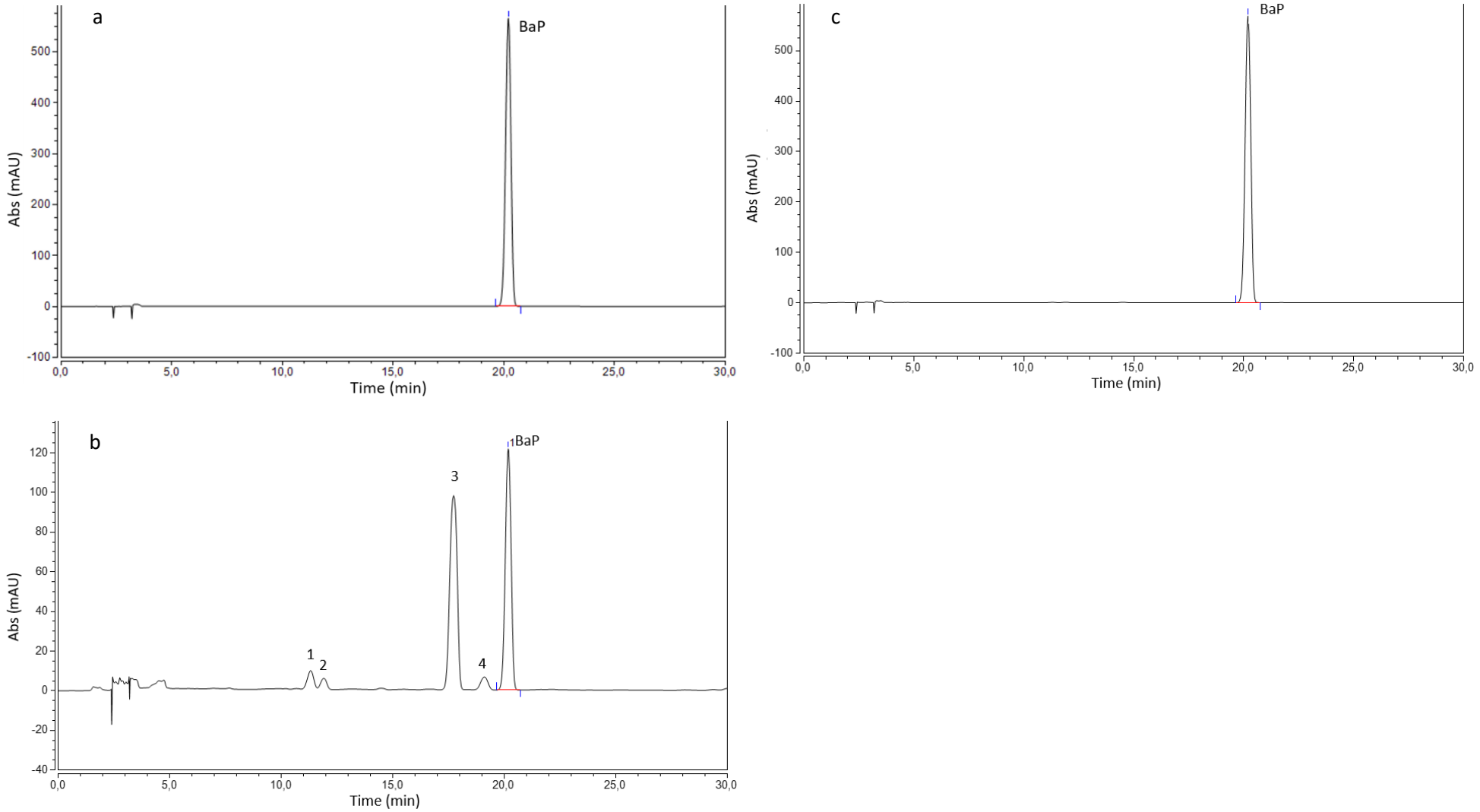

Fig. I.7: Chromatograms obtained after biodegradation in standard MM1 C/N=23 (a), in N-enriched MM1 C/N=8 (b), and for a pure BaP standard (c). BaP is detected as a peak at ~20.2 min.

correspond to BaP derivatives produced during fungal degradation, displaying a lower hydrophobicity since their retention times on the C-18 resin is shorter than that of native BaP.

In non-ligninolytic fungi, including *Cuninghamella elegans* (zygomycetes), *Aspergillus*, *Penicillium, Trichoderma* and *Fusarium* species (ascomycetes), intracellular oxidation through the cytochrome P450 mono-oxygenase pathway appears to be the dominant metabolic pathway for the degradation of aromatics. The initial reaction of conjugated cycles with dioxygen yields unstable arene oxides that are further hydrated by an epoxide hydrolase or non-enzymatically rearranged into a phenol (Cerniglia and Sutherland, 2010). Dihydrodiols have also been identified as products of BaP metabolism through the P450 pathway in *Fusarium sp.* (Chulalaksananukul et al., 2006).

Oxidation products such as dihydrodiols or phenolic compounds, which are more polar than the unsubstituted BaP molecule, could account for the peaks n°1, 2, 3 and 4. Since peak n°3 is the main one, BaP aside, it is likely a stable metabolite that accumulates, or a slowly-degraded intermediate, while peak n°4 could be associated to a transitory intermediate. When summing all peaks for each N-enriched test sample, the total areas were 80.4, 73.1 and 118.8 mAU·min respectively. This result is consistent with the hypothesis of a stable metabolite detected as a peak at 17.8 min: BaP may be first converted to metabolite n°3, which would accumulate until reaching a concentration in the same order of magnitude as the initial BaP concentration. High nitrogen content in the medium thus appears to favor the metabolic pathway responsible for the accumulation of metabolite n°3. However these results are not sufficient to conclude on whether metabolite n°3 is further metabolized at a slower rate than the initial reaction, or whether it is an end-product of degradation in these conditions.

On chromatograms obtained with samples incubated with H_2O_2 at $5 \cdot 10^{-2}$ mol/L, small peaks are visible at 11.5, 12 and 17 min in addition to the main BaP peak at 20.2 min (Fig. I.8). Their elution times are similar to those of peaks n° 1, 2 and 3 observed in samples with N-enriched medium (Fig. I.7.b). In this experiment with H_2O_2, peak n°3 is much lower than it was in N-enriched medium, which suggests that either the metabolic pathway involved is inhibited under these conditions, or that the metabolite is further degraded. As it was pointed out in section 3.3, chemical oxidation rather than biodegradation is likely to be dominant in these samples. The degradation products detected may therefore be formed through an H_2O_2-mediated oxidation mechanism.

Gao et al. (2019) analyzed the degradation products of several PAH by a *Talaromyces verruculosus* strain after 72 h, and obtained chromatograms displaying three peaks occurring earlier during elution than the BaP peak. Taking into account the fact that the authors used different elution conditions, the elution times of these peaks are roughly proportional to those found in our study. The corresponding metabolites are thought to be carboxylic acid, phenol and benzaldehyde derivatives of BaP, possibly

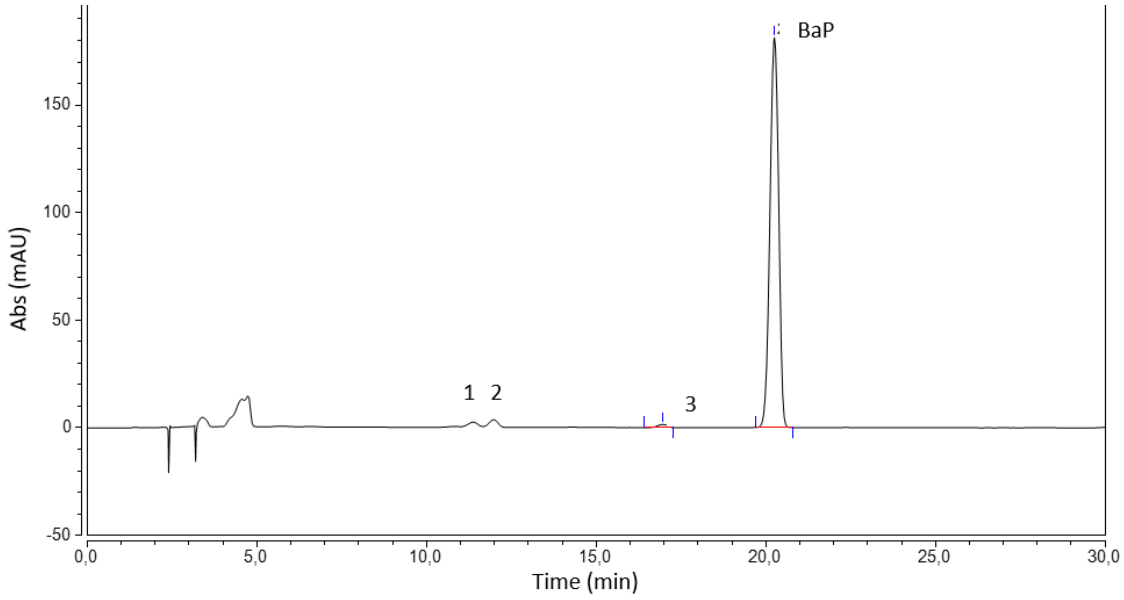

Fig. I.8 : Chromatogram of a sample incubated with *T. helicus*, H_2O_2 $5 \cdot 10^{-2}$ mol/L. BaP is detected at 20.2 min. Additional peaks are visible at 11.5 min, 12 min and 17 min.

ring cleavage products of hydroxylation through the cytochrome P450 (Gao et al., 2019). The production of polar metabolites has also been reported during the degradation of BaP by the ligninolytic fungus *Phanerochaete laevis* (Bogan and Lamar, 1996). The authors observed the production of quinones as degradation intermediates during BaP oxidation, but no accumulation of this compound in the cultures. In the experiments presented here, peak n°3 could correspond to such a quinone derivative: indeed, its elution time is proportional to that reported by Bogan and Lamar (1996), relatively to the elution time of BaP. Quinones are part of the metabolites produced during the biodegradation of PAH by ligninolytic enzymes. The aerobic degradation of PAH by ligninolytic fungi involves the unspecific oxidation of aromatic cycles through the release of reactive oxygen species (ROS) and other oxidated species (such as free radicals or Mn^{3+} ions) by manganese peroxidase (MnP) and laccase (Lac) activities. Although manganese peroxidases are generally considered specific to ligninolytic basidiomycetes, MnP activities have been found in several ascomycetous strains including *T. helicus* during the biodegradation of BaP (Fayeulle, 2013). Some non-basidiomycetous soil dwelling fungi can also present lignin-degrading activities (Saparrat et al., 2000). This is the case of *Fusarium sp.*, which is able to metabolize BaP into BaP-quinones usually typical of the ligninolytic pathway, and into dihydrodiols from the P450 pathway (Verdin et al., 2004; Chulalaksananukul et al., 2006). LiP and Lac activities associated with BaP degradation were also identified in the ascomycete *Lasiodiplodia theobromae* (Cao et al., 2020). These results suggest that the divide between ligninolytic and non-ligninolytic fungi may not be as clear as was previously thought, and underline the importance of such enzymatic activities for the degradation of recalcitrant aromatic pollutants. The production of BaP-

quinones by *T. helicus* should therefore not be excluded, and this hypothesis is consistent with a degradation pathway involving peroxidase activities. Further characterization of the metabolites through mass spectrometry, and identification of enzymatic activities would be needed to elucidate the degradation pathways.

4. Biodegradation in soil microcosms

The biodegradation abilities of *T. helicus* and of the commercial bacterial suspension HC were assessed in soil microcosms, using soil samples from three polluted sites. The use of contaminated environmental samples was chosen over artificial spiking, in order to more accurately reflect the situation of aged contaminations. As time passes, natural attenuation of the most readily available compounds leads to an enrichment of the remaining fraction in recalcitrant and/or the least bioaccessible contaminants. As a result, HOC in freshly contaminated soils are generally regarded as more bioavailable than in an aged contaminated soils (Burgess et al., 2003). Through a partnership with the company Oxbiolab, four soil samples from three contaminated sites were kindly provided for this study, as well as a bacterial suspension for hydrocarbon degradation, commercialized under the name “solution HC”. These soil samples presented very different characteristics described in the following sections, both in terms of physico-chemical properties of the soil matrix, and contamination levels. The soils were left unsterilized to preserve the endogenous micro-organisms, again in order to achieve conditions as close as possible to an actual soil bioremediation. Indeed, competition with autochthonous flora is one of the limitations to the efficient development of exogenous micro-organisms introduced for bioremediation, even when these micro-organisms prove efficient *in vitro*.

4.1. Biodegradation assays in soil from Ecommoy

4.1.1. Effect of endogenous microflora and abiotic factors on contamination

Sample n°2 came from a rural area near Ecommoy in the Pays de la Loire region, and was collected after a construction engine caught on fire, causing a heavy local contamination with hydrocarbons. Oil and tar “patties” visible to the naked eye were found in the sample. The soil was dark colored and contained many plant debris (dead leaves, twigs, etc.), reminiscent of a forest soil. Under the binocular microscope, the texture appears heterogeneous, with coarser particles mixed in a darker humus-like matrix (Fig. I.9.b). Preliminary analysis provided with the soil sample revealed a total hydrocarbon content of 9550 mg/kg. This high hydrocarbon content is very likely due to the contamination being recent, and the sample originating from a location close to the source. No information was available regarding the detailed composition of organic contaminants in soil n°2. However the pH measured after incubation microcosms was neutral (6.8), which suggests favorable conditions for biological

activity and especially bacterial activity. Moreover, the residual organic matter content after this treatment was in the order of 12% in dry weight, which is consistent with visual observations suggesting that it is a humus-rich soil.

The total hydrocarbon content measured in soil 2 after a 30-day incubation in control microcosms without bio-augmentation was 8130 ± 405 mg/kg (Fig. I.10). This value is lower than the initial content measured on site, but remains of the same order of magnitude. The difference could be due to sampling heterogeneity, or contaminant removal either through volatilization during soil drying, abiotic degradation or biodegradation by the endogenous flora.

4.1.2. Effect of bioaugmentation with T. helicus and HC bacteria on total hydrocarbon removal

In microcosms inoculated with *T. helicus*, observations under a binocular magnifier after 30 days of incubation revealed a visible mycelial growth in the vessels (Fig. I.9.b). As shown in the pictures below, the aerial hyphae are colorless, and carry what appear to be cream white conidiophores (indicated with arrows). These morphological characteristics are consistent with observations of *T. helicus* on agar plates (Fig. I.9.c) in terms of color and density of the mycelium.

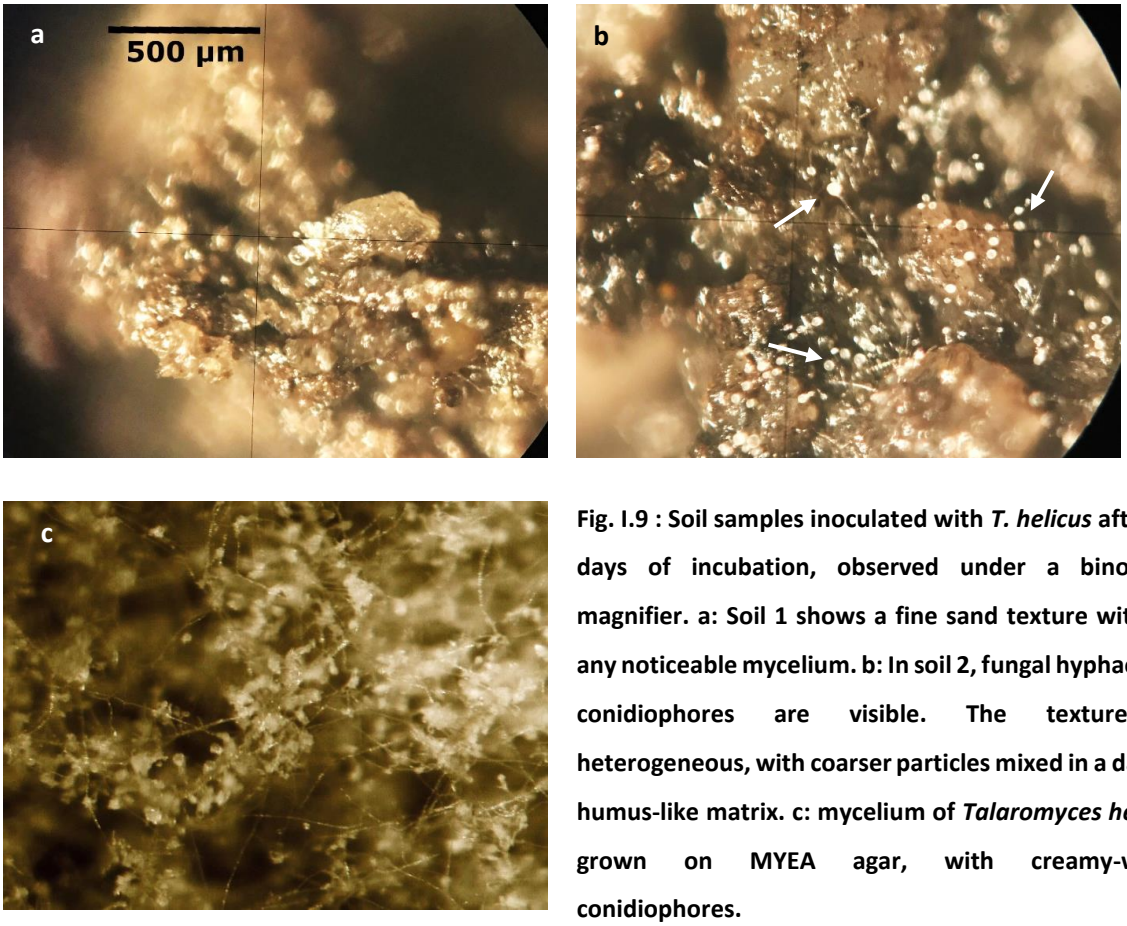

Fig. I.9 : Soil samples inoculated with *T. helicus* after 30 days of incubation, observed under a binocular magnifier. a: Soil 1 shows a fine sand texture without any noticeable mycelium. b: In soil 2, fungal hyphae and conidiophores are visible. The texture is heterogeneous, with coarser particles mixed in a darker humus-like matrix. c: mycelium of *Talaromyces helicus* grown on MYEA agar, with creamy-white conidiophores.

No such mycelial growth was observed in control microcosms without bio-augmentation, nor those inoculated only with bacteria, which strongly suggests that the mycelium observed is *T. helicus* and not a fungus native to the soil. Further investigations, such as observations of the detailed morphology of conidiophores or genetic sequencing would be needed to confirm the identity of the strain.

The percentage of hydrocarbon removal in soil samples after bioaugmentation treatment is shown in Fig. I.10. Samples inoculated with *T. helicus* did not show any significant loss of hydrocarbon compared to the control without bio-augmentation: *T. helicus* did not enhance the biodegradation activity. Yet, mycelium resembling *T. helicus* grew in soil n°2, which shows that the incubation conditions were suitable for fungal development. This means that the strain is likely able to grow in soil n°2 but the conditions of this experiment were not suitable for any significant biodegradation activity towards hydrocarbons. Strains of the genus *Talaromyces* were previously reported to be able to degrade crude oil as sole carbon source (Chaillan et al., 2004), and *T. helicus* itself is known to degrade aromatic compounds (Romero et al., 2005, 2009; Fayeulle et al., 2019), and use phenol or hexadecane as sole carbon sources (Romero et al., 2005). However it is unclear whether this strain can utilize heavier hydrocarbons for growth, and if so, the least recalcitrant compounds are likely to be metabolized first. In this regard, high molecular weight oil fractions may not be an energetically efficient substrate despite their abundance in soil n°2, if this soil also contains more easily degradable organic matter as a carbon source. It should also be noted that the soils were not sterilized prior to the biodegradation tests, and even though *T. helicus* may be able to degrade hydrocarbons, it may not develop properly in this situation due to competition with other organisms, or develop but contribute negligibly to the overall pollutant removal.

Biodegradation in soil n°2 was also tested using a commercial bacterial suspension HC sold by Oxbiolab for the remediation of hydrocarbons, alone or in co-culture with *T. helicus*. Among the bio-augmentation parameters tested, the bacterial suspension is the only one where a significant decrease of the total hydrocarbon content was measured compared to the control (Fig. I.10): 30% of hydrocarbons (w/w) were removed compared to the initial content, which means the bacterial consortium from the HC suspension enhanced degradation. Co-inoculation of *T. helicus* with bacteria did not perform better than each micro-organism separately, however they did not negatively affect each other either (Fig. I.10).

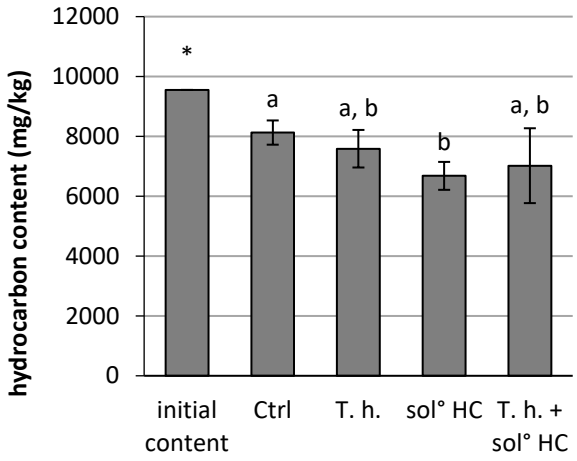

Fig. I.10 : Hydrocarbon content (C10-C40) in soil 2 before and after 30-day treatment with *Talaromyces helicus*, bacterial suspension HC or both. Error bars represent standard errors for each replicate. Groups of values that are not significantly different are indicated with the same letter. Values indicated with a star represent only one measurement, preventing the use of Student's t-test.

4.1.3. Effect of bioaugmentation with T. helicus and HC bacteria on PAH and PCB removal

Analysis of pollutants of interest, including PCB and PAH, was carried out after bio-augmentation treatment in microcosms. No detailed information is available on initial contamination levels with PAH and PCB in soil n°2, however a control experiment without bio-augmentation was conducted to compare with those incubated with microorganisms.

The PCB content after treatment was undetectable in all samples analyzed. Since the initial content in PCB in soil n°2 is not known, it is possible that this soil did not contain any significant amount of PCB in the first place.

PAH contents measured after treatment were in the order of 1 mg/kg. Contamination profiles could be classified into two categories: a first group with a total PAH content between 0.3 and 0.6 mg/kg, containing naphthalene, fluorene, phenanthrene, anthracene and/or pyrene, but little to no other PAH with 4 or more cycles. The second group contained 1.5 to 5.2 mg/kg PAH in total, with all 16 species analyzed detected above the quantification limit of 0.05 mg/kg, including 5 and 6-cycle PAH. These contamination profiles were distributed between all incubation conditions. Generally speaking, the high dispersion of values within each triplicate highlights the heterogeneity of soil samples despite pulverization and mixing prior to the incubation.

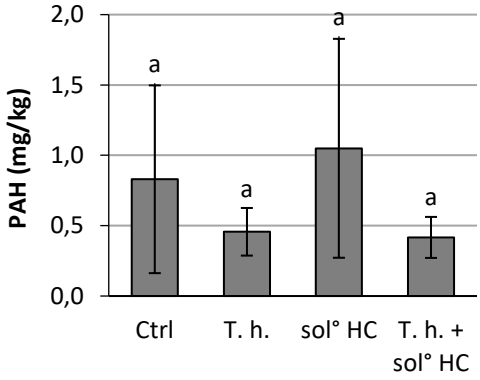

Fig. I.11 : residual PAH content in soil 2 after 30-day treatment with *T. helicus*, HC solution or both. Error bars represent standard errors for each triplicate. Groups of values that are not significantly different are indicated with the same letter.

Bio-augmentation did not significantly reduce the overall PAH content after 1 month of treatment, compared to the control (Fig. I.11). There was no effect of bio-augmentation on any specific type of PAH either. However in microcosms inoculated with *T. helicus*, either alone or in combination with HC bacteria, the PAH content was particularly low on average, with a smaller dispersion of values than for the control and HC-bioaugmented triplicates. As PAH contaminations appears to be globally low in this soil, this observation could be interpreted as a biodegradation of the residual bioavailable PAH fraction by *T. helicus* in samples with higher PAH contents within triplicates inoculated with the fungus, lowering the contamination level to a minimum while reducing the variability. Unfortunately, the low initial content in PAH and the variability between samples did not lead to statistically significant differences within the chosen incubation time, which is short considering PAH bioremediation.

To summarize the results obtained with soil n°2, fungal and bacterial inocula had qualitatively different effects on the soil contaminations: the HC solution tended to lower the overall hydrocarbon content, but had no effect on PAH indicating a preferential use of linear chains. On the contrary, *T. helicus* had little to no effect on the total hydrocarbon content, but may have a specific effect on PAH biodegradation. This result correlates with another bioaugmentation study carried out on aged contaminated soils in microcosms, which showed a statistically significant PAH degradation (26%) by this fungal species within one month (Fayeulle et al., 2019). Besides, our result is of particular interest, because it may indicate a complementarity of bacterial and fungal biodegradation activities for hydrocarbon bioremediation. However no synergic effect of co-cultures could be observed during this experiment, which means that condition of microbial community establishment and compatibility between strains have to be further investigated. The characteristics of soil n°2 appeared to be favorable for microbial development, however PAH contamination was low and incubation time was relatively short for this type of experiment.

4.2. Biodegradation assays in soils from Noisy-le-Sec

4.2.1. Contamination levels and hydrocarbon composition

Soil sample 1 and 3 came from an industrial area in Noisy-le-Sec in the Ile-de-France region. The results of analyses conducted at Eurofins (Saverne, France) was provided for soil excavated from two different areas, detailing total hydrocarbon, PAH and PCB contents. The first site is where sample 1 was taken, and was untreated so far. Sample 3 originates from a different site, where the soil was limed prior to sampling and analysis. With 442 mg/kg in the untreated soil and 94.3 mg/kg in the limed soil, the total hydrocarbon content was about 5-fold higher in the untreated area. The proportion of long-chain and short-chain hydrocarbons however was similar for both sites: indeed, hydrocarbons with chain lengths above C20 initially made up for about 70% of total hydrocarbons (Fig. I.12.a). Both samples also had a similar PAH content, in terms of total quantity and composition (Fig. I.12.b). In addition to hydrocarbons, the limed soil contained unusually high levels of copper (3.13 mg/kg), and exhibited an alkaline pH of 10.5 due to the pre-treatment. It also displayed the lowest initial hydrocarbon contamination among all three sites considered in this study.

Biodegradation tests were conducted over 1 month with two batches of soil from the untreated site (soil sample 1), as well as one batch from site 3 (soil sample 3).

After 1 month of control treatment without bio-augmentation, the residual hydrocarbon content in soil sample 3 represented almost half of that reported initially for site 3, and its relative content in C30-C40 hydrocarbons was slightly lower (Fig. I.12.a). The lower proportion of long carbon chains after treatment can be attributed to an incomplete breakdown of the high-molecular weight hydrocarbons.

Regarding soil samples from site 1, after 1 month of control treatment the residual hydrocarbon content 648.3 mg/kg (Fig. I.12.a). This value should be compared to the initial hydrocarbon content for site 1 which is 442 mg/kg (see section 2.5, Table I.4). The residual content in sample 1 being higher than the content reported for untreated soil from site of origin indicates that the samples were taken from different areas of the site, and their initial hydrocarbon contents must have been different. High molecular weight hydrocarbons dominated in sample 1, while those below C22 accounted for only 18% of the total (Fig. I.12.a). Sample 1 thus presented a hydrocarbon composition similar to the one reported for the corresponding site, both in terms of total quantity and composition. Analysis results provided with the samples are indicative of contamination levels on the site but do not account for its spatial heterogeneity, unless multiple samples are taken in relevant spots, at increasing distances from the suspected source of pollution for example. These results highlight the importance of comparing

bio-augmentation results with control runs with the same soil sample, rather than analysis results for the site only.

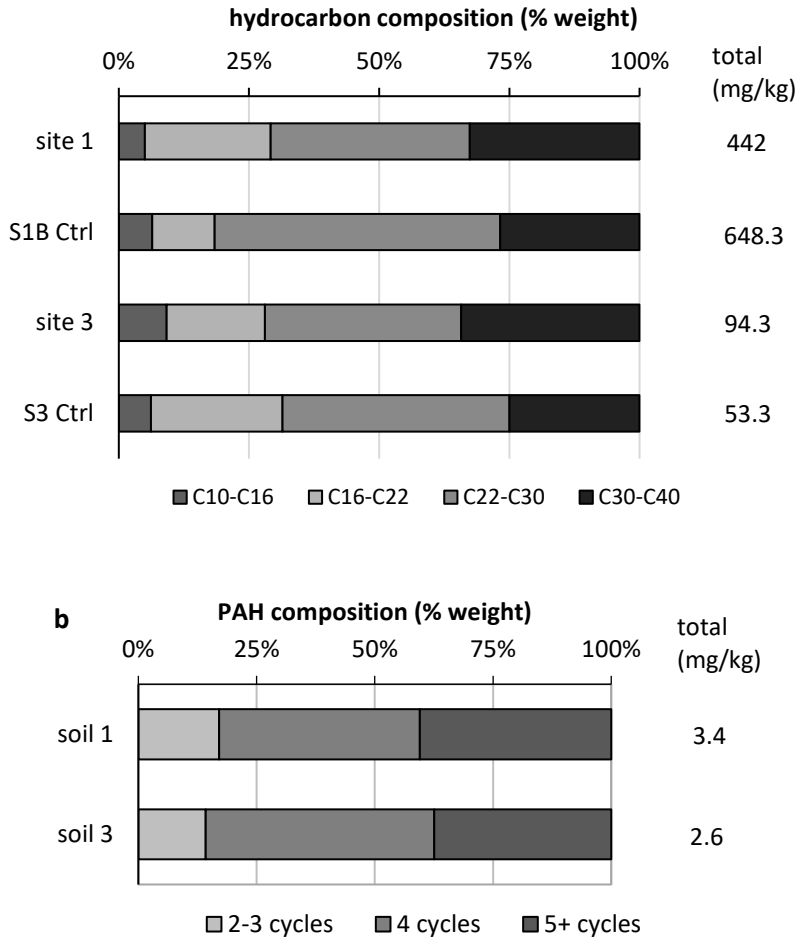

Fig. I.12: a - hydrocarbon composition in soil samples n°1 and 3 after incubation in closed microcosms without bio-augmentation, compared to the reference values for the corresponding sites (% of the total PAH weight per kg of dry soil). Ctrl = after 1 month of incubation without bioaugmentation. in % of the total hydrocarbon weight per kg of dry soil. b - PAH contamination on sites 1 and 3 broken down by number of aromatic cycles, in % of the total PAH weight per kg of dry soil.

4.2.2.Biodegradation assays in a pretreated (limed) soil

The biodegradation potential of *T. helicus* was tested in soil n°3. The total hydrocarbon content measured after bio-augmentation treatment with *T. helicus* was not significantly different from the control, despite being slightly lower than the initial content reported for the site of origin (Fig. I.13). Soil sample n°3 displayed a basic pH due to previous liming and a high copper content, which is unfavorable for microbial activity and especially fungal growth. This can explain why no significant biodegradation of hydrocarbons was observed with *T. helicus*. No significant effect of the bio-

augmentation was apparent either with HC bacteria; i.e. the residual content in hydrocarbons appears even higher in average when bacteria were inoculated than with *T. helicus* alone or without inoculation, but these differences are not significantly different (Fig. I.13).

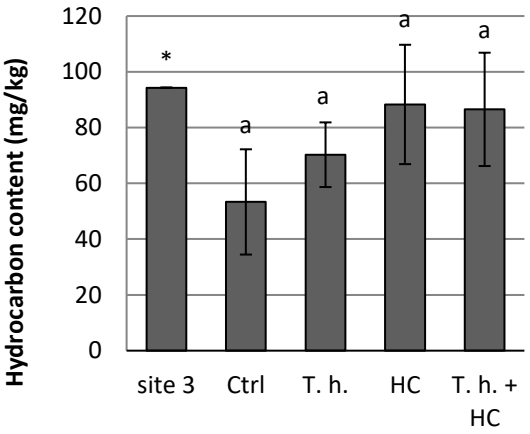

Fig. I.13: Total hydrocarbon content in soil n°3 after a 30-day incubation in microcosms, without bio-augmentation (Ctrl) or with inoculation with *Talaromyces helicus* and/or bacterial solution HC.

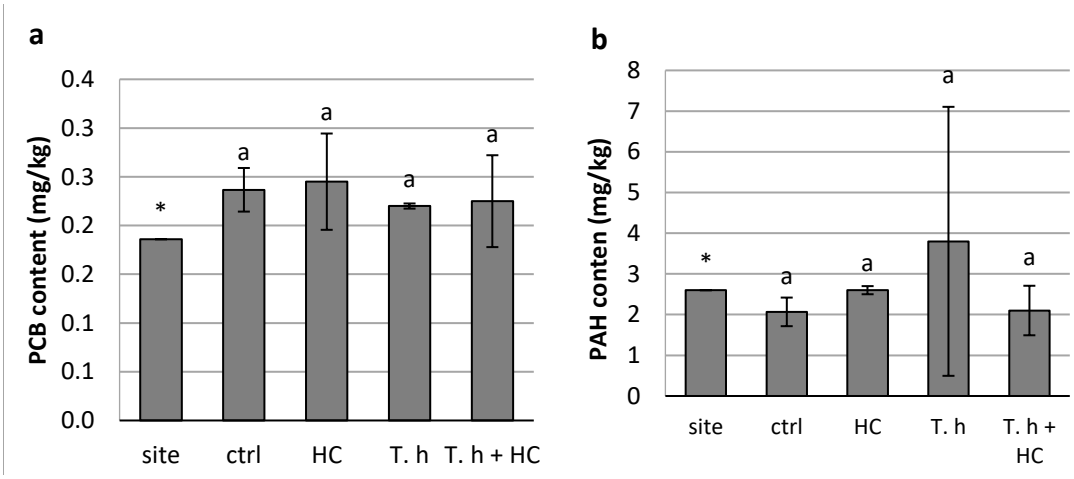

Fig. I.14 : residual content in PCB (a) and PAH (b) in soil n°3 after a 30-day treatment with *Talaromyces helicus*, HC solution or both. Error bars represent standard errors for each triplicate. Groups of values that are not significantly different are indicated with the same letter (values for each soil were analyzed independently). Values indicated with a star represent only one sample, preventing the use of Student's t-test.

Regarding PCB, the residual content measured after the bio-augmentation treatments with either *T. helicus*, HC bacteria or both, are of the same order as the control (2.4 ±0.2 mg/kg) (Fig. I.14.a). No significant biodegradation of PAH was observed either with any of the bio-augmentation conditions (Fig. I.14.b). Again, this suggests a lack of microbial activity in soil n°3 likely due to the previous liming treatment. It can be noticed that the average residual PAH content in samples of soil 3 inoculated with the co-culture of *T. helicus* and HC bacteria was slightly lower than those inoculated with the bacterial

suspension or the fungus alone. However, none of these values are significantly different from each other, and generally speaking the PAH content was not reduced compared to the control. The wide error bars are most likely due to the initial heterogeneity of contamination in soil samples, despite the homogenization efforts.

To summarize the results obtained with soil 3, none of the bio-augmentation conditions resulted in significant improvement of contaminant degradation compared to the control, and on the contrary, the residual hydrocarbon content tended to be higher in samples inoculated with micro-organisms. This may indicate a competition between the endogenous microflora and the bio-augmentation strains added, resulting in overall biodegradation being inhibited in presence of the exogenous strains. The pre-treatment of this site, combined with its copper content, renders it poorly suited for bioremediation using microorganisms. In this particular case, the copper contamination may explain why a chemical treatment was initially chosen rather than the use of microbial agents. When a sequential remediation process with chemical or physical pretreatment followed by biological treatment is planned, it is therefore important to choose pre-treatments that will not alter the soil to a point where microbial development is inhibited, notably in terms of pH. In order to evaluate the potential of micro-organisms for a bio-augmentation treatment, working with untreated soil samples and longer incubation times would thus be more relevant.

4.2.3. Biodegradation assays in untreated soil samples

4.2.3.1. Effect of bioaugmentation with T. helicus and HC bacteria after 4 months

The effect of bio-augmentation on total hydrocarbon, PAH and PCB contamination was tested in soil sample 1. Sites 1 and 3 are in the same geographical area, but site 1 was not limed. Residual contamination levels in soil 1B were measured after a 4-month incubation in microcosms inoculated with *T. helicus*, the bacterial suspension HC or a fungal-bacterial co-culture. For this experiment, a longer incubation time was tested since previous biodegradation results obtained after only one month were mostly inconclusive, even for soil 2 which was the most likely to favor microbial development.

The residual content in hydrocarbons in control microcosms of soil 1 after a 4-month incubation was slightly higher than the contamination reported for site 1, as previously noted in section 4.2.1. This is most probably due to spatial heterogeneity of the site of origin, indicating that the batch of soil used for our experiment was collected an area more heavily contaminated with hydrocarbons than the one where the reference sample was taken.

No significant degradation of total hydrocarbons was observed with *T. helicus* nor with HC bacteria compared to the control without bio-augmentation (Fig. I.15.a), even though the combination of both appears to lower hydrocarbon content compared to *T. helicus* alone. PAH quantities were extremely low, the concentration of each individual PAH being below or barely above the quantification limit (0.05 mg/kg) in most samples regardless of the bio-augmentation conditions (Fig. I.15.b). Residual PAH concentrations tended to be lower on average in microcosms inoculated with bacteria or *T.* compared to the control, but not in those inoculated with both in co-culture. However the differences between samples are not significant and hardly interpretable due to the very low concentrations. The PAH content in this aged contaminated soil probably represents the least bioavailable fraction, requiring additional mobilization strategies.

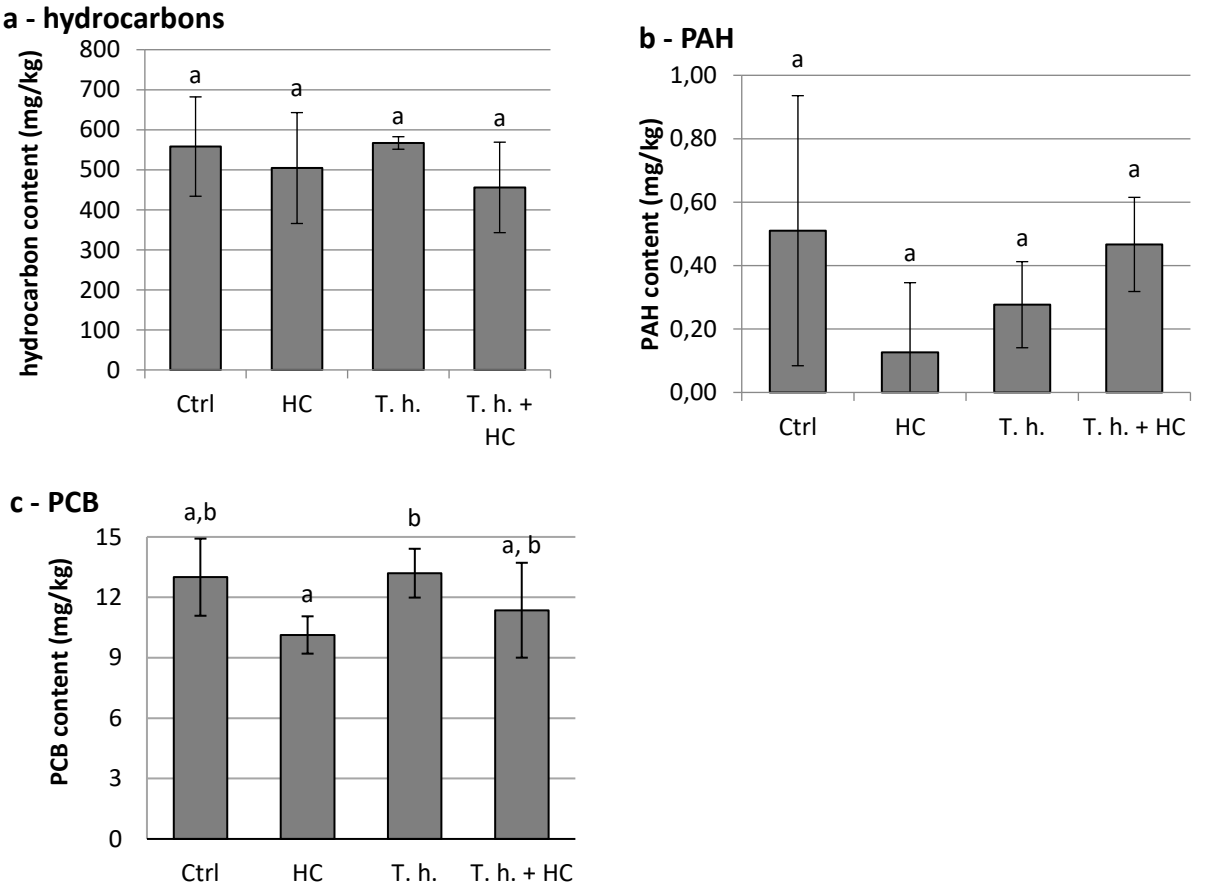

Fig. I.15: Residual hydrocarbon content (a) PAH content (b) and PCB content (c) in soil 1 after a 4-month incubation in microcosms, without bio-augmentation (Ctrl), inoculated with *Talaromyces helicus* (T. h.), bacterial suspension HC, or both. Error bars represent standard errors for each triplicate. Groups of values that are not significantly different are indicated with the same letter. Values indicated with a star represent only one sample, preventing the use of Student's t-test.

By contrast, residual PCB contamination was surprisingly high, being above 9 mg/kg in all microcosms analyzed compared to the initial concentration of 2.46 mg/kg reported for site 1 (Fig. I.15.c). This confirms that the initial contamination levels have been under-estimated: indeed, contaminants can be heterogeneously distributed within a site, and the sample analyzed was probably collected from a different location than the soil batch provided by Oxbiolab. A significant decrease of the PCB concentration was found in microcosms inoculated with the bacterial suspension, compared to *T. helicus* alone. The residual concentration was also lower than found in control conditions, even though the difference is not significant in this case. The co-cultures of *T. helicus* and bacteria did not perform better than bacteria on their own, resulting in less PCB degradation and a higher dispersion of concentrations within the triplicate.

No significant effect on contamination levels was observed after 4 months of bio-augmentation treatment with *T. helicus*, while a slight but significant removal of PCB by HC bacteria was noted, however this effect appeared to be inhibited when bacteria were co-cultured with *T. helicus.* Soil 1 appears to be less favorable for microbial activity compared to soil 2, due to its low organic matter content (1% in dry weight as measured after incubation in microcosms) and alkaline pH of 9 hindering microbial development. (In comparison, soil 2 contained 12% organic matter in dry weight and its pH was close to neutrality). The longer incubation time in this experiment did not allow for a more efficient biodegradation of organic contaminants, therefore time is probably not the main limiting factor in this case. Other parameters may hinder biodegradation in soil 1: the lack of organic matter to sustain fungal growth and serve as a co-substrate, as well as low contaminant bioavailability. Further tests with the addition of mobilizing agents could give a useful insight into the biodegradation kinetics in soil n°1. The mitigated results obtained with fungal-bacterial co-cultures also highlight the importance of selecting compatible strains for an efficient consortium, ensuring that competition between the microorganisms does not cancel the effect of each member.

4.2.3.2. Effect of biostimulation with surfactants or biosurfactant-producing bacteria

The degradation of organic contaminants by *T. helicus* was tested again in soil n°1 either by adding synthetic surfactants, or co-inoculating with the surfactant-producing bacteria *Corynebacterium glutamicum*. *C. glutamicum* is a species of soil-dwelling actinobacteria notable for its atypical outer "mycomembrane" consisting of glycans and peptidoglycans covalently linked to the membrane lipids. Trehalose lipids are notable amphiphilic constituents of this outer membrane, comprised of a trehalose moiety acylated with mycolic acid (Lanéelle et al., 2013). In addition, *C. gluctamicum* is able to utilize a number of aromatic compounds as sole carbon source, including phenol and benzoate, and can take them up thanks to transmembrane active transporters (Shen et al., 2015). Sophoclean, a sophorolipid

detergent synthesized from wheat and vegetable oil, was used for this test in an attempt to enhance the availability of contaminants for biodegradation. Sophorolipids are a class of glycolipid surfactants comprised of a disaccharide polar head and a lipid moiety. A 1 g/L solution of Sophoclean detergent was added to the soil samples in microcosms instead of distilled water.

The control treatment in soil 1 yielded residual hydrocarbon contents higher on average than the initial content, which is likely due to an underestimation of the initial content as already noted previously (see section 4.2.1).

The hydrocarbon content in samples treated with *T. helicus* and sophorolipid decreased significantly after 1 month, while a decrease was observed as well with only *T. helicus* but not significantly different from the control (Fig. I.16.a). These results indicate a stimulating effect of the biosurfactant on hydrocarbon degradation by *T. helicus*. This is likely due to the enhancement of the pollutant bioavailability for the fungus, since it did not significantly enhance hydrocarbon removal in the absence of added surfactants, in the present experiment like in the previous one (see section 4.2.3.1). The addition of a mobilizing agent thus appears to be necessary for biodegradation to occur with *T. helicus* in this type of aged contamination. The addition of only sophorolipid without bio-augmentation did not stimulate biodegradation by the endogenous flora, which indicates that hydrocarbon removal in microcosms inoculated with *T. helicus* is due to addition of the fungus. This hypothesis could be tested by comparing the performance of *T. helicus* in fresh soil and sterilized samples. However, soil sterilization is also likely to alter its physicochemical properties and influence bioavailability parameters.

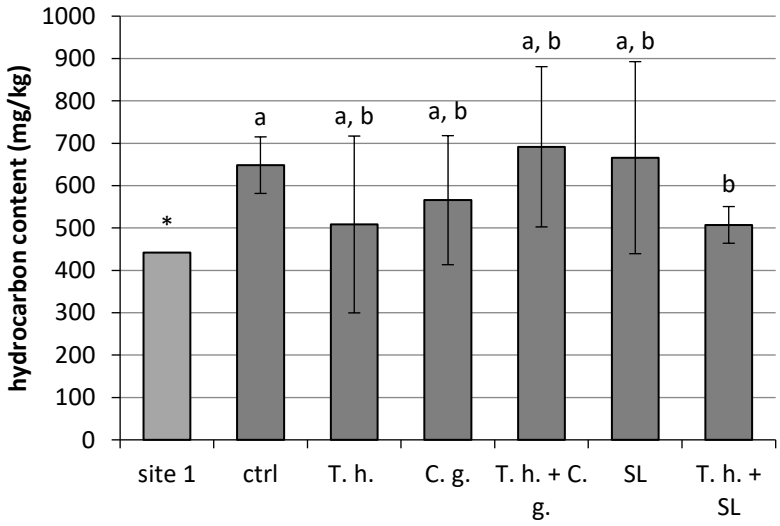

Fig. I.16: Residual hydrocarbon content in soil 1 after 1 month of treatment with *T. helicus* and biostimulation with sophorolipids (SL) or co-culture with *Corynebacterium glutamicum* (C. g.).

Bioaugmentation with *C. glutamicum* did not enable to have a significant effect on hydrocarbon content in particular when combined with *T. helicus*. In addition to competition with endogenous microflora, other parameters may be the reason of poor hydrocarbon degradation, for example low nitrogen content or the presence of metallic elements (not quantified in this sample) hindering microbial development.

The residual PCB concentrations measured were in the range of 10 mg/kg in all microcosms: these values are similar to those previously found after 4 months of incubation. The effect of sophorolipid addition on the PCB content in soil 1 samples was similar to its effect on total hydrocarbons, resulting in a significant decrease of PCB concentrations in microcosms incubated with *T. helicus* combined with sophorolipid, but not with *T. helicus* alone (Fig. I.17.a). This indicates a stimulation of the biodegradation when the surfactant solution is added. The residual PCB content in microcosms treated with only sophorolipids without bio-augmentation was also lower than the control, although not significantly different. *T. helicus* may thus not be the only microorganism responsible for biodegradation, and sophorolipid could also enhance the biodegradation by endogenous flora. A significant effect on PCB content was also observed in samples treated with *C. glutamicum* (Fig. I.17.a), alone or in combination with *T. helicus*. Although the presence the fungus did not significantly enhance the removal of PCB by *C. glutamicum*, it was not inhibited either, which is promising for future co-culture experiments.

Similarly to results previously found after the 4-month incubation, very low concentrations of PAH were measured after incubation, regardless of the conditions tested (Fig. I.17.b). PAH concentrations in this case were so low that the dispersion within each triplicate is of the same order of magnitude as the average value. No significant differences were found between PAH concentrations after bio-augmentation with *T. helicus* or *C. glutamicum*, bio-stimulation with sophorolipids or the control treatment.

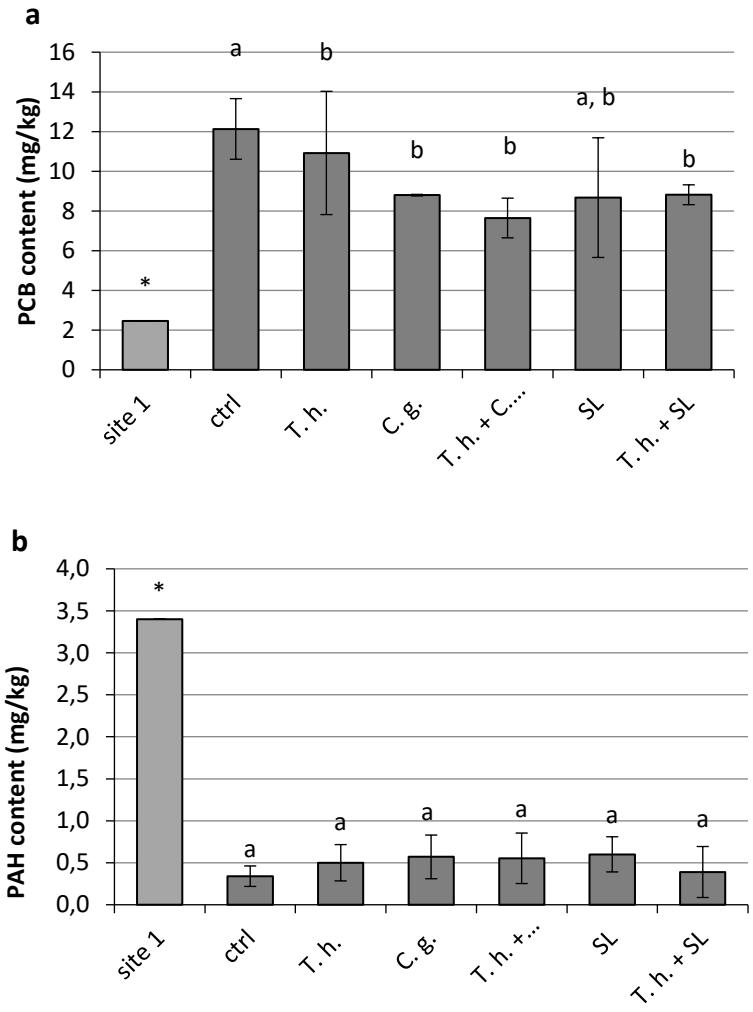

Fig. I.17: Residual PCB content (a) and PAH content (b) in soil 1 after 1 month of treatment with *T. helicus* and biostimulation with sophorolipids (SL) or co-culture with *Corynebacterium glutamicum* (C. g.).

Table I.6 : Summary of the bioremediation results obtained in soil microcosms for each bio-augmentation and biostimulation condition tested. (greyed-out cells correspond to experiments that were not carried out)

	Soil 1	Soil 2	Soil 3
T. helicus	No significant effect	Slightly lowered PAH content. No effect on total hydrocarbons	No significant effect
HC solution	Slight removal of PCB (not significant)	Significant removal of total hydrocarbons	
Sophoclean	Enhanced removal of hydrocarbons and PCB with *T. helicus*		
C. glutamicum	Enhanced removal of PCB, alone or combined with *T. helicus*		

5. Summary and conclusions

Biodegradation experiments in liquid cultures allow quantifying the biodegradation activity of a given organism in homogeneous and controlled conditions. Here the results confirmed the biodegradation abilities of *Talaromyces helicus* towards benzo[*a*]pyrene, its degradation efficiency being stimulated by nitrogen supplementation. Four unidentified polar metabolites of BaP were detected in the cultures after biodegradation by the fungus. Hydrogen peroxide added to test cultures inhibited the growth of *T. helicus*, but caused a chemical oxidation of BaP. The addition of surfactants to enhance the solubilization of BaP did not increase biodegradation percentages, indicating that BaP bioavailability is not a limiting parameter for biodegradation in liquid media.

The results obtained in liquid cultures were poorly predictive of the performance of the same microorganism in an actual contaminated soil. Indeed, bioremediation efficiency differed greatly depending on the soil. *T. helicus* and the bacterial consortium HC performed best on the soil with the highest organic matter content, with the fungus effecting specifically the PAH content, and bacteria the total hydrocarbon content but not PAH. In contrast, they did not enhance pollutant removal from limed soil samples with a basic pH. Interestingly, the addition of a biobased surfactant enhanced the removal of total hydrocarbon and PCB by *T. helicus*. Finally, the biosurfactant-producing strain *C. glutamicum* displayed bioremediation abilities specifically towards PCB. These results underline the

fundamental importance of parameters specific to each contaminated sites to predict bioremediation efficiency. On one hand, physico-chemical properties of the soil matrix including texture, porosity, mineral composition, pH, and nutrient content (carbon/nitrogen ratio) influence both pollutant retention and biological activity. On the other hand, organisms will show variable bioaccumulating and/or biodegrading capacities depending on the nature, abundance and availability of contaminants, as well as possible co-contaminations.

One of the major drawbacks of using soil samples with a classical microcosm approach is the inability to determine the spatial distribution of contaminants, and how it affects bioremediation. Microbial colonization of the soil matrix is also difficult to evaluate in such experimental set-ups, both in terms of growth kinetics and spatial distribution. This double heterogeneity is a source of uncertainty, which can only partially be overcome through mechanical mixing or amendment with surfactants. From a more fundamental point of view, there is relatively little knowledge about the mechanisms underlying pollutant mobilization by fungi, and microcosm experiments are poorly suited to investigate pollutant mobility and transfer mechanisms.

In consequence, there is a need for new experimental models to investigate the complex interactions between micro-organisms, soil matrix and pollutants. Instead of considering bioremediation efficiency averaged over soil samples assumed to be homogeneous materials, another perspective is to consider it as a juxtaposition of micro-environments. The goal of such an approach would be to study biological, mechanical and/or chemical phenomena at a microscale, and gaining a better insight into the parameters affecting pollutant mobilization and biodegradation. In this context, the following chapters focus on investigating how *Talaromyces helicus* affects pollutant mobility and dispersion, by researching the production of potential fungal mobilizing agents, and monitoring BaP incorporation into the mycelium.

Chapter II: Production and characterization of fungal surfactants

1. Introduction

Filamentous fungi, whether they live in or on plant tissues, animal tissues, or the soil, navigate a water-unsaturated environment and come into contact with various surfaces and interfaces. The production of extracellular surfactants is thus involved in several aspects of the fungal lifestyle: surfactants can modulate the surface properties of hyphae themselves, or those of solid surfaces in the fungus surroundings. In soils, surface property regulation is required for hyphal attachment to soil aggregates, crossing air pockets, or substrate mobilization. Hydrophobins are ubiquitous fungal proteins with surface active properties, well-known for coating the surface of aerial hyphae and mediating their interactions with air-water interfaces. In addition to hydrophobins, many terrestrial fungi produce surfactants such as glycolipids, glycoproteins or lipopeptides. Several surfactant-producing strains were isolated from soils (Sena et al., 2018) including hydrocarbon-contaminated soils (Guimarães Martins et al., 2006; Luna-Velasco et al., 2007)

By adsorbing to hydrophobic surfaces and forming micelles, extracellular biosurfactants can be involved in the mobilization of poorly water-soluble substrates that can be used by the fungus as carbon sources, such as lignin, lipids, hydrocarbons, and various other hydrophobic organic compounds (Azin et al., 2018; Zadeh et al., 2018; do Amaral Marques et al., 2019). The role of such mobilizing agents may thus be crucial for accessing hydrophobic contaminants in soils, which can be present as solid deposits on solid particles, or present as non-aqueous phase liquids. For example, polymeric proteoglycans able to flocculate kaolin particles were described in the species *Talaromyces trachyspermus* closely related to *T. helicus* (Fang and Shi, 2016). Culture filtrates of several fungal strains isolated from contaminated soil, including *Fusarium oxysporum*, *Geotrichum candidum* and *Verticillium insectorum,* were found to enhance the desorption of BaP deposited on the side of a glass tube, suggesting the production of extracellular mobilizing agents able to partially stabilize BaP in the water phase (Rafin et al., 2013). Although the chemical nature of these mobilizing agents is not yet elucidated, other studies have shown the ability of fungal surfactants to solubilize or emulsify PAH. This is the case of some hydrophobin-like proteins produced by *Aspergillus brasiliensis* (Sánchez-Vázquez et al., 2018), or a carbohydrate from *Fusarium solani* (Veignie et al., 2012). In some white-rot strains, the production of surfactant or emulsifiers coincides with the production of ligninolytic enzymes and PAH degradation (Nikiforova et al., 2009). Extracellular polymeric flocculants (Fang and Shi, 2016)

The works presented in this chapter focuses on the production of extracellular biosurfactants by *Talaromyces helicus* and their partial characterization. Culture supernatants of *T. helicus* were produced in batch cultures, tested for surface activity, then analyzed to identify their composition. Size-exclusion chromatography and high performance thin layer chromatography were performed to gain information on both the molecular size and chemical nature of the surfactants. This method was chosen because it allows the detection of a wide range of compounds from various biochemical families through the use of appropriate revealing reagents. It is particularly interesting in the case presented here, where the molecules of interest are unknown, and only defined by their ability to lower the surface tension. The possible effect of supernatants on PAH mobilization is then investigated by conducting desorption tests.

2. Materials and methods

2.1. Production of culture filtrates

Shaking flasks containing mineral medium (KCl 0.25 g/L, $NaH_2PO_4.2H_2O$ 1.54 g/L, Na_2HPO_4 $8\cdot10^{-3}$ g/L, $MgSO_4.7H_2O$ 0.24 g/L, NO_3NH_4 1.0 g/L, $ZnSO_4.7H_2O$ $1\cdot10^{-3}$ g/L, $MnCl_2.4H_2O$ $1\cdot10^{-4}$ g/L, $FeSO_4.5H_2O$ $1\cdot10^{-3}$ g/L, $CuSO_4.7H_2O$ $5\cdot10^{-4}$ g/L, $CaCl_2.2H_2O$ $1\cdot10^{-4}$ g/L, MoO_3 $2\cdot10^{-4}$ g/L, glucose 20 g/L) were inoculated with spores of *T. helicus* to reach a final concentration of 10^4 spores/mL. 50 mL flasks containing 10 mL medium were used for the growth kinetics experiment, and 250 mL flasks containing 50 mL medium were used for filtrate production before characterization. Cultures were incubated at 22°C with orbital shaking and a 12 h/12 h light-dark cycle. The mycelium was harvested by vacuum-filtration on quantitative filter paper (VWR 434) with a Büchner funnel. Filtrates were collected, filtered again on a 0.2 µm syringe filter to sterilize them and remove any remaining particle, and frozen at -20°C until use. To quantify fungal growth in 10 mL cultures, the paper filters with mycelium cake were rinsed with distilled water and dried in a 105°C oven for 24 h, then weighted. For the growth kinetics experiments, 10 mL cultures were done in triplicate and filtered separately. For batch production of filtrates in 50 mL flasks, the contents were pooled upon filtration.

2.2. Size-exclusion chromatography

Sephacryl S-200 HR resin, with a molecular weight range of 5-250 kDa for globular proteins, and 1-80 kDa for dextran, was used for size exclusion chromatography. The resin was packed into a column (27 cm high, diameter 13 mm, resulting in a theoretical column volume (CV) of 35.8 mL) connected to a peristaltic pump (Ismatec). The column was then equilibrated in 100 mM ammonium acetate buffer (pH 5.5) as the mobile phase.

The column was first tested using 400 µL of a standard sample containing 0.5 g/L BSA and 1% glucose in order to estimate the column total volume. Low-molecular weight molecules such as glucose, which partition freely between the mobile phase and the resin pores, are expected to be eluted at 1 CV. Protein and glucose were qualitatively detected by visually assessing a color change in the fractions after adding Bradford or DNS reagent respectively.

Before size-exclusion chromatography, culture filtrates harvested after 10 or 13 days were lyophilized in batches of 10 mL and resuspended in 400 µL distillated water. Two runs were performed with samples from the same 13-day culture batch, and one run with a sample from a 10-day batch. The samples were loaded onto the column and eluted at 2 mL/min. 1.5 mL fractions were manually collected in microcentrifuge tubes by shifting the tube rack every 45 s, and fractions were stored at 4°C for up to a week until analysis.

2.3. Surface tension measurements

Surface tension in filtrates was measured on a tensiometer (Krüss K-100) with the Wilhelmy plate method. Alternatively a rod was used instead of a plate for size-exclusion chromatography fractions, due to their small volume (1.5 mL). Each measurement was taken 10 minutes after immersing the plate (or rod) into the sample, to allow the meniscus to equilibrate at room temperature. All measurements were performed on triplicate samples, and results are presented as average values and standard deviations for each triplicate (with the exception of SEC fractions for which only one measurement was taken per fraction).

2.4. Protein quantification

Protein content was quantified by the Bradford method adapted for microplate reading (Bradford, 1976). Bradford reagent was prepared as follows: 10 mg Coomassie Brilliant Blue G-250 (Sigma) was dissolved in 5 mL 95% ethanol, 10 mL 85% phosphoric acid and completed with distillated water for a final volume of 100 mL. The solution was filtered before use to eliminate crystals, and stored in the dark.

Before the assay, the culture filtrates to be tested were concentrated 10 times with a speedvac concentrator (Savant). A protein standard scale was prepared using bovine serum albumine (BSA) in distillated water from 0 to 100 µg/mL in a final volume of 20 µL. 20 µL of each sample to be tested was pipetted into microplate wells. 200 µL of Bradford reagent was then added in each well, the plate was gently shaken then incubated for 15 minutes at room temperature. Absorbances were read at 595 nm using a Multiskan GO spectrophotometer (Tecan).

2.5. Reducing sugar quantification

Reducing sugar content was quantified by the dinitrosalicylic acid (DNS) method adapted for a microplate (Miller, 1959). DNS reagent was prepared as follows: 0.5 g dinitrosalicylic acid, 13 mg Na_2SO_3 and 0.5 g NaOH were dissolved in distillated water for a final volume of 50 mL. A solution of Na/K tartrate 40% was prepared separately.

A glucose standard scale was prepared in distillated water from 0 to 5 g/L. When necessary, samples to be tested were diluted beforehand to avoid absorbance values outside of the linear range. 150 µL of each sample and 150 µL of DNS reagent were pipetted into microplate wells. The plate was gently shaken for homogenization then incubated 5 min at 90°C in a hot bath. The reaction was stopped by adding 50 µL of Na/K tartrate solution in each well and cooling at room temperature. Absorbances were read at 575 nm using a Multiskan GO spectrophotometer (Tecan)

2.6. HPTLC analysis

HPTLC analysis of the SEC fractions was conducted by the CAP DELTA laboratory at Chromacim (Grabels, France) with the CAMAG method. Soy lecithin (1 g/L), BSA (1 g/L) and glucose (1 g/L) were used as positive controls for the detection of lipids, proteins and reducing sugars respectively. 10 µL of each control was deposited on the plate, as well as 50 µL of each fraction and of the crude filtrate. Samples were deposited on a TLC plate coated with F254 silica gel and migrated vertically. The mobile phase was a cosolvent mixture containing $CHCl_3$:MeOH: H_2O:NH_3 32 % (32:15:2:1 in volume)

After migration, the plates were observed under UV light at 254 and 366 nm, then sprayed with reagent solutions to reveal specific chemical functions, and observed at 366 nm after development. The solutions used were the following:

- primulin at 0.1 mg/ml in acetone:water (80:20 by volume) for the detection of aliphatic carbon chains corresponding to lipids

- anisaldehyde (4-methoxybenzaldehyde) at 0.5% (v/v) in MeOH: CH_3COOH:H_2SO_4 (42.5:5:2.5 by volume) for the detection of ketone, aldehyde and alcohol functions corresponding mostly to carbohydrates.

2.7. BaP desorption tests

Culture filtrates harvested after 10 days were used for BaP desorption tests.

50 µg of BaP (62.5 µL of stock solution in acetone at 0.8 g/L) were deposited on a cellulose antibiotic disc. The discs were left to dry under a fume hood to evaporate the acetone, then each one was

transferred to an erlenmeyer flask containing 10 mL of filtrate or MM1 for control. The flasks were agitated for 24 h at room temperature. After incubation, the disks were retrieved from the liquid using tweezers and the liquid medium was transferred to centrifuge tubes. The cellulose disks and empty flasks were dried overnight under the fume hood.

Residual BaP on the cotton disks was extracted by washing each disk three times with 1 mL dichloromethane. The washing solvent was transferred to an HPLC glass vial and concentrated under a nitrogen stream.

Desorbed BaP was extracted from the liquid phase by dispersive liquid-liquid extraction following a protocol modified from Rezaee et al. (2006). 2 mL of acetone (disperser solvent) and 1 mL of dichloromethane (extraction solvent) were added into each liquid sample, and the tubes were shaken manually. The tubes were centrifuged for 10 min at 4000 rpm (3220 *g*) to separate the phases, and the dichloromethane phase at the bottom of the tube was then recovered and transferred to an HPLC glass vial.

All samples were concentrated under a nitrogen stream and supplemented with an equal volume of acetonitrile, then analyzed by HPLC following the protocol described in chapter I for the quantification of residual BaP. Briefly, samples were run on a C18 reverse-phase column (Syncronis aQ, Thermoscientific), with an acetonitrile:water gradient from 75:25 to 100:0 over 25 min, at a solvent flowrate of 1 $mL \cdot min^{-1}$. BaP was detected at 380 nm as a single peak at 20 min of elution, and its concentration was calculated by measuring the peak area and comparing it to the standard scale. The residual mass of BaP in each sample was then calculated in µg by multiplying the concentration with the known sample volume.

3. Results

3.1. Production of extracellular surfactants by *Talaromyces helicus*

Culture filtrates of *Talaromyces helicus* grown in 10 mL mineral medium (MM1) were harvested by filtration after 4, 7, 10 and 13 days of incubation. For each incubation time, three shaking flasks were harvested, and results are presented as average values and standard deviations for each triplicate. Fungal growth was monitored by weighting the dry biomass after filtration. After a lag phase during 4 days, corresponding to the germination of spores, the biomass increased over time in a linear manner, until reaching 188 ± 6 mg after 13 days (Fig. II.1.a). This growth profile is consistent with sigmoidal kinetics typical of microbial biomass evolution in batch cultures (Prosser and Tough, 1991). It appears that cultures were stopped right before the stationary phase, since the biomass curve did not yet reach a plateau.

The surface tension in each filtrate was measured by the Wilhelmy plate method. The initial surface tension measured in fresh, non-inoculated MM1 medium was 69 ± 3.7 mN/m, in the same range as that of pure distillated water (72 mN/m). A significant decrease of the surface tension was observed during fungal growth, up to a minimum of 49.4 ± 0 mN/m after 10 days. This indicates the release of extracellular surface active agents in the medium.

pH measurements in the fresh filtrates and quantification of the residual glucose concentration gave additional information on the development stage of the mycelium. The pH in culture filtrates decreased rapidly over the first days of culture, and reached a minimum of 2.3 after 7 days. After ten days of incubation the pH increased again, and was equivalent to its initial value of 5.1 after 13 days. Many fungi develop well in a relatively wide range of pH, but are usually better adapted to acidic environments, hence the initial pH of the mineral medium used in this study adjusted at 5.5 for optimal fungal growth. They are also known to acidify their environments, through the release of organic acids and CO_2. In soils, this acidification is involved in competition with bacteria, and chemical weathering of the substrate enabling hyphal penetration and nutrition (Magnuson and Lasure, 2004; Scervino et al., 2010).

During fungal growth, the consumption of glucose can be observed as a linear decrease of the reducing sugar concentration over time, from 20 g/L of glucose initially introduced in the culture medium until reaching 1 g/L after 13 days (Fig. II.1.b). This glucose is used as a source of carbon for the synthesis of biomass, and is likely partly converted to organic acids responsible for the acidification, as well as dissolved CO_2 from respiration. The depletion of this primary carbon source results in a shift from active growth to the stationary phase, until autolysis of the mycelium becomes dominant (Prosser and Tough, 1991). The increasing pH in the last days of incubation indicates a shift in metabolism: this alkalinization of the medium occurs when glucose from the medium is nearly totally consumed (Fig. II.1.b). Indeed, alkalinization of the substrate is an indicator of cell death, likely caused the release of cellular contents into the medium upon autolysis (Powell, 1995). Since the acidification appears to be an active process during fungal growth, the disruption of pH regulating mechanisms is an expected consequence of metabolic arrest. Organic acids released during the growth phase may also be consumed as a source of carbon. For the culture conditions considered here, 13 days of culture thus appear to correspond to the beginning of the stationary phase.

Protein concentrations in the filtrates were measured by the Bradford method. Due to the very low concentrations, the samples had to be concentrated beforehand for protein to be quantifiable. The concentrations measured are extremely low, below 3 mg/L. However, the protein concentration is significantly higher from 7 days on, coincidently with the surface tension minimum. The surfactant

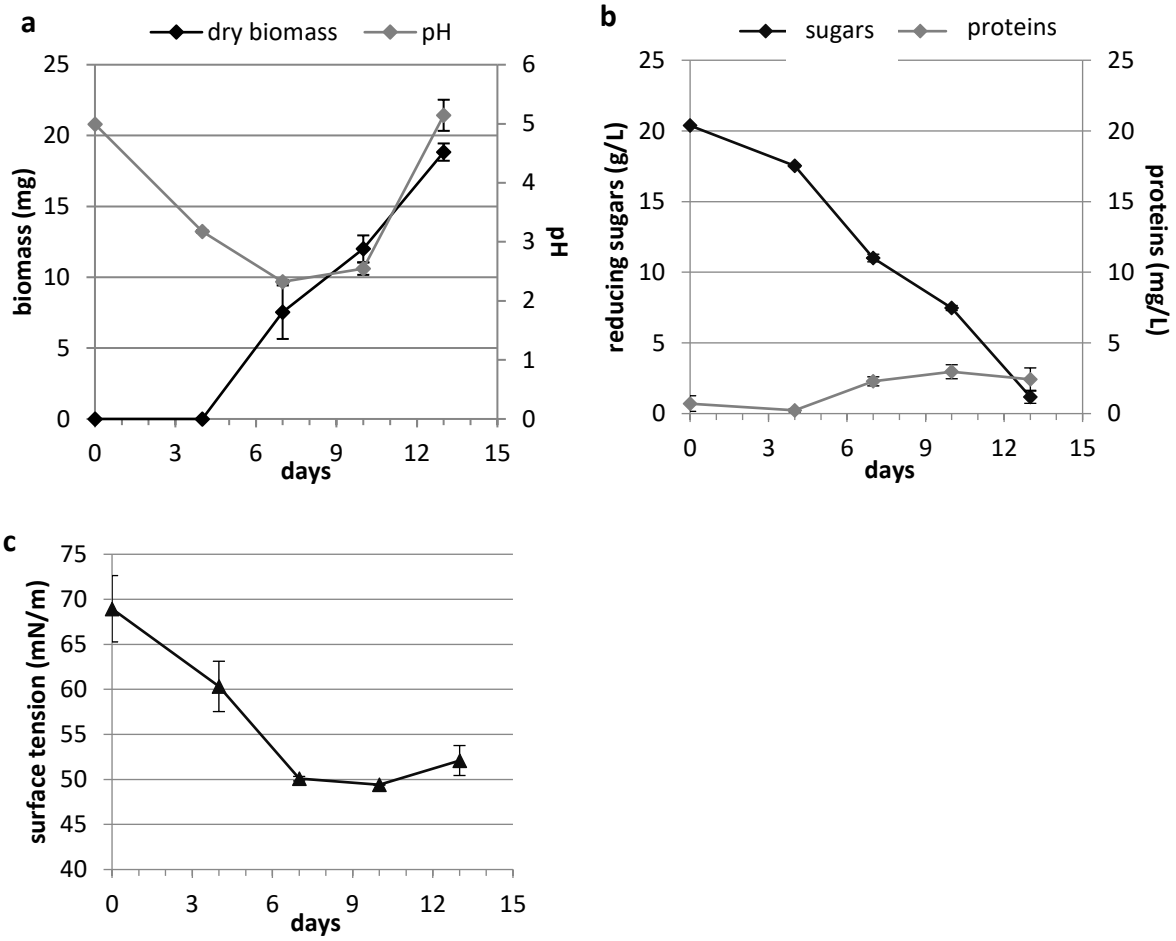

Fig. II.1 : Growth kinetics of *T. helicus* in mineral medium over 14 days and analysis of culture filtrates. a – dry fungal biomass and pH in filtrates – b: reducing sugar and protein concentration in filtrates – c: surface tension of filtrates.

activity in filtrates could thus be due to the production of surface active molecules displaying a protein group, possibly hydrophobins.

Fungal hydrophobins are known to be active at very low concentrations. Indeed, class II hydrophobins from the ascomycete *Trichoderma reesei* at 10^{-6} mol/L are able to lower the surface tension in water phases to up to 25 mN/m (Cox et al., 2007). For the sake of comparison, surface values of 50 mN/m observed in this experiment could be obtained with HFBII concentrations in the range of 10^{-7} to 10^{-6} mol/L according to the data reported by the same authors. Since the molecular mass of hydrophobins is in the order of 10 kDa, these concentrations correspond to about 10^{-2} to 10^{-3} g/L of protein. This is the same concentration range observed in the filtrates of *Talaromyces helicus* analyzed in this study, which means if the proteins detected are indeed hydrophobins, this low concentration is likely to be sufficient for detectable surfactant activity. It must be noted that results obtained with the Bradford

method are relative to the protein used as a standard, here BSA. Since different proteins react more or less strongly with the reagent, quantities may be over or underestimated. However it is still a useful indicator of the concentration order of magnitude, and for comparing concentrations between protein samples of similar composition. Purification and further analysis of the protein fraction from the filtrates is needed to confirm this hypothesis. Other biosurfactants possibly occurring in the culture filtrates could be glycolipids, lipopeptids or glycoproteins/peptidoglycans. To our knowledge no such biosurfactants are reported yet in the genus *Talaromyces*, however lipopeptide and lipopolysaccharide surfactants have been identified in other *Penicillium* species (Camargo-de-Morais et al., 2003; Gautam et al., 2014).

In order to estimate the saturation concentration of the surfactant relatively to its undiluted concentration, surface tension measurements were carried out on a 10 day-old filtrate sample and several dilutions thereof. This test aims at determining whether culture supernatants contain enough surfactant to saturate interfaces, and therefore to form micelles if applicable. The surface tension in the undiluted filtrate was 51.8 ± 0 mN/m (Fig. II.2), which is in the same order as that observed in the previous experiment (49 ± 0 mN/m). The 1/2 dilution displayed a similar surface tension value, only slightly higher than the undiluted filtrate. In contrast, the surface tension significantly increased with subsequent dilutions, and reached a surface tension equivalent to pure distillated water at a 1/16 dilution factor. Based on the profile of this curve, the slope decreases around the 1/2 dilution, which means that the surface saturation concentration is close to that value. As a consequence, saturation appears to be reached in the undiluted filtrate. However, it is important to note that a mixture of surface-active molecules may be present in solution, with different CMC values. The present experiment aims at evaluating the apparent saturation concentration resulting from all compounds present in the medium.

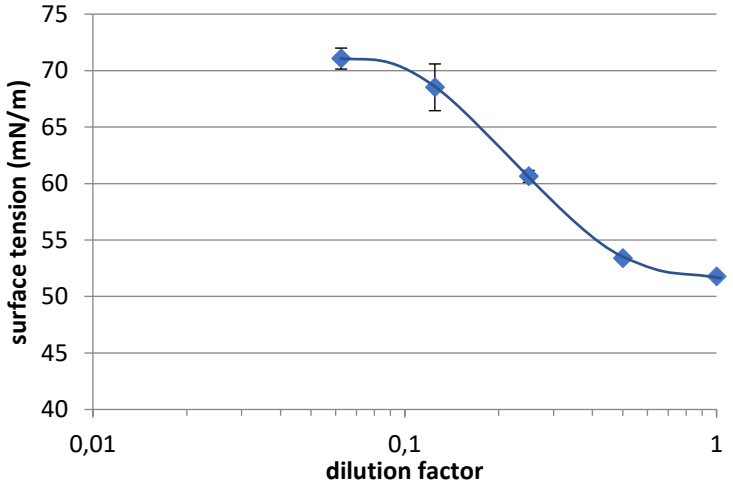

Fig. II.2 : Surface tension in a culture filtrate of *T. helicus* harvested after 10 days, as a function of its relative concentration (1 = undiluted filtrate). The curve is added for visual guidance.

3.2 Identification of surface active fractions in culture filtrates

3.2.1. Bulk fractionation by molecular size

Filtrates harvested after 10 or 13 days of incubation were fractionated using a size exclusion chromatography column. The aim is to fractionate surface active compounds in the filtrate into broad groups depending on their molecular size, rather than measuring their molecular weight (which would require better knowledge of their chemical nature in order to choose appropriate calibration standards). Indeed, surfactants can display a broad range of molecular sizes category: some such as liposan (Cirigliano and Carman, 1985) molecular complexes containing proteoglycans or glycolipids ranging in tens of kDa, while others like sophorolipids or phospholipids are relatively low molecular weight compounds below 1 kDa. Small proteins such as hydrophobins are in an intermediate molecular weight range (about 10 kDa): here, they stand in the lower molecular weight range of the resin used. As a first approach, this method will thus allow the separation of HMW molecular complexes from proteins and smaller molecules, to gain insight into the composition of the filtrates before further analysis of the fractions.

The column was first tested using a standard containing BSA (66.4 kDa) and glucose in order to verify the column total volume and separation. Protein and glucose content were detected qualitatively in the fractions by adding Bradford or DNS reagent respectively. Glucose was detected in fractions corresponding to an elution volume of 28.5 mL and higher. BSA was detected between 16.5 and 19.5 mL of elution volume. The resolution of the column is rather low: the initial 400 µL sample was diluted over 3 fractions with a total volume of 4.5 mL. Dilution is expected during size-exclusion chromatography, and could be limited by minimizing the sample volume while avoiding precipitation. Excessive dilution could be due to uneven column packing and elution caused by the poor control over pressure throughout the experiment. Indeed, improper packing of the resin bed can lead to the formation of preferential flow paths. However, these elution volumes for BSA and glucose are consistent with the expected column volume, and demonstrate that bulk separation of proteins from small solutes can be achieved with the column.

In order to concentrate the filtrates before separation and minimize the samples volumes loaded onto the colum, 10 mL aliquots to be analyzed were lyophilized and re-dissolved in 400 µL distilled water. The elution buffer chosen was adjusted at the same pH as the culture filtrates to avoid protein precipitation due to denaturation. A volatile buffer, ammonium acetate, was chosen to enable fraction concentration by evaporation in a Speedvac. After separation, the surface tension of each fraction was measured by the Wilhelmy method using a metal rod.

A first SEC run was performed on a sample of 10 day-old filtrate, which corresponds to the surface tension minimum (Fig. II.1.c). The filtrate was from the same batch used for the determination of saturation concentration, displaying a surface tension of 51.8 ± 0 mN/m (Fig. II.2). The relative glucose concentration in the fractions was measured by reading the absorbance at 575 nm after adding DNS reagent (Fig. II.3). The glucose concentration increased from 27 mL of elution on, and reached a plateau until the end of measurements at 36 mL. The elution of glucose indicates the end of the run, and occurs at the same time as a decrease of surface tension in the fractions. Four groups of fractions displayed a lowered surface tension: the first one from 5.5 mL to 8 mL, a second one around 18 mL, the third one between 24 and 25.5 mL and the fourth one at the end of the elution from 28.5 mL on (Fig. II.3). Thus, at least four surface-active compounds or groups of compounds with different molecular weights are present in the filtrate. The first one elutes at the beginning of the run, indicating that its molecular weight is above the upper separation limit of the resin of within its higher molecular weight range. The second one could be due to an extracellular protein with a molecular weight close to that of BSA, since it elutes at the same volume. The third compound is detected at the end of the run, right before glucose is eluted. It corresponds to the lower molecular weight range of the resin, and could match the molecular weight of hydrophobins around 10 kDa. The lowered surface tension at the end of the run cannot be due to the presence of glucose, since glucose on the contrary tends to increase surface tension (Docoslis et al., 2000). The filtrate therefore contains other low molecular weight surface-active molecules, smaller than 1 kDa if they are carbohydrates, or 5 kDa in the case of peptides (the separation properties of the resin for lipid conjugates or glycoproteins is not specified, and likely varies depending on their respective structures).

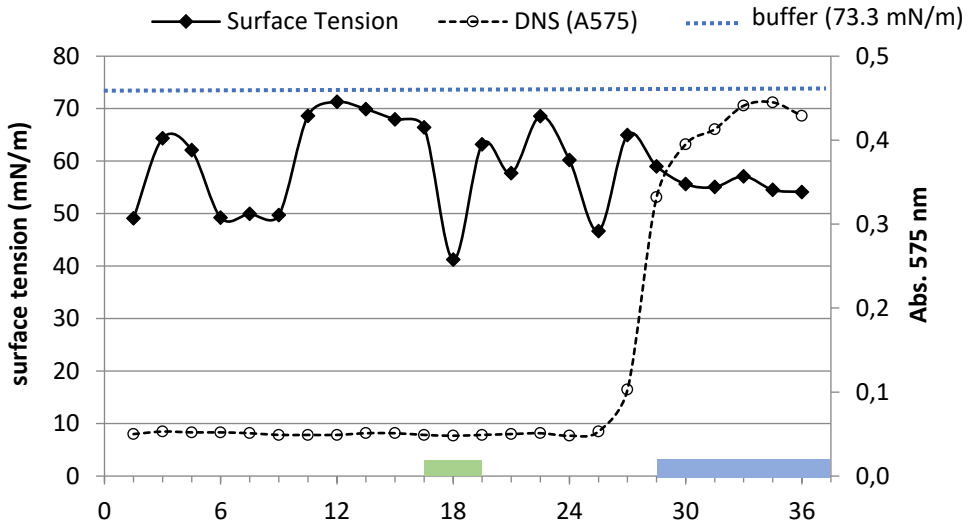

Fig. II.3 : Surface tension and relative glucose concentration in fractions obtained after SEC separation of 10-day filtrate. The elution range of BSA and glucose are highlighted in green and blue respectively.

Two more SEC runs were conducted with the 13-day filtrate, which corresponds to the end of the growth phase, when glucose is almost completely depleted from the medium and the surface activity is slightly above 50 mN/m (Fig. II.1). Both runs yielded similar surface tension profiles over the course of elution (Fig. II.4), but the surface tension profile of fractions was shifted by about 3 mL between each run, which indicates poor precision in the timing of the experiment, and/or deterioration of the column bed. The results differed from those obtained with 10-day filtrates, since less surface activity peaks were found, suggesting a different composition at this later stage of culture. A first group of active fractions was harvested in the early phase of elution (15 to 16.5 mL in run n°1), and a major drop in surface tension was detected at the end of elution once the total column volume was reached. Surface activity was also lowered in fractions collected around 30 mL, but still higher than the other two groups of fractions. This profile indicates that the filtrates contain at least two major surface-active fractions, with molecular weights being respectively close to the upper and lower limits of separation resolution for the resin used, and probably a third one with an intermediate molecular weight. In the second run, the first peak was split into two minima, which may be due to the presence of two compounds of close molecular weight that could not be efficiently separated with this protocol.

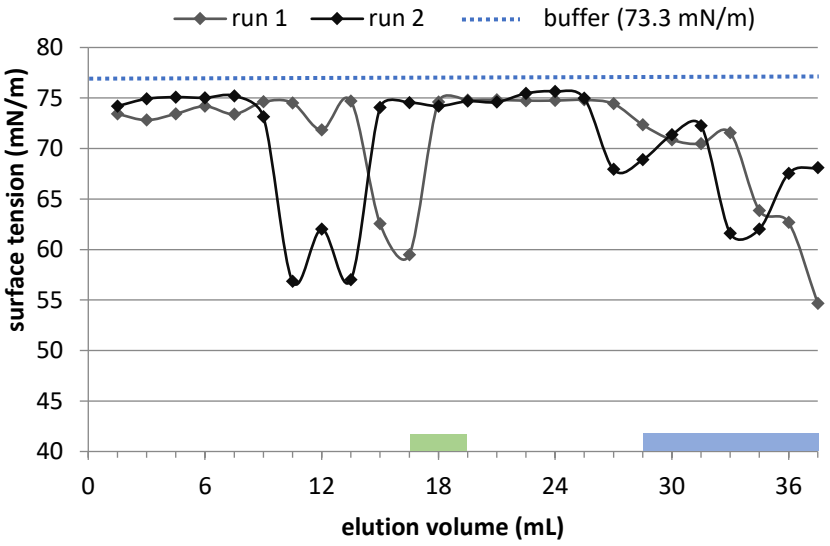

Fig. II.4 : Surface tension in SEC fractions from two runs with the same 13-day filtrate.

3.2.2. Characterization of the filtrates and fractions

In order to better characterize the content of the fractions obtained after SEC separation of 13-day filtrate, samples from run n°2 were analyzed by high-performance thin layer chromatography (HPTLC) at the Chromacim lab. Thin layer chromatography was chosen due to its high separation potential for complex mixtures and the possibility to detect a wide variety of compounds. Since culture filtrates are likely to contain a number of molecules of various biochemical families, this method appeared to be

well-suited. Moreover, the molecules of interest in the filtrates are surfactants, which means molecules with at least some degree of affinity with organic phases. The TLC methods allow using custom mobile phases depending on the polarity of the compounds of interest.

Due to its high molecular weight and insolubility in organic solvents, BSA did not migrate and was detected as a spot at the deposit well. It was visible as an extinction spot under UV at 254 nm, and after revelation with primulin under UV at 266 nm (probably due to the presence of hydrophobic amino-acids), but did not react with anisaldehyde. Glucose was revealed by anisaldehyde as an intense spot at Rf 0.05. Soy lecithin, which is a complex mixture containing mostly phospholipids, was separated into numerous well-defined spots distributed along the migration lane. Three main spots were revealed by primulin staining at Rf ≈ 0.20, 0.30 and 0.38, likely corresponding to different chain lengths and saturation degrees. Many spots including the three main ones were also revealed by anisaldehyde staining.

In the crude filtrate, the observation under UV at 254 nm revealed 5 main spots at Rf ≈ 0.08, 0.14, 0.38, 0.59 and 0.77, in addition to the glucose spot at Rf 0.05. Glucose was also detected as a large saturated spot stained by anisaldehyde. The residual concentration of glucose in filtrates after 13 days is in the order of 1 g/L (Fig. II.1.b). This means the quantity of glucose deposited on the plate is ≈ 50 µg, *i.e*. 5 fold higher than the quantity in the glucose standard, hence the very large and intense spot bleeding into the neighboring lanes. In addition to glucose, four anisaldehyde-positive spots were revealed in the filtrate at Rf ≈ 0.09, 0.17, 0.60 and 0.72. These spots correspond to 3 of the spots detected under UV at 254 nm, but the Rf 0.38 spot did not react with anisaldehyde, and on the contrary the 0.72 spot is barely visible at 254 nm. No spot was revealed in the filtrate after primulin staining, except for a faint fluorescence of glucose due to its very high concentration.

As expected, the culture filtrates appear to contain a mixture of several compounds with differing chemical natures. In addition to glucose, at least 6 main components were detected. Four of these compounds are anisaldehyde-positive, which indicates that they contain carbohydrate moieties, or at least carbonyl or alcohol groups. Two other compounds were detected at 254 nm (Rf 0.38 and Rf 0.77) but did not react with anisaldehyde nor primulin. None of these six compounds were stained with primulin, indicating the lack of hydrocarbon chains. They likely do not contain lipid moieties, and are therefore not glycolipids.

In the SEC fractions analyzed, glucose was found in increasing quantities in fractions n°18 to 25. In the five last fractions, migration was disturbed, probably due to the high concentration of glucose, leading to smeared spots and uneven migration lanes (Fig. II.5). The spots visible in the filtrate at Rf 0.08 and

0.14 were detected in fractions 20 to 25, a third spot at Rf 0.38 appeared in fractions 23 and 24, and the spots at Rf 0.6 and 0.72 were visible in fractions 24 and 25.

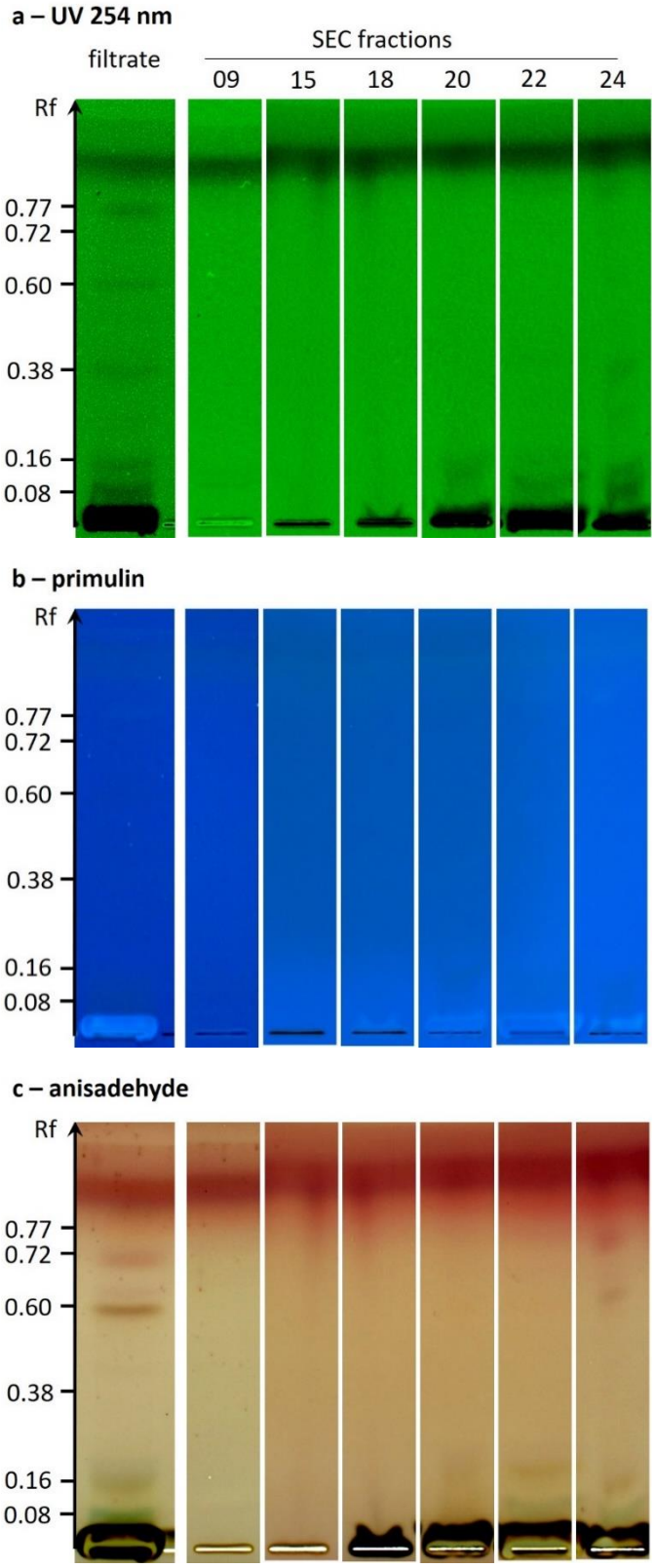

Fig. II.5 : HPTLC analysis of crude filtrates and SEC fractions – a : fluorescence quenching under UV at 254 nm – b : primulin staining under UV at 266 nm – c : anisaldehyde staining under visible light

Fractions n° 7, 8 and 9 displayed the highest surface activity (section 3.2.1, Fig. II.4): this means that they contain surfactants with a relatively high molecular weight, hence their early elution. However, no spot was detected by TLC in these fractions, neither under UV at 254 nm nor after chemical revelation. This could be explained in several ways: (i) - the surfactant has no affinity for the mobile phase and did not migrate: it could be a protein such as BSA, or a high molecular weight carbohydrate soluble in water but not organic solvents. It would then be detected at the deposit spot but the silica gel was damaged due to the high volume loaded, preventing reliable observations. (ii) - the surfactant migrated but was not detected due to the lack of an appropriate revealer; indeed some spots such as spot n°5 were not visible under UV at 254 nm and were only detected after staining with anisaldehyde. In particular, no staining solution for the specific detection of proteins and peptides was available. Other solutions that could be used are $KMnO_4$ for the detection of carbohydrates, nihydrin for free amines (proteins and peptides), α-naphtol for carbohydrates and some proteins.

Table II.1 : Summary of culture filtrate components detected by HPTLC analysis

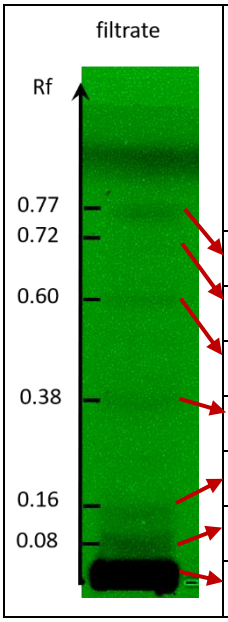

spot	Rf	UV 254 nm	UV 200 nm	anisaldehyde	primulin	fractions	Elution volume (mL)
6	0.77-0.8	+	+	-	-	All?	
5	0.72	-	(+)	+	-	(23) 24-25	34.5-37.5
4	0.58-0.60	+	+	+	-	(23) 24-25	34.5-37.5
3	0.38	+	-	-	-	23-24	33-36
2	0.15-0.17	+	++	+	-	20-25	28.5-37.5
1	0.08-0.09	+	+	+	-	20-25	28.5-37.5
glucose	0.05	+		++	-	18-25	25.5-37.5

As a summary, the native filtrate appears to contain mostly low molecular weight compounds, below the resin lower limit of separation (1 kDa for carbohydrates, 5 kDa for globular proteins). Indeed, all the main filtrate compounds detected in HPTLC were eluted at the end of the SEC run after 25.5 mL. The size exclusion resin chosen was therefore not the best suited to properly separate them. These compounds could be carbohydrates or compounds containing carbohydrate moieties. The presence of protein or peptidic fractions is possible but needs to be confirmed by further tests, either TLC with an appropriate chemical revealer, or SDS-PAGE. In particular, this could be the case of the high molecular weight surfactants in fractions 7 to 9, which was not detected by TLC analysis and the nature of which remains unknown. Although biosurfactants are chemically diverse, most known surfactants produced

by fungi contain a lipid moiety as their hydrophobic domain (see literature review – section 2). Such fungal surfactants can thus be detected through primulin staining after TLC (Park et al., 2005). The lack of lipids detectable in the filtrate and SEC fractions is therefore surprising, however the surfactants may be too diluted to be detected. Indeed, all compounds but glucose appear as faint spots. Concentration of the fractions may be required before TLC analysis, but the high glucose concentration may hinder proper migration. Alternatively, fungal lipid conjugates can be detected with reagents that specifically stain the carbohydrate moiety rather than lipids, including anthrone (Morita et al., 2007; Alimadadi et al., 2018), α-naphtol (Spoeckner et al., 1999), or anisaldehyde (Thanomsub et al., 2004).

3.3 Effect of culture supernatants on BaP desorption

In order to test the ability of surfactants from *T. helicus* to enhance the desorption of BaP from a solid porous matrix, desorption tests were conducted: cellulose discs soaked with BaP were incubated for 24 h in culture filtrates with constant orbital shaking. After 24 h BaP in the paper disc and the liquid phase was quantified separately to estimate the quantity of desorbed BaP.

The recovery rate of BaP upon extraction was about 85%. Out of 50 µg introduced initially, 39.2 ± 0.9 µg remained on the paper disc after 24 hours of incubation in the filtrate, and 2.6 ± 0.6 µg were transferred to the liquid phase (Fig. II.6). The results were similar in the control with pure MM1 medium: 39.8 ± 1.3 µg on the paper disc and 2.5 ± 1.7 µg in the liquid phase. In both cases only 6% of the total amount of BaP was desorbed from the discs and suspended in the liquid phase after 24 h of contact.

In this configuration, the filtrate from *T. helicus* culture did not enhance the transfer of BaP to the aqueous phase. One of the effects expected in this situation is the formation of “loaded” micelles containing BaP that could enhance its stabilization in the water phase. The dispersion of BaP solid flakes could also be promoted through a detergent effect of the filtrate, by coating the surface of BaP particles and enhancing their stability in aqueous suspension. In order for micelle solubilization to happen, the surfactant concentration must be above critical micelle concentration (CMC) (Paria, 2008). In the case of the filtrate used in this experiment, results presented in section 3.1 suggest its concentration is near or above surface saturation concentration. However CMC can vary depending on salt content, pH, and temperature among other factors. Moreover, as we showed in the previous section, the filtrate is a mixture of different molecules. Several of these compounds are likely to contribute to the surfactant properties, but they may not all be involved in the solubilization of hydrophobic compounds.

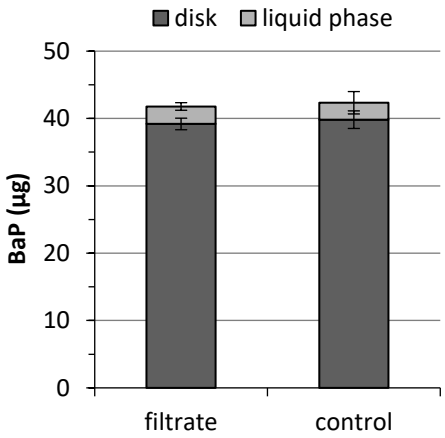

Fig. II.6 : Residual mass of BaP on a cellulose disc (dark grey) and in the liquid phase (light grey) after 24 h incubation in culture filtrates of *T. helicus* or fresh medium (control).

It must be noted that filtrates used in this experiments were produced in the absence of BaP, indeed the surfactant production when in presence of a hydrophobic substrate may differ both in terms of composition and concentration. In addition, surfactant properties of a given compound are not necessarily correlated with detergency and/or micelle formation: the surfactants detected may be involved in cell wall coating or surface conditioning promoting fungal contact with surfaces or interfaces, rather than the mobilization of hydrophobic substrates.

The desorption test was conducted in a large volume of liquid (10 mL) compared to the volume directly surrounding hyphae in soil pores, which would be in the order of microliters. Moreover, the partition of a surfactant between the aqueous phase and interfaces depends on both the surfactant concentration and the surface area available for adsorption. In this regard the batch set-up used here differs greatly from the soil environment, where surface/volume ratios can be extremely high. As a result, for an equivalent fungal biomass the amount of surfactants released in a culture batch is diluted into a large volume, whereas in a confined space the high local concentration can exceed saturation concentration and surfactants are thus more likely to accumulate at interfaces. The porosity and surface properties of the material itself also come into play: here, cellulose disks specifically designed for antibiograms were used, in order to mimic BaP adsorption to a porous matrix. Although cellulose itself is hydrophilic and allows the aqueous medium to soak through, the fiber network is likely to lower the accessibility of the solid BaP and keep particles trapped. The properties of microbial surfactants at a micro-environment scale in soils can thus differ widely from the properties measured in vitro, hence the relevance of approaches to study the interaction of fungal hyphae with solid surfaces and interfaces at a microscale.

4. Conclusions

Results obtained in this chapter show the production of surfactants able to lower the surface tension in filtrates to 49 mN/m. The biosurfactant appears to be saturated in culture batches, but does not show any effect on BaP solubilization in preliminary tests. At least three compounds or groups of compounds with respectively high and low molecular weights appear to contribute to surface activity in the filtrates. However their respective biochemical nature remains to be properly characterized. First results indicate that filtrates contain proteins (possibly hydrophobins) and carbohydrates, but no evidence of the presence of lipids was found. The high molecular weight compound(s) could be separated by size-exclusion chromatography but its chemical nature could not be identified through TLC analysis.

Further tests would need to be conducted to characterize the effect of culture filtrates of *T. helicus* on hydrophobic compounds, including insoluble solids like BaP or organic liquids such as petroleum oils. In particular, some limitations need to be addressed: surfactant production and hyphal surface properties are likely to differ when the fungus is grown in presence of a hydrophobic substrate. Moreover, the scale of batch experiments does not appropriately reflect fungal growth conditions in a porous matrix such as the soil. The role of biosurfactants for the access to hydrophobic substrates may lie in short-distance mobilization or direct contact with the pollutant source, rather than a simple solubilization mechanism. In particular, adsorption and uptake of the pollutant may be mediated by specific compounds modulating the surface properties of the cell wall. For these reasons interactions between the pollutant and the fungus should be investigated at the cellular scale, and the microfluidic device presented in chapter III will be used as a tool to monitor pollutant mobilization at the microscale.

Chapter III: Setting up a compartmentalized model environment using microfluidics

1. Introduction

Microfluidics is the field of study dealing with fluid flows at characteristic dimensions in the sub-millimeter range: at this scale, flows are dominated by capillary effects. As a technology, microfluidics encompasses a set of techniques involving the design and construction of devices to handle such flows in a controlled manner. These devices typically feature circuits with defined geometries, which can be constructed using microporous materials such as paper, or patterned onto silicon, synthetic polymers or glass (Yeo et al., 2011). One of the most popular approaches to microfabrication is the soft lithography technique: first a positive master is patterned by photolithography using a photoresistive resin, then a silicone elastomer, polydimethylsiloxane (PDMS), is cast onto the master, enabling for rapid and reproducible molding of the channel network. Channels can then be sealed by irreversible bonding of the PDMS slab onto a flat surface of glass, PDMS or other silicon-based polymers (Duffy et al., 1998).

The use of microfluidic devices for life science applications, including microbiology, has been increasingly popular since the beginning of the 2000's. Advances in microfluidics notoriously led to the development of DNA chips or microarrays, which greatly reduced sequencing time and cost at the turn of the 21st century, and enabled the amplification of minute amounts of input DNA. The dimensions of channels and chambers is of the same order as real biological structures containing flowing fluids such as blood vessels, plant vessel elements. They can be used to recreate miniaturized versions of animal tissues or organs on chip, being studied as potential alternatives to live animals for biomedical testing. Microfluidic chips enable the experimenter to implement flows, gradients, isolate single cells or cell populations in specific compartments, expose cells to textured or chemically functionalized surfaces, thus allowing a fine control over the cellular microenvironment (Whitesides et al., 2001). Such devices are usually constructed using bio-compatible and transparent polymers, PDMS being the most popular due to its transparency, low toxicity and permeability to gases. More recently, biopolymers and especially hydrogels have also drawn attention as materials for microfluidic applications (Kobel and Lutolf, 2011).

Like animal cells, bacteria and eukaryotic microorganisms live in complex micro-environments and are able to respond to various chemical, mechanical, thermal or electrical stimuli, which can be simulated in microfluidic devices. Microfluidic techniques have been used to investigate various aspects of microbial life including growth and replication, attachment or motility, response to concentration

gradients, communication (Rusconi et al., 2014; Zhou et al., 2019). In particular, microbial cells can be trapped in droplets or specific confined compartments, enabling the single-cell scale monitoring of organisms that would otherwise be studied as populations of millions of cells (Eland et al., 2016). Microfluidic gradient generators can be used to study chemotaxis in bacteria or yeast, a crucial mechanism involved in microbial nutrition and communication (Paliwal et al., 2007; Long and Ford, 2009; Kim et al., 2016)

The first applications for on-chip cultivation of filamentous fungi are the works of Kristi Hanson, Marie Held and co-workers, who designed microfluidic mazes to investigate space-searching strategies and morphogenesis of the model filamentous fungus *Neurospora crassa* in confined environments (Hanson et al., 2006; Held et al., 2010, 2011). Since then, a few studies dealing with the growth behavior of filamentous fungi were conducted using microfluidic platforms. Spore germination was investigated in several of them: Barkal et al. (Barkal et al., 2016) considered spore differentiation and germination of a whole population cultivated in the same chamber, whereas (Geng et al., 2015) trapped single conidia to observe the polarized growth of young hyphae in confined microchannels. Microfluidic devices can also be used as a tool to trap single hyphae in microchannels in order to carry out micro-injections directly into the cytoplasm (Bidanjiri, 2018). Indeed, the soft lithography techniques used to pattern microfluidic circuits allow the fabrication of structures with characteristic dimensions of a few micrometers, in the same order as hyphal diameter (about 2 to 10 µm in true fungi). Spiral-shaped channels were used to guide the rapid growth of *N. crassa* to allow longer observation times, in order to measure circadian changes in hyphal elongation rates (Lee et al., 2016). Thomson et al. (2015) studied hyphal tip asymmetry and growth orientation in response to substrate geometry and texture in micro-patterned chambers. Alternative approaches to microfluidics to monitor the growth of filamentous fungi without confinement involve the use of a sophisticated system for automated imaging and tracking of hyphae (Sánchez-Orellana et al., 2019).

Because they allow fine spatial control, microfluidic platforms are particularly interesting to replicate complex and heterogeneous environments. The modeling of natural porous media, including soil, is one of the applications of microfluidics. In particular, increasing demand from the petroleum industry for more efficient oil recovery techniques has led to the development of a whole field of study on the behavior of fluids, and more specifically oil, in the soil. Model porous media sometimes replicate the geometry of actual samples, such as porous sandstone (Nilsson et al., 2013) or fractured rock (Porter et al., 2015). In other cases, random geometric patterns can be computer-generated (Wu et al., 2011). Such devices can be used to study the behavior of oil/water biphasic systems, foams or unsaturated aqueous phases in a model porous medium (Ma et al., 2012; Conn et al., 2014)

The control over geometry, confinement, flow makes microfluidic platforms interesting tools for the development of "soil-on-chip" models to study not only soil physical properties, but also the soil microbial flora (Stanley et al., 2016). Organisms of interest can be trapped or transferred in a controlled manner in definite compartments, which is useful to study interactions between microorganisms. Physical interactions can thus be visualized in real time: for example bacterial attachment to fungal hyphae (Stanley et al., 2014; Millet et al., 2019) or the fungal colonization of plant roots during the formation of mycorrhizae (Millet et al., 2019). Coupled with metabolomic analysis, on-chip microbial co-cultures were used to investigate metabolic exchanges between bacteria and filamentous fungi (Uehling et al., 2019). Fungal cultivation in a compartmentalized environment highlights the spatial heterogeneity of the organism, and its ability to trigger localized responses to external stimuli: one example is signal translocation during fungal response to a pathogen attack (Schmieder et al., 2019).

Compartmentalization and spatial control over the micro-environment are features of particular interest in the context of our study, which focuses on fungal behavior in presence of unevenly distributed pollutants. In this chapter, we describe the development of a microfluidic device enabling fungal cultivation and the monitoring of pollutant mobilization. This device is intended to serve as a model compartmentalized environment where (i) - the experimenter has control over the location of a water-insoluble pollutant, benzo-[*a*]-pyrene, and (ii) – the pollutant source can be spatially separated from the organism studied, here the BaP-degrading fungus *Talaromyces helicus*.

2. Materials and Methods

2.1. Device requirements

In order to implement a chip design suitable for the cultivation and observation of *T. helicus* in presence of BaP, a number of features had to be considered. The goal was to develop a single versatile design that could be used in a variety of experiments: with or without perfusion, inoculated with an agar plug or mycelium pellets, introducing the pollutant as a solid or dissolved in a non-aqueous liquid phase.

In the context of this thesis, the device was initially developed to investigate whether direct contact with the pollutant source is necessary for intracellular uptake of benzo-[*a*]-pyrene by *Talaromyces helicus*. A physical separation between pollutant source and inoculum needs to be achieved by introducing them in definite compartments, in order to monitor the development of hyphae over time and their encounter with BaP. For this purpose, designs featuring two chambers connected by microchannels were chosen. The microchannels should be large enough to allow at least one hypha to grow through it (which is not a limitation in the case of *T. helicus* considering its hyphal diameter is 2-

3 µm), but thin enough to (i) - confine hyphae and enable the parallel observation of several single hyphae isolated in separate channels, and (ii) – prevent the transport of particles of BaP from the distal camber to the inoculation chamber. Hyphae can thus be tracked over time and changes can be observed at a single-cell level, with a high number of replicates in the same system.

The device should first of all enable the development of mycelium, and the possibility of prolonged cultivation times ranging from a few days to whole weeks. This implies that sufficient moisture and nutrients can be retained inside the cultivation chambers and that gas exchanges can occur, allowing fungal respiration. The materials used should be suitable for hyphal attachment so that the colony growing from its inoculation point is fixed and not floating in the liquid medium. The possibility of microscopic observations is also a requirement, and more specifically fluorescence microscopy: transparent materials with low autofluorescence are therefore needed. Rapid and reproducible fabrication is desired.

Finally, the chip should be suitable for perfusion with a flow of liquid medium: either to feed the culture with nutrients, to introduce effectors to stimulate or inhibit pollutant incorporation, or to inject the contaminant itself, either as a non-aqueous liquid phase or dissolved in an aqueous buffer. Another possible use of perfusion would be the recovery of degradation products or pollutant-induced fungal compounds for further analysis.

2.2. Fungal strains and media

The model species *Neurospora crassa* was obtained from the BCCM/MUCL Agro-food & Environmental Fungal Collection (strain MUCL 041473). *Talaromyces helicus* and *Neurospora crassa* were maintained on malt yeast extract agar medium (refer to chapter I for detailed recipe), at 22°C with a 12 h-12 h light-dark cycle, and transplanted onto fresh medium every ten days. The mineral medium MM1 described in chapter I was used for liquid cultures and to fill the culture chambers of microchips.
Radial colony growth on solid medium was monitored by imaging Petri dishes freshly inoculated with *N. crassa* or *T. helicus* (each strain in triplicate). For the fast-growing *N. crassa* pictures were taken every 6 h for 48 h, and for *T. helicus* pictures were taken every day for four days, then every 2 or 3 days until colonies reached the edge of the dish. For each image, the maximum and minimum diameter of the colony was measured using ImageJ, and the average diameter was calculated. Average and standard deviation were calculated for each triplicate.

2.3. Microchip design

Silicium wafers patterned by photolithography were used as positive masters for the fabrication of microchannels. Custom wafers were obtained from Microfactory (Institut Pierre-Gilles de Gennes, Paris, France). The 2 designs used are pictured in Fig. III.1.

- Ch1 consists in two rectangular chambers (800 µm wide, 4 mm long, 38 µm high) connected by a single 15 µm wide and 14 µm high channel, either 0.5 mm or 2 mm long. Inlets are punched at the end of each chamber.

- Ch50 consists in two chambers with rounded corners, connected by an array of 50 parallel microchannels. Each chamber is 3 mm wide, 5 mm long and 124 µm high. The microchannels are 10 µm high, 5.8 µm wide, and 0.5 or 1 mm long. Each chamber is connected to circular compartments of 2 mm in diameter, where inlets and outlet holes can be punched.

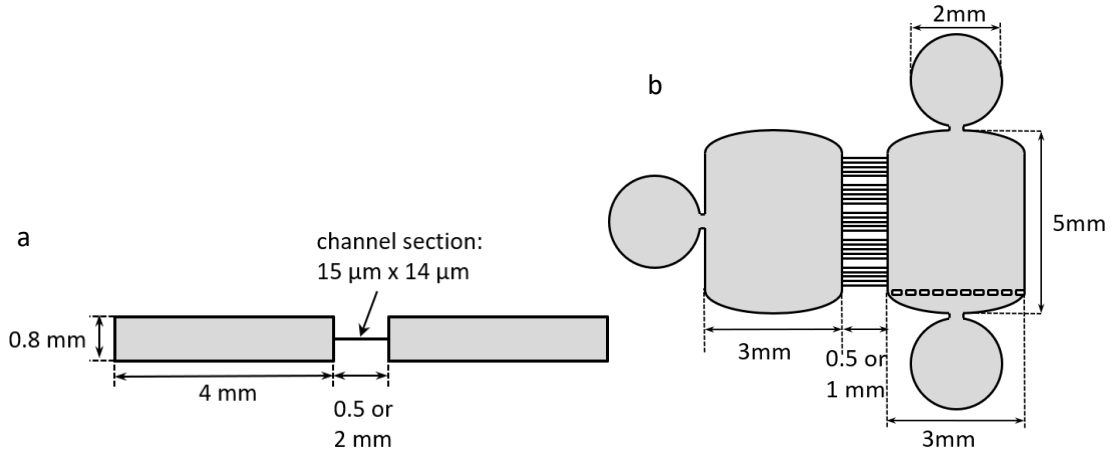

Fig. III.1: Diagram of the microchip patterns. a: Ch1 – b: Ch50

2.4. Microchip fabrication

PDMS chips - Polydimethylsiloxane (PDMS, Sylgard 184, Dow Corning) mixed with 10% reticulating agent was thoroughly degassed under vacuum, then cast against the wafer and left to cure for at least 2 h at 70°C. Inlets were added by punching holes in the PDMS block with a biopsy puncher (1 or 2 mm). The negatively patterned PDMS block was bound to a clean glass microscope slide or cover slip after surface oxidization in an oxygen plasma chamber (Harrick) for 60 s.

PDMS replicas - To avoid intensive handling of the fragile wafers, PDMS replicas of the patterns were made by first casting a negative mold in the same way described previously, then using this mold to cast the replica. In between each casting step, PDMS surfaces of the mold and replica need to receive an anti-adhesive surface treatment, here silanization, to enable unmolding after curing. This is done by activating the surfaces by oxygen plasma treatment for 60 s, followed by incubation of the replica

in a closed vessel filled with trichloro(1*H*,1*H*,2*H*,2*H*-perfluorooctyl)silane vapors (Sigma-Aldrich) for at least 2 h.

PDMS "sticker" chips - Alternatively to the regular PDMS chips described previously, thin PDMS "stickers" were fabricated and mounted between a glass slide and a cover slip. To make the stickers, approximately 100 µL PDMS was deposited on a silanized PDMS replica of the wafer, degassed under vacuum, pressed under a flat silanized PDMS slab and left to cure for at least 2 h at 70°C. Glass coverslips were pierced to form inlet holes using a micro-sandblaster (bipol, Bezannes, France) with 50-80 µm silica grains. The PDMS stickers were carefully unmolded while keeping the slab attached to avoid warping of the pattern, then bound to the pierced cover slip after plasma activation, aligning the inlets with the chambers. The PDMS slab used as support was then removed and the chip was placed on a glass side, PDMS sticker facing down. Inlets/inoculation wells were added by punching holes (1 or 2 mm) with a biopsy puncher in 4 x 4 mm PDMS blocks and by sealing the blocks onto the cover slip.

Double-sided tape chips - An fabrication method even simpler than PDMS casting consists in cutting a design out of 70 µm thick double-sided adhesive film (Aslan) using a programmable laser cutter (Speedy400, Trotec), and mounting it between two glass slides. This technique was only used for a pattern featuring two rectangular chambers (4 mm x 500 µm) joined by a single 1 mm-long channel. This geometry is similar to the Ch1 pattern, but the resolution of the laser cutter is lower resulting in less defined edges, and the channel is about 100 µm wide.

2.5. On-chip fungal culture

2 x 2 mm mycelium explants were collected from the edge of colonies growing on MYEA medium, aged 3 days to 1 week for *T. helicus*, and 1 day for *N. crassa*. The mycelium plugs were placed in the inoculation inlet of the chip previously filled with MM1 medium. A PDMS plug was used to close the inlet and prevent drying, and microchips were placed in a Petri dish sealed with parafilm to maintain a water saturated atmosphere. Chips were incubated at 22°C with a 12 h-12 h light-dark cycle, and growth was monitored by microscopic observations.

2.6. Liquid perfusion

For experiments requiring a dynamic medium flow, Ch50 chips were connected to a perfusion system. After pre-incubation of the chip to let the mycelium grow in the inoculation chamber, the inlet of the distal chamber was connected to a peristaltic pump (Ismatec) using PTFE tubing and mineral medium was fed through the chip at 1.8 µL/min.

In order to test whether concentration gradients could be implemented in the device, a chip featuring 1 mm long channels was filled with distilled water, then perfused with a $1.5 \cdot 10^{-2}$ mol/L fluorescein solution at 1.8 µL/min through the distal chamber using a peristaltic pump. The intensity of fluorescence in the chambers was monitored by fluorescence microscopy over 3 h using the FITC filter.

2.7. Imaging and data analysis

Fungal growth in the chips was imaged in bright field using a DMI-8 inverted microscope (Leica) equipped with a motorized stage and a Fastcam SA3 camera (Photron), or a DFC 3000G camera (Leica).

In Ch1 systems, images of the central channel (1 mm long) were taken every 60 or 90 min for 48 h. The distance between the tip of the leading hypha and the opening of the channel was measured using ImageJ. For long-term growth experiments over 14 days, Ch1 chips featuring 2 mm long channels were used, and the whole system was imaged every 2 or 3 days. Time-averaged elongation rates were calculated as (final length – initial length)/time over the time span of the experiment. When relevant, maximum growth rates were estimated as the slope of the curve during the linear phase.

For the monitoring of growth kinetics on Ch50 chips, images of 5 fields for each chip were taken at a 10x magnification every 10 min for *T. helicus* and every 5 min for *N. crassa*, for at least 10 h. In each channel, the distance between the tip of the longest growing hypha and the opening of the channel was measured using ImageJ. Unless indicated otherwise, channels presenting obvious signs of drying or disbonding from the glass slide were excluded from analysis, as well as those already filled with a hypha longer than half the length of the channel at the beginning of the observations. Time-averaged growth rates were calculated as (final length – initial length)/time over a maximum time of 10 h. For hyphae reaching the extremity of the channel earlier than 10 h, the last picture with a visible hyphal tip was taken into account. Spatio-temporal diagrams were generated using the KymoGraph plugin to visualize elongation rate variations.

Epifluorescence microscopy observations were performed using either an OLYMPUS BX60 microscope mounted with an Infinity 3-6UR camera (Lumenera) or the DMI-8 inverted microscope (Leica) equipped with a DFC 3000G camera (Leica). A DAPI emission filter selecting wavelengths between 435 and 485 nm was used to observe the autofluorescence of BaP, near its maximum emission peak at 405 nm. The FITC filter (maximum excitation 494 nm, maximum emission 518 nm) was used to observe the fluorescence of fluorescein.

2.8. BaP diffusion test

A PDMS slab mounted on a glass microscope slide was photobleached by exposing it to UV light using a UV Kub insolator (Kloe, Montpellier, France) at 100% power for 1 h.

1 µL of BaP stock solution was pipetted onto the PDMS slab, and the diffusion of BaP through the polymer was monitored by epifluorescence microscopy. Images of the slab were taken for up to 12 days after the time of deposit, and were analyzed with ImageJ by calculating the mean RGB value for each of the 7 measurement points between 0 to 16 mm from the deposit.

3. Results and discussion

3.1. Suitability for fluorescence observations

BaP is auto-fluorescent under UV light, presenting maximum excitation at 297 nm and maximum emission at 405 nm. Its localization can thus be directly observed under an epifluorescence microscope. BaP is able to enter fungal cells, staining the mycelium and more specifically intracellular vesicles, as observed in *F. solani* (Verdin et al., 2005; Fayeulle et al., 2014). The aim was to verify which kind of chip was best suited to observe the details of intracellular localization, and intracellular structures. The mycelium was imaged in bright field and epifluorescence microscopy, to evaluate the quality of observations in different chip designs.

3.1.1.Sources of background fluorescence in PDMS chips

Polydimethylsiloxane (PDMS) is a transparent material, however it displays autofluorescence properties: when excited at 403 nm, it is 3 times more fluorescent than borosilicate glass, and the autofluorescence is more intense towards shorter excitation wavelengths (Piruska et al., 2005). This can be a drawback for its use in epifluorescence applications with excitation in the UV range, causing a fluorescent background noise and interfering with the observation of faintly stained structures. One of the solutions to this problem is the photobleaching of PDMS chips prior to their use. Works previously conducted in the lab (Xue Sun, 2016, unpublished) concluded that 1 h of exposition to UV light using an insolator (UV Kub, Kloe, Montpellier, France) at 100% power was sufficient to bleach any detectable autofluorescence.

One of the problems encountered with PDMS is absorption of BaP into the PDMS matrix. Indeed, the absorption of PAH and other hydrophobic compounds into PDMS was already described, and possible applications for solid-phase extraction of PAH from water samples were proposed based on these observations (Mayer et al., 2000). Other lipophilic molecules including fluorescent dyes such as

Rhodamine B or Nile Red used as fluorescent markers are able to diffuse through the silicone matrix when injected into PDMS microfluidic chips (Toepke and Beebe, 2006; Robinson et al., 2009).

When BaP was introduced in microfluidic chips, it caused a high fluorescence background around the deposit, interfering with epifluorescence observations. The thicker the PDMS layer above the sample, the stronger the fluorescent background was: this observation led to tests using thin PDMS stickers to limit diffusion through the polymer, described in section 3.1.2.

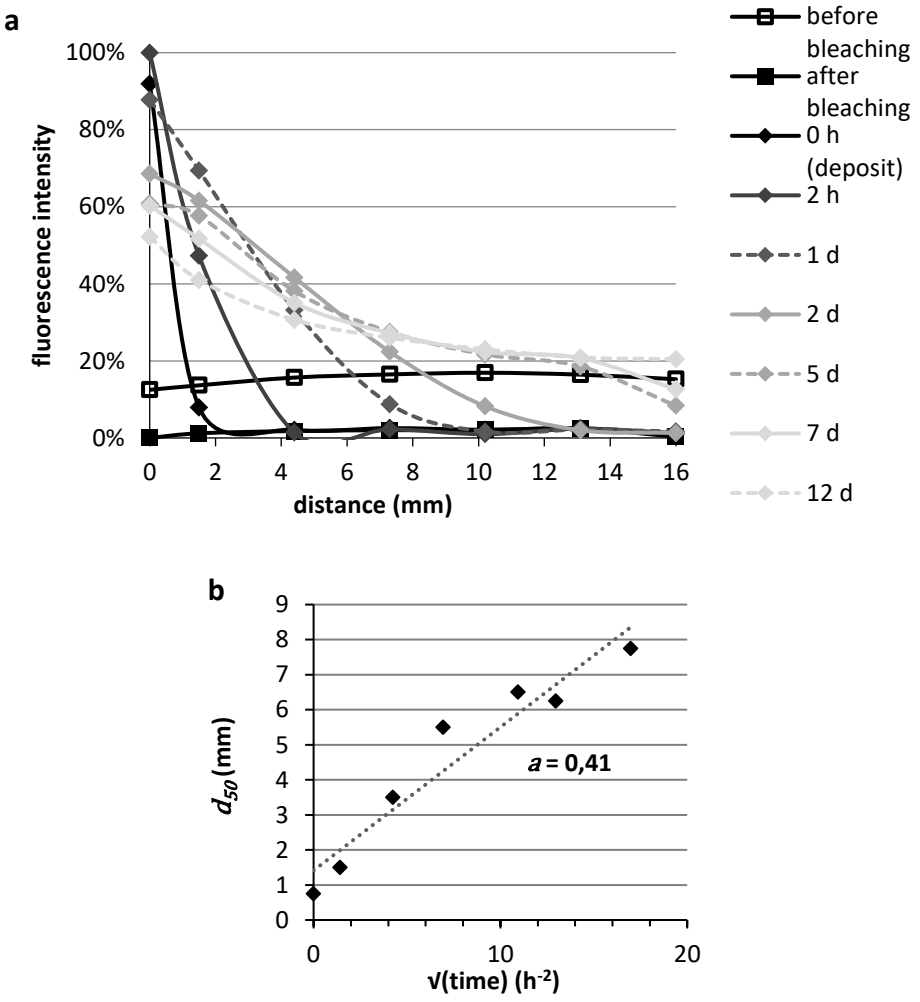

Fig. III.2: Fluorescence intensity on a PDMS slab around a BaP spot. a: Intensity profiles (as % of the fluorescence intensity at the deposit spot at T = 0) depending on the distance from the deposit spot, measured after several incubation times. b: d_{50} (distance at 50% of relative intensity for each time point) plotted against the square root of time.

The diffusion behavior of BaP in PDMS was tested by pipetting 1 µL of BaP stock solution onto a previously photobleached PDMS slab. Epifluorescence microscopy images of the slab taken at each time point were analyzed to measure the fluorescence intensity at each measurement point. The maximal intensity of fluorescence was located at the deposit spot, and the fluorescence intensity

decreased as the distance from the spot increased, along a bell-shaped curve (Fig. III.1a). At the deposit point, the maximum fluorescence intensity decreased over time, reaching 57% of its initial intensity after 16 days. Simultaneously, the BaP spot spread out around the deposit, with fluorescence being detected at increasing distances from the center. Considering in first approximation that the fluorescence intensity is proportional to the local BaP concentration, the diffusion coefficient D of BaP in PDMS can be evaluated by using the approximation equation of diffusion time for diffusion in two dimensions: $d_{50} = \sqrt{4Dt}$. d_{50}, the distance of half-intensity for each time point, is graphically determined based on the graph in Fig. III.2.a and plotted against the square root of time (Fig. III.2.b). The slope of this curve is a = 0.41, which entails that $D \approx (a^2/4) = 4.2 \cdot 10^{-2}$ mm^2/h or $1.5 \cdot 10^{-4}$ m^2/s.

3.1.2. On-chip observations of mycelium staining

In order to verify the quality of epifluorescence observations in several types of systems, liquid cultures of *T. helicus* were incubated for 48 h with BaP, then injected into the chamber of each tested system using a micropipette. Three different types of microchips were compared: a PDMS-on-glass system, a PDMS "sticker" system mounted between a glass slide and cover slip, and a double-sided tape system mounted between a glass slide and cover slip. As a reference, a droplet of liquid culture containing mycelium pellets was directly mounted between a glass microscope slide and cover slip.

On microscope slides used as a control, strong staining was observed, with sharp outlines (Fig. III.3.a). The background fluorescence was low, ensuring good contrast. Fluorescence is specifically localized in intracellular vesicles appearing as brighter areas with a clear outline, against septa and at the cell periphery. Other areas display a more diffuse fluorescence in the cytoplasm.

In PDMS-on-glass systems, the fluorescent staining was faint and diffuse. No stained intracellular structures were discernable, and no preferential localization of BaP was apparent (Fig. III.3.b). Despite previous bleaching, a strong fluorescent background interfered with the observations. Since the delay between mycelium injection and observation was too short for any significant diffusion of BaP, this background fluorescence may be due to the diffraction of emitted fluorescence through the relatively thick PDMS layer (≈ 3 mm). Impurities entrapped into the polymer, or reticulation heterogeneity may be responsible for such diffraction. Moreover, PDMS presents a higher refractive index for shorter wavelengths (Schneider et al., 2009), which may amplify this phenomenon when observations are carried out in the blue range.

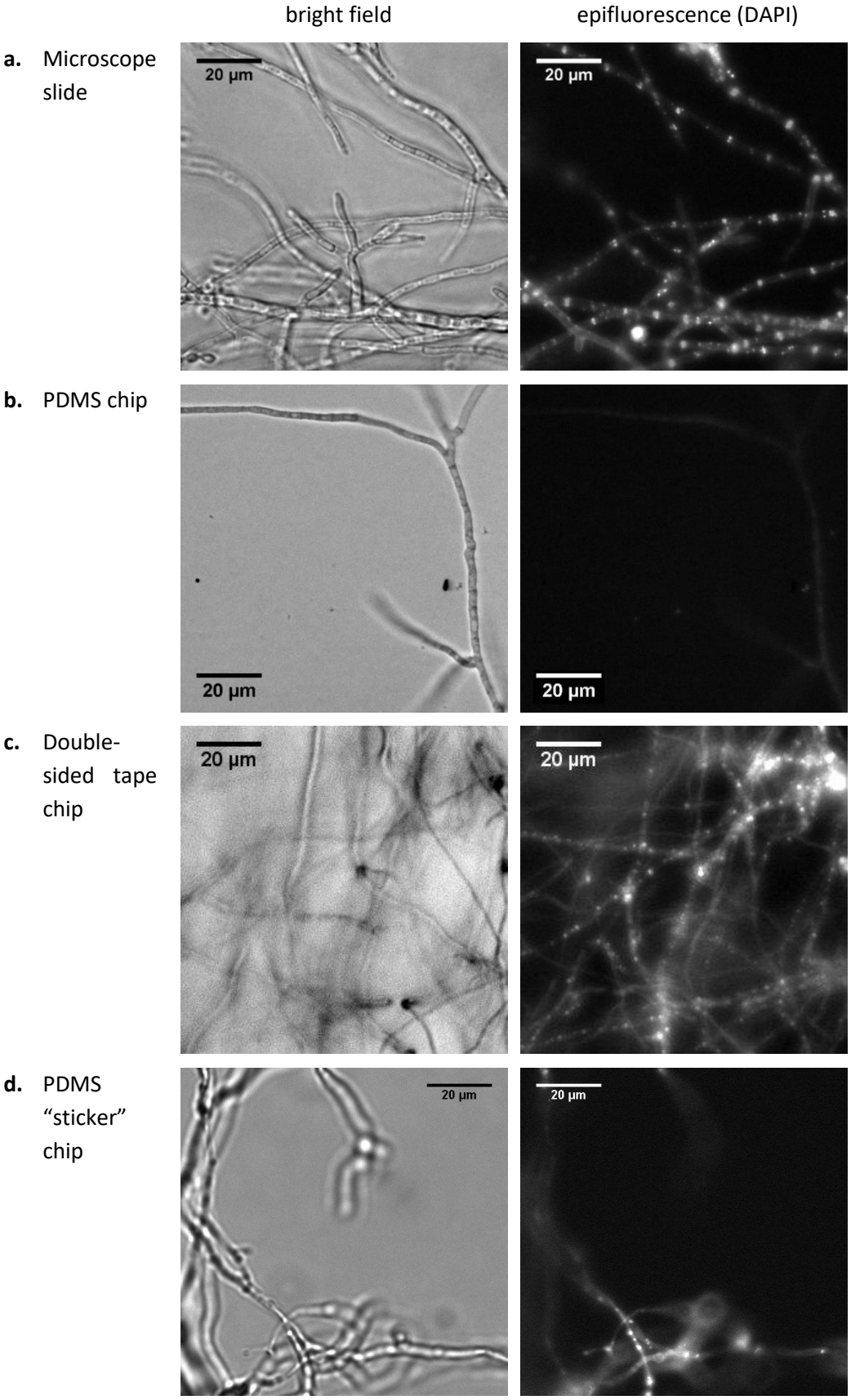

Fig. III.3 : Mycelium of *T. helicus* observed in bright field and epifluorescence microscopy, displaying a fluorescent marking after 48 h of incubation with BaP. Mycelium samples were mounted on a glass microscope slide (a), or injected in three different types of microfluidic chips (b, c, d)

In double-sided tape systems, the observation of intracellular structures was possible: hyphae appeared strongly stained, with visible intracellular vesicles (Fig. III.3.c). However, the degree of observable detail was still lower compared to images obtained with a regular glass slide.

In PDMS "sticker" systems, a strong staining of hyphae was observed, with some visible vesicles. The background was less fluorescent than it was in classical PDMS chips. However the outline of stained cellular structures did not appear as sharp as on a glass microscope slide. Out of the three chip configurations tested, double-sided tape systems and "sticker" systems appeared to be better suited for fluorescence observations than thick PDMS chips, yielding images with lower quality than a regular glass slide, but with a satisfactory sharpness and low to no background fluorescence. In the case of double-sided tape systems, there is no other material than glass on the optical trajectory. Double-sided tape systems are particularly cheap and fast to fabricate, however channels fabricated with this method cannot be narrower than 100 µm due to the thickness of the tape and resolution limitations of the laser cutter. The sealing of such systems is also not optimal due to the roughness of the tape surface: prolonged culture of filamentous fungi in this type of chip may result in hyphae growing into the gaps between the tape and the glass slide.

In systems made out of PDMS, the PDMS layer covering the sample caused a blurring of the image and a fluorescent background. This is a hindrance for clear observation of the fluorescent staining in hyphae, especially when attempting to observe intra-cellular structures at the micrometer scale. The effect is stronger, the thicker the layer of PDMS: a thin PDMS sticker thus yielded better results than a standard PDMS block. The PDMS sticker appears to be the best compromise to ensure precise and reproducible control over the channel geometry, and limit background fluorescence. However, the manual fabrication of such devices is particularly tedious, and PDMS stickers were frequently teared or warped during unmolding, preventing sealing. As a consequence only a few chips could be successfully constructed with this method: for routine experiments, PDMS-on-glass chips were finally chosen for further experiments, and a get-around to the background fluorescence issues was found by using a laser scanning confocal microscope for imaging.

3.2. On-chip fungal culture

3.2.1. Hyphal growth through a single channel

Fungal growth tests were first carried out in chips patterned with the Ch1 design, featuring two rectangular chambers connected by a single 2 mm long channel with a 15 x 14 µm section.

Culture chambers sometimes dried out before the mycelium could reach the opening of the channel, in which case they were excluded from analysis. In some cases, the mycelium was able to form

conidiophores in the air-filled chambers (Fig. III.4.a). The conidiophores exhibited a biverticillate morphology ending in chains of conidia. Coiled hyphae typical of the *Talaromyces helicus* species (Stolk and Samson, 1972) were also observed (Fig. III.4.a). Another problem encountered was imperfect sealing of the PDMS slab from the glass slide, causing PDMS to peel off from the glass slide under the effect of mycelial growth. Hyphal tips growing between the glass slide and PDMS appeared thicker with many branches and visible vesicles (Fig. III.4.b). Microchannels were also sometimes deformed due to the growth of multiple hyphae in a single channel. Deformations due to hyphae pushing against PDMS walls was already described and used to quantify tip forces during hyphal elongation (Thomson et al., 2015). Fungi appear to be able to develop considerable turgor pressures driving hyphal penetration into host tissues or solid substrates (Roper and Seminara, 2019). In order to ensure containment of the fungus in the culture chamber, weak sealing of the chips should be avoided. Impurities at the surface of the PDMS slab or the glass slide, or imperfect flatness of the surface, can be avoided as much as possible by ensuring the cleanliness of all materials and tools. Channels must also be separated by a sufficient distance to ensure tight sealing and prevent hyphae from causing disbonding and growing into neighboring channels.

In some cases, fragments of mycelium or spores from the inoculum were pushed through the channel into the distal chamber, and as a result mycelium grew from both directions. In order to retain mycelium fragments in the inoculation chambers, narrower channels could be a solution. The mycelium plug must also be collected from the edge of a relatively young colony (less than 1 week old) to avoid introducing spores, which can be easily transported from one chamber to the other by convective flows.

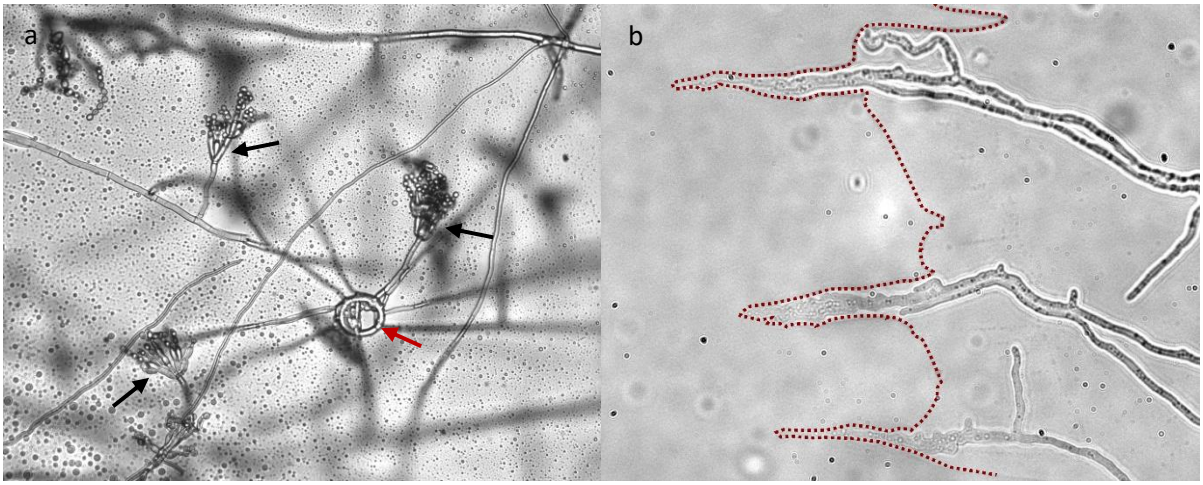

Fig. III.4 - a : Aerial mycelium of *T. helicus* growing in a dried out chamber, with coiled hyphae and biverticillate conidiophores (indicated by red and black arrows respectively) - b : hyphae growing between the glass slide and the disbonded PDMS slab (disbonding front highlighted with a dotted red line)

Hyphal growth through a 2 mm long channel was monitored over 14 days in 4 chips. Over the duration of observations in each chip, the mycelium grew respectively by 548, 517, 513 and 139 µm/day on average. This translates to an average elongation rate of 17.9 ± 8.1 µm/h. In 3 out of 4 chips, elongation tended to accelerate once the opposite chamber was reached. This was not observed in the fourth chip, where a lower average elongation velocity was measured. This first experiment was useful to gain information about the time scales needed to cultivate *T. helicus* in such chips. However a higher measurement frequency would be needed to study hyphal elongation behavior over shorter time periods.

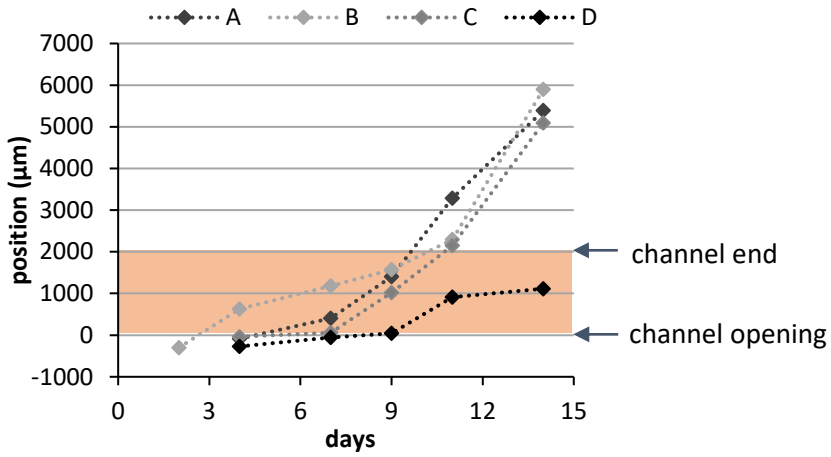

Fig. III.5: Elongation profile of *T. helicus* in 4 Ch1 chips (A, B, C and D) with a 2 mm long channel, over 14 days of observation. The opening of the channel corresponds to the 0 position.

In order to investigate the growth behavior of *T. helicus* more specifically inside the channel, chips featuring a shorter channel (0.5 mm) were inoculated so that the fungus would be able to reach the opposite chamber in less than 3 days. The growth was monitored in time-lapse over 72 h, with automated imaging. Since the chips were incubated for an extended period of time in the open air on the microscope, several of them dried out and did not yield any interpretable data.

Only two of the growth time-lapse experiments in Ch1 systems resulted in data that could be analyzed, with time-averaged growth speeds in the channel of 45 and 23 µm/h respectively. The elongation rate of hyphae in the channel was variable over time, as the elongation profiles presented in Fig. III.6.a show. In one of the systems, a first rapid growth phase with a maximum elongation rate of 105 µm/h was followed by complete growth arrest 7.5 h after entering the channel. In the other system, two linear elongation phases were observed separated by a growth arrest for 3 h. The maximal elongation rate in this system was 39 µm/h.

Several hyphae were able to enter the channel and branch inside of it, due to its being wider than hyphal diameter. Frequent branching could be a reason for variable elongation rates over time: indeed,

arrest of hyphal growth prior to branching events was also observed in experiments studying the unconstrained growth of single hyphae (Sánchez-Orellana et al., 2019). Drying occurred during observation time, as air bubbles formed in the distal chamber until reaching the channel (visible on Fig. III.6.b), which could also explain slower or arrested growth.

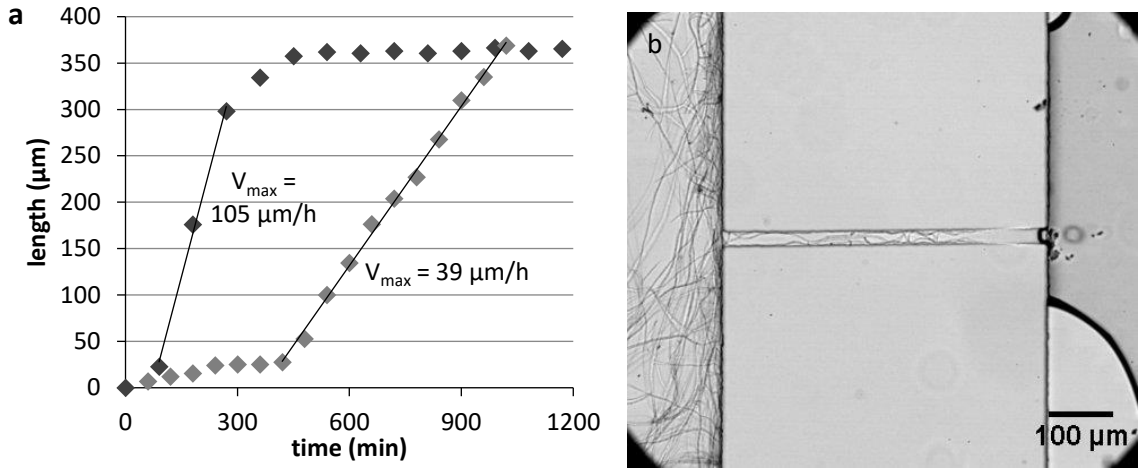

Fig. III.6 : a - Elongation profile of *T. helicus* mycelium through a single microchannel in the Ch1 microchip, observed over 48 h. Each curve represents one chip. b - Mycelial growth through a single channel observed at 20x magnification.

Due to the presence of a single channel in the Ch1 design, the number of elongation measurements in parallel is limited, or requires the use of a high number of chips. Fabrication defects such as deformations or the presence of dust blocking the channel can render the whole chip unusable or greatly affect the results. A design featuring multiple channels would save time by permitting a higher number of parallel observations on the same chip, and reduce the impact of individual defective channels. Moreover, the channel is relatively wide compared to the diameter of hyphae: narrower channels would help achieve higher confinement and better compartmentation, preventing mycelial fragments from escaping the inoculation chamber.

Finally, evaporation of the liquid medium leading to bubbles or even complete drying of the chambers was a recurrent problem in experiments carried out with Ch1 chips, especially when these were left on the microscope stage for several hours for automated imaging. This issue led to a number systems being eliminated from analysis. Bigger culture chambers could partially solve this problem, by storing a higher volume of liquid. The opening of large contact interfaces with air directly in the chamber could be prevented by the introduction of specific compartments for punching inlet and outlet holes, separated from the main chamber by a constriction.

3.2.2. Hyphal growth through an array of parallel channels

The chip design "Ch50" was designed to overcome several limitations of the Ch1 geometry: it features 2 larger chambers joined by 50 narrow parallel channels (described in Fig. III.1.b), allowing many parallel observations and increasing the degree of confinement. In order to verify the suitability of the Ch50 device for fungal culture, the growth behavior of *T. helicus* in microchannels was monitored. *N. crassa* was chosen as a reference to compare the results obtained here with data available in the literature, since the growth behavior of this species is well studied and it has already been used in several microfluidic studies on filamentous fungi (Hanson et al., 2006; Held et al., 2011; Lee et al., 2016). The comparison with *N. crassa,* rather than other extensively studied model fungal species such as *Candida albicans,* is also justified by its lifestyle similar to *T. helicus*: *N. crass*a is a saprotrophic ascomycete found in soils. In contrast to *N. crassa*, little information is available on the growth and morphology of *T. helicus*, or other species of the *Talaromyces* genus.

In order to monitor hyphal growth of *T. helicus* and *N. crassa* in confined conditions, Ch50 chips were inoculated with mycelium plugs, and the linear elongation rate of individual hyphae was measured for both species during their growth through the microchannels. The mycelium was left to grow until reaching the opening of microchannels before being mounted on a microscope for time-lapse observations. Hyphal growth was monitored in parallel in multiple channels over 10 h, and the hyphal tip position in each channel was measured to calculate elongation rates. The experiment was repeated at least 3 times for each species, with and without mineral medium perfusion. Growth was measured in a total of 280 channels from 15 separate chips, 6 in static conditions and 9 in dynamic conditions.

In *N. crassa*, mycelial growth was faster than in *T. helicus*, consistently with observations of colonies growing on agar (see section 3.2.3). Hyphae of *N. crassa* filled the inoculation chamber and reached the opening of the channels about 12 h after inoculation of the chip, compared to 2 to 3 days for *T. helicus*. Hyphal diameter in *N. crassa* is about 10 µm, in contrast to *T. helicus,* which exhibits hyphae ranging from 2 µm (for young, growing hyphal tips) to 5 µm (for older, septate and vacuolized hyphae) in diameter. As a consequence, single hyphae of *N. crassa* fit tightly into the microchannels, while each microchannel can contain multiple hyphae of *T. helicus,* which sometimes branch inside the channels until forming a bundle of parallel filaments (Fig. III.7.b).

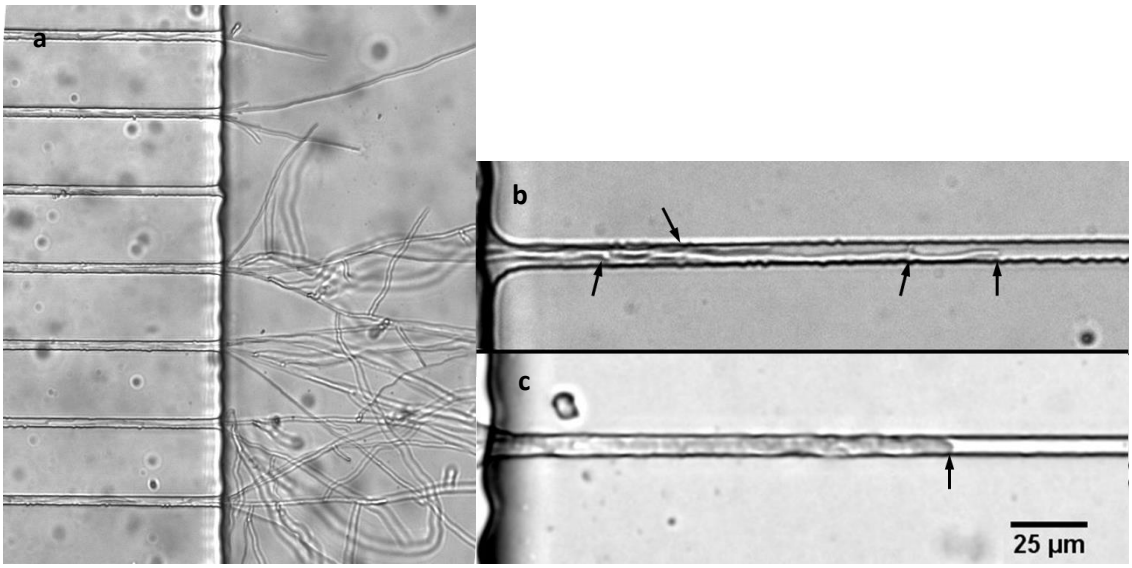

Fig. III.7: Fungal growth through parallel microchannels in Ch50 chips (inoculation point on the left side of images) – a: mycelium of *T. helicus* exiting the channels and entering the distal chamber – b: Comparison of hyphae of *T. helicus* (top) and *N. crassa* (bottom) growing in 5.8 wide microchannels. Hyphal tip and branching points are indicated by arrows.

Time-averaged elongation velocities were considered and compared between a large number of channels. Significant variations in average elongation velocities were observed from one chip to the other for *T. helicus* (Fig. III.8): this could be due to inconsistent inoculum size or different metabolic state when the mycelium plug was collected. The age of the agar plate used to collect the inoculum could impact growth rates, as well as the quantity of nutrient agar transferred along with the mycelium. The average elongation velocity without perfusion (45 channels analyzed from 3 different chips) was 47 ± 19 µm/h, which is consistent with values found in the Ch1 system (see section 3.2.1). In *N. crassa,* the elongation velocity was 190 ± 46 µm/h on average, and did not differ significantly between chips inoculated on the same day with plugs from the same culture.

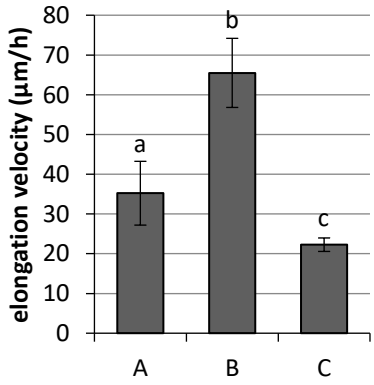

Fig. III.8 : Comparison of average elongation velocities of *T. helicus* in three microfluidic chips without perfusion Values that are significantly different (p<0.05) are indicated with different letters.

3.2.3. Effect of confinement

Radial extension velocities of fungal colonies on agar were measured and compared to the hyphal elongation velocities in confined microchannels. Mycelium plugs of *Neurospora crassa* and *Talaromyces helicus* were inoculated at the center of Petri dishes and left to grow until the colony reached the edge. Radial growth profiles showed a similar trend: a short lag phase was observed at the beginning of incubation, followed by second phase where the colony radius increased linearly (Fig. III.9). The slope of the curve during this second phase was calculated by linear regression to reflect the maximum extension velocity, which reached 25 mm/day for *N. crassa*, and 2.7 mm/day in *T. helicus*. Both strains displayed consistent colony sizes between replicates. *T. helicus* grew colonies of 33.4 ± 0.1 mm in diameter after 7 days, which is consistent with values of 25 to 33 mm reported in the literature (Yilmaz et al., 2014). The colony extension velocity found on Petri dishes for *N. crassa* was consistent with those found by Steele and Trinci (1975), which were 23.7 and 21.2 mm/d for two different strains. This radial extension velocity, equivalent to 17.4 µm/min, is also in the same range as that of unconstrained hyphal elongation velocity in *N. crassa* reported by (Potapova et al., 2016), which is 24 µm/min.

Radial colony growth of *T. helicus* on agar was about 2.5-fold faster than the elongation rate in microchannels, while the same was 5.5-fold faster for *N. crassa*. Confinement and limited nutrient availability during on-chip culture have decisive influence on the growth rates for both species. However, *N. crassa* was more affected than *T. helicus*: this difference could be explained by the faster growth of *N. crassa* in general. Indeed, a higher growth rate implies faster nutrient consumption of nutrients, which are in large excess on an agar plate but in short supply in the microfluidic chambers.

It must be noted that radial colony extension does not necessarily coincide with hyphal extension rates: Indeed, radial extension depends on both the extension velocity of individual leading hyphae at the edge, and the direction of their growth. A significant difference between colony extension and hyphal extension velocities would mean that hyphae at the edge do not typically grow radially from the center but in various directions. As a result, the tip elongation velocity of single leading hyphae is not sufficient to predict the volume of substrate covered by the mycelium. A fixed hyphal length can correspond to a diversity of morphologies, depending on branching distance, angle and frequency.

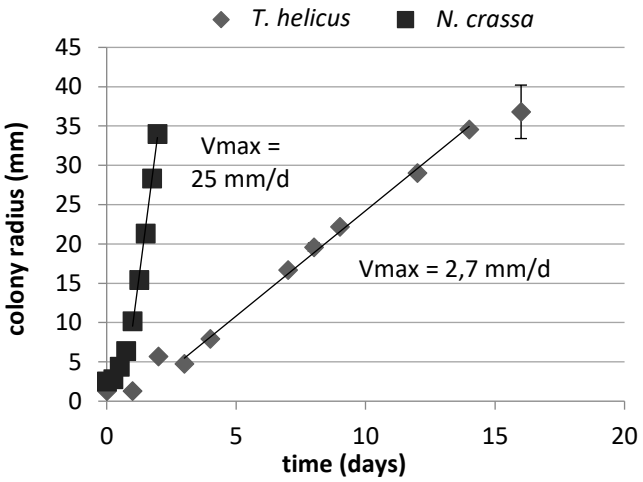

Fig. III.9 : Average colony radius over time for *N. crassa* and *T. helicus* grown on MYEA agar (average and standard deviation for triplicates). Trend lines were computed by linear regression for the linear growth phase and plotted on the graph.

For *T. helicus*, branching events occurred during growth through the straight channels and were usually associated with a brief pause or a decrease in elongation velocity. Pauses before branching events were also noted in *Trichoderma atroviride*, another soil ascomycete (Sánchez-Orellana et al., 2019), and have been reported for apical branching in *N. crassa* as well (Riquelme and Bartnicki-Garcia, 2004). Due to the different hyphal diameter in each species, the degree of confinement in microchannels differs, which may impact elongation rate, branching frequency and directionality. Hyphae of *N. crassa* were able to cross the 500 µm long channels without forming any lateral branches, which suggests it adapted its branching length to the geometrical constraints of the microsystems. Indeed, branching distances reported in the literature for *N. crassa* in the case of unconstrained growth on agar are in the range of 200 µm (Held et al., 2010; Potapova et al., 2016). Held et al. (2010) observed that the branching distance dropped from 219 µm on agar to 23 µm for confined growth in microfluidic channels arranged in a complex maze. In contrast, branching distances of 369 µm on average were observed when growing hyphae of *N. crassa* on agar after isolation from the parent colony, compared to 175 µm for hyphal tips still attached to the colony (Potapova et al., 2016). In the experiment we performed, the straight geometry of the channels can explain the suppression of branching over distances longer than 500 µm, exceeding the average unconfined branching distance. These results confirm that the branching distance in *N. crassa* can be adapted in response to mechanical constraints, stress or resource shortage. Such adaptations of growth behavior in the soil can be an advantage for scouting solid substrates upon nutrient limitation. A longer branching distance allows increasing the overall area of the colony while keeping the hyphal density low, thus saving energetic resources. On

the contrary, a high branching frequency associated with short branching distances increases the chances to find an exit when growing through a tortuous network of pores.

3.3. Implementation of a perfusion

Ch50 chips were designed to allow the implementation of a perfusion through one of the chambers, in a perpendicular direction to the channels. In order to evaluate the characteristic time of solute transfer from the perfusion chamber to the inoculation chamber (which is a dead end in this case), perfusion experiments were performed with a fluorescein solution without mycelium. A chip featuring 1 mm long channels was perfused with a 50 mg/L fluorescein solution at a flow rate of 9 µL/min. The fluorescence intensity in each chamber was monitored over time.

The fluorescence intensity in the perfused chamber reached its maximum 10 min after starting the perfusion. Since the depth of both chambers is the same, local fluorescein concentrations can be calculated as a function of fluorescence intensity, with the maximal fluorescence intensity being used as a reference for 50 mg/L. Over the whole experiment time, fluorescence intensity in the inoculation chamber remained significantly lower than the chamber perfused with fluorescein solution. After an increase in the first 30 min, it stabilized for the remaining two hours (Fig. III.10.a). A concentration gradient can thus be achieved by perfusing one of both chambers, resulting in a polarized environment that can be maintained in a relatively stable state over several hours. In this regard, the geometry chosen is reminiscent of some microfluidic gradient generators featuring a row of microchannels joining two perfusion chambers, which have been used to implement concentration gradients with co-current or countercurrent perfusions. Using specific nutrients or signal molecules, such concentration gradients can be used to orientate cell growth or migration (Zhang and van Noort, 2011; Kim et al., 2016).

Depending on the distance to the perfusion inlet, the plateau value varied: the fluorescent intensity was lower in the downstream part of the chamber (Fig. III.10.b). Since the chamber has no open outlet, fluid transfers can only occur through the channels. In first approximation, the fluid in the inoculation chamber was considered to be static. However, concentration variations along the length of the chamber cannot entirely be explained by fluorescein diffusion: a fraction of the input flow in the perfusion chamber leaks into the inoculation chamber through the channels closest to the inlet, thus increasing the local fluorescein concentration. As a consequence, liquid flows in the reverse direction through the channels close to the outlet, so that an equal amount of fluid enters and leaves the chamber. The flow rate through the microchannels can be predicted using a simple one-dimensional model of fluid flow presented in appendix : this flow rate is dependent on the microchannel position along the chamber, in a linear manner. This is consistent with the fluorescence profiles described in

Fig. III.10. In upstream channels, accelerated transport of solutes towards the inoculation chamber occurs, slows down then reverts back towards the perfusion chamber in the downstream part of the chip, the flow rate through microchannels located at the middle of the chambers being null.

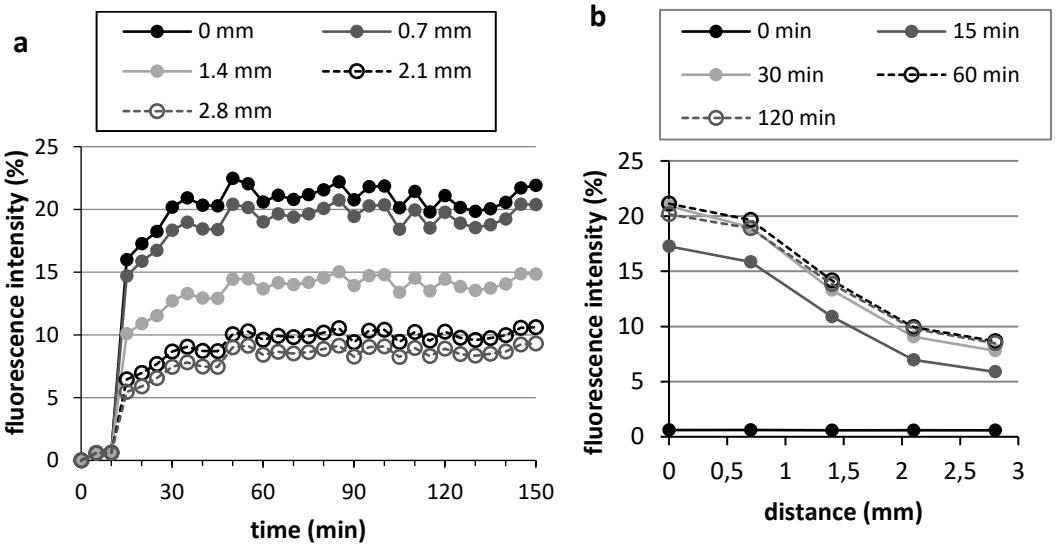

Fig. III.10: relative fluorescence intensity in the inoculation chamber during perfusion of the system with a fluorescein solution through the opposite chamber – a: fluorescence intensity over time at 5 different positions along the chamber – b: fluorescence intensity profile across the chamber at 5 different times after the start of the perfusion.

Natural soils are porous media with a high heterogeneity in pore size and distribution, and can be subjected to variations in water saturation and infiltration rates depending on weather conditions. As a result, average infiltration rates through a given volume of soil can vary from a few millimeters to a few tens of centimeters per hour, while local flow velocities vary greatly depending on pore size and saturation, reaching up to 50 cm/s in centimeter-wide macropores (Beven and Germann, 1982). In this regard, the microfluidic set-up described here is a plausible situation mimicking laminar flow through water-saturated pores at the millimeter and micrometer scales.

3.3.1. Effect of a nutrient perfusion on fungal growth

On-chip fungal cultures were carried out as described in section 2.5 with or without perfusion with fresh mineral medium. This perfusion prevented nutrient depletion in the chamber opposite to the inoculation point, in order to maintain a stable concentration in glucose and salts. It efficiently prevented drying and bubble formation, thus allowing longer observation times. In such conditions, one could expect oriented and/or faster growth of the fungus towards the nutrient source. A low flow rate was chosen in order to minimize shear stress on hyphae and medium consumption: with a flow

rate of 1.8 µL/min and chamber dimensions of 3 mm by 130 µm the average speed in the perfusion chamber was 77 µm/s and the flow regime is laminar (Re = 0.23).

The distribution of elongation rates for both strains is plotted in Fig. III.11. In *T. helicus*, the implementation of medium circulation did not result in any significant difference in elongation rates compared to static conditions. In contrast to *T. helicus*, medium perfusion resulted in faster growth rates for *N. crassa* compared to static conditions: hyphae grew at 190 ± 46 µm/h on average without circulation of medium and 300 ± 128 µm/h with circulation (Fig. III.11). This result in consistent with the hypothesis of *N. crassa* growth being limited by nutrient availability in this set-up (see section 3.2.3): continuous feeding through a perfusion indeed results in faster growth. In contrast, the growth rate of *T. helicus* in these conditions may be limited mainly because of low oxygen availability or geometric constraints, rather than access to nutrients.

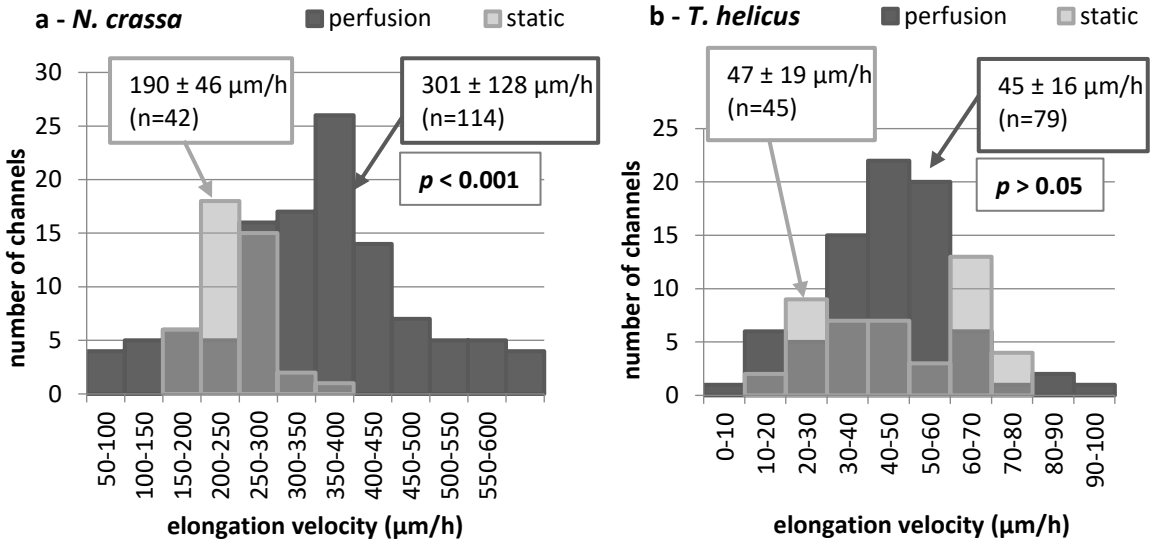

Fig. III.11. Distribution of hyphal elongation velocities in microchannels, with and without perfusion. The average elongation velocity, standard deviation and size of each sample are displayed in labels. Student's t-test was performed for each strain and the p-value is labeled on each graph– a. *N. crassa* – b. *T. helicus*

Characteristic times for nutrient transfer from the perfusion chamber to the growth chamber should be compared to the time needed for each strain to grow through the channels: indeed the addition of a nutrient source may have little effect on growth rates if the establishment of a gradient is slower than hyphal elongation. In the previous section we showed that solutes could be transferred from the perfusion chamber to the inoculation chamber through convection in less than an hour. The diffusion coefficient of glucose ($0.6 \cdot 10^{-11}$ m^2/s) (Stein and Litman, 2014) is 100 times smaller than that of fluorescein ($0.64 \cdot 10^{-9}$ m^2/s) (Galambos and Forster, 1998). This means that glucose transport in the mycelial growth experiments relies mostly on convective transport, at least at the beginning of the perfusion.

For *T. helicus*, elongation velocities in each measured channel were plotted against the distance between the perfusion inlet and the channel. As shown in Fig. III.12, the velocity did not depend on the relative position of the channel, indicating that the implementation of a nutrient perfusion did not cause growth disparities among the channels, and the growth conditions were homogeneous.

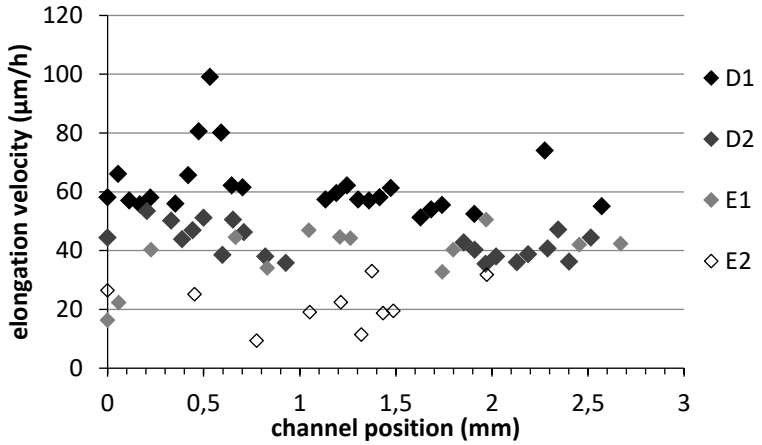

Fig. III.12: hyphal elongation velocity in individual channels depending on their relative position, in dynamic conditions (with x=0 corresponding to the position of the channel closest to the perfusion inlet)

3.3.2. Temporal variations of the elongation velocity

The images series acquired during fungal growth in Ch50 chips were used to construct spatio-temporal diagrams for each channel analyzed: on such diagrams, the x axis represents the distance in µm, and the y axis represents time. A constant elongation velocity thus appears as a straight line cutting diagonally from the top left of the image to the bottom right, acceleration of the elongation as a convex curve and deceleration as a concave curve (Fig. III.13).

Temporary elongation arrests were observed in some channels, followed by a resume of growth. These pauses were usually associated with branching events in *T. helicus*. Indeed, due to the relative thinness of its hyphae, *T. helicus* was able to branch and develop multiple hyphae in the same channel. This was not the case for *N. crassa*, where branching rarely occurred inside the channels despite their length being higher than the average branching distance of about 200 µm (Held et al., 2010; Potapova et al., 2016), and pauses were rather associated with local irregularities of the channel due to microfabrication defects (narrowed or bent channels for example). Growth of *T. helicus* in static conditions tended to be mostly constant (64% of all channels) or decelerating (27%), while profiles noted in chips with perfusion were constant (56%) or accelerating (43%). In a small percentage of channels (7% in static conditions and 1% in dynamic conditions) hyphal growth presented alternating phases of acceleration and deceleration, as showed in Fig. III.13.b.

The presence of a flow in the perfusion chamber thus appears to influence the growth behavior of *T. helicus*, although it did not significantly affect the average elongation velocities.

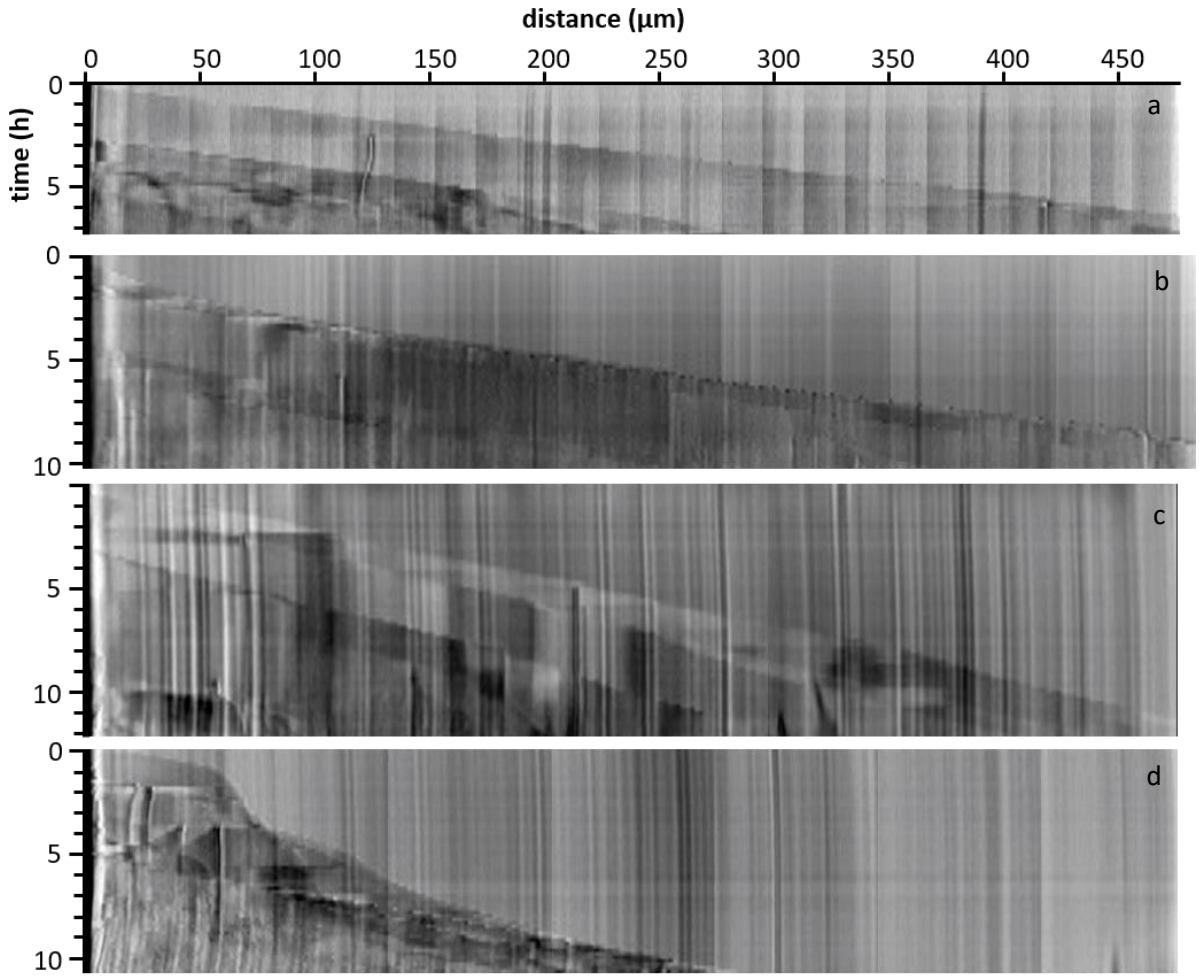

Fig. III.13: spatio-temporal diagrams representing different elongation patterns of *T. helicus* in microchannels – a: linear pattern – b: acceleration – c: deceleration – d: variable elongation profile, with a deceleration phase followed by an acceleration

4. Summary and conclusions

Several microfluidic chip designs with different channel patterns and construction methods were tested to evaluate their suitability for fungal cultures and fluorescence microcopy observations. Glass "sticker" devices presented the best optical properties, but either did not allow precise and reproducible control over channel geometry (when double-sided tape was used), or were particularly tedious to fabricate (in the case of PDMS stickers). Usual PDMS-on-glass chips appeared to be the simplest and fastest solution to enable fungal growth while enabling high reproducibility of the geometry. A new "Ch50" pattern featuring two chambers connected by 50 parallel microchannels was designed, with a chamber volume ≈ 10 times higher than in Ch1, which greatly reduced desiccation issues and allowed easier injection of mycelium pellets. Moreover, the chambers are high enough to accommodate particles or beads up to a few tens of µm, which could be used as carriers to introduce the pollutant adsorbed onto a solid substrate.

Fungal growth rates in such chips were evaluated, giving useful insight into the growth kinetics and time scales needed to perform future experiments in presence of a pollutant. Growth speed of *T. helicus* in microfluidic chips was more than 2 fold slower than on agar plates, which means that confinement and nutrient availability affect hyphal elongation. The effect of confinement appears to be more marked for strains with higher energetic needs, as the results obtained with the fast-growing mold *Neurospora crassa* show. The chips can be perfused with a stream of fresh medium, which can partially compensate nutrient consumption by the fungus, and avoid evaporation. Perfusion experiments conducted using fluorescein indicate that the concentration differences between upstream and downstream channels are minimal, and that the parallel channels can be treated as replicates of the same culture conditions.

PDMS chips on glass coverslips were chosen for the monitoring of BaP incorporation over time, described in the following chapter. The use of a confocal laser scanning microscope solves the background fluorescence issue by allowing the selective excitation of fluorophores at the desired Z-position, and imaging of a very narrow field depth. However BaP diffusion through the PDMS network remains a drawback, since the transport of BaP may not only occur through the channels.

Chapter IV : BaP mobilization and uptake by *Talaromyces helicus*

1. Introduction

The first research conducted on hydrocarbon uptake into fungal cells dates back to the 70's, with emphasis on oleaginous yeasts such as *Candida lipolytica* and hydrocarbon-utilizing fungi including the "kerosene fungus" *Cladosporium resinae*. Early proposed mechanisms of alkane uptake into fungal cells involved a two-step mechanism with adsorption onto the fungal cell surface followed by active incorporation (Lindley and Heydeman, 1986). The induction of cell wall structure modifications during alkane adsorption in yeast was also shown (Käppeli et al., 1984). The interaction between fungal cell surface and hydrophobic substrates has since been subject to further research, however the mechanisms at play are still not fully understood, especially when mobilization in complex substrates like the soil is considered.

Mobilization mechanisms are already at play before lipophilic compounds reach the cell surface: some filamentous fungi produce extracellular biosurfactants able to emulsify neutral hydrocarbons and lipids (Camargo-de-Morais et al., 2003; Luna-Velasco et al., 2007). A carbohydrate able to partially solubilize benzo-[a]-pyrene was also identified in *Fusarium solani* (Veignie et al., 2012). How these mobilizing agents interact with the cell surface, and their possible relation with the first stages of incorporation, remains unclear. In yeast, the agglutination of cells with alkane droplets depends on their respective size and hydrophobicity of the compound, and the degree of substrate emulsification may play a regulation role limiting the absorption rate of hydrocarbons (Komarov and Ganin, 2004). Solubilization and adsorption mechanisms may greatly differ depending on a given compound's solubility in water, since some lipophilic compounds are still moderately soluble in water (*i.e.* naphtalene, phenanthrene, functionalized aromatic compounds such as dyes or pharmaceuticals) while others are almost completely immiscible (*i.e.* alkanes, oils). Whether they are found as non-aqueous phase liquids or as solids may also play a decisive role, since in the first case they are susceptible to emulsification, and in the latter they present as adsorbed or suspended particles. High molecular weight PAH such as BaP or higher alkanes for example are typically solid at 20°C.

Verdin et al. (2005) first observed the intracellular storage of BaP in filamentous fungi, in organelles identified as lipid bodies. The authors also showed that internalization occurred even when the mycelium was exposed to metabolic inhibitors or incubated at 4°C, indicating that that BaP transport to the lipid bodies is a passive process. However, later works at higher concentrations of inhibitors taking into consideration the protective effect of the fungal cell wall present contradictory conclusions, showing that BaP uptake in the same fungal species involves an active cytoskeleton-dependent

mechanism that still needs to be further characterized (Fayeulle et al., 2014). Active hydrocarbon uptake has been described in other organisms: in bacteria, active transmembrane pumps able to transport PAH were identified, apparently selectively transporting molecules with a log K_{ow} > 4 out of the cell (Bugg et al., 2000). Although similar pumps could be responsible for the absorption of HOC into the cytoplasm of fungal cells, there is no evidence of their existence so far. Besides, transmembrane transporters may not be the only route for uptake: indeed, PAH are lipophilic compounds, and several works report PAH behaving in a similar way to neutral lipids in terms of storage sites and intracellular transport (Verdin et al., 2005; Furuno et al., 2012; Delsarte et al., 2018). Endocytosis has also been proposed as an active uptake route (Fayeulle et al., 2014).

In this chapter, the uptake of BaP into live cells of *Talaromyces helicus* is investigated, relying on the natural autofluorescence of BaP to detect its localization through fluorescence microscopy. The microfluidic device "Ch50" developed in the previous chapter was used to implement a compartmentalized culture environment, allowing the monitoring of BaP uptake over a week without initial contact with the pollutant source.

2. Materials and methods

2.1. Strains and media

Talaromyces helicus was maintained on MYEA at 22°C. Mineral medium MM1 was used for incorporation experiments in shaking flasks, and for on-chip cultures. All culture media used in this chapter are described in Chapter I, section 2.2.

2.2. Fungal cultures with BaP and *in vivo* staining

Pre-cultures of *T. helicus* were prepared in 50 mL MPYC medium without BaP by inoculating with spores of *T. helicus* harvested from a colony to reach 10^4 spores/mL. Cultures were incubated at 22°C under orbital shaking, with a 12 h – 12 h light-dark cycle. The mycelium was harvested after 3 days by filtration on a Büchner funnel, rinsed with mineral medium without glucose, and weighted in sterile conditions.

BaP (100 µg) was deposited at the bottom of clean glass shaking flasks by pipetting 125 µL of stock solution at 0.8 g/L and evaporating the acetone under a fume hood. 10 mL of MM1 medium were then added to each flask, and glucose after autoclaving to reach a final concentration of 20 g/L. The flasks containing BaP were then inoculated either with spores of *T. helicus* collected from a colony on solid medium, or with 150 mg of fresh mycelium harvested by filtrating a 3-day old pre-culture. Control flasks without BaP were prepared as well. Cultures were incubated at 22°C under orbital shaking, with

a 12 h – 12 h light-dark cycle. Samples were taken by pipetting 20 µL of the culture after 30 min, 2 h 30, 6 h, 24 h and 48 h of incubation, and mounted on a microscope slide for epifluorescence observations.

BODIPY 500/510 C_4, C_9 lipid dye (Invitrogen) was used for the live staining of lipids in fungal mycelium. BODIPY dyes display a green fluorescence with a maximum excitation 505 nm and, maximum emission at 510 nm. A BODIPY solution (1 µmol/L) was prepared in DMSO, and 4 µL was added to 36 µL of fungal suspension on a microscope slide to achieve a final concentration of 0.1 µmol/L. The suspension was gently mixed by pipetting up and down and incubated for 4 hours in the dark, at room temperature, before microscopic observations.

2.3. Germination test with BaP

Spores of *T. helicus* harvested from a solid culture were suspended in mineral medium at a final concentration of 10^4 spores/mL and seeded in microplate wells. Each well was filled with mineral medium up to a final volume of 300 µL. A BaP solution at 0.8 g/L was prepared in dimethyl sulfoxide (DMSO) and used to prepare a range of dilutions. BaP was added by pipetting 20 µL of appropriate dilutions in DMSO into each culture well, to obtain ratios of 0.1, 1 and 5 µg BaP per mL of medium. Two wells were seeded for each concentration, and a control without BaP was prepared with 20 µL of DMSO. Non-inoculated blanks were prepared for each BaP concentration. The plate was sealed with parafilm and incubated at 22°C in a water-saturated atmosphere. Absorbance measurements at 600 nm were taken with a Multiskan GO spectrophotometer (Thermo Scientific). Relative absorbance was calculated for each well by subtracting the blank absorbance value for the corresponding BaP ratio.

2.4. Microfabrication and on-chip fungal cultures

Microfluidic chips for fungal culture were fabricated as described in Chapter III, section 2.4. Briefly, polydimethylsiloxane (PDMS, Sylgard 184, Dow Corning) mixed with 10% reticulating agent was cast against the wafer and allowed to cure for at least 2 h at 75°C. Inlets were added by punching holes through the PDMS with a biopsy puncher (2 mm for the inoculation well, 1 mm for medium injection inlets). The negatively patterned PDMS slab was bound to a clean glass microscope slide or cover slip after surface oxidization in an oxygen plasma chamber (Harrick) for 60 s.

2 x 2 mm mycelium explants were collected from the edge of non-sporulating colonies of *T. helicus* growing on MYEA medium, aged 3 days to 1 week. The mycelium plugs were placed in the inoculation well of the chip previously filled with MM1 medium. A PDMS plug was used to close the inoculation well and prevent drying. 1 µL of BaP stock solution in acetone was pipetted into one of the injection inlets on the opposite side to the inoculation chamber. The microchips were then placed in a Petri dish

sealed with parafilm to maintain a water-saturated atmosphere. Chips were incubated at 22°C with a 12 h - 12 h light cycle, and growth and BaP uptake were monitored by observations in laser scanning confocal microscopy.

2.5. Imaging

Mycelium of *T. helicus* grown in liquid cultures with BaP, and co-stained with BODIPY lipid dye was imaged in bright field and epifluorescence using an OLYMPUS BX60 microscope mounted with a color Infinity 3-6UR camera (Lumenera). Time-lapse epifluorescence microscopy observations were performed using a DMI-8 inverted microscope (Leica) equipped with a motorized stage and a DFC 3000G camera (Leica). The autofluorescence of BaP was observed with a standard DAPI emission filter set, and BODIPY with the FITC filter set.

Microchips inoculated with *T. helicus* and spiked with BaP were imaged using a confocal laser scanning microscope (LSM 710 Axio Observer, Carl Zeiss). The fluorescent signal of BaP was detected using the DAPI filter (excitation 405 nm, emission 453 nm) and that of BODIPY using the FITC filter (excitation 488 nm, emission 563 nm).

2.6. In silico simulation

The penetration of BaP through a model lipid bilayer was simulated using the IMPALA method as first described by (Ducarme et al., 1998), courtesy of Dr Magali Deleu, Laboratoire de Biophysique Moléculaire aux Interfaces, University of Gembloux in Liège, Belgium. IMPALA is a simulation method initially developed to predict the conformation of integral membrane proteins. Using an atomic model of the molecule of interest, its interaction with membrane lipids is modeled by a field of restraints.

3. Results and discussion

3.1. BaP uptake by *T. helicus* and intracellular localization

3.1.1. Absorption of BaP by mycelium pellets in liquid cultures

BaP is a highly hydrophobic molecule, being quasi insoluble in water with an aqueous solubility of $3.8 \cdot 10^{-3}$ mg/L at 25°C and an octanol-water partition coefficient log K_{ow} = 6.35 (IARC, 2012). When added to liquid culture media for microbiological uses, it is therefore found in the form of solid yellow crystals (Fig. IV.1.a). Theses crystals can be observed in epifluorescence microscopy, appearing brightly fluorescent in the blue and green range, branched with serrated edges. Smaller (≈ 10 µm wide), flat blue crystals with a characteristic 4-pointed star shape can also be found (Fig. IV.1.c).

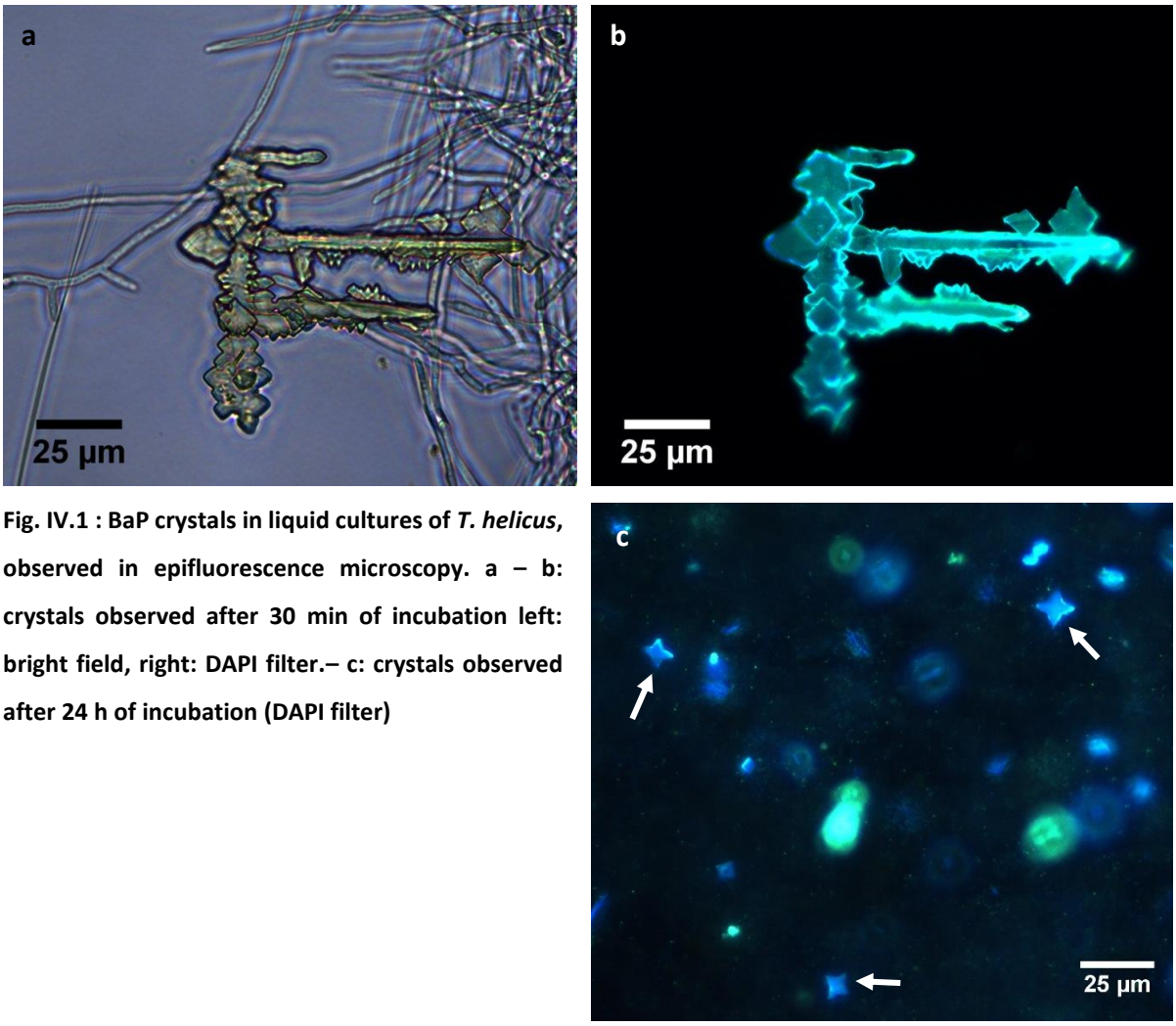

Fig. IV.1 : BaP crystals in liquid cultures of *T. helicus*, observed in epifluorescence microscopy. a – b: crystals observed after 30 min of incubation left: bright field, right: DAPI filter.– c: crystals observed after 24 h of incubation (DAPI filter)

Since BaP presents autofluorescence properties, emitting a blue fluorescent signal when excited with UV light, its incorporation into the fungal biomass can be visualized directly in epifluorescence microscopy. 4-day old mycelium pellets of *T. helicus* incubated with BaP for 24 h were thus observed under the epifluorescence microscope. In control flasks without BaP, a slight fluorescence of the mycelium was visible under UV. This fluorescent signal without addition of any fluorophore corresponds to the autofluorescence of parietal components. Indeed, fungal hyphae are known to emit blue autofluorescence when exposed to UV light (330-385 nm) due to the presence of chitin in the fungal wall (Jabaji-Hare et al., 1984; Dreyer et al., 2006). This faint fluorescence appears to be uniform along hyphae and does not highlight any structure in particular.

After 24 h of incubation with BaP, the staining was not uniform: pellets appeared brightly fluorescent at their core, which could be due to the immediate contact with BaP crystals. As pictured in Fig. IV.1.a, BaP crystals tended to get tangled into bigger mycelium pellets.

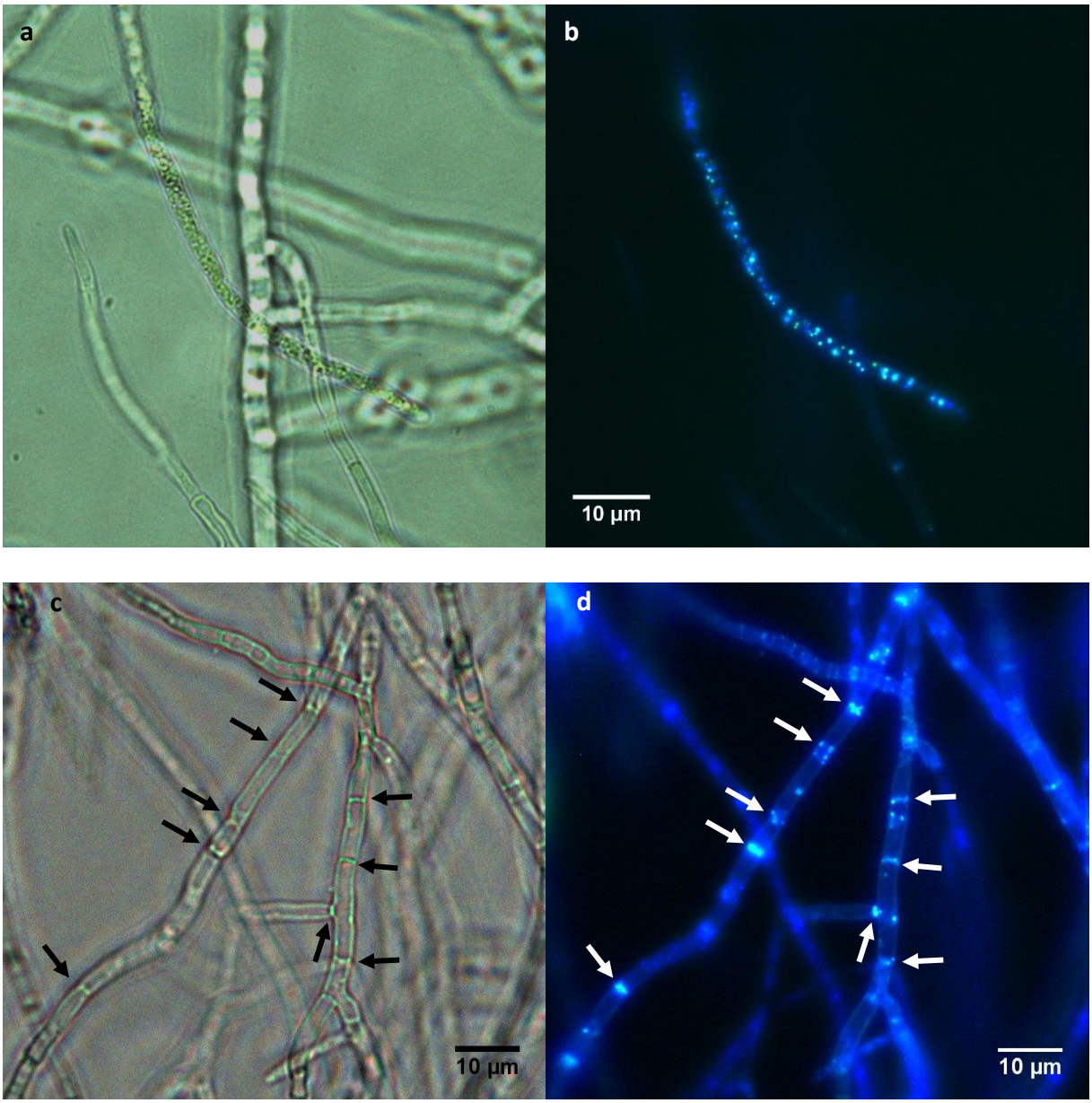

Fig. IV.2 : Mycelium of *T. helicus* after 24 h of incubation wih BaP, observed in bright field (left) and epifluorescence using the DAPI excitation filter (right). a, b – hyphal tip with numerous stained intracellular vesicles. c, d – mature vacuolized hyphae with small vesicles localized against septa (indicated by arrows).

Diffuse blue fluorescence was detected along hyphae, with cell walls and septa appearing brighter than the cytoplasm (Fig. IV.2.d). Many intracellular vesicles were visible in bright field, and appeared brightly fluorescent. At hyphal tips, these vesicles were distributed in the cytoplasm (Fig. IV.2.b). Measurements performed on 79 vesicles visible in the apex imaged in Fig. IV.2.b yielded diameters ranging from 0.16 to 0.85 µm, with an average of 0.41 ± 0.16 µm. In mature hyphae, the vesicles were localized against the walls and septa, while the vacuoles were not stained (Fig. IV.2.d). The intracellular storage of PAH in such vesicles, identified as lipid bodies, was previously observed in other filamentous species including *Fusarium solani* (Verdin et al., 2005) and the oomycete *Phytium ultimum* (Schamfuß et al., 2013), although in the latter the morphology of these organelles differed.

3.1.2. In silico simulation of the behavior of BaP in a lipid bilayer

In order to predict the interaction of BaP with biological membranes, its penetration into a model symmetrical lipid bilayer was simulated by the IMPALA method. The simulated membrane is 36 Å thick and planar, with constant properties along its surface but hydrophobicity varying in a symmetrical manner along the X axis crossing through the membrane. The method yields a profile of interaction energy for positions along the X axis, the most stable positions being those with minimal energy (Fig. IV.3.a). As expected for a hydrophobic molecule, the profile displayed a sharp contrast between the positions corresponding to the water phase surrounding the membrane and those corresponding to the hydrocarbon core of the membrane. The most stable positions for BaP, displaying negative interaction energies, are located within 14 Å on each side of the membrane center, and correspond to the dehydrated alkane core of the lipid bilayer. In contrast, the interaction energy is maximal starting for positions at 22 Å and further from the center, and decreases sharply between 22 Å and 14 Å. This decrease coincides with positions where the BaP molecule is in contact with the membrane, and still partially surrounded by water. Indeed, for a 36 Å thick membrane, the hydrated phosphate heads of the amphiphilic lipids are located between 14 and 18 Å.

These results are consistent with the low solubility in water of BaP, which tends to minimize its contact surface with aqueous phases. From the energy profile obtained, it is apparent that BaP can penetrate a lipid bilayer and stabilize at its core, which means it can diffuse laterally in the hydrophobic core layer. This is consistent with the lipophilic nature of BaP, already highlighted by its storage in intracellular lipid reserves. It is also consistent with observations of a surface adsorption of dodecane followed by its absorption into cells of the "kerosene fungus" *Cladosporium resinae*, which was the first proposed mechanism of hydrocarbon absorption in filamentous fungi (Lindley and Heydemann 1984). Passive transport of phenanthrene, fluoranthene and anthracene through the plasma membrane was shown in the PAH-degrading resistant bacterium *Pseudomonas fluorescens* (Bugg et al. 2000), which confirms the ability of PAH to diffuse through the plasma membrane. A major difference between BaP and those low molecular weight PAHs is their higher solubility in water (from 0.044 mg/L for anthracene to 1.15 mg/L for phenanthrene at 25°C, compared to $3.8 \cdot 10^{-3}$ mg/L), which means that despite their affinity for lipids, they are susceptible to diffuse through the aqueous phase and into the cytosol depending on concentration gradients. It is very unlikely for BaP to be present in water in the molecular form and diffuse freely through the extracellular aqueous medium: for BaP to be absorbed into membranes, it would need to be already in close vicinity to the cell surface. Transport phenomena, other than passive diffusion, must therefore occur earlier in the incorporation process and bring the pollutant in contact with the cell surface.

Biological membranes are typically 7 to 10 nm thick, with polar heads forming a 0.7 to 1 nm thick layer on each side. Moreover, they contain up to 50% protein, a heterogeneous lipid composition and they are not symmetrical: in particular the lipids composition differs between the external and internal layers of the plasma membrane. Various biomolecules including polysaccharides and proteins are tethered to the membrane through covalent bonds with the polar heads, or associated with transmembrane proteins (Freedman 2012 – Cell Biology). The *in silico* membrane model used in this simulation is therefore very simplified and not an accurate representation of the fungal plasma membrane in all its complexity, however it gives a useful insight into the behavior of an extremely hydrophobic compound such as BaP in the vicinity of biological lipid bilayers. *In vivo*, cell wall components may facilitate the transfer of BaP to the plasma membrane by adsorbing BaP prior to internalization. Indeed, the fungal cell wall consists mainly in microfibrillar glucans and chitin, which are insoluble polymers and may play a significant role in PAH adsorption on the surface of fungal hyphae (Ma et al., 2016). Moreover, filamentous fungi produce hydrophobins that modulate the surface hydrophobicity of the cell wall, and affect cell adhesion to hydrophobic substances including hydrocarbons (Zhang et al., 2011).

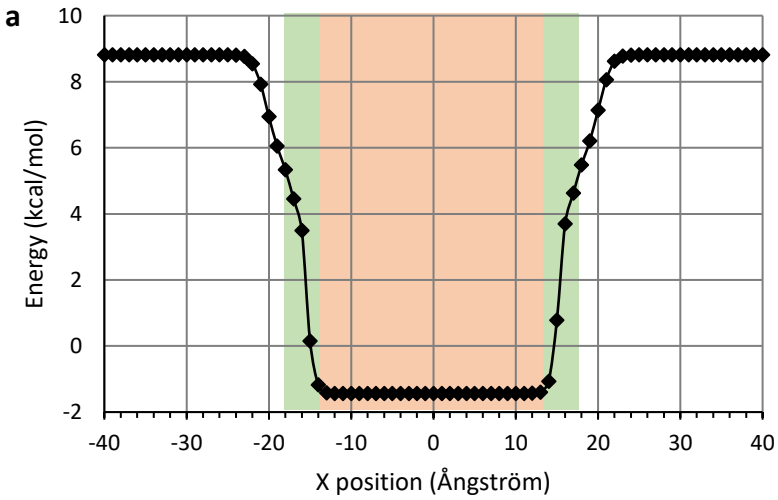

Fig. IV.3 : Simulation of BaP penetration across a model lipid bilayer using the IMPALA method. X-axis: position of the mass center of BaP relatively to the center of the lipid bilayer; Y-axis: interaction energy. The position of the membrane is highlighted in orange (core hydrocarbon chains) and green (polar heads).

3.1.3. Localization of BaP in lipid bodies

BODIPY lipid analogs undergo similar transport mechanisms and metabolism as native neutral lipids in cells (Bai and Pagano, 1997), and as a result highlight cellular structures containing lipids with fluorescence in the green range. Mycelium pellets of *T. helicus* grown in mineral medium were harvested and incubated with BODIPY. After four hours, a faint fluorescence was visible in the whole

cell, likely due to the staining of membrane lipids in organelles and vesicles (Fig. IV.4). Septa and cell walls were not stained. Some parts of the cytoplasm appear more intensely stained than others, with clear delimitations: the less intensely stained parts are likely to be vacuoles, while the rest of the cytoplasm contains various membrane-rich organelles. The most striking feature visible is the bright staining of small intracellular vesicles measuring less than a micrometer in diameter, corresponding to lipid bodies (Kamisaka and Noda, 2001; Chang et al., 2015). These vesicles appear in bright field observations as highly refractive circular objects.

Lipid bodies or oleosomes are intracellular organelles ubiquitous in Eukaryotes, containing lipid reserves in the form of triglycerides. They are formed in conditions of lipid accumulation, especially in oleaginous yeasts and fungi such as *Yarrowia* (*Candida*) *lipolytica* or *Mortierella ramanniana* (Kamisaka et al., 1999). They can be stained using specific lipophilic fluorescent dyes including Nile red (Kamisaka et al., 1999; Bago et al., 2002) or BODIPY conjugated short-chain lipids (Kamisaka and Noda, 2001; Chang et al., 2015) which were chosen for this experiment. Lipids are a form of energy and carbon storage, and the cytoskeleton-dependent transport of lipid bodies along hyphae contributes to resource redistribution within the mycelium (Welte, 2009). The case of mycorrhizal fungi is a notable example of this transport, where vesicles are translocated from carbon-absorbing areas (mycorrhizes) to actively growing areas which consume lipids (hyphal tips in extension in the soil) (Bago et al., 2002).

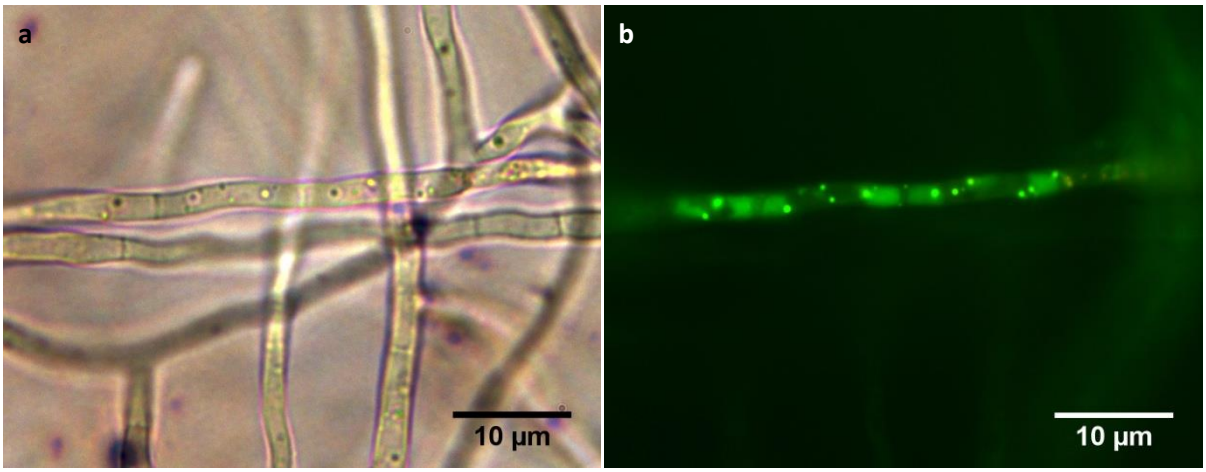

Fig. IV.4 : Mycelium of *T. helicus* stained with BODIPY observed in epifluorescence microscopy, highlighting intracellular lipid bodies – a: bright field – b: fluorescent signal of BODIPY observed using the FITC filter

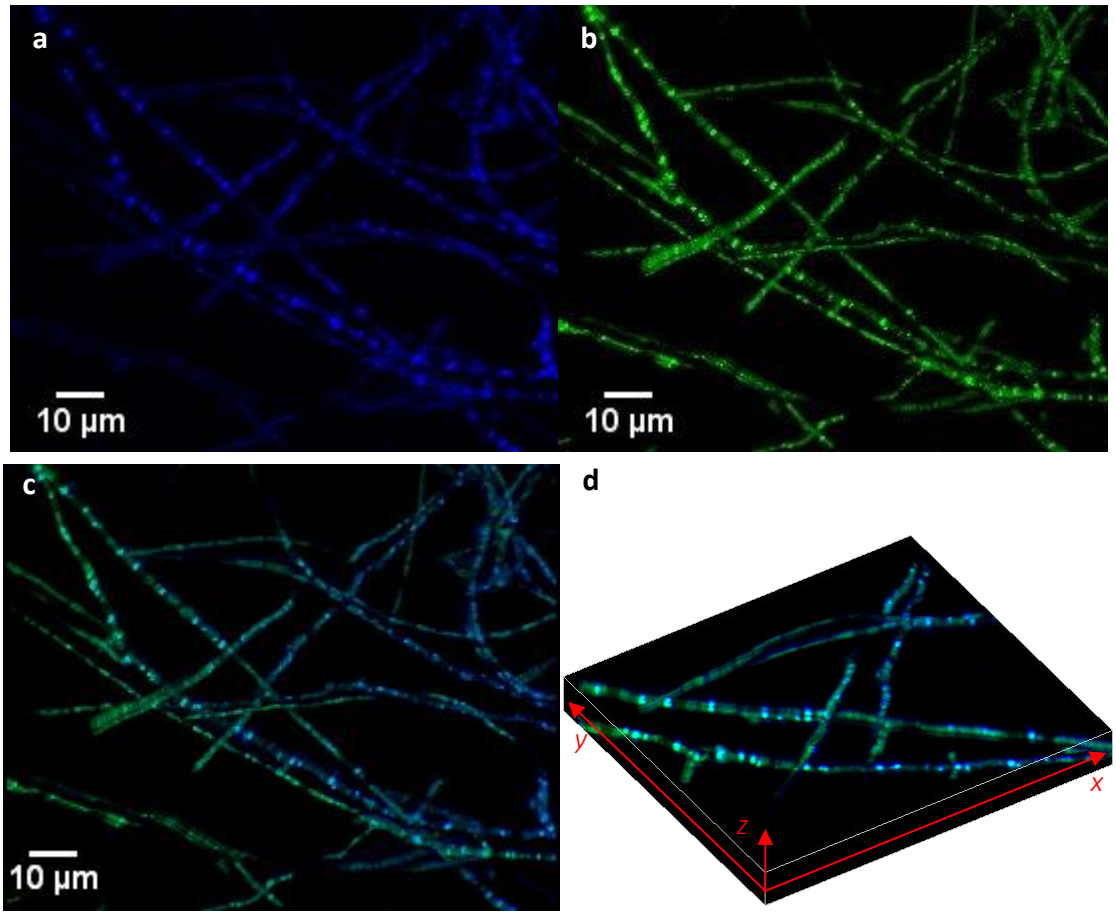

Fig. IV.5 : Mycelium of *T. helicus* incubated with BaP and stained with BODIPY, observed in confocal microscopy at 40 x magnification (maximum intensity projection of a 41 images stack with a 0.38 µm increment). BaP appears in blue and BODIPY in green. Structures stained with both fluorescent molecules appear in cyan shades. – a : DAPI filter – b: FITC filter – c: merged DAPI and FITC channels – d: 3D view of stained hyphae, dimensions 70 x 63 x 7 µm (x:y:z)

Mycelium incubated for 24 h with BaP in shaking flasks was stained with BODIPY lipophilic dye to reveal lipid bodies, and observed in confocal microscopy. When mycelium previously incubated with BaP was stained with BODIPY, blue and green fluorescence co-localized in the same cellular structures, i.e. lipid bodies and some parts of the cytoplasm (Fig. IV.5.c). When viewed in 3D projection, the placement of the fluorescent spots along hyphae confirms their intracellular location (Fig. IV.5.d). The intensity of fluorescence was not uniform for each dye, indicating that the absorption of BODIPY is not uniform and/or the heterogeneous intracellular accumulation of BaP prior to BODIPY staining prevents the uniform absorption of the BODIPY dye in all lipid-rich organelles.

These observations confirm that BaP is absorbed into the cells of *T. helicus* and stored in lipid bodies. Similar observations were made in the saprotrophic fungus *Fusarium solani* (Verdin et al., 2005; Fayeulle et al., 2014). Accumulation of lipophilic toxins in lipid bodies may be a defense mechanism against oxidative stress in fungi: Chang et al. (2015) found that the formation of large lipid bodies in

Candida albicans was associated with mycotoxin resistance, and that toxins were stored in lipid bodies. The authors propose a protection mechanism against oxidative stress caused by the oxidation of aromatic rings involving quenching of reactive oxygen species by triacyglycerols making up the bulk of storage lipids. Incidentally, the accumulation of PAH in intracellular vesicles was described in other species of filamentous fungi and fungus-like organisms which are inefficient at PAH degradation, including *Saccharomyces cerevisiae*, the white rot *Phanerochaete chrysosporium* (Verdin et al., 2005), and the oomycete *Pythium ultimum* (Furuno et al., 2012). Intracellular PAH storage thus appears to be independent from degradation, which is consistent with the hypothesis of a protective mechanism. A similar strategy in *Talaromyces helicus* may serve as a protection against adverse effects of BaP and other lipophilic organic compounds.

Not only is *T. helicus* able to incorporation BaP, it can also metabolize it, as shown in Chapter I. Intracellular storage sites may thus also host biodegradation. The main PAH degradation pathway identified in non-ligninolytic fungi involves P450 mono-oxygenases: Class II P450 cytochromes are membrane-bound enzymes found in the endoplasmic reticulum, performing the hydroxylation of carbon chains including alkanes and fatty acids (Črešnar and Petrič, 2011). Since lipid bodies are known to be mobile in the cytoplasm (Welte, 2009) and interact with various organelles including the endoplasmic reticulum and peroxisomes (Murphy et al., 2009), intracellular transport *via* lipid bodies could be one of the ways bringing BaP to P450 cytochromes.

Previous works have demonstrated that lipophilic contaminants, including alkanes and PAH, can also follow the same metabolic pathways as neutral lipids (Singh, 2006; Peter et al., 2012; Boll et al., 2015; Al-Hawash et al., 2019). This is consistent with the intracellular accumulation of BaP in lipid storage organelles we observe here, and with the enhanced biodegradation of BaP when lipids (vegetable oil) are used as carbon source rather than glucose (Delsarte et al., 2018). Delsarte et al. (2018) propose a degradation pathway taking place in lipid bodies, involving H_2O_2 transfer from peroxisomes to lipid bodies. Indeed, lipid bodies and peroxisomes are located in close vicinity of each other and membrane hemifusion may occur between the compartments (Murphy et al., 2009). Peroxisomes notably host the beta-oxidation of fatty acids. Aside from H_2O_2 diffusion between those compartments, the exchange of neutral lipids and other lipophilic molecules could happen in the same way, allowing BaP transfer from lipid bodies to the core leaflet of peroxisome membrane where it can be oxidized.

3.1.4. Anti-fungal effect of BaP and detoxification mechanisms

Germination assays were conducted with increasing quantities of BaP in a fixed volume of mineral medium. Fungal growth in microplate wells filled with 300 µL of medium was evaluated by measuring

the absorbance at 600 nm. This method enables to rapidly evaluate biomass production during germination, without the need to manually count germinating spores (Broekaert et al., 1990).

Without BaP, germination started 4 days after seeding, and the relative absorbance measured reached 0.232 on average after 10 days (Fig. IV.6). In wells containing 0.1 µg/mL BaP (30 ng/well), germination was delayed by 3 days, and the relative absorbance was 0.152 after 10 days. No growth occurred with higher concentrations of BaP. This indicates a total inhibition of germination for concentrations as low as 1 µg/mL. These results show the toxicity of BaP towards the fungus used in this study, especially at early development stages. Fungi can display very different sensitivities to PAH exposure, as shown by Reyes-César et al. (2014) for several non-ligninolytic strains. The authors found *Talaromyces spectabilis* to be one of the most resistant among the strains studied, as it can withstand PAH concentrations up to 1 mg/mL without significant growth inhibition on agar plates. However these results cannot be quantitatively compared to germination assays in liquid medium, since the route of exposure and growth stages investigated are different. The highest concentration used for degradation assays in chapter I is equivalent to 25 µg/mL (250 µg in a total volume of 10 mL). These conditions are therefore not suitable to enable the germination of spores of *T. helicus*, hence the necessity to seed the flasks with mycelium grown in BaP-free pre-cultures.

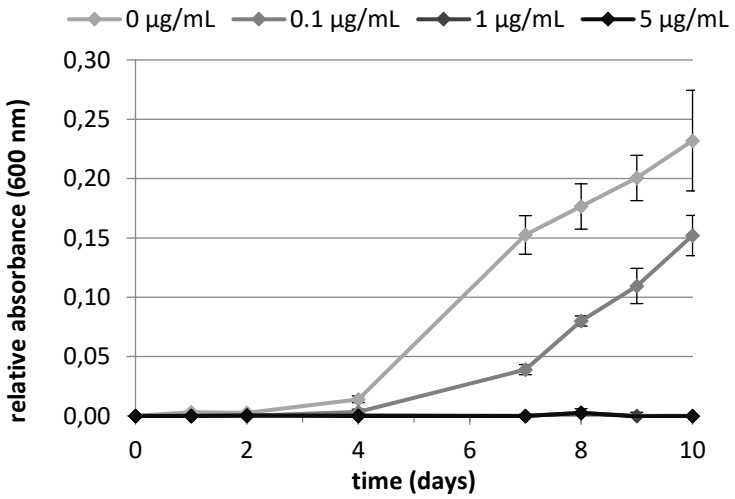

Fig. IV.6 : Absorbance of *Talaromyces helicus* cultures measured at 600 nm during spore germination in presence of increasing BaP proportions in the medium.

Veignie et al. (2004) highlighted the possible role of non-enzymatic oxidation of PAH through free radicals during their biodegradation by non-ligninolytic fungi. Based on these results, as well as earlier works showing higher biodegradation rates during germination than exponential growth phase (Veignie et al., 2002), a multi-step degradation model was proposed involving an oxidative burst during germination causing BaP oxidation through reactive oxygen species (Rafin et al., 2006). The inability of

T. helicus to germinate in presence of high concentrations of BaP could be explained by the inability of the fungus to protect itself from the contaminant at early stages of its development, before resistance mechanisms can be established, in this case sequestration through intracellular storage (as discussed in section 3.1.3) or detoxification through biodegradation.

3.2. Kinetics of BaP incorporation in liquid cultures

3.2.1. Incorporation over 48 h

When incubated with BaP, the mycelium of *T. helicus* displayed a fluorescent staining as soon as 30 min after the start of incubation. This early staining appeared as a diffuse fluorescent signal homogeneous along hyphae, except in some hyphal tips where stained vesicles were visible (Fig. IV.7.a). This diffuse labeling could be due to early adsorption of BaP to the cell wall or penetration of the plasma membrane, before internalization. Accumulation of BaP at the periphery of fungal cells was described in fungal mycelium where actin polymerization was inhibited (Fayeulle et al., 2014). The authors propose a two-step mechanism involving an early adsorption step onto the cell surface, and active internalization through a cytoskeleton-dependent process, possibly endocytosis. Our observations appear to support this hypothesis.

After 2h30 of incubation, stained lipid bodies were observed in other parts of hyphae and not only apices, and appeared to be distributed in the cytoplasm (Fig. IV.7.b). After 24h, the localization of the lipid bodies followed the typical patterned described previously in section 3.1.1, with many of them distributed in the cytoplasm of some tip compartments, and others against the septa of mature hyphae (Fig. IV.7.d-e). As Fig. IV.7.e shows, conidiospores were not stained with BaP, even though they were formed after the incorporation of BaP into the mycelium.

The solubilization of BaP into cell membranes could be a determinant step for its internalization: indeed, the constant recycling of membrane lipids implies that BaP dissolved in the plasma membrane could quickly be internalized in endocytosis vesicles, and thereby reach the membrane of intracellular organelles. This mechanism was proposed as a route for phospholipid transport to intracellular lipid bodies in *Mortierella ramanniana* (Kamisaka and Noda, 2001). It would explain the faint and homogeneous fluorescent staining of hyphae observed during early contact with BaP (Fig. IV.7.a, Fig. IV.9) before the apparition of a fluorescent staining in lipid bodies. However, our results do not allow to differentiate between BaP localization in the cell wall or the cell membrane.

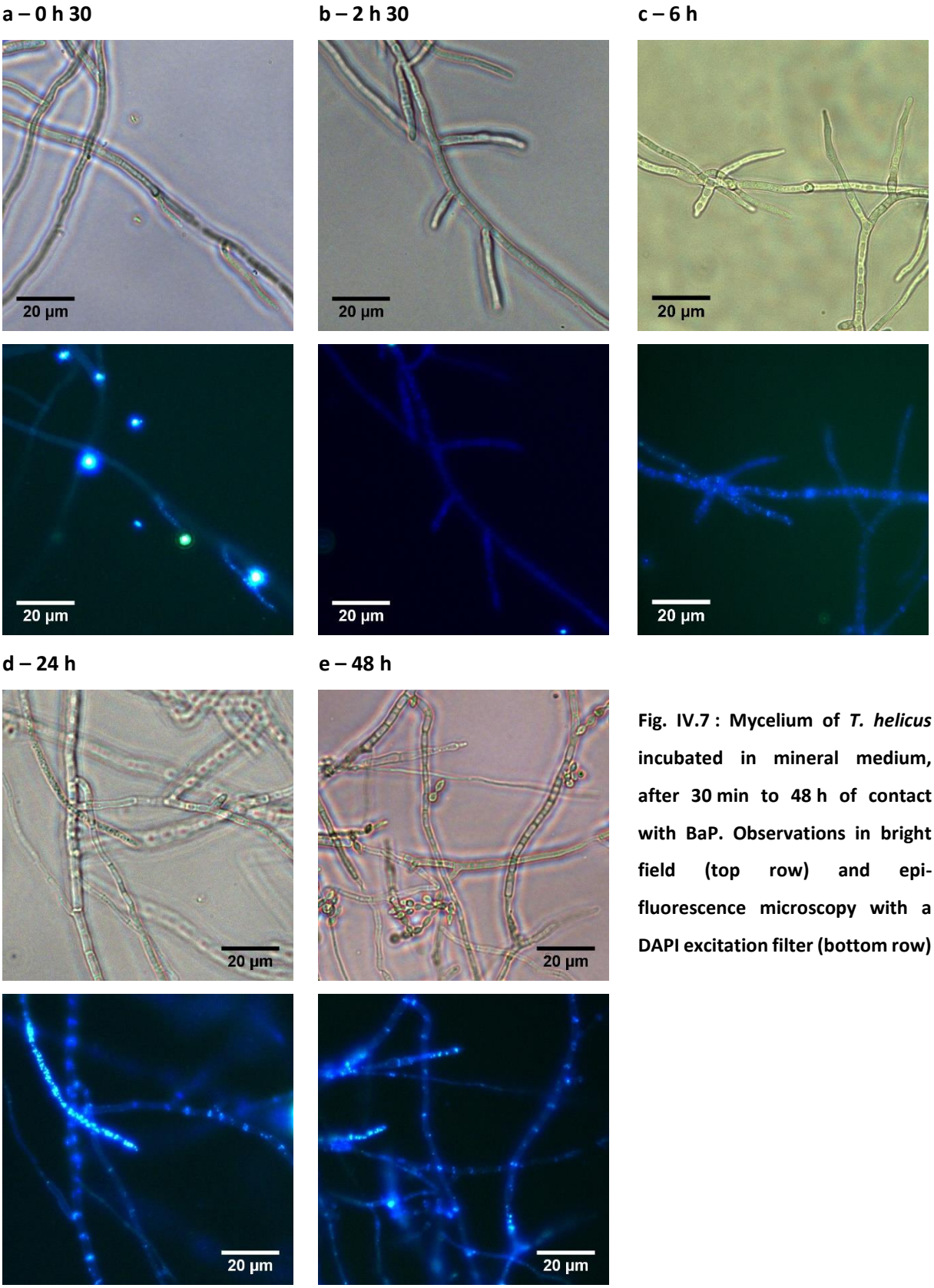

Fig. IV.7 : Mycelium of *T. helicus* incubated in mineral medium, after 30 min to 48 h of contact with BaP. Observations in bright field (top row) and epi-fluorescence microscopy with a DAPI excitation filter (bottom row)

3.2.2. Early stages of incorporation

In order to gain a better insight into the early stages of BaP incorporation into fungal cells, mycelium pellets were mounted on a microscope slide right after addition of BaP to the medium, and observed in time-lapse epifluorescence microscopy at 10 min intervals for 24 h. In contrast to the previous experiment, this set-up allows monitoring the spatial progression of the staining a single pellet over time, instead of sampling and observing new pellets for every time point. The temporal resolution was also increased thanks to automated imaging. Images of the pellet at several time points are presented in Fig. IV.8.

At the beginning of the observations, a faint fluorescence of the mycelium was already visible, either due to early BaP adsorption onto the cell wall, or to cell wall autofluorescence (as observed in Chapter III). Two bright fluorescent spots were visible at the center of the pellet, likely corresponding to solid particles of BaP (Fig. IV.9.a). Fluorescence intensity in the mycelium pellet increased over time. The mycelium was stained simultaneously in all visible parts of the pellet, and not only in hyphae close to the BaP spot. Fluorescent spots resembling the vesicles observed in section 3.1.1 were first visible along hyphae after 2 h of incubation (Fig. IV.9.b) (these were visible as early as 30 min in the previous experiment, for which the camera used allows the detection of smaller objects and fainter fluorescent signals). The accumulation of BaP in these intracellular structures, appearing brightly stained, seems to happen as a second step after early biosorption that results in a diffuse marking of the mycelium.

One of the brightly fluorescent BaP particles visible in first images decreased in fluorescence intensity, until it completely disappeared after 7 hours. Quite remarkably, fluorescent staining of the mycelium appeared stable after that point. This suggests that the whole crystal was progressively fragmented or dissolved and incorporated into mycelium pellets. The images show that BaP was translocated from a single source point to all branches of the pellet within a few hours, which constitutes further evidence of a hypha-mediated PAH dispersion mechanism as described by Furuno et al. (2012). It is no clear whether direct contact with the fungal pellet was necessary for BaP uptake in this set-up, although it may explain its rapid incorporation. Fungal mobilizing agents, either cell wall components or freely dissolved surfactants, may be involved in the observed breakdown of the BaP source. A. Fayeulle (2013) demonstrated that preventing direct contact between the mycelium of *F. solani* and solid BaP flakes strongly decreased biosorption, while the same was not true for phenanthrene. Morphological differences at the surface of hyphae induced by the incubation with benzo[*a*]pyrene were observed in an *Aspergillus* strain, which displayed a roughness attributed to BaP deposits (Wu et al., 2009). These results suggest that the removal of highly hydrophobic molecules such as BaP from the medium is

dependent on their prior adsorption onto the mycelium, while moderately soluble compounds such as phenanthrene or fluorene could be directly recovered from the aqueous phase.

Stained vesicles were observed inside the hyphae, but did not move within the mycelium over the period of observation, nor did they undergo any significant change in size. No hyphal elongation was observed during the experiment either, despite the 24 h time span allowing measurable growth both in microchips and on agar (see chapter III). This may be due to the limited access to oxygen when mycelium pellets are incubated between two glass slides. These observations demonstrate that BaP is not necessarily incorporated in actively growing parts of the mycelium. This apparent immobility of the stained lipid droplets may simply be due the absence of cytoplasmic flows associated with growth. In fungi, lipid droplets can be transported through bulk cytoplasmic flows, as observed in *N. crassa* where artificially injects lipid droplets moved with velocities of about 5 µm/s (Lew, 2005). The average velocity of cytoplasmic flows in growing hyphae is in the same range as hyphal tip extension velocity (Suelmann et al., 1997; Lew, 2005). For comparison, the apical extension velocities measured for *T. helicus* in chapter III were in the range of tens of nanometers per second. However, lipid transfer between membranes and storage sites through vesicular transport could occur *via* smaller vesicles not detectable at the spatio-temporal resolution of our observations. Indeed, cytoskeleton-dependent migration of lipid bodies occurs with speeds in the range of several hundreds of nm per second (Welte, 2009). Furuno et al. (2012) directly observed vesicular translocation of PAH along hyphae of *P. ultimum* through video imaging, at an average velocity of 13 µm/min, which is consistent with reported velocities of lipid body translocation. Based on these observations and the faster diffusion of PAH in presence of hyphae, the authors proposed a mechanism of PAH dispersion through cytoplasmic transport of lipid bodies. Moreover, the works of Fayeulle et al. (2014) demonstrated a cytoskeleton-dependent uptake of BaP into hyphae of *F. solani* is, further supporting these arguments.

PAH lateral diffusion in cellular membranes, as discussed earlier in section 3.1.2, fits within this model of fungal-mediated dispersion: indeed, it could be a first incorporation step when BaP comes into contact with the cell surface, prior to internalization through endocytosis. Lateral diffusion in membranes could occur as an alternative or complementary route to intracellular vesicular traffic. Such a diffusion mechanism could also explain rapid BaP diffusion to all parts of the mycelium without any noticeable organelle migration, as observed in this time-lapse experiment. In order to confirm this hypothesis, the translocation velocity in the mycelium should be quantified and compared with PAH diffusion rates in lipidic phases.

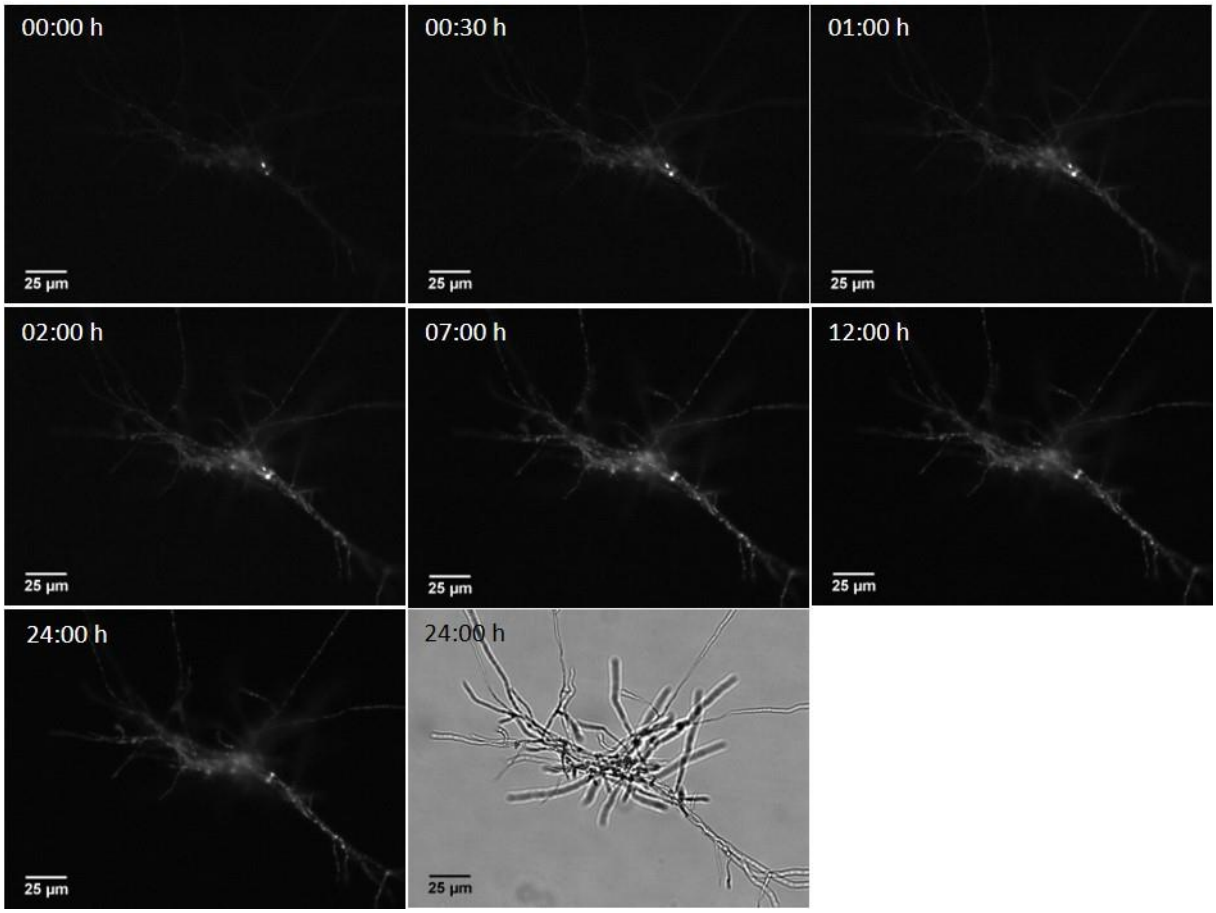

Fig. IV.8 : Time-lapse imaging of BaP incorporation in a mycelium pellet over 24h, visualized in epifluorescence microscopy (DAPI filter).

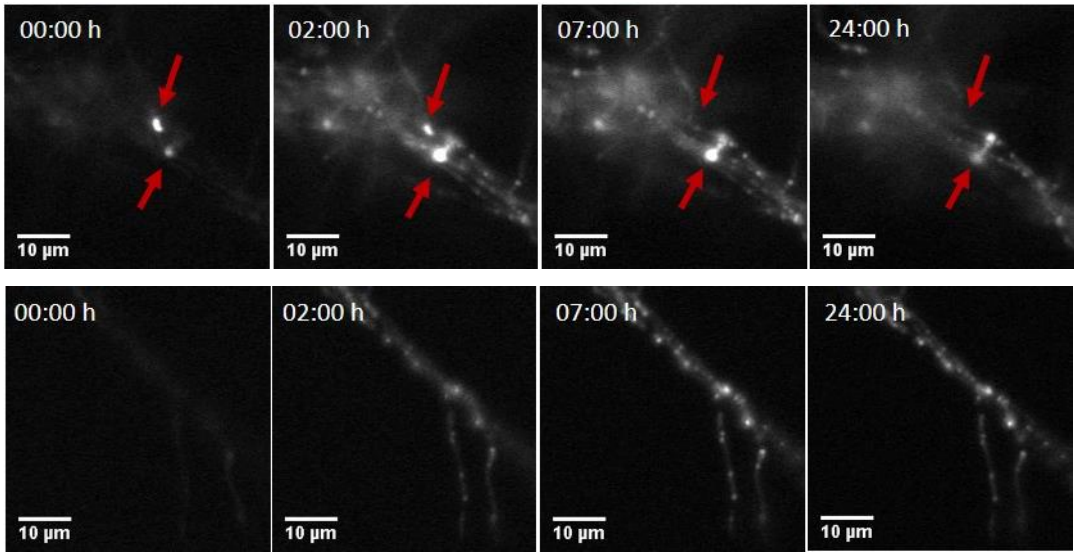

Fig. IV.9 : Details of BaP incorporation in a mycelium pellet visualized in time-lapse epifluorescence microscopy (DAPI filter). a – core of the pellet. b – peripheral hyphae and apices.

3.3. Mobilization in a compartmentalized environment

T. helicus was grown in microfluidic chips, seeded in one of the chambers while BaP was deposited into the opposite chamber, and the mycelium was left to grow until it reached the solid BaP crystals.

After 3 days of culture, the mycelium had not yet reached the opposite chamber containing the BaP deposit. Hyphae appeared stained, without any particular structure being highlighted (Fig. IV.10.a). 3D image stacks obtained in confocal microscopy show a fluorescent staining throughout the width of hyphae, indicating that the cytoplasm is fluorescent and not only the cell walls. With a resolution of 1.01 µm along the Z axis, the thickness of each stack layer is lower than the diameter of the largest hyphae, which allows distinguishing structures located inside the cytoplasm from those at the cell surface. Since such fluorescence is not observed in mycelium incubated without BaP, it cannot be solely due to parietal autofluorescence.

After 6 days, fungal hyphae grew into the chamber containing the solid BaP deposit, that appears in fluorescent microscopy as brightly fluorescent crystals indicated by red arrows in images presented in Fig. IV.10.c-d. Confocal images reveal that some hyphae are in direct contact with these crystals, and these hyphae are also those that display the brightest staining, with numerous visible lipid bodies. These results are consistent with previous observations made with mycelium pellets from liquid cultures, where the core of pellets containing entrapped BaP crystals displayed a more intense staining that peripheral areas (see section 3.1.1). Contact between the solid pollutant deposit and the hyphal surface thus appears to locally enable higher rates of absorption and intracellular storage. Staining of the mycelium was also observed in areas which were not in direct contact with the crystals (Fig. IV.10.b), in these areas the staining pattern was similar to that observed after 3 days: the cytoplasm appears to be stained, but no intracellular vesicles are visible. The high fluorescence intensity in microchannels is due to the high hyphal density in this area, however individual hyphae are not more intensely fluorescent.

The absorption of BaP into fungal cells implies that the pollutant can be transported to the site of absorption in the first place, and that it can cross the cell wall. Considering the extremely low solubility of BaP in water ($3.8 \cdot 10^{-3}$ mg/L), free diffusion cannot occur at a rate fast enough to allow transfer through the aqueous phase, unless it is facilitated by mobilizing agents. One of the proposed mechanisms for bioavailability enhancement of hydrophobic contaminants involves their inclusion in micelles and facilitated diffusion, as reported for bacteria (Brown, 2007). The partial solubilization of BaP when incubated in fungal culture supernatants was previously reported in filamentous fungi (Fayeulle, 2013; Rafin et al., 2013). However preliminary experiments to test the solubilization of BaP by culture filtrates of *T. helicus* did not show any significant desorption from a solid porous matrix, as

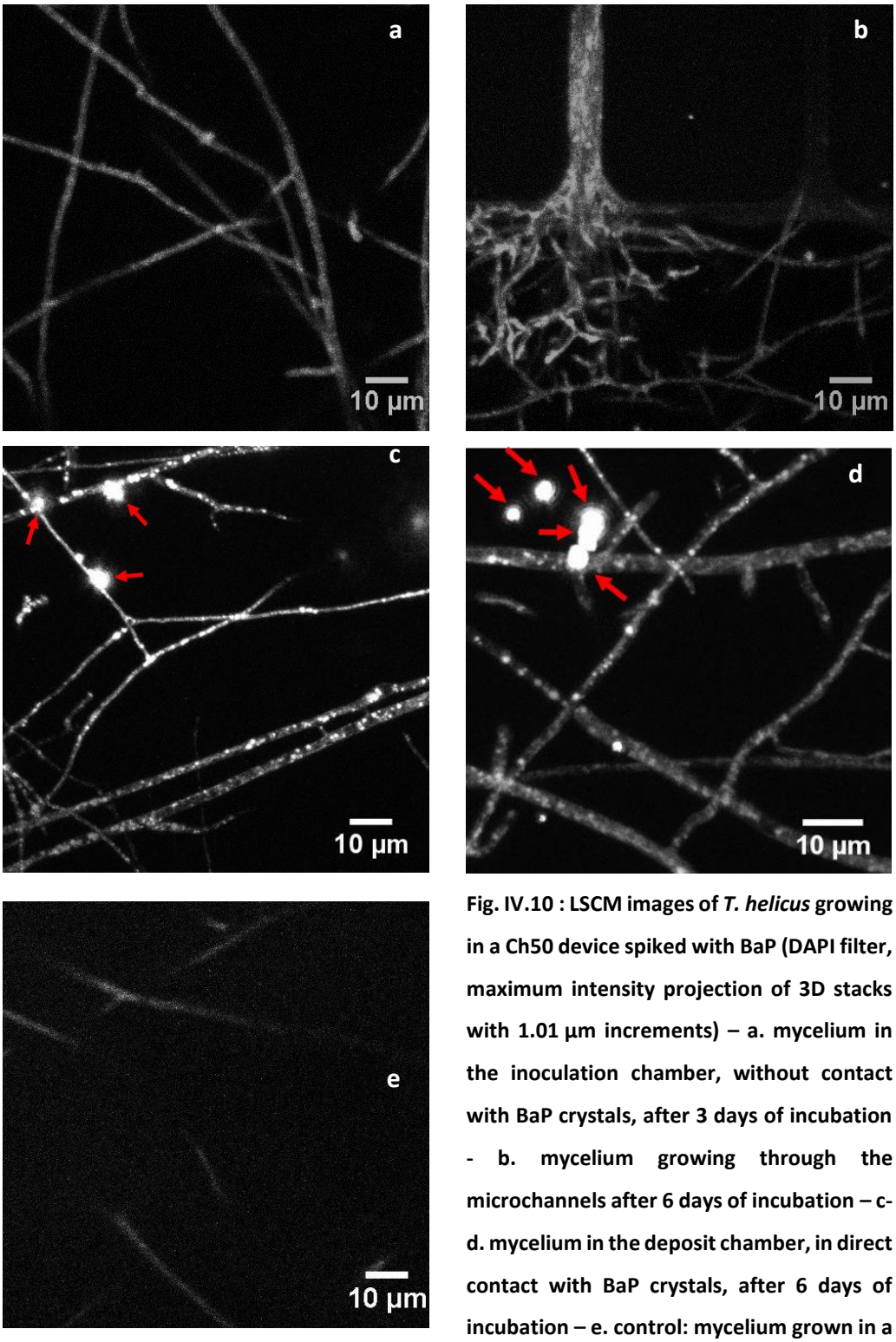

Fig. IV.10 : LSCM images of *T. helicus* growing in a Ch50 device spiked with BaP (DAPI filter, maximum intensity projection of 3D stacks with 1.01 µm increments) – a. mycelium in the inoculation chamber, without contact with BaP crystals, after 3 days of incubation - b. mycelium growing through the microchannels after 6 days of incubation – c-d. mycelium in the deposit chamber, in direct contact with BaP crystals, after 6 days of incubation – e. control: mycelium grown in a chip without BaP, after 6 days of incubation.

presented in chapter II. Previous desorption tests conducted by (Fayeulle, 2013), with the same species but following a different protocol, did not show any solubilization of BaP above the aqueous solubility limit either. Rather than actual solubilization, surfactants in culture supernatants may promote the fractionation of large crystals such as the one pictured in Fig. IV.1.a and their stabilization into smaller particles susceptible to easier transport in liquid cultures. This could explain the diffuse staining of hyphae before the solid BaP deposit is reached. Although the dispersion of non-aqueous phase liquids by microbial surfactants is well documented, there is little data available about their effect on solid PAH crystals. As previously discussed in chapter II, fungal surfactants likely behave differently towards BaP in a confined microenvironment as opposed to large culture volumes, due to higher local concentrations. They may thus be most effective at a close range, which is consistent with observations of preferential uptake into hyphae close to the BaP source. Alternatively, surfactants may act as mediators of the direct contact between hyphae and hydrophobic PAH crystals, rather than solubilizing agents.

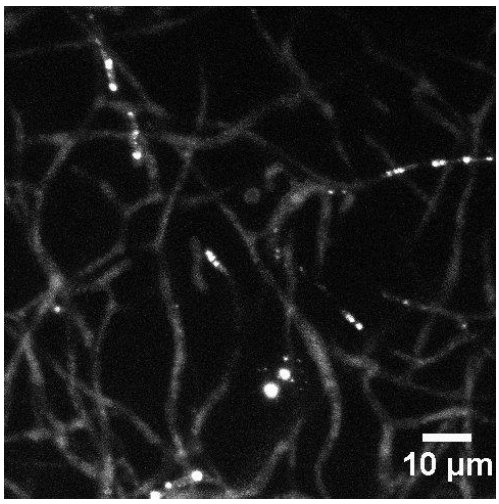

Fig. IV.11 : LSCM image of *T. helicus* growing in a Ch50 device, separated from the BaP source by a 4 mm thick PDMS wall, after 6 days of incubation (DAPI filter, maximum intensity projection of a 13 images stack with 1.01 µm increments).

As reported in Chapter III (section 3.1.1), BaP is able to diffuse through the PDMS matrix, which can also explain how it is transported from the deposit to the fungus in the inoculation chamber before hyphae can reach the crystals. This implies that the fungus is able to retrieve BaP from the polymer. In order to verify this hypothesis, *T. helicus* was grown in a microfluidic chamber, and BaP deposited in a neighboring chamber separated from the inoculum by a 4 mm thick PDMS wall, ensuring that the fungus could not grow towards the deposit and come into direct contact with the crystals. After 6 days of incubation, the mycelium was visibly stained, with a diffuse fluorescence along hyphae and some apices presenting bright spots similar to the previously observed intracellular lipid bodies (Fig. IV.11).

According to the results obtained in Chapter III, BaP is able to diffuse over a distance of 13 mm after 6 days, which is greater than the width of the PDMS walls separating the growth chamber from the BaP deposit. This result therefore shows the ability of *T. helicus* to access BaP diffusing through a solid organic phase, in this case PDMS. These images also tend to support the hypothesis of a preliminary incorporation through metabolically active hyphal tips. This is consistent with the internalization model through lipid membranes, since intense membrane trafficking takes place at hyphal tips.

4. Conclusions

Talaromyces helicus, like other species of filamentous fungi, is able to incorporate BaP (used here as a model of insoluble hydrophobic pollutant) into its cells. BaP is internalized and stored in the dissolved form in lipid droplets where it is present in high concentrations, and in other lipid-rich cellular components. These results add elements to the already existing evidence of connections between fungal lipid metabolism, intracellular lipid trafficking and the detoxification of hydrophobic organic contaminants. It is consistent with an incorporation model involving lateral diffusion in the cellular membranes, internalization through endocytosis and transfer to the internal organelles, and most specifically lipid bodies, via the constitutive membrane cycling and lipid trafficking of the cell.

We observed a preferential absorption of BaP into hyphae in direct contact with BaP crystals, occurring within a few minutes only. Adsorption to the cell wall thus appears to be a determining step preliminary to internalization, as also suggested by previous works with yeast and other filamentous fungi.

Incorporation can also occur without contact with the solid crystals, as demonstrated by implementing a spatial compartmentation in on-chip fungal cultures: in this case transport mechanisms prior to the incorporation remain unclear. BaP is likely to diffuse through NAPL, and as well as through the solid PDMS used to construct the microfluidic chips used here. Micelle-facilitated transport in the aqueous phase may also be involved. Fungal mobilizing agents may act on BaP in two complementary ways: a detergent effect detaching BaP crystals from solid surfaces, and a stabilizing effect suspending small particles in the aqueous phase.

In this regard, further research is needed to elucidate the possible role of fungal mobilizing agents in the transport of BaP, and more specifically that of extracellular surfactants highlighted in chapter II. Current evidence indicate that BaP behaves in a similar way as neutral lipids in the fungal cell, and extracellular mobilization as well as internalization mechanisms are likely to be the same as other lipophilic substrates. Moreover, BaP degradation in non-ligninolytic filamentous fungi is thought to be a co-metabolism, serving a non-specific detoxification function.

Intracellular transport via vesicle trafficking or bulk cytoplasmic flows along hyphae cannot be confirmed or infirmed from these results, however experiments to answer this question could be designed using the same microfluidic set-up with a higher resolution in time, in order to observe changes in overall fluorescent signal over time.

Conclusion générale

Ce travail de thèse a été réalisé dans le but d'une meilleure compréhension des mécanismes impliqués dans la mobilisation de polluants récalcitrants des sols, dans un contexte de bioremédiation. Les champignons saprotrophes du sol présentent en effet des caractéristiques prometteuses pour ces applications, du fait de leurs capacités de bioaccumulation de polluants organiques, et de leur adaptation à l'environnement du sol. *Talaromyces helicus*, dont le potentiel pour la bioremédiation de métaux lourds et de composés aromatiques est connu depuis seulement une dizaine d'années, est une de ces espèces. Les objectifs étaient donc de mieux caractériser le potentiel de cette souche émergente pour la bioremédiation des HAP d'une part, et d'autre part de mieux comprendre les mécanismes de mobilisation et d'incorporation de polluants hydrophobes par les champignons filamenteux via la mise en place d'un dispositif microfluidique reproduisant un environnement compartimenté.

Principaux résultats obtenus

Des tests de biodégradation ont été menés en milieu minéral liquide pour le benzo[*a*]pyrène, ainsi que dans des échantillons de sols pollués. Les résultats des tests en milieu liquide confirment la capacité de *T. helicus* à dégrader le BaP en présence du glucose comme unique cosubstrat carboné. Au moins quatre métabolites non identifiés, plus polaires que le BaP, ont été détectés par HPLC au cours de la dégradation. Ils pourraient être des quinones, dihydrodiols ou composés phénoliques dérivés du BaP. La biodégradation du BaP apparaît stimulée par l'enrichissement en azote en milieu liquide, tandis que de précédents travaux suggéraient l'effet opposé dans des échantillons de sol. Un des métabolites détectés en particulier s'accumule dans des conditions d'excès d'azote, ce qui indique la favorisation d'une voie métabolique responsable de sa formation. Les résultats obtenus en milieu liquide suggèrent en effet la coexistence de la voie de détoxification des cytochrome P450 monooxygénases avec une ou des voies de biodégradation impliquant des activités peroxydases, et des oxydations non spécifiques par des espèces réactives de l'oxygène. La voie des CYP450 est une voie intracellulaire impliquant notamment des monooxygénases membranaires qui pourraient interagir avec les organites de stockage et de transit des lipides. Or, *T. helicus* absorbe le BaP dans ses cellules où il est incorporé dans les corps lipidiques, ce qui a été confirmé par des observations en microscopie confocale à balayage laser en utilisant un marqueur fluorescent des lipides. Ces observations sont donc cohérentes avec une dégradation intracellulaire. Cependant, on ne peut affirmer à ce stade que l'incorporation au sein des cellules est un préalable nécessaire à la dégradation chez *T. helicus*.

Des tests de bio-augmentation en sol ont été menés en microcosmes et en conditions aérobies, en utilisant des échantillons de sols provenant de véritables sites pollués et présentant des contaminations multiples aux hydrocarbures, HAP, PCB et métaux. Un développement mycélien a été observé dans l'échantillon le plus riche en matières organiques, qui était également celui où la biodégradation des hydrocarbures totaux était la plus efficace. L'efficacité de biodégradation de *T. helicus* inoculé seul dans ces sols est faible, probablement en raison du pH élevé, de la faible teneur en matières organiques et de la présence de cuivre dans un des échantillons. La bio-augmentation avec *T. helicus* a également été testée en présence de tensioactifs et de bactéries en coculture : une stimulation significative de la biodégradation des PCB a ainsi pu être observée en présence de sophorolipides, ainsi que de *Corynebacterium glutamicum.*

La production de biosurfactants extracellulaires par *T. helicus* a été montrée pour la première fois à notre connaissance chez cette espèce. Ces surfactants libérés dans le milieu de culture sont responsables d'un abaissement de la tension de surface jusqu'à 49 mN/m pendant la phase de croissance du mycélium. Les filtrats de culture présentant une activité de surface ont été analysés par gel filtration et chromatographie sur couche mince à haute performance, afin de caractériser les molécules tensioactives. Au moins trois fractions de tailles différentes, présentent une activité de surface, ont été séparées par gel filtration. L'analyse par HPTLC ne révèle aucun groupement lipidique dans ces fractions, mais elles pourraient contenir des hydrophobines ou des tensioactifs présentant un groupement sucre.

Des cultures fongiques dans un environnement compartimenté ont été mises en place grâce à la fabrication par lithographie douce de puces microfluidiques en verre et polydiméthylsiloxane (PDMS). Une géométrie de canaux personnalisée a été dessinée spécifiquement à cette fin: le motif « Ch50 » comprend deux chambres pouvant être remplies de milieu nutritif, séparées par des microcanaux dont les dimensions transversales sont du même ordre de grandeur que le diamètre des hyphes de *T. helicus*. Ce dispositif permet d'observer en temps réel la progression du mycélium à travers des porosités, et sa mise en présence du BaP, sans qu'il y ait initialement contact entre la source de polluant et le mycélium. La vitesse de croissance de *T. helicus* dans les microcanaux a ainsi été mesurée, et était deux fois plus lente que sur milieu gélosé MYEA agar plates, ce qui indique que l'élongation des hyphes est affectée par le confinement et la disponibilité des nutriments. Les observations en microsystèmes montrent une incorporation du BaP dans les cellules fongiques au niveau de vésicules intracellulaire lorsque le mycélium a atteint la source de BaP, confirmant les observations préalablement faites sur du mycélium cultivé en milieu liquide additionné de BaP. Un marquage précoce du mycélium est également observé avant le contact des hyphes avec les cristaux solides. L'incorporation a donc lieu même sans contact direct des hyphes avec le dépôt de polluant. L'existence

d'un mécanisme de transport via la phase aqueuse reste à vérifier, mais la production de biosurfactants par *T. helicus* démontrée ici pourrait expliquer une solubilisation partielle et un transport facilité du BaP. D'autre part, le mycélium apparaît capable de mobiliser le BaP qui diffuse à travers une paroi de PDMS, sans que des canaux remplis de milieu aqueux relient l'inoculum au dépôt de polluant. La diffusion du BaP dans la matrice du PDMS suggère une autre voie possible de mobilisation, via la diffusion du BaP dans des phases organiques non miscibles avec l'eau. Ainsi la présence d'hydrocarbures aliphatiques comme co-contaminants pourrait permettre un meilleure efficacité de biodégradation non seulement en raison de leur utilisation comme cosubstrat, mais également par une meilleure mobilisation du BaP via sa solubilisation dans la phase organique.

Limites et perspectives futures

De nombreuses pistes restent à explorer sur chacun des axes de recherche développés dans ce travail de thèse. En particulier, le lien entre production de biosurfactants, incorporation et dégradation chez *T. helicus* n'est pas établi. D'une part, plusieurs voies métaboliques intracellulaires et extracellulaires pourraient participer à la biodégradation, l'identification des activités enzymatiques exprimées ainsi qu'une caractérisation des métabolites produits permettraient d'évaluer plus précisément la contribution de chaque voie. D'autre part, le rôle potentiel des tensioactifs fongiques dans la stabilisation de composés organiques hydrophobes en phase aqueuse et leur entrée dans la cellule reste à déterminer.

Les premiers tests de désorption réalisés en batch ne montrent pas d'effet des surnageants de culture sur la solubilisation ou la mise en suspension du BaP. Cependant ces expériences demandent à être répétées dans différentes conditions. Une des modifications possibles est de tester le lessivage du BaP dans un écoulement, avec un dépôt sur une surface ou imbibé sur un support poreux. Cette méthode permettrait d'introduire une contrainte mécanique. Le dispositif microfluidique pourrait également présenter un intérêt pour ce type de test : en effet, la quantité de tensioactifs produits par le champignon peut-être efficace à l'échelle du micro-environnement des hyphes en milieu poreux, mais négligeable lorsque diluée dans le du volume d'une culture en erlenmeyer. D'autre part, des tests d'émulsification avec de l'huile végétale ou des hydrocarbures permettraient de tester un éventuel effet des tensioactifs fongiques sur les phases liquides non aqueuses qui peuvent contenir du BaP, plutôt que sur des particules solides. La nature des tensio-actifs fongiques produits par *T. helicus* reste également à élucider plus précisément, à cette fin la chromatographie sur couche mince est une technique versatile et prometteuse. A l'aide d'une résine de gel filtration de plus haut pouvoir séparateur pour les petites masses moléculaires, un meilleur fractionnement en fonction de la taille pourrait être réalisé préalablement à l'HPTLC. L'utilisation d'échantillons plus concentrés et de

révélateurs de fonctions chimiques spécifiques et à envisager. La chromatographie d'interaction hydrophobe est une autre piste d'analyse pour isoler des tensio-actifs, en les séparant selon leur affinité pour des groupements hydrophobes.

Le rôle de la paroi comme interface entre les cellules fongiques et les xénobiotiques présents dans le milieu extérieur reste mal connu. Certains composants pourraient jouer un rôle d'adsorbant, comme première étape avant une internalisation. La purification de composants de la paroi pourrait permettre de tester leur affinité pour divers substrats hydrophobes. La détection de changements de l'hydrophobie de surface des hyphes reste un défi technique, les techniques usuelles utilisées pour les levures et bactéries étant mal adaptées à la morphologie des champignons filamenteux. En ce qui concerne d'éventuels transports intracellulaires des HAP après incorporation, et leur redistribution dans le mycélium, les observations microscopiques en time-lapse à une fréquence temporelle suffisamment élevée semblent une solution simple à mettre en œuvre, et combinable avec un marquage fluorescent du cytosquelette et des lipides.

Plusieurs modèles de puces microfluidiques ont été explorés au cours de ce projet de thèse, avec pour objectif la mise au point d'un environnement compartimenté et contrôlé pour la culture fongique. Cependant, aucun de ces modèles n'était parfaitement satisfaisant, soit parce que le bruit de fond fluorescent était trop important, soit parce qu'elles ne permettaient pas un confinement et un contrôle de la géométrie des canaux suffisants, et plusieurs compromis ou contournements ont dû être recherchés. Le principe des puces à « sticker » de PDMS mériterait d'être exploité de manière plus poussée pour des observations en épifluorescence, ce qui n'a finalement pas été réalisé dans les travaux présentés ici. Une des limites majeures de ce système microfluidique est la perméabilité du PDMS à certaines molécules organiques hydrophobes, dont le BaP. L'interprétation des observations réalisées est donc à faire au regard de la vitesse de diffusion du BaP dans le polymère. La fabrication de systèmes entièrement en verre serait beaucoup plus longue, coûteuse et incompatible avec la diffusion du dioxygène nécessaire à la croissance fongique. Quant à la plupart des autres matériaux plastiques utilisés pour la microfabrication, dont les cyclo-oléfines, polycarbonates, ou le PMMA, ils ne présentent pas d'aussi bonnes propriétés optiques et sont également imperméables aux échanges gazeux ce qui rend leur utilisation en biologie limitée.

A partir de ce modèle simplifié visant à élucider des mécanismes biologiques, la perspective à plus long terme serait de développer un modèle versatile dans une perspective « soil-on-chip ». Le design présenté ici nécessite d'être amélioré et complexifié pour intégrer de nouveaux paramètres expérimentaux. Ainsi des géométries de canaux reproduisant plus fidèlement les porosités de la matrice du sol pourraient être conçues, ainsi que la mise en place d'écoulements, des traitements de

surface, des milieux biphasés avec une phase organique ou hétérogènes avec des particules en suspension. La grande variabilité des sols en terme de structure, de composition et de biodiversité d'une part, et la diversité des pollutions en terme de nature chimique, de concentration et de biodisponibilité d'autre part, rendent la prédiction des résultats d'un procédé de remédiation difficile. Le changement d'échelle expérimentale, de l'erlenmeyer au microcosme puis du microcosme à l'essai sur site, occasionne souvent des résultats très différents. En effet les études en laboratoires, en sol ou en milieu liquide ne rendent pas compte des conditions hétérogènes et dynamiques d'un site réel. Afin de mettre en place un outil de diagnostic permettant de mimer les paramètres d'un sol donné de manière customisée, le défi technique est important. L'enjeu est donc de comparer les résultats obtenus avec un tel modèle à ceux obtenus sur site, afin de vérifier leur prédictibilité selon plusieurs paramètres jugés pertinents: en particulier, la colonisation du milieu par le micro-organismes, les activités métaboliques exprimés, la mobilisation du polluant et/ou son accessibilité, finalement sa dégradation. Enfin, l'étape suivante serait l'utilisation de ce type de dispositif pour tester différentes stratégies de biostimulation en amont de la mise au point d'un protocole de bioremédiation. Parmi ces stratégies figurent l'ajout de tensioactifs, des amendements visant à fournir une source de carbone supplémentaire ou modifier la teneur en azote et phosphore du sol, des ajustements du pH, la chélation de métaux, ou des co-inoculations avec d'autres micro-organismes dans le but de former des synergies de dégradation. L'identification de métabolites de dégradation mobiles en phase aqueuse pourrait également être réalisée avec des puces sous perfusion, en récoltant et en analysant l'efflux de sortie.

General Conclusion

This work was conducted aiming to better understand the mechanisms involved in persistent pollutant mobilization in soil in the context of bioremediation. Soil saprotrophic fungi indeed display promising traits for such applications, due to their ability to bioaccumulate organic pollutants, and their adaptation to the soil environment. *Talaromyces helicus*, of which the potential for the bioremediation of heavy metals and aromatic compounds has been known only for a decade, is one of these species. The goals were thus to better characterize the properties of this emerging strain for the remediation of PAH on one hand, and on the other hand to gain insight on hydrophobic pollutant mobilization and uptake mechanisms in filamentous fungi, through the implementation of microfluidic device replicating a compartmentalized and confined environment.

Main results

Biodegradation tests were conducted in liquid mineral medium for benzo[*a*]pyrene, and in polluted soil samples. The results obtained in liquid media confirm the ability of *T. helicus* to degrade BaP in presence of glucose as the sole carbon-containing co-substrate. At least four unidentified metabolites more polar than BaP were detected by HPLC analysis during biodegradation experiments. These could be quinone, dihydrodiol or phenolic BaP derivatives. The biodegradation of BaP appears to be stimulated by nitrogen enrichment in liquid media, in contrast to previous works suggesting the opposite effect in soils. One of the metabolites detected in particular accumulates in conditions of excess nitrogen, indicating the stimulation of a specific metabolic pathway responsible for its formation. Indeed, the results obtained in liquid media suggest the co-existence of cytochrome P450 - mediated detoxification with one or more degradation pathways involving peroxidases or non-specific oxidations through reactive oxygen species. The CYP450 pathway is intracellular involving membrane-bound mono-oxigenases which could interact with lipid storage and transport organelles. Incidentally, *T. helicus* absorbs BaP into its cells where it is incorporated in lipid bodies, as was confirmed by observations in laser scanning confocal microscopy using a fluorescent lipid marker. These observations are thus consistent with an intracellular biodegradation route. However, it is still unsure at this stage whether BaP uptake into the cells is a necessary preamble to biodegradation in *T. helicus*.

Bio-augmentation tests were conducted as well in soil microcosms in aerobic conditions, using samples from real polluted sites and presenting multiple contaminations with hydrocarbons, PCB, PAH and metals. In the soil that with the highest organic matter content, mycelial development was observed, coincidentally with the highest rate of total hydrocarbon degradation. The biodegradation efficiency of *T. helicus* inoculated by itself was generally low, probably because of the high pH, the low organic

matter content and he presence of copper in one of the soils. Bio-augmentation with *T. helicus* was also tested with the addition of surfactants and bacteria in co-cultures : a significant stimulation of PCB biodegradation was thus observed when sophorolipid surfactants were used, and in presence of *Corynebacterium glutamicum.*

The production of extracellular biosurfactants by *T. helicus* was described in this species for the first time to our knowledge. These surfactants released in the culture supernatant are responsible for lowering the surface tension to 50 mN/m during the mycelium growth phase. Culture filtrates displaying a surfactant activity were analyzed by gel filtration and high performance thin layer chromatography, in order to characterize the surface-active molecules. At least three surface-active fractions with different molecular sizes were separated through gel-filtration. The HPTLC analysis of these fractions does not reveal any lipid moiety, but they could consist in hydrophobins or surfactants containing sugars as the hydrophilic group.

Fungal cultures were implemented in a compartmentalized environment thanks to the making of glass and polydimethylsiloxane (PDMS) microfluidic chips using a soft lithography technique. A custom channel geometry was designed specifically for this purpose : the « Ch50 » pattern included two culture chambers that can be filled with growth medium, joined by microchannels with section dimensions of the same order as hyphal diameter. This device allows the real-time observation of mycelial growth through porosities, and its coming in contact with BaP, while enabling initial separation between the inoculum and pollutant source. The growth velocity of *T. helicus* in microchannels was thus measured, and was twice slower than it was on MYEA plates, which indicates that elongation is affected by confinement and nutrient availability. Observations in the microfluidic chips show BaP uptake into the fungal cells, into intracellular vesicles once the mycelium has reached the BaP source. These observations confirm the previous results obtained with mycelium cultivated in liquid medium supplemented with BaP. Early staining of the mycelium was also observed before contact occurs between the hyphae and BaP crystals. Uptake therefore takes place even without direct contact with the BaP deposit. A possible transport mechanism through the aqueous phase remains to be confirmed, but the production of biosurfactants by *T. helicus* demonstrated here could explain a partial solubilization and facilitated transport of BaP. Besides, the mycelium appears to be able to mobilize BaP diffusing through a PDMS wall, without channels filled with aqueous medium joining the inoculum to the pollutant source. The diffusion of BaP through the PDMS matrix suggests another possible mobilization route, involving the diffusion of BaP through organic phases. Thus, the presence of alkanes as co-contaminants could allow a better biodegradation efficiency, not only because of their use as co-substrates, but also by enhancing BaP mobilization through its solubilization in the organic phase.

Limitations and future prospects

A number of avenues are still to be investigated along each of the research axes laid out in this work. In particular, the relationship between biosurfactant production, BaP uptake and biodegradation in *T. helicus* is not established. On one hand, several intracellular and extracellular metabolic pathways may participate in BaP degradation, and the identification of enzymatic activities as well as a characterization of the produced metabolites could allow to evaluate more precisely the contribution of each pathway. On the other hand, the potential role of fungal surfactants in stabilizing hydrophobic organic compounds in the aqueous phase and facilitating their entry into the cell remains to be determined.

The first desorption tests do not show any significant effect of culture supernatants on the solubilization or suspension of BaP. However, this experiment needs to be repeated in different conditions. One of the possible modifications would be to test BaP washing in a dynamic flow, with the pollutant deposited on a surface or soaked into a porous substrate. This way, mechanical constraints could be introduced. The microfluidic device could also be of interest for this type of test : indeed, the quantity of surfactants produced may be efficient at the scale of hyphal micro-environment in a porous matrix, but negligible when diluted in the volume of a shaking flask culture. In addition, emulsification tests with vegetable oil or alkanes would allow testing of a possible effect of fungal surfactants on nonaqueous phase liquids containing BaP, rather than solid particles. The nature of the fungal surfactants produced by *T. helicus* should also be determined more precisely. For this purpose, thin-layer chromatography appears as a versatile and promising technique. Using a gel filtration resin with a higher resolution for low molecular weights, fractionation before HPTLC analysis could be improved. The use of more concentrated samples and of relevant detection reagents for specific chemical functions should be considered. Hydrophobic interaction chromatography is another possibility to purify surfactants, separating them according to their affinity for hydrophobic functions.

The role of the cell wall as an interface between fungal cells and xenobiotics in the outside environment is poorly known. Some components could act as adsorbents, in a first step prior to internalization. The purification of parietal components could allow their affinity for various hydrophobic substrates to be tested. The detection of changes in surface hydrophobicity of hyphae is still a technical challenge, as techniques used for yeast and bacteria are poorly adapted to the morphology of filamentous fungi. Regarding the intracellular transport of PAH after uptake, and their distribution within the mycelium, time-lapse microscope observations with a relevant acquisition frequency are a rather simple solution, that can be used in combination with a fluorescent marking of the cytoskeleton, lipids or other cellular components.

Several microfluidic chip designs were tested during the course of this project, aiming at setting up a compartmentalized and controlled environment for fungal culture. However, none of these designs were ultimately perfectly satisfying, either because the fluorescent background was too high, or because they did not enable a sufficient control over confinement and channel geometry, hence, compromises or workarounds had to be found. The principle of PDMS « sticker » chips should be further explored for epifluorescence microscopy applications, which was ultimately not done within the frame of the present work. One of the major limits of these devices is the permeability of PDMS to small hydrophobic organic molecules including BaP. The observations must therefore be interpreted in relationship to the speed of BaP diffusion in the polymer. The fabrication of devices entirely made of glass would be longer, more expensive and not compatible with oxygen diffusion required for fungal growth. Most of the other synthetic materials commonly used for microfabrication, including cyclo-olefins, polycarbonates, or polymethyl methacrylate, do not present optical properties as good as PDMS, and are impervious to gas exchanges which limits their uses for biological applications.

Starting from this simplified model, designed to elucidate fundamental biological mechanisms, a longer-term perspective is to develop a versatile model in a “soil-on-chip” approach. The present set-up requires to be improved and complexified to incorporate new experimental parameters. Thus, channel geometries more closely replicating soil porosities could be designed, as well as the implementation of flows, surface treatments, biphasic media with an organic and aqueous phase, or heterogeneous media with suspended particles. The great variability of soils in terms of structure, composition and biodiversity on one hand, and the diversity of pollutions in terms of chemical nature, amount and bioavailability on the other hand, make it difficult to predict the results of a given bioremediation protocol. Experimental scale-up, from the shake flask to soil microcosms and then to field trials, often results in very different outcomes. Indeed, laboratory-scale studies, either in soils or liquid medium, do not account for the heterogeneous and dynamic conditions on a real site. In order to implement an assessment tool allowing the experimenter to mimic characteristics of a given soil in an adaptable manner, technical challenges remain. Results obtained with such a device will have to be compared with on-site results, in order to verify their predictability regarding several relevant parameters; in particular, substrate colonization by the microorganisms, metabolic activity, pollutant availability and its mobilization, and its eventual degradation. Finally, the next step would be the use of this type of device to test biostimulation strategies before proposing a bioremediation protocol. Among these strategies are the addition of surfactants, medium modifications to modulate the carbon or nitrogen supply, pH adjustments, metal chelation, co-inoculation with other micro-organisms with the aim of forming biodegradation synergies. Microchips under perfusion could also be used to identify

degradation metabolites that are mobile in the aqueous in the aqueous phase, by harvesting and analysis the downstream efflux.

References

Acevedo F., L. Pizzul, M. del P. Castillo, R. Cuevas and M.C. Diez (2011). Degradation of polycyclic aromatic hydrocarbons by the Chilean white-rot fungus Anthracophyllum discolor. J. Hazard. Mater. *185*, 212–219.

Al-Hawash A.B., X. Zhang and F. Ma (2019). Removal and biodegradation of different petroleum hydrocarbons using the filamentous fungus Aspergillus sp. RFC-1. MicrobiologyOpen *8*, e00619.

Alimadadi N., M.R. Soudi and Z. Talebpour (2018). Efficient production of tri-acetylated mono-acylated mannosylerythritol lipids by Sporisorium sp. aff. sorghi SAM20. J. Appl. Microbiol. *124,* 457–468.

do Amaral Marques N.S.A., T. Alves Lima e Silva, R. F. da Silva Andrade, J.F. Branco Júnior, K. Okada and G.M. de Campos-Takaki (2019). Lipopeptide biosurfactant produced by *Mucor circinelloides* UCP/WFCC 0001 applied in the removal of crude oil and engine oil from soil. Acta Sci. - Technol. *41*.

Amellal N., J.-M. Portal, and J. Berthelin (2001). Effect of soil structure on the bioavailability of polycyclic aromatic hydrocarbons within aggregates of a contaminated soil. Appl. Geochem. *16*, 1611–1619.

Amézcua-Vega C., H.M. Poggi-Varaldo, F. Esparza-García, E. Ríos-Leal and R. Rodríguez-Vázquez (2007). Effect of culture conditions on fatty acids composition of a biosurfactant produced by Candida ingens and changes of surface tension of culture media. Bioresour. Technol. *98*, 237–240.

Andersson B.E. and T. Henrysson (1996). Accumulation and degradation of dead-end metabolites during treatment of soil contaminated with polycyclic aromatic hydrocarbons with five strains of white-rot fungi. Appl. Microbiol. Biotechnol. *46*, 647–652.

Andrade Silva N.R., M.A.C. Luna, A.L.C.M.A. Santiago, L.O. Franco, G.K.B. Silva, P.M. de Souza et al. (2014). Biosurfactant and bioemulsifier produced by a promising *Cunninghamella echinulata* isolated from caatinga soil in the Northeast of Brazil. Int. J. Mol. Sci. *15*, 15377–15395.

Arutchelvi J.I., S. Bhaduri, P.V. Uppara and M. Doble (2008). Mannosylerythritol lipids: a review. J. Ind. Microbiol. Biotechnol. *35*, 1559–1570.

Ásgeirsdóttir S.A., O.M.H de Vries and J.G.H Wessels (1998). ldentification of three differentially expressed hydrophobins in *Pleurotus ostreatus* (oyster mushroom). Microbiol. *144*, 2961–2969.

Azin E., H. Moghimi, and R. Heidarytabar (2018). Petroleum degradation, biosurfactant and laccase production by *Fusarium neocosmosporiellum* RH-10: a microcosm study. Soil Sediment Contam. Int. J. *27*, 329–342.

Bago B., P.E. Pfeffer, W. Zipfel, P. Lammers, and Y. Shachar-Hill (2002). Tracking metabolism and imaging transport in arbuscular mycorrhizal fungi. pp. 189–197 *In*: S.E. Smith and F.A. Smith, [eds.]. Diversity and Integration in Mycorrhizas. Springer Netherlands, Dordrecht, Netherlands.

Bai J., and R.E. Pagano (1997). Measurement of spontaneous transfer and transbilayer movement of BODIPY-labeled lipids in lipid vesicles. Biochemistry *36*, 8840–8848.

Banitz, T., K. Johst, L.Y. Wick, S. Schamfuß, H. Harms and K. Frank (2013). Highways versus pipelines: contributions of two fungal transport mechanisms to efficient bioremediation. Environ. Microbiol. Rep. *5*, 211–218.

Baranger C., L. Creusot, X. Sun, I. Pezron, A. Le Goff and A. Fayeulle (2018). Microfluidic approaches for improved bioremediation: monitoring pollutant uptake in a soil fungus. NewTech'18: 184. Madrid, Spain

Baranger C., A. Fayeulle, and A. Le Goff (2020). Microfluidic monitoring of the growth of individual hyphae in confined environments. R. Soc. Open Sci. *7*, 191535.

Baranger C., I. Pezron, A. Le Goff, A. Fayeulle (2020). Fungal influence on hydrophobic organic pollutants dynamics within the soil matrices. *In*: V. Kumar, [ed.]. Rhizomicrobiome Dynamics in Bioremediation. CRC Press (in press)

Barkal L.J., N.M. Walsh, M.R. Botts, D.J. Beebe, and C.M. Hull (2016). Leveraging a high resolution microfluidic assay reveals insights into pathogenic fungal spore germination. Integr. Biol. *8*, 603–615.

Barkay T., S. Navon-Venezia, E.Z. Ron and E. Rosenberg (1999). Enhancement of solubilization and biodegradation of polyaromatic hydrocarbons by the bioemulsifier alasan. Appl. Environ. Microbiol. *65*, 2697–2702.

Batista R.M., R.D. Rufino, J.M. de Luna, J.E.G de Souza and L.A. Sarubbo (2010). Effect of medium components on the production of a biosurfactant from *Candida tropicalis* applied to the removal of hydrophobic contaminants in soil. Water Environ. Res. *82*, 418–425.

Bell-Pedersen D., J.C. Dunlap and J.J Loros (1992). The *Neurospora* circadian clock-controlled gene, ccg-2, is allelic to eas and encodes a fungal hydrophobin required for formation of the conidial rodlet layer. Genes Dev. *6*, 2382–2394.

Berger B.W. and N.D. Sallada (2019). Hydrophobins: multifunctional biosurfactants for interface engineering. J. Biol. Eng. *13*, 10.

Beven K., and P. Germann (1982). Macropores and water flow in soils. Water Resour. Res. *18*, 1311–1325.

Bhardwaj G. (2013). Biosurfactants from fungi: a review. J. Pet. Environ. Biotechnol. *4*, 6

Bhardwaj G., S.S. Cameotra and H.K. Chopra (2015). Isolation and purification of a new enamide biosurfactant from *Fusarium proliferatum* using rice-bran. RSC Adv. *5*, 54783–54792.

Bidanjiri M. (2018). Mass flow in hyphae of the oomycete *Achlya bisexualis*. University of Canterbury, Christchurch, New Zealand

Blesic M., V. Dichiarante, R. Milani, M. Linder and P. Metrangolo (2018). Evaluating the potential of natural surfactants in the petroleum industry: the case of hydrophobins. Pure Appl. Chem. *90* (2), 305–314.

de Boer, W., L.B. Folman, R.C. Summerbell and L. Boddy (2005). Living in a fungal world: impact of fungi on soil bacterial niche development. FEMS Microbiol. Rev. *29*, 795–811.

Bogan B.W., and R.T. Lamar (1996). Polycyclic aromatic hydrocarbon-degrading capabilities of Phanerochaete laevis HHB-1625 and its extracellular ligninolytic enzymes. Applied and Environmental Microbiology *62*, 1597–1603.

Boll E.S., A.R. Johnsen, and J.H. Christensen (2015). Polar metabolites of polycyclic aromatic compounds from fungi are potential soil and groundwater contaminants. Chemosphere *119*, 250–257.

Bonfante, P. and A. Genre (2010). Mechanisms underlying beneficial plant–fungus interactions in mycorrhizal symbiosis. Nat. Commun. *1*, 1–11.

Bonnard N., M.-T. Brondeau, T. Clavel, M. Falcy, D. Jargot, M. Lafontaine, M. Reynier, and O. Schneider (2007). Benzo[a]pyrène - Fiche toxicologique n°144.

Bradford M.M. (1976). A rapid and sensitive method for the quantitation of microgram quantities of protein utilizing the principle of protein-dye binding. Anal. Biochem. *72*, 248–254.

Breedveld G.D., and D.A. Karlsen (2000). Estimating the availability of polycyclic aromatic hydrocarbons for bioremediation of creosote contaminated soils. Appl. Microbiol. Biotechnol. *54*, 255–261.

Brignon J.M., and S. Soleille (2006). Hydrocarbure aromatique polycyclique (HAP).pdf (INERIS).

Broekaert W.F., F.R.G. Terras, B.P.A. Cammue, and J. Vanderleyden (1990). An automated quantitative assay for fungal growth inhibition. FEMS Microbiol. Lett. *69*, 55–59.

Brown D.G. (2007). Relationship between micellar and hemi-micellar processes and the bioavailability of surfactant-solubilized hydrophobic organic compounds. Environ. Sci. Technol. *41*, 1194–1199.

Bugg T., J.M. Foght, M.A. Pickard, and M.R. Gray (2000). Uptake and active efflux of polycyclic aromatic hydrocarbons by *Pseudomonas fluorescens* LP6a. Appl. Environ. Microbiol. *66*, 5387–5392.

Burgess R.M., M.J. Ahrens, C.W. Hickey, P.J. den Besten, D. ten Hulscher, B. van Hattum, J.P. Meador, and P.E.T. Douben (2003). An overview of the partitioning and bioavailability of PAHs in sediments and soils. pp. 99–126 *In*: P.E.T. Douben [ed.], PAHs: An Ecotoxicological Perspective. John Wiley & Sons, UK

Cachada A., R. Pereira, E.F. da Silva and A.C. Duarte (2014). The prediction of PAHs bioavailability in soils using chemical methods: State of the art and future challenges. Sci. Total Environ. *472*: 463–480.

Camargo-de-Morais M.M., S.A.F. Ramos and M.C.B Pimentel (2003). Production of an extracellular polysaccharide with emulsifier properties by *Penicillium citrinum*. World J. Microbiol. Biotechnol. *19*, 191–194.

Cameron D.R., D.G. Cooper and R.J. Neufeld (1988). The mannoprotein of *Saccharomyces cerevisiae* is an effective bioemulsifier. Appl. Environ. Microbiol. *54*, 1420–1425.

Cao H., C. Wang, H. Liu, W. Jia, and H. Sun (2020). Enzyme activities during Benzo[a]pyrene degradation by the fungus *Lasiodiplodia theobromae* isolated from a polluted soil. Sci Rep *10*, 865.

Cerniglia C.E. (1992). Biodegradation of polycyclic aromatic hydrocarbons. Biodegradation *3*, 351–368.

Cerniglia C.E., and J.B. Sutherland (2010). Degradation of polycyclic aromatic hydrocarbons by fungi. pp. 2079–2110 *In:* K.N. Timmis [ed.]. Handbook of Hydrocarbon and Lipid Microbiology. Springer Berlin Heidelberg, Germany

Chaillan F., A. Le Flèche, E. Bury, Y. Phantavong, P. Grimont, A. Saliot, and J. Oudot (2004). Identification and biodegradation potential of tropical aerobic hydrocarbon-degrading microorganisms. Res. Microbiol. *155*, 587–595.

Chang W., M. Zhang, S. Zheng, Y. Li, X. Li, W. Li, G. Li, Z. Lin, Z. Xie, Z. Zhao, et al. (2015). Trapping toxins within lipid droplets is a resistance mechanism in fungi. Sci. Rep. *5*, 1–11.

Chau H.W., B.C. Si, Y.K. Goh and V. Vujanovic (2009). A novel method for identifying hydrophobicity on fungal surfaces. Mycol. Res. *113,* 1046–1052.

Chau H.W., Y.K Goh, B.C. Si and V. Vujanovic (2010). Assessment of alcohol percentage test for fungal surface hydrophobicity measurement. Lett. Appl. Microbiol. *50*, 295–300.

Chen M., P. Xu, G. Zeng, C. Yang, D. Huang, and J. Zhang (2015). Bioremediation of soils contaminated with polycyclic aromatic hydrocarbons, petroleum, pesticides, chlorophenols and heavy metals by composting: Applications, microbes and future research needs. Biotechnol. Adv. *33*, 745–755.

Chen S., J. Wang, M.G. Waigi and Y. Gao (2018). Glomalin-related soil protein influences the accumulation of polycyclic aromatic hydrocarbons by plant roots. Sci. Total Environ. *644*, 465–473.

Chiewpattanakul P., S. Phonnok, A. Durand, E. Marie and B.W. Thanomsub (2010). Bioproduction and anticancer activity of biosurfactant produced by the dematiaceous fungus *Exophiala dermatitidis* SK80. J. Microbiol. Biotechnol. *20*, 1664–1671.

Chulalaksananukul S., G.M. Gadd, P. Sangvanich, P. Sihanonth, J. Piapukiew, and A.S. Vangnai (2006). Biodegradation of benzo(a)pyrene by a newly isolated *Fusarium sp.* FEMS Microbiol. Lett. *262*, 99–106.

Cicatiello P., A.M. Gravagnuolo, G. Gnavi, G.. Varese and P. Giardina (2016). Marine fungi as source of new hydrophobins. Int. J. Biol. Macromol. *92*, 1229–1233.

Cirigliano M.C. and G.M. Carman (1985). Purification and characterization of Liposan, a bioemulsifier from *Candida lipolytica*. Appl. Environ. Microbiol. *50*, 846–850.

Conn C.A., K. Ma, G.J. Hirasaki, and S.L. Biswal (2014). Visualizing oil displacement with foam in a microfluidic device with permeability contrast. Lab. Chip *14*, 3968–3977.

Cooper, D.G. and D.A. Paddock (1984). Production of a biosurfactant from *Torulopsis bombicola*. Appl. Environ. Microbiol. *47*, 173–176.

Costa Sperb, J.G., T.M. Costa, S.L. Bertoli and L. Benathar Ballod Tavares (2018). Simultaneous production of biosurfactants and lipases from *Aspergillus niger* and optimization by response surface methodology and desirability functions. Braz. J. Chem. Eng. *35*, 857–868.

Cox A.R., F. Cagnol, A.B. Russell, and M.J. Izzard (2007). Surface properties of class II hydrophobins from *Trichoderma reesei* and influence on bubble stability. Langmuir *23*, 7995–8002.

Črešnar B., and Š. Petrič (2011). Cytochrome P450 enzymes in the fungal kingdom. BBA - Proteins Proteom. *1814*, 29–35.

Cui, X., P. Mayer and J. Gan (2013). Methods to assess bioavailability of hydrophobic organic contaminants: Principles, operations, and limitations. Environ. Pollut. *172*, 223–234.

Dashti N., H. Al-Awadhi, M. Khanafer, S. Abdelghany, and S. Radwan (2008). Potential of hexadecane-utilizing soil-microorganisms for growth on hexadecanol, hexadecanal and hexadecanoic acid as sole sources of carbon and energy. Chemosphere *70*, 475–479.

Delsarte I., C. Rafin, F. Mrad, and E. Veignie (2018). Lipid metabolism and benzo[*a*]pyrene degradation by *Fusarium solani*: an unexplored potential. Environ. Sci. Pollut. Res. *25*, 12177–12182.

Deng, Y., Y. Zhang, A.-L. Hesham, R. Liu and M. Yang (2010). Cell surface properties of five polycyclic aromatic compound-degrading yeast strains. Appl. Microbiol. Biotechnol. *86*, 1933–1939.

Déziel, E., G. Paquette, R. Villemur, F. Lépine and J.-G. Bisaillon (1996). Biosurfactant production by a soil *Pseudomonas* strain growing on polycyclic aromatic hydrocarbons. Appl. Environ. Microbiol. *62* (6), 1908–1912

Docoslis A., R.F. Giese, and C.J. van Oss (2000). Influence of the water–air interface on the apparent surface tension of aqueous solutions of hydrophilic solutes. Colloids Surf. B Biointerfaces *19*, 147–162.

Domingo J.L., and M. Nadal (2015). Human dietary exposure to polycyclic aromatic hydrocarbons: A review of the scientific literature. Food Chem. Toxicol. *86*, 144–153.

Dreyer B., A. Morte, M. Pérez-Gilabert, and M. Honrubia (2006). Autofluorescence detection of arbuscular mycorrhizal fungal structures in palm roots: an underestimated experimental method. Mycol. Res. *110*, 887–897.

Driver, J.D., W.E. Holben and M.C. Rillig (2005). Characterization of glomalin as a hyphal wall component of arbuscular mycorrhizal fungi. Soil Biol. Biochem. *37*, 101–106.

Ducarme Ph., M. Rahman, and R. Brasseur (1998). IMPALA: A simple restraint field to simulate the biological membrane in molecular structure studies. Proteins *30*, 357–371.

Duffy D.C., J.C. McDonald, O.J.A. Schueller, and G.M. Whitesides (1998). Rapid prototyping of microfluidic systems in poly(dimethylsiloxane). Anal. Chem. *70*, 4974–4984.

Eland L.E., A. Wipat, S. Lee, S. Park, and L.J. Wu (2016). Microfluidics for bacterial imaging. pp 69-111 *In:* Methods in Microbiology. Elsevier

Fang D., and C. Shi (2016). Characterization and flocculability of a novel proteoglycan produced by *Talaromyces trachyspermus* OU5. J. Biosci. Bioeng. *121*, 52–56.

Fayeulle A. (2013). Etude des mécanismes intervenant dans la biodégradation des Hydrocarbures Aromatiques Polycycliques par les champignons saprotrophes telluriques en vue d'applications en bioremédiation fongique de sols pollués. Université du Littoral Côte d'Opale, Dunkerque, France.

Fayeulle A., E. Veignie, C. Slomianny, E. Dewailly, J.-C. Munch, and C. Rafin (2014). Energy-dependent uptake of benzo[*a*]pyrene and its cytoskeleton-dependent intracellular transport by the telluric fungus *Fusarium solani*. Environ. Sci. Pollut. Res. *21*, 3515–3523.

Fayeulle A., E. Veignie, R. Schroll, J.C. Munch, and C. Rafin (2019). PAH biodegradation by telluric saprotrophic fungi isolated from aged PAH-contaminated soils in mineral medium and historically contaminated soil microcosms. J. Soils Sediments *19*, 3056–3067.

Fomina, M., E.P. Burford and G.M. Gadd (2006). Fungal dissolution and transformation of minerals: significance for nutrient and metal mobility. pp. 236-266 *In*: G.M. Gadd [ed.]. Fungi in Biogeochemical Cycles. Cambridge University Press, Cambridge, UK

Frautz, B., S. Lang and F. Wagner (1986). Formation of cellobiose lipids by growing and resting cells of *Ustilago maydis*. Biotechnol. Lett. *8,* 757–762.

Fuchs U., K.J. Czymmek and J.A. Sweigard (2004). Five hydrophobin genes in *Fusarium verticillioides* include two required for microconidial chain formation. Fungal Genet. Biol. *41*: 852–864.

Furuno S., K. Päzolt, C. Rabe, T.R. Neu, H. Harms and L.Y. Wick (2010). Fungal mycelia allow chemotactic dispersal of polycyclic aromatic hydrocarbon-degrading bacteria in water-unsaturated systems. Environ. Microbiol. *12*, 1391–1398.

Furuno S., S. Foss, E. Wild, K.C. Jones, K.T. Semple, H. Harms, and L.Y. Wick (2012a). Mycelia promote active transport and spatial dispersion of polycyclic aromatic hydrocarbons. Environ. Sci. Technol. *46*, 5463–5470.

Furuno S., R. Remer, A. Chatzinotas, H. Harms and L.Y. Wick (2012b). Use of mycelia as paths for the isolation of contaminant-degrading bacteria from soil. Microb. Biotechnol. *5*, 142–148.

Gadd, G.M., Y.J. Rhee, K. Stephenson and Z. Wei (2012). Geomycology: metals, actinides and biominerals. Environ. Microbiol. Rep. *4*, 270–296.

Gadkar, V. and M.C. Rillig. 2006. The arbuscular mycorrhizal fungal protein glomalin is a putative homolog of heat shock protein 60. FEMS Microbiol. Lett. *263*, 93–101.

Gao, Y., Z. Zhou, W. Ling, X. Hu and S. Chen (2017). Glomalin-related soil protein enhances the availability of polycyclic aromatic hydrocarbons in soil. Soil Biol. Biochem. *107*, 129–132.

Gao R., D.C. Hao, W. Hu, S. Song, S.Y. Li, and G.B. Ge (2019). Transcriptome profile of polycyclic aromatic hydrocarbon-degrading fungi isolated from *Taxus* rhizosphere. Curr. Sci. *116*, 11.

Galambos P., and F.K. Forster (1998). Micro-fluidic diffusion coefficient measurement. pp. 189–192 *In*: D.J. Harrison and A. van den Berg, [eds.]. Micro Total Analysis Systems ’98. Springer Netherlands, Dordrecht, Netherlands

Garay, L.A., I.R. Sitepu, T. Cajka, J. Xu, H.E. Teh, J.B. German, et al. (2018). Extracellular fungal polyol lipids: A new class of potential high value lipids. Biotechnol. Adv. *36*, 397–414.

Garcia-Junco, M., C. Gomez-Lahoz, J.-L. Niqui-Arroyo, and J.J. Ortega-Calvo (2003). Biosurfactant- and biodegradation-enhanced partitioning of polycyclic aromatic hydrocarbons from nonaqueous-phase liquids. Environ. Sci. Technol. *37*, 2988–2996.

Gautam G., V. Mishra, P. Verma, A.K. Panday, and S. Negi (2014). A cost effective strategy for production of bio-surfactant from locally isolated *Penicillium chrysogenum* SNP5 and its applications. J. Bioprocess. Biotech. *4*.

Geng T., E.L. Bredeweg, C.J. Szymanski, B. Liu, S.E. Baker, G. Orr, J.E. Evans, and R.T. Kelly (2015). Compartmentalized microchannel array for high-throughput analysis of single cell polarized growth and dynamics. Sci. Rep. *5*, 16111.

González-Chávez, M.C., R. Carrillo-González, S.F. Wright and K.A. Nichols (2004). The role of glomalin, a protein produced by arbuscular mycorrhizal fungi, in sequestering potentially toxic elements. Environ. Pollut. *130*, 317–323.

Grünbacher, A., T. Throm, C. Seidel, B. Gutt, J. Röhrig, T. Strunk et al (2014). Six hydrophobins are involved in hydrophobin rodlet formation in *Aspergillus nidulans* and contribute to hydrophobicity of the spore surface. PLoS One *9*, e94546.

Guimarães Martins V., S.J. Kalil, T.E. Elit, and J.A. Vieira Costa (2006). Solid state biosurfactant production in a fixed-bed column bioreactor. Z. Für Naturforschung C *61*, 721–726.

Gunderson, J.J., J.D. Knight and K.C.J Van Rees (2007). Impact of ectomycorrhizal colonization of hybrid poplar on the remediation of diesel-contaminated soil. J. Environ. Qual. *36*, 927–934.

Gunsch, C.K., Q. Cheng, K.A. Kinney, P.J. Szaniszlo and C.P. Whitman (2005). Identification of a homogentisate-1,2-dioxygenase gene in the fungus *Exophiala lecanii-corni*: analysis and implications. Appl. Microbiol. Biotechnol. *68*, 405–411.

Haas Jimoh Akanbi, M., E. Post, A. Meter-Arkema, R. Rink, G.T. Robillard, X. Wang et al. (2010). Use of hydrophobins in formulation of water insoluble drugs for oral administration. Colloids Surf. B: Biointerfaces *75*, 526–531.

Hai, F.I., O. Modin, K. Yamamoto, K. Fukushi, F. Nakajima and L.D. Nghiem (2012). Pesticide removal by a mixed culture of bacteria and white-rot fungi. J. Taiwan Inst. Chem. Eng. *43*, 459–462.

Han, H.-L., J. Tang, H. Jiang, M.-L. Zhang and Z. Liu (2008). Synergy between fungi and bacteria in fungi-bacteria augmented remediation of petroleum-contaminated soil. Huan Jing Ke Xue *29*: 189–195.

Hanson K.L., D.V. Nicolau, L. Filipponi, L. Wang, A.P. Lee, and D.V. Nicolau (2006). Fungi use efficient algorithms for the exploration of microfluidic networks. Small *2*, 1212–1220.

Harms H., D. Schlosser, and L.Y. Wick (2011). Untapped potential: exploiting fungi in bioremediation of hazardous chemicals. Nat. Rev. Microbiol. *9*, 177–192.

Harvey, J.V. (1952). Relationship of aquatic fungi to water pollution. Sewage Ind. Waste *24,* 1159–1164.

Hazen, K.C. (1990). Cell surface hydrophobicity of medically important fungi, especially *Candida* species. pp. 249–295 *In*: R.J. Doyle and M. Rosenberg [eds.]. Microbial Cell Surface Hydrophobicity. American Society for Microbiology, Washington DC, USA.

He, X., S. Li and S.G.W. Kaminskyj (2018). Overexpression of *Aspergillus nidulans* α-1,3-glucan synthase increases cellular adhesion and causes cell wall defects. Med. Mycol. *56*: 645–648.

Heister, K., S. Pols, J.P.G. Loch and T.N.P. Bosma (2013). Desorption behaviour of polycyclic aromatic hydrocarbons after long-term storage of two harbour sludges from the port of Rotterdam, The Netherlands. J. Soils Sediments *13,* 1113–1122.

Held M., A.P. Lee, C. Edwards, and D.V. Nicolau (2010). Microfluidics structures for probing the dynamic behaviour of filamentous fungi. Microelectron. Eng. *87*, 786–789.

Held M., C. Edwards, and D.V. Nicolau (2011). Probing the growth dynamics of *Neurospora crassa* with microfluidic structures. Fungal Biol. *115*, 493–505.

Hoffmann J., and J. Altenbuchner (2014). Hyaluronic acid production with *Corynebacterium glutamicum*: effect of media composition on yield and molecular weight. J. Appl. Microbiol. *117*, 663–678.

Holder D.J., B.H. Kirkland, M.W. Lewis and N.O. Keyhani (2007). Surface characteristics of the entomopathogenic fungus *Beauveria* (*Cordyceps*) *bassiana*. Microbiol*. 153*: 3448–3457.

Huang L.H., and J.A. Schmitt (1975). Ohio ascomycete notes II. *Talaromyces* from soils of southern Ohio. Ohio J. Sci. *75*, 75–81.

Hunt, L.M., J.R. Fairweather and F.J. Coyle (2003). Public understandings of biotechnology in New Zealand: factors affecting acceptability rankings of five selected biotechnologies. Research report No. 266, Agribusiness and Economics Research Unit, Lincoln University, Canterbury, N.Z.

IARC (2012). Benzo[*a*]pyrene. In Chemical Agents and Related Occupations, (World Health Organization), pp. 111–144.

Inoue H., S.R. Decker, L.E. Taylor, S. Yano, and S. Sawayama (2014). Identification and characterization of core cellulolytic enzymes from *Talaromyces cellulolyticus* (formerly *Acremonium cellulolyticus*) critical for hydrolysis of lignocellulosic biomass. Biotechnol. Biofuels *7*, 151.

INRS (2018). Classement des agents biologiques. Références en santé au travail 19–26.

Ishaq, U., M.S. Akram, Z. Iqbal, M. Rafiq, A. Akrem, M. Nadeem et al. (2015). Production and characterization of novel self-assembling biosurfactants from *Aspergillus flavus*. J. Appl. Microbiol. *119*: 1035–1045.

Ivshina I., L. Kostina, A. Krivoruchko, M. Kuyukina, T. Peshkur, P. Anderson, and C. Cunningham (2016). Removal of polycyclic aromatic hydrocarbons in soil spiked with model mixtures of petroleum hydrocarbons and heterocycles using biosurfactants from *Rhodococcus ruber* IEGM 231. J. Hazard. Mater. *312*, 8–17.

Jabaji-Hare S.H., C.J. Perumalla, and W.B. Kendrick (1984). Autofluorescence of vesicles, arbuscules, and intercellular hyphae of a vesicular–arbuscular fungus in leek (*Allium porrum*) roots. Can. J. Botany *62*, 2665–2669.

Jaynes, W.F. and S.A. Boyd (1991). Hydrophobicity of siloxane surfaces in smectites as revealed by aromatic hydrocarbon adsorption from water. Clays Clay Miner. *39*, 428–436.

Jennings A.A. (2012). Worldwide regulatory guidance values for surface soil exposure to carcinogenic or mutagenic polycyclic aromatic hydrocarbons. J. Environ. Manage. *110*, 82–102.

de Jonge, L.W., C. Kjaergaard and P. Moldrup (2004). Colloids and colloid-facilitated transport of contaminants in soils: an introduction. Vadose Zone J. *3*, 321–325.

Kamisaka Y., N. Noda, T. Sakai, and K. Kawasaki (1999). Lipid bodies and lipid body formation in an oleaginous fungus, *Mortierella ramanniana* var. *angulispora*. BBA - Mol. Cell Biol. L. *1438*, 185–198.

Kamisaka Y. and N. Noda (2001). Intracellular transport of phosphatidic acid and phosphatidylcholine into lipid bodies in an oleaginous fungus, *Mortierella ramanniana* var. *angulispora*. J. Biochem. *129*, 19–26.

Komarov E.V., and P.G. Ganin (2004). ζ-potential of n-alkane emulsion droplets and its role in substrate transport into yeast cells. Appl. Biochem. Microbiol. *40*, 272–279.

Kan, A.T., W. Chen and M.B. Tomson (2000). Desorption kinetics of neutral hydrophobic organic compounds from field-contaminated sediment. Environ. Pollut. *108,* 81–89.

Käppeli O., P. Walther, M. Mueller, and A. Fiechter (1984). Structure of the cell surface of the yeast *Candida tropicalis* and its relation to hydrocarbon transport. Arch. Microbiol. *138*, 279–282.

Kaufman, D.D. and J. Blake (1970). Degradation of atrazine by soil fungi. Soil Biol. Biochem. *2*, 73–80.

Khalid, S., M. Shahid, N.K. Niazi, B. Murtaza, I. Bibi and C. Dumat (2017). A comparison of technologies for remediation of heavy metal contaminated soils. J. Geochemi. Explor. *182*, 247–268.

Kim H.S., and W.J. Weber (2003). Preferential surfactant utilization by a PAH-degrading strain: effects on micellar solubilization phenomena. Environ. Sci. Technol. *37*, 3574–3580.

Kim B.J., I. Chu, S. Jusuf, T. Kuo, M.A. TerAvest, L.T. Angenent, and M. Wu (2016). Oxygen tension and riboflavin gradients cooperatively regulate the migration of *Shewanella oneidensis* MR-1 revealed by a hydrogel-based microfluidic device. Front. Microbiol. *7*.

Kiran, G.S., T.A. Hema, R. Gandhimathi, J. Selvin, T.A. Thomas, T. Rajeetha Ravji and K. Natarajaseenivasan (2009). Optimization and production of a biosurfactant from the sponge-associated marine fungus *Aspergillus ustus* MSF3. Colloids Surf. B: Biointerfaces *73*, 250–256.

Kitamoto, D., H. Yanagishita, T. Shinbo, T. Nakane, C. Kamisawa and T. Nakahara (1993). Surface active properties and antimicrobial activities of mannosylerythritol lipids as biosurfactants produced by *Candida antarctica*. J. Biotechnol. *29*, 91–96.

Kjær, J., V. Ernstsen, O.H. Jacobsen, N. Hansen, L.W. de Jonge and P. Olsen (2011). Transport modes and pathways of the strongly sorbing pesticides glyphosate and pendimethalin through structured drained soils. Chemosphere *84*, 471–479.

Kobel S., and M.P. Lutolf (2011). Biomaterials meet microfluidics: building the next generation of artificial niches. Curr. Opin. Biotechnol. *22*, 690–697.

Kotterman M.J.J., H.-J. Rietberg, A. Hage, and J.A. Field (1998). Polycyclic aromatic hydrocarbon oxidation by the white-rot fungus Bjerkandera sp. strain BOS55 in the presence of nonionic surfactants. Biotechnology and Bioengineering *57*, 220–227.

Leonardi V., V. Šašek, M. Petruccioli, A. D'Annibale, P. Erbanová, and T. Cajthaml (2007). Bioavailability modification and fungal biodegradation of PAHs in aged industrial soils. Int. Biodeter. Biodegr. *60*, 165–170.

Lacroix, H. and P.D. Spanu (2009). Silencing of six hydrophobins in *Cladosporium fulvum*: Complexities of simultaneously targeting multiple genes. Appl. Environ. Microbiol. *75*, 542–546.

Lade H.S., T.R. Waghmode, A.A. Kadam and S.P. Govindwar. (2012). Enhanced biodegradation and detoxification of disperse azo dye Rubine GFL and textile industry effluent by defined fungal-bacterial consortium. Int. Biodeterior. Biodegradation *72*, 94–107.

Lanéelle M.-A., M. Tropis, and M. Daffé (2013). Current knowledge on mycolic acids in *Corynebacterium glutamicum* and their relevance for biotechnological processes. Appl Microbiol Biotechnol *97*, 9923–9930.

Lee K.K., L. Labiscsak, C.H. Ahn, and C.I. Hong (2016). Spiral-based microfluidic device for long-term time course imaging of *Neurospora crassa* with single nucleus resolution. Fungal Genet. Biol. *94*, 11–14.

Lew R.R. (2005). Mass flow and pressure-driven hyphal extension in *Neurospora crassa*. Microbiology *151*, 2685–2692.

Linder, M.B. (2009). Hydrophobins: Proteins that self-assemble at interfaces. Curr. Opin. Colloid Interface Sci. *14*: 356–363.

Lindley N.D., and M.T. Heydeman (1986). Mechanism of dodecane uptake by whole cells of *Cladosporium resinae*. Microbiology *132*, 751–756.

Lladó S., A.M. Solanas, J. de Lapuente, M. Borràs, and M. Viñas (2012). A diversified approach to evaluate biostimulation and bioaugmentation strategies for heavy-oil-contaminated soil. Sci. Total Environ. *435–436*, 262–269.

Lladó S., S. Covino, A.M. Solanas, M. Viñas, M. Petruccioli and A. d'Annibale (2013). Comparative assessment of bioremediation approaches to highly recalcitrant PAH degradation in a real industrial polluted soil. J. Hazard. Mater. *248–249*, 407–414.

Lohrasbi-Nejad A., M. Torkzadeh-Mahani and S. Hosseinkhani (2016). Heterologous expression of a hydrophobin HFB1 and evaluation of its contribution to producing stable foam. Protein Expr. Purif. *118*, 25–30.

Long T., and R.M. Ford (2009). Enhanced Transverse Migration of Bacteria by Chemotaxis in a Porous T-Sensor. Environ. Sci. Technol. *43*, 1546–1552.

Loureiro dos Reis, C.B., L.M.B. Morandini, C.B. Bevilacqua, F. Bublitz, G. Ugalde, M.A. Mazutti et al. (2018). First report of the production of a potent biosurfactant with α,β-trehalose by *Fusarium fujikuroi* under optimized conditions of submerged fermentation. Braz. J. Microbiol. *49*, 185–192.

Lourenço L.A., M.D. Alberton Magina, L. Benathar Ballod Tavares, S.M.A. Guelli U. de Souza, M. García Román and D. Altmajer-Vaz (2018). Biosurfactant production by *Trametes versicolor* grown on two-phase olive mill waste in solid-state fermentation. Environ. Technol. *39,* 3066–3076.

Lu B. (2016). Evaluation of physico-chemical properties of biorefinery-derived amphiphilic molecules and their effects on multi-scale biological models. PhD Thesis. Université de Technologie de Compiègne.

Lugones L.G., J.S. Bosscher, K. Scholtmeyer, O.M.H. de Vries and J.G.H. Wessels (1996). An abundant hydrophobin (ABH1) forms hydrophobic rodlet layers in *Agaricus bisporus* fruiting bodies. Microbiol. *142*, 1321–1329.

Lugones L.G., H.A.B. Wös and J.G.H. Wessels (1998). A hydrophobin (ABH3) specifically secreted by vegetatively growing hyphae of *Agaricus bisporus* (common white button mushroom). Microbiol. *144*, 2345–2353.

Lukondeh T., N.J. Ashbolt and P.L. Rogers (2003). Evaluation of *Kluyveromyces marxianus* FII 510700 grown on a lactose-based medium as a source of a natural bioemulsifier. J. Ind. Microbiol. Biotechnol. *30*, 715–720.

Lumsdon S.O., J. Green and B. Stieglitz (2005). Adsorption of hydrophobin proteins at hydrophobic and hydrophilic interfaces. Colloids Surf. B: Biointerfaces *44*, 172–178.

de Luna J.M., R.D. Rufino, A.M.A.T. Jara, P.P.F. Brasileiro and L.A. Sarubbo (2015). Environmental applications of the biosurfactant produced by *Candida sphaerica* cultivated in low-cost substrates. Colloids Surf. A: Physicochem. Eng. Asp. *480*, 413–418.

de Luna J.M., L.A. Sarubbo and G.M. de Campos-Takaki (2009). A new biosurfactant produced by *Candida glabrata* UCP 1002: characteristics of stability and application in oil recovery. Braz. Arch. Biol. Technol. *52*, 785–793.

Luna-Velasco M.A., F. Esparza-García, R.O. Cañízares-Villanueva and R. Rodríguez-Vázquez (2007). Production and properties of a bioemulsifier synthesized by phenanthrene-degrading *Penicillium sp*. Process Biochem. *42*, 310–314.

Ma B., X. Lv, Y. He, and J. Xu (2016). Assessing adsorption of polycyclic aromatic hydrocarbons on *Rhizopus oryzae* cell wall components with water–methanol cosolvent model. Ecotox. Environ. Safe. *125*, 55–60.

Ma K., R. Liontas, C.A. Conn, G.J. Hirasaki, and S.L. Biswal (2012). Visualization of improved sweep with foam in heterogeneous porous media using microfluidics. Soft Matter *8*, 10669–10675.

Ma, X.-J., H. Li, D.-X. Wang and X. Song (2014). Sophorolipid production from delignined corncob residue by *Wickerhamiella domercqiae* var. sophorolipid CGMCC 1576 and *Cryptococcus curvatus* ATCC 96219. Appl. Microbiol. Biotechnol. *98*, 475–483.

Machín-Ramírez, C., D. Morales, F. Martínez-Morales, A.I. Okoh and M.R. Trejo-Hernández (2010). Benzo[*a*]pyrene removal by axenic- and co-cultures of some bacterial and fungal strains. Int. Biodeterior. Biodegradation *64*, 538–544.

Magnuson J.K., and L.L. Lasure (2004). Organic acid production by filamentous fungi. pp. 307–340 *In*: J.S. Tkacz and L. Lange, [eds.]. Advances in Fungal Biotechnology for Industry, Agriculture, and Medicine. Springer US, Boston, MA

Mankel, A., K. Krause and E. Kothe (2002). Identification of a hydrophobin gene that is developmentally regulated in the ectomycorrhizal fungus *Tricholoma terreum*. Appl. Environ. Microbiol. *68*, 1408–1413.

Manoch L., and T. Dethoup (2011). A potential use of *Talaromyces* species as biological agents against plant pathogenic fungi. Thai J. Agr. Sci. *44*, 81–91.

Marco-Urrea E., I. García-Romera, and E. Aranda (2015). Potential of non-ligninolytic fungi in bioremediation of chlorinated and polycyclic aromatic hydrocarbons. New Biotechnol. *32*, 620–628.

Mayer P., W.H.J. Vaes, and J.L.M. Hermens (2000). Absorption of Hydrophobic Compounds into the Poly(dimethylsiloxane) Coating of Solid-Phase Microextraction Fibers: High Partition Coefficients and Fluorescence Microscopy Images. Anal. Chem. *72*, 459–464.

Meharg A.A. and J.W.G. Cairney (2000). Ectomycorrhizas - extending the capabilities of rhizosphere remediation? Soil Biol. and Biochem. *32*, 1475–1484.

Méndez-Castillo L., E. Prieto-Correa and C. Jiménez-Junca (2017). Identification of fungi isolated from banana rachis and characterization of their surface activity. Lett. in Appl. Microbiol. *64*, 246–251.

Meneses D.P., E.J. Gudiña, F. Fernandes, L.R.B. Gonçalves, L.R. Rodrigues and S. Rodrigues (2017). The yeast-like fungus *Aureobasidium thailandense* LB01 produces a new biosurfactant using olive oil mill wastewater as an inducer. Microbiol. Res. *204*, 40–47.

Mersch-Sundermann V., S. Mochayedi, and S. Kevekordes (1992). Genotoxicity of polycyclic aromatic hydrocarbons in *Escherichia coli* PQ37. Mutat. Res. Genet.Tox. *278*, 1–9.

Miller G.L. (1959). Use of dinitrosalicylic acid reagent for determination of reducing sugar. Anal. Chem. *31*, 426–428.

Millet L.J., J. Aufrecht, J. Labbé, J. Uehling, R. Vilgalys, M.L. Estes, C. Miquel Guennoc, A. Deveau, S. Olsson, G. Bonito, et al. (2019). Increasing access to microfluidics for studying fungi and other branched biological structures. Fungal Biol. Biotechnol. *6*, 8.

Morita T., M. Konishi, T. Fukuoka, T. Imura, H.K. Kitamoto and D. Kitamoto (2007). Characterization of the genus *Pseudozyma* by the formation of glycolipid biosurfactants, mannosylerythritol lipids. FEMS Yeast Res. 7, 286–292.

Morita T., M. Konishi, T. Fukuoka, T. Imura and D. Kitamoto (2008). Identification of *Ustilago cynodontis* as a new producer of glycolipid biosurfactants, mannosylerythritol lipids, based on ribosomal DNA sequences. J. Oleo Sci. *57*, 549–556.

Morita T., Y. Ishibashi, T. Fukuoka, T. Imura, H. Sakai, M. Abe and D. Kitamoto (2009). Production of glycolipid biosurfactants, mannosylerythritol lipids, by a smut fungus, *Ustilago scitaminea* NBRC 32730. Biosci. Biotechnol. Biochem. *73*, 788–792.

Morita T., T. Fukuoka, T. Imura and D. Kitamoto (2013). Accumulation of cellobiose lipids under nitrogen-limiting conditions by two ustilaginomycetous yeasts, *Pseudozyma aphidis* and *Pseudozyma hubeiensis*. FEMS Yeast Res. *13*, 44–49.

Mousavi, F., K. Beheshti-Maal and A. Massah (2015). Production of sophorolipid from an identified current yeast, *Lachancea thermotolerans* BBMCZ7FA20, isolated from honey bee. Curr. Microbiol. *71*, 303–310.

Murphy S., S. Martin, and R.G. Parton (2009). Lipid droplet-organelle interactions; sharing the fats. BBA - Mol. Cell Biol. L. *1791*, 441–447.

Murugesan K., A. Selvam, and J.W.C. Wong (2014). Flocculation and dewaterability of chemically enhanced primary treatment sludge by bioaugmentation with filamentous fungi. Biores. Technol. *168*, 198–203.

Nakkharat P., and D. Haltrich (2006). Purification and characterisation of an intracellular enzyme with β-glucosidase and β-galactosidase activity from the thermophilic fungus *Talaromyces thermophilus* CBS 236.58. J. Biotechnol. *123*, 304–313.

Nikiforova S.V., N.N. Pozdnyakova, and O.V. Turkovskaya (2009). Emulsifying agent production during PAHs degradation by the white rot fungus *Pleurotus ostreatus* D1. Curr. Microbiol. *58*, 554–558.

Nilsson M.A., R. Kulkarni, L. Gerberich, R. Hammond, R. Singh, E. Baumhoff, and J.P. Rothstein (2013). Effect of fluid rheology on enhanced oil recovery in a microfluidic sandstone device. J. Non-Newton. Fluid Mech. *202*, 112–119.

Niu, Y., L. Fan, D. Gu, J. Wu and Q. Chen (2017). Characterization, enhancement and modelling of mannosylerythritol lipid production by fungal endophyte *Ceriporia lacerate* CHZJU. Food Chem. *228*, 610–617.

Nyanhongo, G.S., S.R. Couto and G.M. Guebitz (2006). Coupling of 2,4,6-trinitrotoluene (TNT) metabolites onto humic monomers by a new laccase from *Trametes modesta*. Chemosphere *64*, 359–370.

Nylund L., P. Heikkilä, M. Hämeilä, L. Pyy, K. Linnainmaa, and M. Sorsa (1992). Genotoxic effects and chemical compositions of four creosotes. Mutat. Res. - Fund. Mol. M. *265*, 223–236.

Oje, O.A., V.E. Okpashi, J.C. Uzor, U.O. Uma, A.O. Irogbolu and I.N.E. Onwurah (2016). Effect of acid and alkaline pretreatment on the production of biosurfactant from rice husk using *Mucor indicus*. Res. J. Environ. Toxicol. *10*, 60–67.

Olagoke O.A. (2014). Amylase activities of some thermophilic fungi isolated from municipal solid wastes and palm-kernel stack. Am. J. Microbiol. Biotechnol. *1*, 64–70.

Ortega-Calvo J.J., M.C. Tejeda-Agredano, C. Jimenez-Sanchez, E. Congiu, R. Sungthong, J.L. Niqui-Arroyo, and M. Cantos (2013). Is it possible to increase bioavailability but not environmental risk of PAHs in bioremediation? J. Hazard. Mater. *261*, 733–745.

Osono, T., Y. Ono and H. Takeda (2003). Fungal ingrowth on forest floor and decomposing needle litter of *Chamaecyparis obtusa* in relation to resource availability and moisture condition. Soil Biol. Biochem. *35*, 1423–1431.

Oudot J., J. Dupont, S. Haloui, and M.F. Roquebert (1993). Biodegradation potential of hydrocarbon-assimilating tropical fungi. Soil Biol. Biochem. *25*, 1167–1173.

Paliwal S., P.A. Iglesias, K. Campbell, Z. Hilioti, A. Groisman, and A. Levchenko (2007). MAPK-mediated bimodal gene expression and adaptive gradient sensing in yeast. Nature *446*, 46–51.

Paria S. (2008). Surfactant-enhanced remediation of organic contaminated soil and water. Adv. Colloid Interface Sci. *138*, 24–58.

Park C., B. Bennion, I.E.J.A. François, K.K.A. Ferket, B.P.A. Cammue, K. Thevissen, and S.B. Levery (2005). Neutral glycolipids of the filamentous fungus *Neurospora crassa* : altered expression in plant defensin-resistant mutants. J. Lipid Res. *46*, 759–768.

Patist A., S.S. Bhagwat, K.W. Penfield, P. Aikens, and D.O. Shah (2000). On the measurement of critical micelle concentrations of pure and technical-grade nonionic surfactants. J. Surfact. Deterg. *3*, 53–58.

Pele, M.A., D.R. Ribeaux, E.R. Vieira, A.F. Souza, M.A.C. Luna, D.M. Rodríguez et al (2019). Conversion of renewable substrates for biosurfactant production by *Rhizopus arrhizus* UCP 1607 and enhancing the removal of diesel oil from marine soil. Electron. J. Biotechnol. *38*, 40–48.

Peng, X., E. Masai, H. Kitayama, K. Harada, Y. Katayama and M. Fukuda (2002). Characterization of the 5-carboxyvanillate decarboxylase gene and its role in lignin-related biphenyl catabolism in *Sphingomonas paucimobilis* SYK-6. Appl. Environ. Microbiol. *68*, 4407–4415.

Peter S., M. Kinne, X. Wang, R. Ullrich, G. Kayser, J.T. Groves, and M. Hofrichter (2012). Selective hydroxylation of alkanes by an extracellular fungal peroxygenase. FEBS J. *278*, 3667–3675.

Piruska A., I. Nikcevic, S.H. Lee, C. Ahn, W.R. Heineman, P.A. Limbach, and C.J. Seliskar (2005). The autofluorescence of plastic materials and chips measured under laser irradiation. Lab. Chip *5*, 1348.

Plant A.L., D.M. Benson, and L.C. Smith (1985). Cellular uptake and intracellular localization of benzo(a)pyrene by digital fluorescence imaging microscopy. J. Cell Biol. *100*, 1295–1308.

Porter M.L., J. Jiménez-Martínez, R. Martinez, Q. McCulloch, J.W. Carey, and H.S. Viswanathan (2015). Geo-material microfluidics at reservoir conditions for subsurface energy resource applications. Lab. Chip *15*, 4044–4053.

Potapova T.V., L.Yu. Boitsova, S.A. Golyshev, and A.Ya. Dunina-Barkovskaya (2016). Tip growth of *Neurospora crassa* upon resource shortage: Disturbances of the coordination of elongation, branching, and septation. Cell Tissue Biol. *10*, 486–499.

Powell W.A. (1995). Vegetative incompatibility and mycelial death of *Cryphonectria parasitica* detected with a pH indicator. Mycologia *87*, 738–741.

Price, N.P.J., P. Manitchotpisit, K.E. Vermillion, M.J. Bowman and T.D Leathers (2013). Structural characterization of novel extracellular liamocins (mannitol oils) produced by *Aureobasidium pullulans* strain NRRL 50380. Carbohydr. Res. *370*, 24–32.

Prosser J.I., and A.J. Tough (1991). Growth mechanisms and growth kinetics of filamentous microorganisms. Crit. Rev. Biotechnol. *10*, 253–274.

Puchkov, E.O., U. Zähringer, B. Lindner, T.V. Kulakovskaya, U. Seydel and A. Wiese (2002). The mycocidal, membrane-active complex of *Cryptococcus humicola* is a new type of cellobiose lipid with detergent features. Biochim. Biophys. Acta - Biomembranes *1558*, 161–170.

Rafin C., E. Veignie, F. Cazier, P. Woisel, and G. Surpateanu (2006). New potential of a deuteromycete fungus *Fusarium solani* in benzo[*a*]pyrene degradation: an eco-physiological hypothesis? New frontiers in environmental research. Nova Science, New York, 165-179

Rafin C., B. de Foucault, and E. Veignie (2013). Exploring micromycetes biodiversity for screening benzo[*a*]pyrene degrading potential. Environ. Sci. Pollut. Res. *20*, 3280–3289.

Ren C.-G., C.-C. Kong, B. Bian, W. Liu, Y. Li, Y.-M. Luo et al (2017). Enhanced phytoremediation of soils contaminated with PAHs by arbuscular mycorrhiza and rhizobium. Int. J. Phytoremediat. *19*, 789–797.

Ren C.-G., C.-C. Kong, S.-X. Wang and Z.-H. Xie (2019). Enhanced phytoremediation of uranium-contaminated soils by arbuscular mycorrhiza and rhizobium. Chemosphere *217*, 773–779.

Ren X., G. Zeng, L. Tang, J. Wang, J. Wan, Y. Liu et al. (2018). Sorption, transport and biodegradation – An insight into bioavailability of persistent organic pollutants in soil. Sci. Total Environ. *610–611*, 1154–1163.

Reyes-César A., Á.E. Absalón, F.J. Fernández, J.M. González, and D.V. Cortés-Espinosa (2014). Biodegradation of a mixture of PAHs by non-ligninolytic fungal strains isolated from crude oil-contaminated soil. World J. Microb. Biot. *30*, 999–1009.

Rezaee M., Y. Assadi, M.-R. Milani Hosseini, E. Aghaee, F. Ahmadi, and S. Berijani (2006). Determination of organic compounds in water using dispersive liquid–liquid microextraction. J. Chromatogr. A *1116*, 1–9.

Rillig, M.C. (2004). Arbuscular mycorrhizae, glomalin, and soil aggregation. Can. J. Soil. Sci. 84, 355–363.

Rillig, M.C. (2005). A connection between fungal hydrophobins and soil water repellency? Pedobiologia *49*, 395–399.

Rillig, M.C., B.A. Caldwell, H.A.B. Wösten and P. Sollins (2007). Role of proteins in soil carbon and nitrogen storage: controls on persistence. Biogeochemistry *85*, 25–44.

Riquelme M., and S. Bartnicki-Garcia (2004). Key differences between lateral and apical branching in hyphae of *Neurospora crassa*. Fungal Genet. Biol. *41*, 842–851.

Ritter, L., K.R. Solomon, J. Forget, M. Stemeroff and C. O'Leary (1995). Persistent organic pollutants: an assessment aeport on DDT, aldrin, dieldrin, endrin, clordane, heptachlor-, hexachlorobenzene, mirex, toxaphene, polychlorinated biphenyls, dioxins, and furans. The International Programme on Chemical Safety *95.39*. World Health Organization

Ritz, K. and I.M. Young (2004). Interactions between soil structure and fungi. Mycologist *18*, 52–59.

Rivera-Figueroa A.M., K.A. Ramazan, and B.J. Finlayson-Pitts (2004). Fluorescence, absorption, and excitation spectra of polycyclic aromatic hydrocarbons as a tool for quantitative analysis. J. Chem. Educ. *81*, 242.

Robinson T., Y. Schaerli, R. Wootton, F. Hollfelder, C. Dunsby, G. Baldwin, M. Neil, P. French, and A. deMello (2009). Removal of background signals from fluorescence thermometry measurements in PDMS microchannels using fluorescence lifetime imaging. Lab. Chip *9*, 3437.

Rodrigues A., R. Nogueira, L.F. Melo, and A.G. Brito (2013). Effect of low concentrations of synthetic surfactants on polycyclic aromatic hydrocarbons (PAH) biodegradation. Int. Biodeter. Biodegr. *83*, 48–55.

Rodrigues A.G., P.-A. Mårdh, C. Pina-Vaz, J. Martinez-de-Oliveira and A.F. Fonseca (1999). Germ tube formation changes surface hydrophobicity of *Candida* cells. Infect. Dis. Obstet. Gynecol. *7*, 222-226

Romero M.C., E. Hammer, R. Hanschke, A.M. Arambarri, and F. Schauer (2005). Biotransformation of biphenyl by the filamentous fungus *Talaromyces helicus*. World J. Microb. Biot. *21*, 101–106.

Romero M.C., E. H. Reinoso, M.I. Urrutia, and A. Moreno Kiernan (2006). Biosorption of heavy metals by *Talaromyces helicus*: a trained fungus for copper and biphenyl detoxification. Electron. J. Biotechnol. *9*, 0–0.

Romero M.C., M.I. Urrutia, E.H. Reinoso, and A. Moreno Kiernan (2009). Wild soil fungi able to degrade the herbicide isoproturon. Rev. Mex. Micol. *29*, 1–7.

Romero M.C., M.I. Urrutia, H.E. Reinoso, and M.M. Kiernan (2010). Benzo[*a*]pyrene degradation by soil filamentous fungi. J. Yeast Fungal Res. *1*, 025–029.

Roper M., and A. Seminara (2019). Mycofluidics: The fluid mechanics of fungal adaptation. Annu. Rev. Fluid Mech. *51*, 511–538.

Rosenberg, M. (2006). Microbial adhesion to hydrocarbons: twenty-five years of doing MATH. FEMS Microbiol. Lett. *262*, 129–134.

Rusconi R., M. Garren, and R. Stocker (2014). Microfluidics expanding the frontiers of microbial ecology. Annu. Rev. Biophys. *43*, 65–91.

Sánchez-Orellana G., S. Casas-Flores, and B. Gutiérrez–Medina (2019). Automated, continuous video microscopy tracking of hyphal growth. Fungal Genet. Biol. *123*, 25–32.

Sánchez-Vázquez V., K. Shirai, I. González, and M. Gutiérrez-Rojas (2018). Polycyclic aromatic hydrocarbon-emulsifier protein produced by *Aspergillus brasiliensis (niger)* in an airlift bioreactor following an electrochemical pretreatment. Bioresour. Technol. *256*, 408–413.

Saparrat M.C.N., M.J. Martinez, H.A. Tournier, M.N. Cabello, and A.M. Arambarri (2000). Production of ligninolytic enzymes by *Fusarium solani* strains isolated from different substrata. World J. Microb. Biot. *16*, 799–803.

Scervino J.M., M.P. Mesa, I. Della Mónica, M. Recchi, N. Sarmiento Moreno, and A. Godeas (2010). Soil fungal isolates produce different organic acid patterns involved in phosphate salts solubilization. Biol. Fertil. Soil *46*, 755–763.

Schamfuß S., T.R. Neu, J.R. van der Meer, R. Tecon, H. Harms, and L.Y. Wick (2013). Impact of mycelia on the accessibility of fluorene to PAH-degrading bacteria. Environ. Sci. Technol. *47*, 6908–6915.

Schmieder S.S., C.E. Stanley, A. Rzepiela, D. van Swaay, J. Sabotič, S.F. Nørrelykke, A.J. deMello, M. Aebi, and M. Künzler (2019). Bidirectional propagation of signals and nutrients in fungal networks via specialized hyphae. Curr. Biol. *29*, 217-228.e4.

Schneider F., J. Draheim, R. Kamberger, and U. Wallrabe (2009). Process and material properties of polydimethylsiloxane (PDMS) for optical MEMS. Sens. Actuators Phys. *151*, 95–99.

Semple, K.T., K.J. Doick, K.C. Jones, P. Burauel, A. Craven and H. Harms (2004). Defining bioavailability and bioaccessibility of contaminated soil and sediment is complicated. Environ. Sci. Technol. *38*, 228–231.

Sen S., S.N. Borah, A. Bora, and S. Deka (2017). Production, characterization, and antifungal activity of a biosurfactant produced by *Rhodotorula babjevae* YS3. Microb. Cell Fact. *16*, 95.

Sena H.H., M. A. Sanches, D.F. Silva Rocha, W.O. P. Filho Segundo, É.S. de Souza and J.V. B. de Souza (2018). Production of biosurfactants by soil fungi isolated from the Amazon forest. Int. J. Microbiol. *2018*, 5684261.

Shen X.-H., T. Li, Y. Xu, N.-Y. Zhou, and S.-J. Liu (2015). Transport, degradation and assimilation of aromatic compounds and their regulation in *Corynebacterium glutamicum*. pp. 83-110 *In*: A. Burkovski [ed.] Corynebacterium Glutamicum. Caister Academic Press.

Silva-Castro G.A., B. Rodelas, C. Perucha, J. Laguna, J. González-López, and C. Calvo (2013). Bioremediation of diesel-polluted soil using biostimulation as post-treatment after oxidation with Fenton-like reagents: Assays in a pilot plant. Sci. Total Environ. *445–446*, 347–355.

Singh H. (2006a). Fungal Metabolism of Petroleum Hydrocarbons. *In*: Singh, H. Mycoremediation: Fungal Bioremediation. John Wiley & Sons, Hoboken NJ, USA. 115–148

Singh H. (2006b). Fungal degradation of polychlorinated biphenyls and dioxins. *In*: Singh, H. Mycoremediation: Fungal Bioremediation. John Wiley & Sons, Hoboken NJ, USA. 149-180

Siqueira, V. and N. Lima (2012). Surface hydrophobicity of culture and water biofilm of *Penicillium spp*. Curr. Microbiol. *64*, 93–99.

Smith, K.E.C., M. Thullner, L.Y. Wick and H. Harms (2009). Sorption to humic acids enhances polycyclic aromatic hydrocarbon biodegradation. Environ. Sci. Technol. *43*, 7205–7211.

Smith, K.E.C., M. Thullner, L.Y. Wick and H. Harms (2011). Dissolved organic carbon enhances the mass transfer of hydrophobic organic compounds from nonaqueous phase liquids (NAPLs) into the aqueous phase. Environ. Sci. Technol. *45*, 8741–8747.

Smits, T.H.M., L.Y. Wick, H. Harms and C. Keel (2003). Characterization of the surface hydrophobicity of filamentous fungi. Environ. Microbiol. *5*, 85–91.

Spoeckner S., V. Wray, M. Nimtz, and S. Lang (1999). Glycolipids of the smut fungus *Ustilago maydis* from cultivation on renewable resources. Appl. Microbiol. Biotechnol. *51*, 33–39.

Stanley C.E., M. Stöckli, D. van Swaay, J. Sabotič, P.T. Kallio, M. Künzler, A.J. deMello, and M. Aebi (2014). Probing bacterial–fungal interactions at the single cell level. Integr. Biol. *6*, 935–945.

Stanley C.E., G. Grossmann, X. Casadevall i Solvas, and A.J. deMello (2016). Soil-on-a-Chip: microfluidic platforms for environmental organismal studies. Lab Chip *16*, 228–241.

Steele G.C., and A.P.J. Trinci (1975). Morphology and growth kinetics of hyphae of differentiated and undifferentiated mycelia of *Neurospora crassa*. J. Gen. Microbiol. *91*, 362–368.

Stein W.D., and T. Litman (2014). Channels, Carriers, and Pumps: An Introduction to Membrane Transport (Elsevier).

Stolk A.C., and R.A. Samson (1972). The genus *Talaromyces*: Studies on *Talaromyces* and related genera II. Stud. Mycol. *2*.

Suelmann R., N. Sievers, and R. Fischer (1997). Nuclear traffic in fungal hyphae: in vivo study of nuclear migration and positioning in *Aspergillus nidulans*. Mol. Microbiol. *25*, 757–769.

Szilvay, G.R., A. Paananen, K. Laurikainen, E. Vuorimaa, H. Lemmetyinen, J. Peltonen et al. (2007). Self-assembled hydrophobin protein films at the air−water interface: Structural analysis and molecular angineering. Biochem. *46*, 2345–2354.

Talbot, N.J., M.J. Kershaw, G.E. Wakley, O.M.H. de Vries, J.G.H. Wessels, and J.E. Hamer (1996). MPG1 encodes a fungal hydrophobin involved in surface interactions during infection-related development of *Magnaporthe grisea*. Plant Cell *8*, 985–999.

Talbot, N.J. (1997). Fungal biology: Growing into the air. Curr. Biol. 7, R78–R81.

Tchuenbou-Magaia, F.L., I.T. Norton and P.W. Cox (2009). Hydrophobins stabilised air-filled emulsions for the food industry. Food Hydrocoll. *23*, 1877–1885.

Texeira Souza, K.S., E.J. Gudiña, Z. Azevedo, V. de Freitas, R.F. Schwan, L.R. Rodrigues et al. (2017). New glycolipid biosurfactants produced by the yeast strain *Wickerhamomyces anomalus* CCMA 0358. Colloids Surf. B: Biointerfaces *154*, 373–382.

Thanomsub B., T. Watcharachaipong, K. Chotelersak, P. Arunrattiyakorn, T. Nitoda, and H. Kanzaki (2004). Monoacylglycerols: Glycolipid biosurfactants produced by a thermotolerant yeast, *Candida ishiwadae*. J. Appl. Microbiol. *96*, 588–592.

Thion, C., A. Cébron, T. Beguiristain and C. Leyval (2012). PAH biotransformation and sorption by *Fusarium solani* and *Arthrobacter oxydans* isolated from a polluted soil in axenic cultures and mixed co-cultures. Int. Biodeterior. Biodegradation *68*, 28–35.

Thomson D.D., S. Wehmeier, F.J. Byfield, P.A. Janmey, D. Caballero-Lima, A. Crossley, and A.C. Brand (2015). Contact-induced apical asymmetry drives the thigmotropic responses of *Candida albicans* hyphae. Cell. Microbiol. *17*, 342–354.

Toepke M.W., and D.J. Beebe (2006). PDMS absorption of small molecules and consequences in microfluidic applications. Lab. Chip *6*, 1484.

Tuohy M.G., and M.P. Coughlan (1992). Production of thermostable xylan-degrading enzymes by *Talaromyces emersonii*. Biores. Technol. *39*, 131–137.

Uehling J.K., M.R. Entler, H.R. Meredith, L.J. Millet, C.M. Timm, J.A. Aufrecht, G.M. Bonito, N.L. Engle, J.L. Labbé, M.J. Doktycz, et al. (2019). Microfluidics and metabolomics reveal symbiotic bacterial–fungal interactions between *Mortierella elongata* and *Burkholderia* include metabolite exchange. Front. Microbiol. *10*.

Valderrama B., M. Ayala, and R. Vazquez-Duhalt (2002). Suicide Inactivation of Peroxidases and the Challenge of Engineering More Robust Enzymes. Chemistry & Biology *9*, 555–565.

Veignie E., C. Rafin, P. Woisel, A. Lounes-Hadj Sahraoui, and F. Cazier (2002). Metabolization of the polycyclic aromatic hydrocarbon benzo(a)pyrene by a non-white rot fungus (*Fusarium solani*) in a batch reactor. Polycycl. Aromat. Comp. *22*, 87–97.

Veignie E., C. Rafin, P. Woisel, and F. Cazier (2004). Preliminary evidence of the role of hydrogen peroxide in the degradation of benzo[*a*]pyrene by a non-white rot fungus *Fusarium solani*. Environ. Pollut. *129*, 1–4.

Veignie E., E. Vinogradov, I. Sadovskaya, C. Coulon, and C. Rafin (2012). Preliminary characterizations of a carbohydrate from the concentrated culture filtrate from *Fusarium solani* and its role in benzo[*a*]pyrene Solubilization. Adv. Microbiol. *2*, 375–381.

Velioglu, Z. and R.O. Urek (2016). Physicochemical and structural characterization of biosurfactant produced by *Pleurotus djamor* in solid-state fermentation. Biotechnol. Bioprocess Eng. *21*, 430–438.

Verdin A., A. Lounès-Hadj Sahraoui, and R. Durand (2004). Degradation of benzo[*a*]pyrene by mitosporic fungi and extracellular oxidative enzymes. Int. Biodeter. Biodegr. *53*, 65–70.

Verdin A., A. Lounès-Hadj Sahraoui, R. Newsam, G. Robinson and R. Durand. (2005). Polycyclic aromatic hydrocarbons storage by *Fusarium solani* in intracellular lipid vesicles. Environ. Pollut. *133*, 283–291.

Verdin A., A. Lounès-Hadj Sahraoui, J. Fontaine, A. Grandmougin-Ferjani and R. Durand (2006). Effects of anthracene on development of an arbuscular mycorrhizal fungus and contribution of the symbiotic association to pollutant dissipation. Mycorrhiza *16,* 397–405.

Vicuña, R., B. González, D. Seelenfreund, C. Rüttimann and L. Salas (1993). Ability of natural bacterial isolates to metabolize high and low molecular weight lignin-derived molecules. J. Biotechnol. *30*, 9–13.

Villholth, K.G., N.J. Jarvis, O.H. Jacobsen and H. de Jonge (2000). Field investigations and modeling of particle-facilitated pesticide transport in macroporous soil. J. Environ. Qual. *29*, 1298-1309

de Vries, O.M.H., M.P. Fekkes, H.A.B. Wösten and J.G.H. Wessels (1993). Insoluble hydrophobin complexes in the walls of *Schizophyllum commune* and other filamentous fungi. Arch. Microbiol. *159*, 330–335.

Watkinson S., D. Bebber, P. Darrah, M. Fricker, M. Tlalka, and L. Boddy (2006). The role of wood decay fungi in the carbon and nitrogen dynamics of the forest floor. pp. 151–181 *In*: G.M. Gadd [ed.]. Fungi in Biogeochemical Cycles. Cambridge University Press, Cambridge, UK

Welte M.A. (2009). Fat on the move: intracellular motion of lipid droplets. Biochem. Soc. T. *37*, 991–996.

Whitesides G.M., E. Ostuni, S. Takayama, X. Jiang, and D.E. Ingber (2001). Soft lithography in biology and biochemistry. Annu. Rev. Biomed. Eng. *3*, 335–373.

WHO. Some non-heterocyclic polycyclic aromatic hydrocarbons and some related exposures (2010) Lyon, France.

Wösten, H.A.B. (2001). Hydrophobins: multipurpose proteins. Ann. Rev. Microbiol. *55*, 625–646.

Wösten, H.A.B., M.-A. van Wetter, L.G. Lugones, H.C. van der Mei, H.J. Busscher and J.G.H. Wessels (1999). How a fungus escapes the water to grow into the air. Curr. Biol. *9*, 85–88.

Wu H., L. Wu, J. Wang, Q. Zhu, S. Lin, J. Xu, C. Zheng, J. Chen, X. Qin, C. Fang, et al. (2016). Mixed phenolic acids mediated proliferation of pathogens *Talaromyces helicus* and *Kosakonia sacchari* in continuously monocultured *Radix pseudostellariae* rhizosphere soil. Front. Microbiol. *7*, 335.

Wu M., F. Xiao, R.M. Johnson-Paben, S.T. Retterer, X. Yin, and K.B. Neeves (2011). Single- and two-phase flow in microfluidic porous media analogs based on Voronoi tessellation. Lab. Chip *12*, 253–261.

Wu, N., S. Zhang, H. Huang and P. Christie. (2008). Enhanced dissipation of phenanthrene in spiked soil by arbuscular mycorrhizal alfalfa combined with a non-ionic surfactant amendment. Sci. Total Environ. *394*, 230–236.

Wu, Y.-R., T.-T. He, J.-S. Lun, K. Maskaoui, T.-W. Huang and Z. Hu. (2009). Removal of benzo[*a*]pyrene by a fungus *Aspergillus sp*. BAP14. World J. Microbiol. Biotechnol. *25*, 1395–1401.

Yang, Z., Y. Shi, Y. Zhang, Q. Cheng, X. Li, C. Zhao and D. Zhang (2018). Different pathways for 4-n-nonylphenol biodegradation by two *Aspergillus* strains derived from estuary sediment: Evidence from metabolites determination and key-gene identification. J. Hazard. Mater. *359*, 203–212.

Yeo L.Y., H.-C. Chang, P.P. Chan, and J.R. Friend (2011). Microfluidic devices for bioapplications. Small *7*, 12–48.

Yilmaz N., C.M. Visagie, J. Houbraken, J.C. Frisvad, and R.A. Samson (2014). Polyphasic taxonomy of the genus *Talaromyces*. Stud. Mycol. 175–341.

Yoshida E., H. Fujimoto, M. Baba, and M. Yamazaki (1995). Four new chlorinated azaphilones, helicusins A-D, closely related to 7-epi-sclerotiorin, from an ascomycetous fungus, *Talaromyces helicus*. Chem. Pharm. Bull. *43*, 1307–1310.

Yu L., L. Duan, R. Naidu, and K.T. Semple (2018). Abiotic factors controlling bioavailability and bioaccessibility of polycyclic aromatic hydrocarbons in soil: Putting together a bigger picture. Sci. Total Environ. *613–614*, 1140–1153.

Zadeh P.H., H. Moghimi, and J. Hamedi (2018). Biosurfactant production by *Mucor circinelloides*: Environmental applications and surface-active properties. Eng. Life Sci. *18*, 317–325.

Zhang C., and D. van Noort (2011). Cells in Microfluidics. pp. 295–321 *In:* B. Lin [ed.]. Microfluidics. Springer Berlin Heidelberg, Germany

Zhang, J.-H., Q.-H. Xue, H. Gao, X. Ma and P. Wang (2016). Degradation of crude oil by fungal enzyme preparations from *Aspergillus spp*. for potential use in enhanced oil recovery. J. Chem. Technol. Biotechnol. *91*, 865–875.

Zhang S., Y.X. Xia, B. Kim, and N.O. Keyhani (2011). Two hydrophobins are involved in fungal spore coat rodlet layer assembly and each play distinct roles in surface interactions, development and pathogenesis in the entomopathogenic fungus, *Beauveria bassiana*. Mol. Microbiol. *80*, 811–826.

Zhang, X., S.M. Kirby, Y. Chen, S.L. Anna, L.M. Walker, F.R. Hung et al. (2018). Formation and elasticity of membranes of the class II hydrophobin cerato-ulmin at oil-water interfaces. Colloids Surf. B: Biointerfaces 164, 98–106.

Zhao J., Y. Chi, Y. Xu, D. Jia, and K. Yao (2016). Co-metabolic degradation of β-cypermethrin and 3-phenoxybenzoic acid by co-culture of *Bacillus licheniformis* B-1 and *Aspergillus oryzae* M-4. PLoS ONE *11*, e0166796.

Zhou, D., X. Zhang, Y. Du, S. Dong, Z. Xu and L. Yan (2014). Insights into the synergistic effect of fungi and bacteria for reactive red decolorization. J. Spectrosc (Hindawi) *2014*, 237346

Zhou W., J. Le, Y. Chen, Y. Cai, Z. Hong, and Y. Chai (2019). Recent advances in microfluidic devices for bacteria and fungus research. Trends Anal. Chem. *112*, 175–195.

Directive 2001/18/EC of the European Parliament and of the Council on the deliberate release into the environment of genetically modified organisms. Official Journal of the European Union L106, 17.04.2001, pp 1-39

(1998). Council Directive 98/83/EC of 3 November 1998 on the quality of water intended for human consumption.

(2001). Directive 2001/18/EC of the European Parliament and of the Council of 12 March 2001 on the deliberate release into the environment of genetically modified organisms.

Agrobiobase (2013). Retrieved August 9, 2019, from http://www.agrobiobase.com/fr/annuaire/bioproduits/detergence/Sophoclean

A Appendix : Fluid velocity in the parallel microchannels

The mean velocity $\bar{v}$ in a rectangular channel is defined by the flow rate q divided by the cross section S:

$$\bar{v} = q/S \tag{1}$$

The flow rate q is proportional to the pressure difference ΔP between the entrance and the exit of the channel, as Poiseuille discovered for cylindrical pipes, and the prefactor is called hydraulic resistance: $\Delta P = R_h q$. The hydraulic resistance of a shallow rectangular microchannel can be expressed as a function of its length l, its width w, its depth $h < w$ and the viscosity μ of the fluid [1]:

$$R_h = \frac{12\mu l}{h^3 w}\left[1 - \Sigma_{n,odd}\frac{192}{(n\pi)^5}\frac{h}{w}\tanh\left(n\pi\frac{w}{2h}\right)\right]^{-1} \tag{2}$$

Let us denote by P_p and P_i the pressures in the perfusion and inoculation chambers respectively. If we assume that the leaks through microchannels represent only a small perturbation of the main flow in the perfusion chamber, we expect P_p to decrease with y in a linear manner:

$$P_p(y) = P_p(y=0) - \frac{y}{L}\Delta P_p \tag{3}$$

with $\Delta P_p = P_p(y=0) - P_p(y=L)$ the pressure difference between the inlet and the outlet of the perfusion chamber, computed using equation (2) with the dimensions $W \times H \times L$ of the perfusion chamber and the flow rate Q imposed by the pump. Since the two chambers are of comparable dimensions, if the leak through the parallel microchannels is negligible in comparison with the main flow in the perfusion chamber, then the pressure drop ΔP_i in the inoculation chamber is much smaller than the pressure drop ΔP_p in the perfusion chamber. We can thus consider that the pressure is constant in the inoculation chamber: $P_i \simeq$ cst.

All the microchannels have the same dimensions $w \times h \times l$ and thus the same hydraulic resistance $R_{h,channel}$. Each of them is located at a different position y and exposed to a pressure difference $P_p(y) - P_i = P_p(0) - P_i - \frac{y}{L}\Delta P_p$, from which we can compute the flow rate through the microchannel towards the inoculation chamber:

$$q(y) = \frac{P_p(y) - P_i}{R_{h,channel}} = \frac{P_p(0) - P_i}{R_{h,channel}} - \frac{\Delta P_p}{R_{h,channel}}\frac{y}{L} \tag{4}$$

q decreases linearly with y. Knowing that the inoculation chamber has no inlet or outlet apart from the microchannel, the amount of fluid flowing in and out of the microchannels has to be null. This implies that $q(y = L/2) = 0$ and allows to compute $P_i = P_p(0) - \Delta P_p/2$. The flow rate in the microchannel reaches its maximum when $y = 0$ and $y = L$, close to the inlet and outlet of the perfusion chamber:

$$q_{max} = \frac{\Delta P_p}{2R_{h,channel}} = Q\frac{R_{h,chamber}}{2R_{h,channel}} \tag{5}$$

Finally, the mean velocity in the microchannel, which is proportional to q, is equal to 0 at the middle of the chamber and maximal in $y = 0$ and $y = L$, as sketched in figure 1.

We can compute its maximal value:

$$\bar{v}_{max} = \frac{Q}{hw}\frac{R_{h,chamber}}{2R_{h,channel}} \tag{6}$$

In the following table we present the experimental parameters used to compute the numerical values of $\bar{v}_{max}$. We check that the flow rate q in the microchannels is indeed negligible compared with the perfusion rate Q and even with Q/N, $N = 50$ being the number of parallel channels. This is in agreement with the assumptions made at the beginning of the calculation (unperturbed perfusion flow, negligible pressure drop in the inoculation chamber).

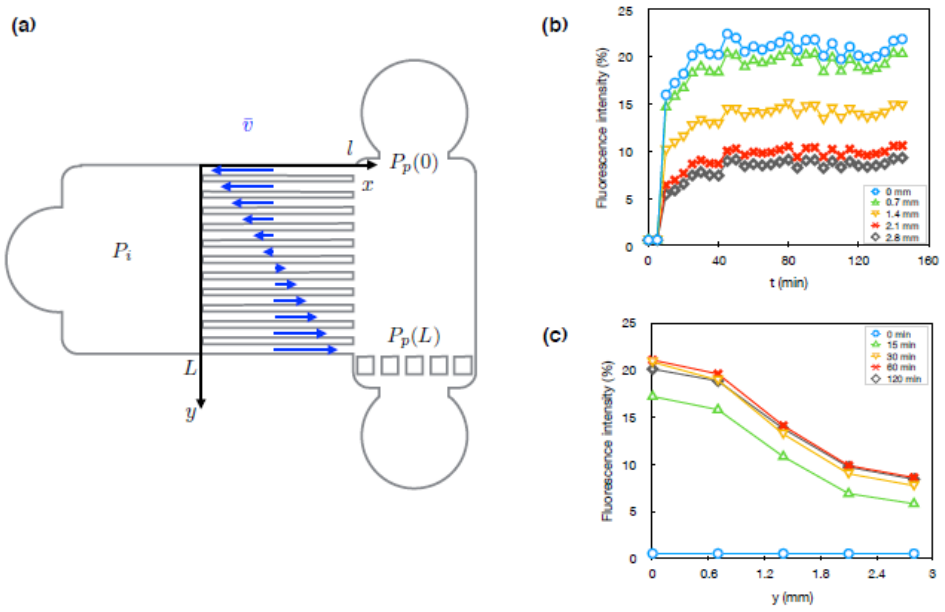

Figure 1: (a) Sketch of the device. The blue arrows indicate the direction and amplitude of the fluid velocity in the parallel microchannels. (b) Measurements of the fluorescence intensity over time in the inoculation chamber for different positions. (c) Axial dependency of fluorescence intensity in the inoculation chamber at different times.

	channel	chamber
w (μm)	10	3000
h (μm)	6	124
l (μm)	1000	3000
R_h (S.I.)	$8.88 \cdot 10^{15}$	$6.46 \cdot 10^{9}$
q (μL/min)	$6.55 \cdot 10^{-7}$	9
$\bar{v}$ (mm/min)	0.05	24.19

References

[1] Henrik Bruus. *Theoretical Microfluidics*. Oxford University Press, 2008.

Annexe B : Liste des publications et communications

Publications écrites :

Baranger C., A. Fayeulle, and A. Le Goff (2020). Microfluidic monitoring of the growth of individual hyphae in confined environments. R. Soc. Open Sci. *7*, 191535.

Baranger C., I. Pezron, A. Le Goff, A. Fayeulle (2020). Fungal influence on hydrophobic organic pollutants dynamics within the soil matrices. *In*: V. Kumar, [ed.]. Rhizomicrobiome Dynamics in Bioremediation. CRC Press (in press)

Communications orales à des conférences internationales :

Baranger, C., Creusot, L., Sun, X., Pezron, I., Le Goff, A., and Fayeulle, A. (2018). Microfluidic Approaches for Improved Bioremediation: Monitoring Pollutant Uptake in a Soil Fungus. NewTech'18 Proceedings, Madrid, Spain

Baranger, C. "Myco-fluidics" for soil remediation. Developing a microfluidic tool to monitor the solubilization and uptake of a persistant soil pollutant in filamentous fungi. 46th World Congress on Microbiology, September 18th, 2017, Dublin, Ireland

Communications orales à des conférences nationales :

Baranger C., Creusot L., Pezron I., Le Goff A., Fayeulle A. Développement de nouveaux outils microfluidiques pour l'étude et l'optimisation de la bioremédiation de polluants organiques dans les sols. 17ème Congrès de la Société Française de Génie des Procédés, 15-17 octobre 2019, Nantes, France

Baranger C., Sun X., Pezron I., Le Goff A., Fayeulle A. « Myco-fluidique » pour la remédiation des sols. Congrès National de la Société Française de Microbiologie, 1-3 octobre 2018, Cité des Sciences et de l'Industrie, Paris

Baranger C., Creusot L., Pezron I., Le Goff A., Fayeulle A. Bioremédiation des sols : mobilisation, incorporation et dégradation d'un HAP par un champignon filamenteux, *Talaromyces helicus*. Congrès Intechem Process, 7-8 mars 2018, ESCOM, Compiègne

Posters :

Baranger C., Le Goff A., Fayeulle A. Incorporation du benzo-[*a*]-pyrene par un champignon filamenteux du sol, *Talaromyces helicus*. 4ème Rencontres Nationales de la Recherche sur les Sites et Sols Pollués, 26-27 novembre 2019, Montrouge, France

Baranger C., Sun X., Pezron I., Le Goff A., Fayeulle A. « Myco-fluidique » pour la remédiation des sols : étude microfluidique de la désorption et de l'incorporation des HAPs par un champignon filamenteux. Colloque de Prospective Surfaces et Interfaces Continentales, 9-11 octobre 2017, Conservatoire National des Arts et Métiers, Paris (Poster)